**UNIVERSITY OF CRETE**
*Department of Materials Science and Technology*

**FOUNDATION FOR RESEARCH AND TECHNOLOGY**
*Institute of Electronic Structure and Lasers*


# "Smart polymer coatings for antimicrobial surfaces"

A DISSERTATION
*submitted in partial fulfillment of*
*the requirements for the degree of*
DOCTOR OF PHILOSOPHY

by

Koufakis Eleftherios

December 2019

To my family and Elmina

*"Science is the Poetry of Reality"*

*Richard Dawkins*

# Acknowledgements

To begin with, I would like to express my deepest gratitude to my supervisor *Prof. Maria Vamvakaki*, who gave me the opportunity to work on this project and for all the guidance she has provided me throughout these years. Working in her synthesis laboratory was a life-time experience and I am grateful for her patience, support, enthusiasm, motivation, encouragement and mostly the freedom she offered me to express my curiosity and my ideas.

I would like to sincerely thank *Prof. Spiros Anastasiadis,* who supervised a part of this work and gave me the opportunity to work in his laboratories of the Institute of Electronic Structure and Laser of the Foundation of Research and Technology.

I am greatly honored to be working with *Dr. Theodore Manouras*, who acted altruistically, closely advised me through this project and introduced me in the solid-state surface science. I would also like to express my thanks to *Dr. Ioanna Peraki* for initiating me in the basic methods for bacterial cultures and antimicrobial applications.

In addition, I would like to thank *Prof. Andreas Fery* and *Prof. Petra Uhlmann*, who gave me the benefit to work in their laboratories of the Leibniz Institute of Polymer Research (IPF) in Dresden. *Dr. Maximilian Seuss* and *Mrs. Inga Melnyk* for fruitful conversations and guidance in FFM measurements.

Moreover, I would like to thank all my colleagues at the Materials Synthesis Group through these years, namely *Maria Kalyva, Fanis Krassanakis, Panagiotis Falireas, Elmina Kabouraki, Daniel Gherca, Epameinondas Orfanoudakis, Kostas Christodoulakis, Eva Vasilaki, Lucille Chambon, Christina Orfanou, Antonis Papadopoulos, Maria Psarrou, Kostas Parkatzidis. Niki Iliadi, Chara Flouraki* and *Maria Kissamitaki* for the positive work environment.

Special thanks to *Prof. Demetrios Ghanotakis* and his laboratory members, *Harris, Eleftheria, Napoleon* and *Manos*, to *Ass. Prof. Eleftherios Iliopoulos* for the Ellipsometry measurements and *Mrs. Aleka Manousaki* and *Mrs. Katerina Tsagkaraki* for the FE-SEM and AFM measurements, respectively.

Last but not least, I would like to thank *my family* for their support and the love of my life *Elmina Kabouraki* for her inspiration, support, understanding and patience.

The present PhD Thesis has been performed at the Materials Synthesis Group of the Materials Science and Technology Department, Univ. of Crete and the Institute of Electronic Structure and Laser of the Foundation of Research and Technology.

The thesis has been co-financed by the European Union (European Social Fund – ESF) and Greek national funds through the operational programs "Education and Lifelong Learning" of the National Strategic Reference Framework (NSRF) – Research Funding Programs:

(a) THALES. Investing in knowledge society through the European Social Fund. Project title: "Development of Novel Functional Copolymers and Surfaces with Permanent and/or Controlled released biocidal species" (MIS:379523).

(b) EDVM 34. Supporting researchers with emphasis on young researchers. Project title: "Novel hybrid biocidal surfaces with self-renewal properties and direct detection of their antimicrobial activity" (MIS: 5006044).

# Abstract

"Smart" polymer coatings enable to tune the interfacial physico-chemical properties of a variety of organic and inorganic materials, at will. Polymer brushes, are ideal coatings for numerous applications, ranging from "smart", controllable adhesive, biosensing and antimicrobial surfaces. This thesis presents the synthesis and characterization of novel, well-defined polymer brushes, bearing desirable functionalities, via surface-initiated atom transfer radical polymerization (SI-ATRP). The surface properties and the antimicrobial performance of the brushes were studied rendering them attractive for use as lubricants with responsive behavior and/or dual-functional antimicrobial surfaces in the solid state.

Homopolymer brushes based on 2-(dimethylamino)ethyl metahcrylate, (DMAEMA), or fluorinated methacrylates, were synthesized, via SI-ATRP, on glass and silicon substrates. PDMAEMA brushes comprise a convenient model-system to investigate the surfaces properties upon a facile post-modification reaction introducing different alkyl chain lengths (ACL) on the side groups of the end-grafted polymer chains. Three fluorinated methacrylates, with different fluorinated alkyl chain lengths (FCLs = 1, 4 and 6 fluorocarbon atoms) in their side-groups, referred to as TFEMA, OFPMA and TDFOMA, respectively, were utilized. The variations in the hydrophilicity/hydrophobicity and the surface free energy of the brush, as a function of the FCL of the side group and the ACL of the quaternization agent, were determined. A hydrophilic to hydrophobic transition of the surfaces and a significant decrease of the degree of quaternization of the DMAEMA moieties was found upon increasing the ACL of the quaternization agent above six carbon atoms, allowing to tune the wettability, the thickness and the pH-response of the brushes. Next, the adhesion and friction properties of the polymer brushes in the solid state against a sliding inorganic surface were examined. Finally, the hydrophilic, PDMAEMA and quaternized PDMAEMA, brushes are shown to be unstable in water due to the degrafting of the polymer chains, by the hydrolysis of the labile ester or siloxane bonds of the surface-bound initiator, that is mechanically driven by the tension on the chains. On the other hand, all fluorinated brushes were stable due to the inhibition of the penetration of water molecules at the polymer-substrate interphase.

In the second part of the present study, amphiphilic diblock copolymer and binary mixed polymer brushes were prepared, comprising PDMAEMA and PTFEMA, POFPMA or PTDFOMA chains. The reorganization of the polymer chains and the switching of the film wettability, upon exposure to selective solvents for the two polymers, were observed. In addition, the mixed brushes exhibited tunable friction and surface energies, in response to

external stimuli, which renders them attractive for use as “smart” surfaces in the dry state. Quaternization of the DMAEMA groups, diminished the responsive behavior of the brushes, which as attributed to the large $\chi$ value between the two very dissimilar blocks (charged PQDMAEMA and semi-fluorinated polymethacrylates). Finally, evidence of unwanted chain degrafting of the diblocks was found again, attributed to hydrolysis, after exposure of the brushes in aqueous media for prolonged time periods, whereas the amphiphilic mixed polymer brushes exhibited a remarkable stability in aqueous media with the fluorinated polymer acting as a barrier to shield the labile initiator bonds from hydrolysis.

In the final part of this thesis, quaternized PDMAEMA brushes bearing quaternary ammonium groups of different ACLs were assessed as biocidal coatings. The effect of the ACL of the quaternary ammonium groups on the contact killing efficiency of the surfaces, against *E. coli* and *B. cereus* bacteria, was investigated. Antimicrobial tests revealed that the hydrophilic polymer brushes exhibited enhanced bactericidal activity, whereas the hydrophobic surfaces showed a significant deterioration of the *in vitro* bactericidal performance. In another approach, the antifouling activity of the semi-fluorinated homopolymer brushes, bearing different FCLs on the polymer side groups, was found to increase with the number of fluorocarbon atoms. These results elucidate the antimicrobial action of the quaternized polymer brushes and the low-surface energy fluorinated brushes, dictating the appropriate choice of the ACL or FCL, for the development of coatings that effectively inhibit biofilm formation on surfaces either by killing or by releasing the bacteria. Finally, dual functional coatings, comprising mixed polymer brushes of the bacterial-releasing fluorinated chains, PTFEMA, POFPMA or PTDFOMA, and the bactericidal PQDMAEMA chains, were shown to possess significantly improved antimicrobial performance, against both *E. coli* and *B. cereus*, due to their combined antifouling and bacteria killing action.

# Table of Contents

# Abbreviations & Notations

| | |
|---|---|
| m | meters |
| mm | Milimeters = $10^{-3}$ m |
| μm | Micrometers = $10^{-6}$ m |
| nm | Nanometers = $10^{-9}$ m |
| $^{1}$H NMR | proton nuclear magnetic resonance |
| AA | allyl alcohol |
| ABIB | allyl 2-bromoisobutyrate |
| ACL | alkyl chain length |
| AFM | atomic force microscopy |
| AGET ATRP | atom generated electron transfer ATRP |
| AO7 | (sodium 4-((2E)-2-(2-oxonaphthalen-1-ylidene)hydrazinyl) benzenesulfonate or acido range 7 |
| APDES | (3-aminopropyl)dimethylethoxysilane |
| APTES | (3-aminopropyl)triethoxysilane |
| ATR-FTIR | attenuated total reflectance fourier transform infrared spectroscopy |
| ATRA | atom transfer radical addition |
| ATRP | atom transfer radical polymerization |
| BDE | bond dissociation energy |
| BIBAPDES | (3-(2-bromoisobutyramido)propyl)dimethylethoxysilane |
| BIBB | 2-bromoisobutyryl bromide |
| BIBPTES | (3-(2-bromoisobutyryl)propyl)triethoxysilane |
| BIDS | (3-(2-bromoisobutyryl)propyl)dimethylethoxysilane |
| BMPA | 2-bromo-2-methyl-N-pentylpropanamide |
| CA | contact angle |
| CD | charge density |
| $CDCl_3$ | deuterated chloroform |
| CRP | controlled/ “living” polymerization |
| Cu(I)Br | copper(I) bromide |
| Cu(II)Br | copper(II) bromide |
| $DQ$ | degree of quaternization |
| DMAEMA | 2-dimethylaminoethyl methacrylate |

| | |
|---|---|
| DMEOS | dimethylethoxysilane |
| DMF | Dimethylformamide |
| dNbpy | 4,4'-dinonyl-2,2'-bipyridine |
| DP or N | degree of polymerization |
| EBIB | ethyl 2-bromoisobutyrate |
| EtOH | ethanol |
| FCL | fluorinated alkyl chain length |
| FRP | free radical polymerization |
| FTIR | fourier transform infra-red spectroscopy |
| GPC | gel permeation chromatography |
| h | dry polymer film thickness |
| $H_2O_2$ | hydrogen peroxide |
| $H_2SO_4$ | sulfuric acid |
| HCl | hydrochloric acid |
| HFiP | 1,1,1,3,3,3-hexafluoro-2-propanol |
| HMTETA | 1,1,4,7,10,10-hexamethyltriethylenetetramine |
| $L_n$ | ligand |
| LCST | lower critical solution temperature |
| LFM | lateral force microscopy |
| LRP | living radical polymerization |
| M | Monomer |
| MetOH | methanol |
| $M_n$ | number-average molecular weight |
| $M_w$ | weight-average molecular weight |
| MMA | methyl methacrylate |
| $Mt^m$/Ligand | metal complex at lower oxidation state |
| $N_A$ | Avogadro's number |
| OFPMA | 2,2,3,3,4,4,5,5-(octafluoro)pentyl methacrylate |
| P2VP | poly(2-vinyl pyridine) |
| P4VP | poly(4-vinyl pyridine) |
| PAA | poly(acrylic acid) |
| PBS | Phosphate-burffered saline |
| PCBMA | poly(carboxy-betaine methacrylate) |

| | |
|---|---|
| PCM | plate counting method |
| PDMAEMA | poly(2-dimethylaminoethyl methacrylate) |
| PEL | polyelectrolyte |
| PEO | poly(ethylene oxide) |
| $pK_a$ | dissociation constant |
| PMETAC | poly(2-methacrylolyloxyethyltrimethylammonium chloride) |
| PMMA | poly(methyl methacrylate) |
| POFPMA | poly(2,2,3,3,4,4,5,5-(octafluoro)pentyl methacrylate) |
| PPEGMA | poly(polyethylene glycol) methacrylate |
| PQDMAEMA | quaternized PDMAEMA |
| PS | polystyrene |
| PTDFOMA | poly(3,3,4,4,5,5,6,6,7,7,8,8,8-(tridecafluoro)octyl methacrylate) |
| PTFEMA | poly(2,2,2-(trifluoro)ethyl methacrylate) |
| RAFT | reversible addition-fragmentation chain transfer |
| $R_g$ | radius of gyration of the free chain in solution |
| RH | relative humidity |
| RI | refractive index |
| RT | room temperature |
| SAM | self-assembled monolayer |
| SE | spectroscopic ellipsometer |
| SEC | size-exclusion chromatography |
| SEM | scanning electron microscopy |
| SFE | surface free energy |
| SI-ATRP | surface-initiated atom transfer radical polymerization |
| SI-CRP | surface-initiated controlled radical polymerization |
| $SiO_2$ | silicon dioxide |
| $T_g$ | glass transition temperature |
| TDFOMA | 3,3,4,4,5,5,6,6,7,7,8,8,8-(tridecafluoro)octyl methacrylate |
| TEA | triethylamine |
| TEOS | triethoxysilane |
| TFEMA | 2,2,2-(trifluoro)ethyl methacrylate |
| TFT | α,α,α-trifluorotoluene |
| THF | tetrahydrofuran |

| | |
|---|---|
| UCST | upper critical solution temperature |
| UV/Vis | ultraviolet/visible spectroscopy |
| WCA | water contact angle |
| X-$Mt^{m+1}$/Ligand | metal complex at higher oxidation state |
| $\sigma$ | grafting density |

# Chapter 1

# Introduction

## 1.1 Polymer coatings

### 1.1.1 Introduction to polymer brushes

The design of functional interfaces can alter the surface properties of solid substrates and the materials' interactions with their surrounding environment, and plays a vital role in nearly all applications. Coatings of soft materials such as polymers, can serve as a protective interface - exploiting the material's intrinsic bulk properties - to battle against environmental effects (e.g. UV-radiation, moisture), chemical degradation, corrosion and biocorrosion, but more interestingly they often allow to tune the surface properties on demand for any intended application. The modification of surfaces with synthetic or natural polymers has been thoroughly explored during the past years, and still constitutes a major research focus. The development of multi-functional polymer coatings exhibiting (super)hydrophilic/(super)hydrophobic, anticorrosive, antireflective, lubricative, self-cleaning, antifouling and biocidal-antimicrobial properties to protect surfaces is an active area of research.

Polymer coatings can be deposited on solid substrates by facile techniques, that rely on physical interactions between the polymeric material and the substrate, comprising spin coating, dip coating, spray coating, painting or droplet evaporation. More complicated methods have been also employed such as the adsorption of monolayers of homo- and block copolymers, the layer-by-layer (LbL) and the Langmuir-Blodgett-Kuhn technique. All these techniques require simple set-ups to generate the polymer coatings and offer the desirable results under favorable conditions. Nevertheless, these films often exhibit instabilities under certain unfavorable external conditions e.g. dewetting above the glass transition temperature ($T_g$) or delamination below the polymer $T_g$, displacement by other molecules with higher affinity for the surface and desorption upon solvent exposure. Self-assembled monolayers (SAMs) have been also widely employed for the preparation of well-controlled interfaces, and use small organic molecules having a reactive head-group for their immobilization onto any material, by forming covalent bonds with specific chemical functionalities, which are present on the surface of the material.[1] Characteristic examples are silanes on oxide surfaces, thiols on gold surfaces, and phosphates on metal surfaces. Figure 1.1 illustrates schematically some typical SAM structures based on different choices of the chemical groups (e.g. head groups, spacer types and functional/end groups) and the types of substrates that

are used.[2] Due to the fact that, a SAM provides more or less a two-dimensional arrangement, conversely, there are strict limitations in several applications that require control of the polymer film thickness and the grafting density of the chains.

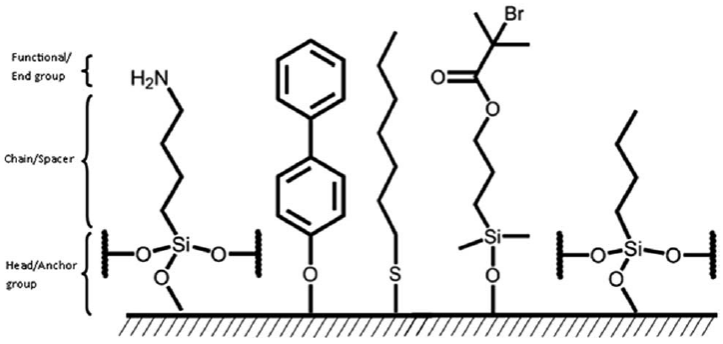


**Figure 1.1.** Schematic illustration of typical SAMs on various substrates using a variety of head groups, spacer types, and functional groups.[2]

Therefore, the need for straightforward and robust surface modification approaches has led to the sophisticated preparation of covalently anchored polymer chains onto surfaces to form the so-called polymer brush architectures. Surface modification via the deployment of polymer brushes is based on the tethering of one end of a polymer chain to a hard surface or an interface. In general sense, polymer brushes are defined as dense covalently attached polymer chains to a surface, where the distance between two anchoring points is a lot lesser than the unperturbed dimensions of the tethered chains, thus the polymer chains become crowded and are stretched away from the surface.[3]

The extension of the tethered polymer chains is determined by the distance between two grafting points, D, calculated as $2R_g\sigma^{1/2}$, where $R_g$ is the radius of gyration of the free chain in solution and $\sigma$ (chains/nm$^2$) is the grafting density. The grafting density can be calculated by Equation 1.1:

$$\sigma = \frac{d \times N_A \times h}{M_n} = \frac{1}{D^2} \tag{1.1}$$

Where, $h$ is the dry polymer film thickness, $d$ is the bulk density of the grafted polymer, $M_n$ is the number-average molecular weight of the chains grafted on the surface assumed to be the same as that of the polymer chains in solution obtained by size-

exclusion chromatography (SEC), and $N_A$ is the Avogadro's number ($6.023\times10^{23}$). The effect of grafting density can be even more pronounced by the solvent interactions, with highly swollen and collapsed states of the polymer brushes found after immersion in good and bad solvents, respectively. The polymer brush conformation can be divided into four different regimes: (a) pancake and (b) mushroom, for $D > R_g$, (b) moderate brush for $D < R_g$ and (c) high-density brush regime for $D << R_g$.[4] Figure 1.2 illustrates the effect of grafting density on the polymer brush thickness.

From the above, it becomes clear that the grafting density is a significant parameter in polymer films as it defines the final structure of the tethered polymer chains. For simplicity, the term "polymer brush" is often used for all the grafted polymer chains, nevertheless, it should be termed only under specific conditions, when the behavior of the grafted polymer layer is defined by strong interactions between densely-grafted polymer chains ($D < R_g$).

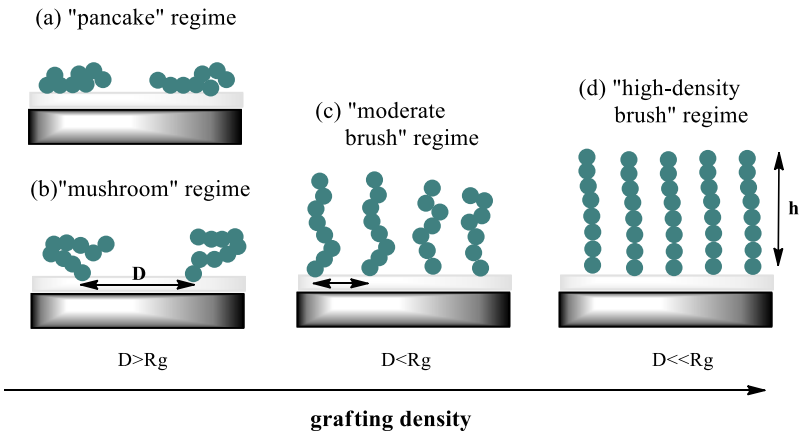


**Figure 1.2.** Schematic representation of the various polymer film regimes depending on the grafting density.

Polymer chains can be covalently grafted onto a large variety of substrates, such as polymeric materials including chitosan (CS), cellulose, polypropylene, polyurethane, polyimide, poly(methyl methacrylate) (PMMA), nylon, polystyrene (PS), poly(dimethyl siloxane) (PDMS), as well as organic and inorganic materials e.g. steel, silicon, glass, mica, diamond, carbon nanotubes, zirconium phosphonate, etc. These may result in planar brushes on flat substrates, cylindrical brushes on fiber- or rod-like-substrates and spherical brushes on spherical substrates.[5]

### 1.1.2 Synthetic processes and methods for the preparation of polymer brushes

A polymer brush can be attached onto a substrate either by physical attachment namely physisorption or covalent-bonding known as chemisorption. In general, physisorption can be attained using block copolymer chains, where, one of the two blocks interacts strongly with the surface and adsorbs on it, while the other does not. Hadjiioannou et. al. were the first to report the physisorption of polystyrene-*b*-poly(2-vinylpyridine) (PS-*b*-P2VP) block copolymer chains on mica.[6] Nevertheless, the attachment in physisorption is based on van der Waals and hydrogen bonding interactions, which render the process reversible, and thus such brushes have limited stability. Covalent bonding between the substrate and the polymer chains can overcome these limitations. Covalently attached polymer brushes are mainly accessible by two approaches: (a) the "grafting-to" and (b) the "grafting-from", along with a third, less reported (c) "grafting-through" method (Figure 1.3).

In the case of "grafting-to", polymer brushes can be attained either by (i) polymer chain physisorption of block copolymers, where one block of the polymer chains interacts with the surface, with the other block interacts with the solvent forming the brush layer, or by (ii) chemisorption, where preformed end-functionalized polymer chains diffuse from the solution towards a proper pre-functionalized (by SAMs or coupling agents) substrate and chemically react with its functional groups (conjugating sites) under appropriate conditions.[7] The chemisorption "grafting-to" method is illustrated in Figure 1.3a. The main advantages of the "grafting-to" approach rely on the synthesis of polymer chains with well-controlled $M_n$'s and narrow polydispersities. As a matter of fact, the degree of polymerization and the polymer chain length are known before the covalent attachment, which promotes a better and more thorough characterization of the final polymer brush films. Nevertheless, the grafting density of the polymer chains constitutes a disadvantage, since a small number of functional polymer chains can avoid the barrier of the increasing polymer film during the process and diffuse through it and react with the "free" reactive sites of the surface. Thus, the film thickness and the grafting density of the polymer brush are restricted using the "grafting-to" method.[8]

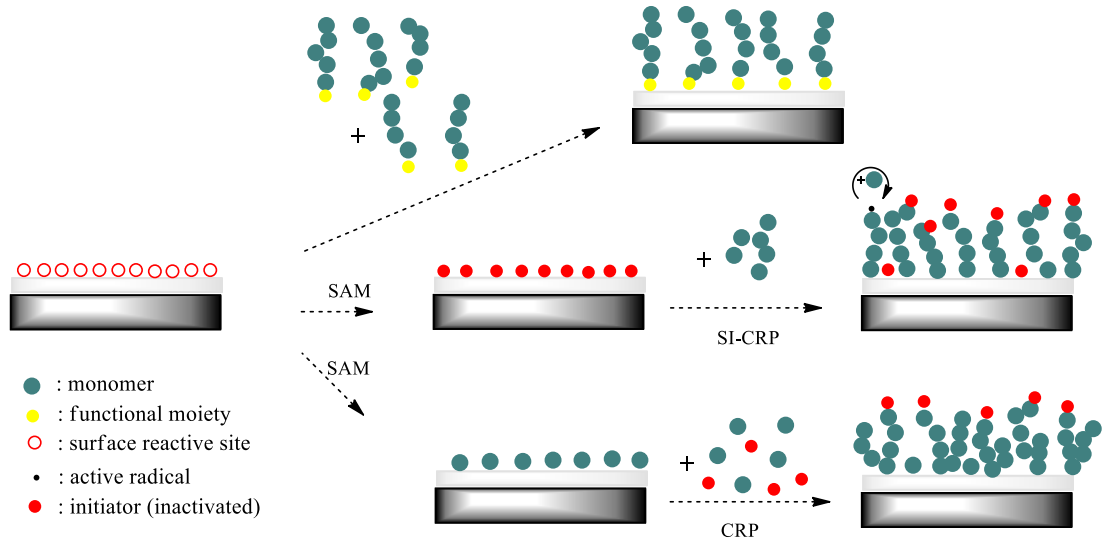


**Figure 1.3.** Schematic illustration of the (a) "grafting-to" approach using "click" chemistry, (b) "grafting-from" approach via the SAM technique and the *in-situ* SI-CRP method and the (c) "grafting-through" approach using CRP.

To avoid these drawbacks, the "grafting-from" technique can be employed. In the "grafting-from" process, polymer chains are *in situ* synthesized on a pre-functionalized (by SAM of a polymerization initiator) surface to form surface-anchored polymer films.[3b, 9] This method is also referred as surface initiated polymerization (SIP) method. Figure 1.3b illustrates the "grafting-from" approach via the widely exploited surface-initiated atom transfer polymerization. "Grafting-from" is the most commonly employed technique for the synthesis of polymer brushes, because it exerts control over the growth of the polymer chains, since the polymer chains are grown uniformly, starting from the substrate, by the addition of monomers in contrast to the diffusion of long macromolecules described in the "grafting-to" method.[10] As a result, much thicker and densely grafted polymer brushes can be synthesized. Nonetheless, a substantial drawback of the "grafting-from" method is the lack of quantitative characterization of the polymer brushes, in terms of the $M_n$ and the polydispersity (Đ) of the grafted polymer chains. The polymer chains can be cleaved from the surface after the polymerization; however, it is crucial to have vast surface area covered by polymer brushes to obtain a sufficient amount of polymer for subsequent characterization. An indirect method, but widely exploited in the literature, is the utilization of a "sacrificial" free initiator during the polymerization reaction, which correlates the polymer chains that are growing from the surfaces with the free polymers in the solution. A lot of

controversy has been posed by the scientific community regarding the correlation of the molecular weights of the polymer in solution and the surface-grafted polymer.[8] Lately, Spencer et al investigated the growth rate of polymers in solution and on surfaces and concluded that these two can be correlated under certain conditions such as propagation rate, temperature and grafting density.[11]

Finally, surfaces can be functionalized by the "grafting-through" method, which involves the *in situ* bulk polymerization reaction of a monomer-modified surface with monomers or growing polymer chains during the polymerization procedure. This method is illustrated in Figure 1.3c. The advantage of this method is that it is compatible with existing bulk polymerization processes (free radical and controlled/"living" radical polymerizations).[12] Nevertheless, similar to the "grafting-to" method, only limited grafting densities can be achieved.

The polymerization methods used for the preparation of polymer brushes are anionic, cationic, ring-opening, ring-opening metathesis and controlled radical polymerization.[13] Controlled/"living" radical polymerization (CRP, also termed reversible-deactivation radical polymerization, RDRP) techniques such as atom transfer radical polymerization (ATRP), reversible addition-fragmentation chain transfer (RAFT) and nitroxide mediated polymerization (NMP) are primarily employed for the synthesis of polymer brushes using the "grafting-from" approach or surface-initiated controlled radical polymerization (SI-CRP).[14] SI-CRP allows strict control over the polymer brush thickness, composition and architecture; thus, it is the most widely used approach, in the recent years, to tailor the surface properties of materials. The common principle in all these techniques is the activation – deactivation process of the radicals or the growing polymer chains. Figure 1.4 illustrates the basic mechanism of the SI-CRPs, in which the dormant species, which are halogen-capped radicals ($P_n$-X), are activated to the propagating species, which are radicals ($P_n$*), and react in the presence of monomers (M), until the reverse deactivation of the radicals. Surface-initiated atom transfer radical polymerization (SI-ATRP) is the predominant SI-CRP technique to prepare polymer brushes. In this thesis, SI-ATRP is the technique employed for the synthesis of polymer brushes of different architectures on flat surfaces, thus it will be described in detail in the subsequent section.

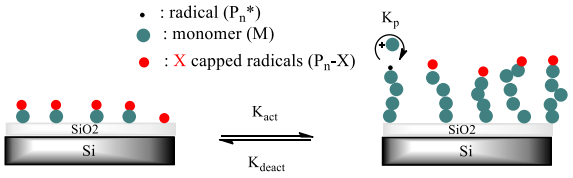


**Figure 1.4.** Schematic illustration of the reversible chain activation-deactivation process in a SI-CRP.

### 1.1.3 Atom Transfer Radical Polymerization (ATRP)

ATRP is the most widely employed method for the synthesis of polymers and polymer brushes. The method was introduced for the first time in 1995 and has been widely used for controlled polymerizations since it has been proved to be versatile, reliable and robust.[15] Mechanistically it is considered as an extension of the transition mediated atom transfer radical addition (ATRA) reactions.[16] In ATRA, a free radical mechanism is involved by the addition of a polyhalogenated alkane to an alkene in the presence of an initiator. A transition metal complex is utilized for the catalysis of the ATRA reaction.

#### 1.1.3.1 Mechanism and ATRP equilibrium

The mechanism of the traditional or "normal" ATRP reaction is shown in Figure 1.5. ATRP is based on an equilibrium between the propagating species, which are the (macro)radicals ($P_n$*) and the dormant species, which are halogen- or pseudohalogen-capped radicals ($P_n$-X), with the metal complexes acting as reversible (pseudo)halogen atom-transfer reagents moving to lower ($Mt^m$/Ligand) and higher (X-$Mt^{m+1}$/Ligand) oxidation states. The radicals react reversibly with the metal complexes in a deactivation/activation process. X-$Mt^{m+1}$/Ligand deactivates the radicals to form dormant species and $Mt^m$/Ligand re-activates the radicals to reform the activator. The polymer chains grow by the addition of monomer units to the generated radicals, similarly to the free radical polymerization with a rate constant of propagation ($k_p$), before they are deactivated by X-$Mt^{m+1}$/Ligand through the halogen atom transfer. This reversible transfer process of the halogen atom occurs with a rate constant of activation ($k_{act}$) and deactivation ($k_{deact}$). The monomers which are added during activation are

minimum, thus $k_{deact}$ is much higher than $k_p$. The reaction equilibrium is shifted to the left side, and thus the free radical concentration is kept low during the polymerization. This means that the contribution of the rate constant of radical termination ($k_t$) to the reaction is vastly reduced. At the final stage of the polymerization, when the amount of monomer units is exhausted, the polymer chains are halogen-capped due to the halogen exchange, and thus can act as macroinitiators for another ATRP.

Termination reactions occur in ATRP, mainly through radical coupling and disproportionation; however, in a well-controlled ATRP, no more than a few percent (~5%) of the polymer chains undergo termination. At the initial stages of the polymerization, the concentration of deactivator is low to ensure a fast rate of the deactivation process. As a result, initiator-initiator termination reactions will take place, which will lead to the formation of the appropriate amount of deactivator needed to obtain a controlled polymerization. This accumulation reduces the equilibrium active radical concentration minimizing further termination reactions. It is estimated that only a small number of radicals are sacrificed (~5%), due to the persistent radical effect based on the coupling of initiators, at the early stages of the polymerization. The persistent radical effect is thought to reduce $P_n^*$- $P_n^*$ termination as well as increase the control, whilst accelerating the polymerization.[2] Addition of an amount of deactivator (<10% of all metal species) at the beginning of the polymerization can result in further reduction of the termination reactions of the growing polymer chains.[17]

Similar to living polymerizations, the degree of polymerization and the theoretical molecular weight can be calculated by the Equation 1.2:

$$DP = [M]_0/[\mathrm{Pn-X}]_0 \times p \qquad (1.2)$$

Where, $[M]_0$ is the initial monomer concentration, $[\mathrm{Pn-X}]_0$ is the initiator concentration, and p is the monomer conversion. For a successful ATRP, the DP should be equimolar to the monomers converted to polymer over the initial initiator added to the reaction mixture.

The molecular weight distribution ($M_w$ / $M_n$) of polymers prepared by ATRP may be lower than 1.1 under certain conditions.[18] In the absence of chain termination and transfer reactions, the polydispersity relates to the concentration of initiator [$P_n$-X] and

deactivator [X-$Mt^{m+1}$/Ligand], the rate constants $k_p$ and $k_{deact}$ and monomer conversion, p, as shown in Equation 1.3[19]:

$$\frac{M_w}{M_n} = 1 + \left(\frac{k_p([\mathrm{Pn{-}X}]_0 - [\mathrm{Pn{-}X}])}{k_{deact}[X{-}Mt^{m+1}]}\right)\left(\frac{2}{P} - 1\right) \quad (1.3)$$

Thus, for the same monomer, a lower polydispersity can be achieved if the catalyst system deactivates the growing chains faster (lower $k_p/k_{deact}$) or the deactivator concentration is increased, or the targeted molecular weights are high.

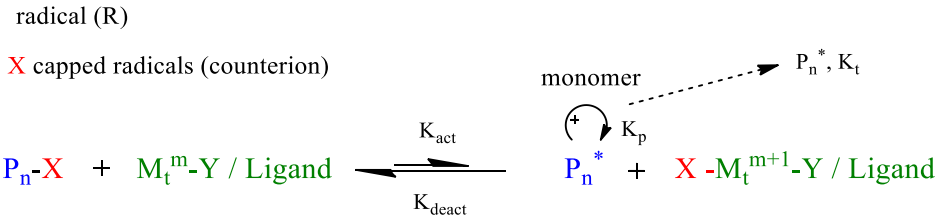


**Figure 1.5.** Representation of the traditional ATRP equilibrium (Note: $k_{act} << k_{deact}$).[20]

In traditional ATRP, the rate of polymerization ($R_p$) is given by Equation 1.4, which depends on the concentration of reagents, the rate constant of propagation ($k_p$) and the ATRP ($K_{ATRP}$) constant:[20]

$$R_p = k_p[P_n^*][M] = k_p K_{ATRP} \frac{[PX][Mt^m L_n]}{[Mt^{m+1} L_n X]}[M] \quad (1.4)$$

In a polymerization reaction, the quantification of $K_{ATRP}$ is significant for the evaluation of the catalyst's activity and is determined by the strength of both the $P_n$ ─X and the $Mt^{m+1}$ ─X bonds. $K_{ATRP}$, is given by Equation 1.5 and is the ratio of $k_{act}$ and $k_{deact}$, which can profoundly be affected by the nature of the Ligand ($L_n$), and the monomer (M), as well as the reaction conditions (temperature, solvent, pressure).[21]

$$K_{ATRP} = \frac{k_{act}}{k_{deact}} = \frac{[P_n^*][Mt^m L_n]}{[Mt^{m+1} L_n X][[PX]} \quad (1.5)$$

### 1.1.3.2 ATRP components

ATRP is a multicomponent catalytic process, and a number of factors that affect the outcome of the polymerization need to be considered, in order to choose the proper conditions for the preparation of well-defined polymeric materials. As discussed previously, ATRP comprises a monomer, an initiator, a catalyst system and solvent

(optional) at different conditions of temperature and pressure, and the presence of an external stimulus (optional).

**Monomers.** The range of vinyl monomers polymerized by ATRP include meth(acrylates), styrenes, (meth)acrylamides and acrylonitrile and is profoundly wide. Amongst them, several functional monomers have been polymerized by ATRP including monomers containing -OH groups (2-(hydroxy)ethyl methacrylate (HEMA)), 4-vinyl pyridine (4VP), glycidyl (meth)acrylate (G(M)A), precursors of ionic monomers (2-(dimethylamino)ethyl methacrylate (DMAEMA), 2-(dimethylethylammonium)ethyl methacrylate bromide) (QDM) and ionic liquid monomers.[5] Nevertheless, challenges, such as the polymerization of acidic ((meth)acrylic acid, phosphonic or sulfonic acids) or strongly coordinating monomers, in the presence of which the deactivator halidophilicity is quite low, still remain. These monomers react rapidly with the catalysts forming metal carboxylates, which are "difficult-to-activate alkyl halides" chain-ends, and thus provide ineffective catalysts for ATRP. In addition, monomers have different reactivity, which means that the $K_{ATRP}$ is affected, and thus a regulation of the $k_{deact}$ is needed in order to maintain a controlled polymerization.

**Initiators.** In ATRP, alkyl halides (R─X) are typically utilized as initiators.[22] The ATRP initiators should possess sufficient reactivity to initiate the polymerization of the monomers. $K_{ATRP}$ is correlated with the bond dissociation energy (BDE) of the initiators. The reactivity of the initiator depends on the structure of the alkyl group as well as the halogen or pseudohalogen itself. Figure 1.6 shows an overview of the activation rate constants of various known ATRP initiators. For a given catalyst system and solvent, the $K_{ATRP}$ depends on the energy needed for the homolysis of the alkyl halide bond. The activation rate constants of tertiary alkyl halides have been shown to be higher than those with secondary and primary carbon atoms. Moreover, the activation rate constants follow the order Br ~ I > Cl of the leaving atoms of the alkyl halide, which overall have higher reactivities than alkyl pseudohalides. This is attributed to the difference in the BDE for C-Cl or C-Br bond cleavage.[23]

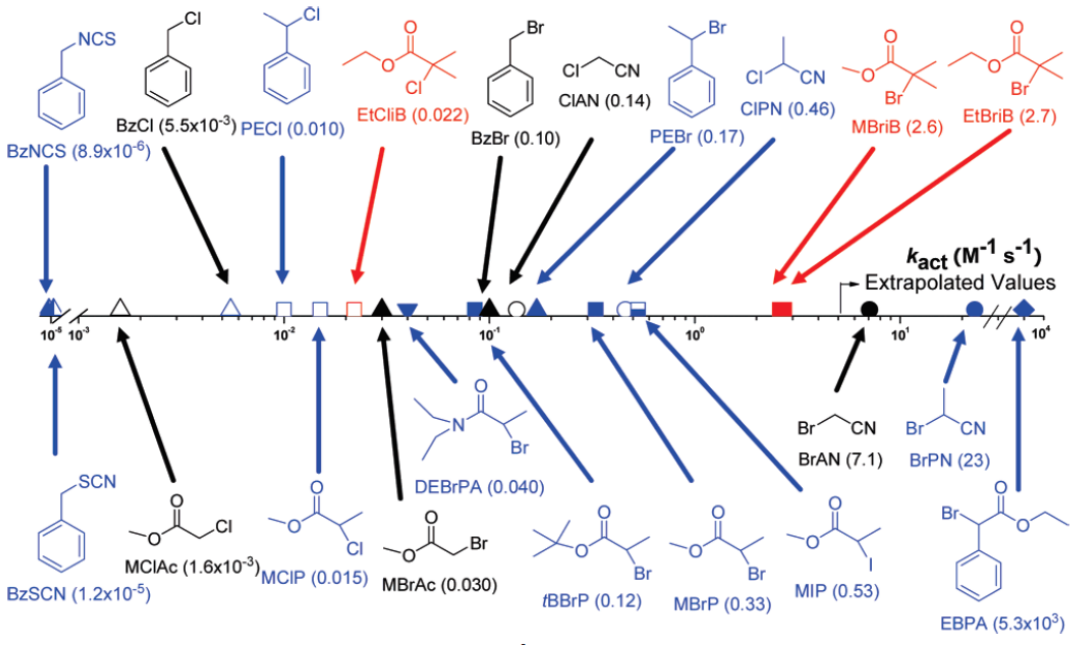


**Figure 1.6.** ATRP activation rate constants of various initiators in the presence of TPMA and Cu$^{I}$Br in MeCN.[23]

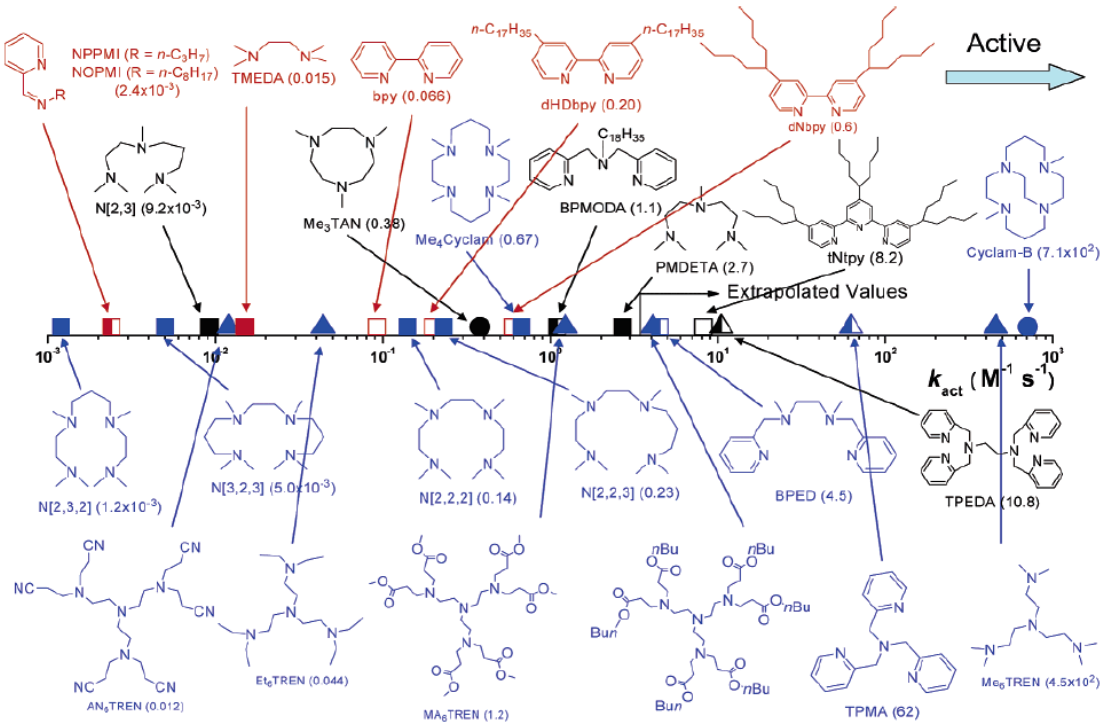


**Figure 1.7.** ATRP activation rate constants of various ligands in the presence of EBIB and Cu$^{I}$Br in MeCN.[21b]

**Catalyst System.** The key component of ATRP is the catalyst system, which is a metal complex based on a transition metal and an appropriate ligand. The transition metal usually has at least two oxidation states separated by one electron and low affinity for atoms such as alkyl radicals and hydrogen atoms, and high affinity towards halogen atoms. Many metal complexes have been employed, including Ti, Re, Rh, Ru, Fe, Ni, Pd, Co, Os and Cu for the establishment of a good control over the polymerization.[24] The most commonly used metal catalyst for ATRP is a copper salt, due to the fact that they are commercially available, inexpensive, and versatile.

The selection of the $L_n$ plays a profound role in solubilizing the metal salt in the reaction media and adjusting the redox chemistry of the metal complex. Various $L_n$'s have been employed to form the metal complexes such as nitrogen- and phosphorus-based ligands. Although several transition metals have shown catalytic properties toward various organic halides used as initiators, copper complexes with nitrogen ligands are the most used catalysts thanks to their low cost and easy handling; typically, they are prepared in situ by adding the $L_n$ to a cuprous halide salt.[21b] Figure 1.7 shows representative examples of nitrogen-based ligands for ATRP. In general, the activity of the ligands follows the order bidentate < tetradentate (linear) < tridentate <tetradentate (linear, branched, cyclic-bridged) and the order aromatic amine < imine < amine.

**Solvents.** A wide range of solvents have been utilized for ATRP, including common organic solvents and "greener" ones i.e. protic solvents (alcohols, water), ionic liquids, supercritical $CO_2$ and poly(ethylene oxide) (PEO).[25] ATRP can be conducted in bulk, solution or heterogeneous media. The choice of the solvent primarily depends on the solubility of the monomer, the polymer and catalyst system and heat transfer considerations. In conventional free radical polymerization, the quality of the solvent can affect the polymerization due to changes in the values of the rate constant of propagation, $k_p$, or due to viscosity effects on the rates of termination, $k_t$. Specifically, in ATRP, the solvent can react with the catalytic metal complexes in both oxidation states, imposing profound differences on the reaction rate, and thus the control of the polymerization (by $X\text{-}Mt^{m+1}$/Ligand dissociation or competitive complexation).[26] In addition, in the presence of solubility issues of monomers or polymers during an ATRP, the use of slightly acidic or coordinating solvents may be required, however in such mixtures, the utilization of more-halidophilic catalysts is needed. In non-polar solvents

usually ATRP cannot be conducted at RT thus the reaction requires heating. Finally, ATRP is accelerated in more polar solvents, at high temperatures and pressures.[26]

**Temperature and Pressure.** The reactivities of all species present in an ATRP and the stability of the catalyst can be affected by the modulation of the temperature. The complexation is an exothermic process and thus at elevated temperatures, destabilization of both oxidation states of the catalyst system can occur.[27] In addition, ATRP under high pressures has been shown to result in high molecular weight polymers compared to ambient pressure, due to the increase of the ratio $k_p/k_{deact}$.[26c]

A major drawback of traditional ATRP is associated with the relatively high concentration of catalyst at equimolar ratio with the initiator (in the range of 0.1─1 mol % *vs* monomer).[15a] High concentration of catalyst is required to overcome the radical termination effects in the presence of low activity catalysts.[25a] (a) Purification methods, including passing the polymer solution through an alumina column, stirring with an ion exchange resin, precipitation into a non-solvent, utilization of a heterogeneous catalyst which can be easily isolated after the polymerization reaction, and (b) polymerization techniques using higher activity catalysts that acquire lower amounts (ppm) of catalyst, have been employed for the elimination of the catalyst.[5] According to equation 1.3, ATRP does not depend on the concentration of catalyst, but rather on the ratio of the concentrations of activator and deactivator. Based on traditional ATRP, several ways have been shown to set up the ATRP equilibrium, including "reverse" ATRP, simultaneous reverse and normal initiation (SR&NI) ATRP, activators generated by electron transfer (AGET) ATRP, activator regenerated by electron transfer (ARGET) ATRP, initiators for continuous regeneration (ICAR) ATRP, supplemental activator and reducing agent (SARA) ATRP, ATRP mediated through electrochemistry (eATRP),[28] and finally photoinduced (photoATRP) and ultrasound-induced (sonoATRP) ATRP. These polymerization techniques are beyond the scope of this thesis and are discussed thoroughly in a review paper published recently by Matyjaszewski.[20]

#### 1.1.3.3 Surface Initiated Atom Transfer Radical Polymerization (SI-ATRP)

ATRP can be employed for the preparation of well-defined polymer brushes on various substrates, both organic and inorganic, with flat, concave or convex surfaces.[29] In 1997,

Huang et al. obtained for the first time polyacrylamide brushes grafted from a benzyl chloride monolayer on silica particles via SI-ATRP, whereas in 1998 Fukuda et al. grafted PMMA brushes from flat silicon surfaces.[30] The utilization of a surface-anchored initiator results to the SI polymerization. In general, the chemistry of SI-ATRP is based on the same principles as ATRP in solution, which involves initiation, propagation, activation/deactivation and termination processes. Nevertheless, there are certain differences, mainly due to the presence of the functionalized inorganic surface. Figure 1.8 shows a typical SI-ATRP from a flat substrate. According to traditional ATRP, the metal complex is transformed into its higher oxidation state due to the halogen transfer, which results in the formation of a radical at the initiator site on the surface. The reaction of the free radical with the monomer present in solution is disrupted by a halogen transfer which deactivates the active chain end. The main reactions involved in SI-ATRP are initiation, propagation and termination.

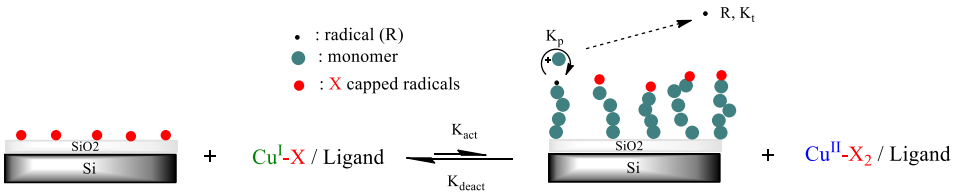


**Figure 1.8.** Schematic representation of the SI-ATRP process from flat ATRP initiator-functionalized substrates.

**Initiation.** As discussed above, the first requirement of SI-ATRP is an ATRP initiator-functionalized substrate using the SAM technique, prior to polymerization.[30b] The advantage of SI-ATRP for the preparation of polymer brushes is the facile functionalization of the surfaces using easily synthesized or commercially available functional α-haloesters or benzyl halides.[31] The most commonly employed surfaces for SI-ATRP are silicon/glass substrates. The functionalization process involves the facile reaction of the silanol groups which are present on the silicon surfaces with appropriate reactive groups (i.e. mono-chloro-silanes, mono-(m)ethoxy-silanes) leading to the formation of stable siloxane bonds. The use of tri-ethoxy or tri-chloro-silanes result in a network formation of silsesquioxanes providing better stability, compared to single bond anchored initiators. A plethora of functional ATRP initiators have been successfully tethered onto organic and inorganic materials, to synthesize polymer brushes with unique properties that are primarily affected by the grafting density of the

initiator.[32] The polymer grafting density can be tuned by several ways, with the most common techniques being the utilization of mixtures of active and non-active or "dummy" initiators or by varying the concentration of the initiator or the reaction time during the SAM process.[31, 33]

Similar to traditional ATRP in solution, the appropriate initiating functionality should be used in the SAM to ensure that the rate of activation is at least equal to the rate of propagation and provide high initiation efficiency and narrow polydispersities. The constant rate of activation follows again the order Br ~ I > Cl halogen atom, tertiary > secondary > primary substitution, and CN > Ph > ester radical stabilizing group.[23] Moreover, the length and hydrophobicity of the spacer between the initiator and the solid surface can affect the efficiency, with the increase of the grafting density and the initiation efficiency upon increasing the carbon spacer length of the initiator.[34] Apart from the grafting density and the type of initiator, the monomer, catalyst and the surface curvature can all affect the initiation efficiency.[34]

**Propagation.** The polymer chains grow from the surface as the monomers diffuse towards the surface and find the chain ends. The monomer diffusion may affect the rate of propagation, and thus the overall kinetics of the polymerization.[35] Ideally, for SI-ATRP from flat surfaces, the rate of propagation is proportional to the polymer film thickness, (if the grafting density is high) and thus the latter is increasing linearly with the polymerization time.[36] In order to achieve a well-controlled ATRP, a sufficient amount of deactivator must be present in the reaction. Due to the fact that, the concentration of attached surface initiators is quite low in SI-ATRP, the generation of the persistent radical effect based on initiator-initiator reactions is impossible. This results to the slow formation of deactivators, no reversible deactivation takes place, and irreversible on-surface radical termination governs.[37] For this reason, two approaches have been utilized; the addition of either a "sacrificial" free initiator, that has similar structure to the surface attached initiator, or a fraction of $Cu^{II}$ based catalyst, to invoke control over the polymerization reaction and ensure the presence of sufficient amount of deactivator during the process.[30a, 35]

Simulation and experimental studies, on these two approaches in SI-ATRP, have shown that: (a) the addition of the deactivator in the reaction mixture at the beginning of the polymerization results in a linear increase of the polymer brush thickness with the

polymerization time. Moreover, higher grafting densities and thicker polymer brushes with uniform growth can be prepared with this method;[37a] (b) on the other hand, addition of sacrificial initiator at the beginning of the polymerization, can generate deactivator only during the propagation, whereas at low polymerization times the concentration of deactivator is low that results to low control. Compared to the addition of deactivator, the addition of free initiator results in lower grafting densities by the partial loss of initiator, due to termination reactions, and to a decrease of the thickness growth rate, due to excessive monomer consumption by the untethered initiators. Nevertheless, the latter method enables the determination of the molecular weight and the grafting density of the polymer chains, assuming that the generation of the polymer chains in solution and on the surface are similar, which is significant for the proper characterization of the polymer brushes.[38]

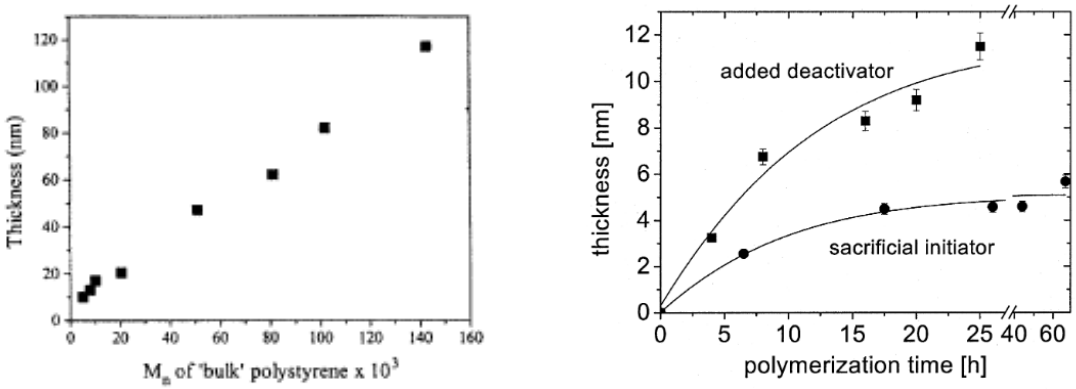


**Figure 1.9.** (a) Linear dependence of the polymer brush thickness with the molar mass of untethered PS chains.[39] (b) Growth profile of PS brushes obtained via SI-ATRP from silicon substrates using sacrificial initiator or deactivator.[40]

As described above the addition of free initiator or deactivator ideally results to a linear growth rate of the polymer brushes with time, assuming that the polymerization rates of the free polymer chains grown in solution and the surface anchored chains are similar. Figure 1.9a shows the increase in thickness of a PS brush with the molecular weight of the PS chains grown in solution using a sacrificial initiator. Figure 1.9b shows the brush growth rate profiles, for the two methods described above, using free initiator or deactivator. It is obvious that, the rate of polymerization is not constant as expected and the growth profile deviates as the ATRP reaction proceeds.[40] This deviation can be

explained by considering that at high levels of monomer consumption the rate of propagation will slow down excessively and end group functionalities can be also lost.[18]

**Termination.** The termination process in SI-ATRP is inevitable due to the nature of the radicals. Mainly there are two ways of possible termination on flat surfaces. The first involves disproportionation of two surface radicals or two solution radicals or a surface and a solution radical, when a "sacrificial" initiator is present in the solution. On the contrary, when no free initiator is employed, termination can only occur between two surface radicals. Figure 1.10 (left) illustrates the possible termination pathways involved in SI-ATRPs on flat surfaces. Since the free chains grown in the solution mixture are mobile, the termination between a surface radical and a solution radical or two solution radicals can occur easily. On the other hand, termination between two randomly activated surface radicals is more unlikely.[41]

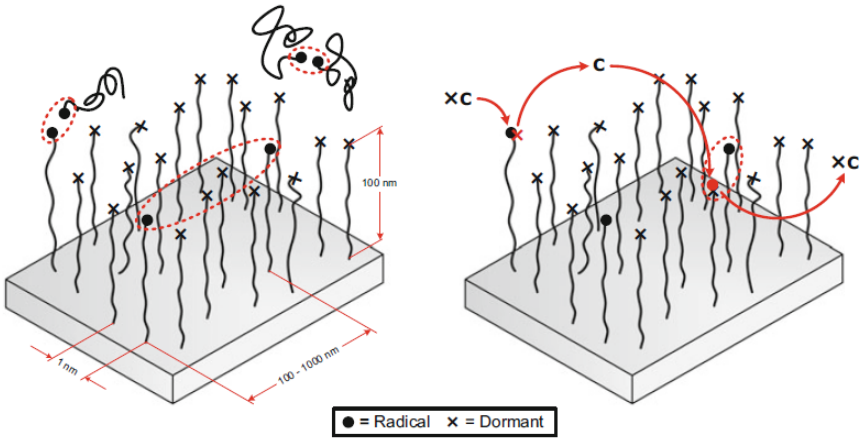


**Figure 1.10.** Left: Possible pathways for termination in SI-ATRP on flat surfaces. Right: Migration effect of surface radicals through activation/deactivation in SI-ATRP and subsequent termination between surface radicals.[41]

Figure 1.10 (Right) shows a schematic illustration of simulation studies of a SI-ATRP from a flat surface and the plausible occurrence of two surface radicals' termination. The film thickness is 100 nm, the grafting density is 0.3 polymer chains/nm$^2$ and the average distance of the grafted chains is 1.83 nm, values that correspond to typical experimentally obtained polymer brushes in the literature. The radical concentration is $3\times10^{-6}$ chains/nm$^2$ with an average distance of two active radicals at 577 nm. In the polymer brush, the grafted polymer chains are crowded, however crowding does not lead to termination on the surface as it is believed. The polymer chains are grafted from

the one end to the surface, thus cannot diffuse freely compared to those in solution, with the crowding further limiting their movement. The average distance between two radicals is 577 nm which renders impossible the direct bimolecular chain termination. Then termination can only occur when the catalyst activates a dormant specie in close proximity to an active radical, and the radicals would instantly terminate as described by the "migration effect".[37a, 41] For ATRP, the constant ratio of the concentrations of activator and deactivator catalyst system is expected to address a constant polymerization rate, since the low number of polymer chains grown in solution do not affect the activator/deactivator ratio throughout the polymerization mixture. Nevertheless, in SI-ATRP an experimental decrease in the growth rate is observed with the increase of the catalyst concentration. For this reason, the termination rate constant should be proportional to the catalyst concentration, due to the fact that higher amounts of catalyst can result in a higher possibility for termination.

In conclusion, higher rates of polymerization result in more termination reactions and thus lower film thicknesses with time, whereas low rates of polymerization result in lower concentrations of active radicals present at the same time and thus lower possibility of termination but non-reasonable polymerization times. So, there is an optimal rate of polymerization, which depends on multiple parameters, such as the solvent quality, catalyst type and ratio of the activator to deactivator, for which higher polymer film thicknesses are obtained at reasonable times.

**Materials.** As mentioned above, SI-ATRP can be applied to various modified substrates, both organic and inorganic, with flat, concave or convex surfaces. The selection of the surface geometry depends on the targeted application, nevertheless, the different geometries may affect differently the effectiveness of the SI-ATRP process. For flat surfaces, the amount of initiator is profoundly low, therefore the molecular weight and the polydispersity of the polymer grown from the surface cannot be directly evaluated by SEC characterization. Moreover, for concave surfaces, the control over the molecular weight and polydispersity might be compromised, due to confinement effects (steric hindrance) between the growing polymer chains. Therefore, the selection of the polymerization conditions in these systems is crucial. Finally, convex systems, provide a large amount of initiator for further characterization, however they can lead to macroscopic gelation, as predicted by Flory's gelation theory.[42] In the next

paragraphs, the theory and the architecture of polymer brushes grown from flat substrates, which is the focus of the present thesis, are described.[20]

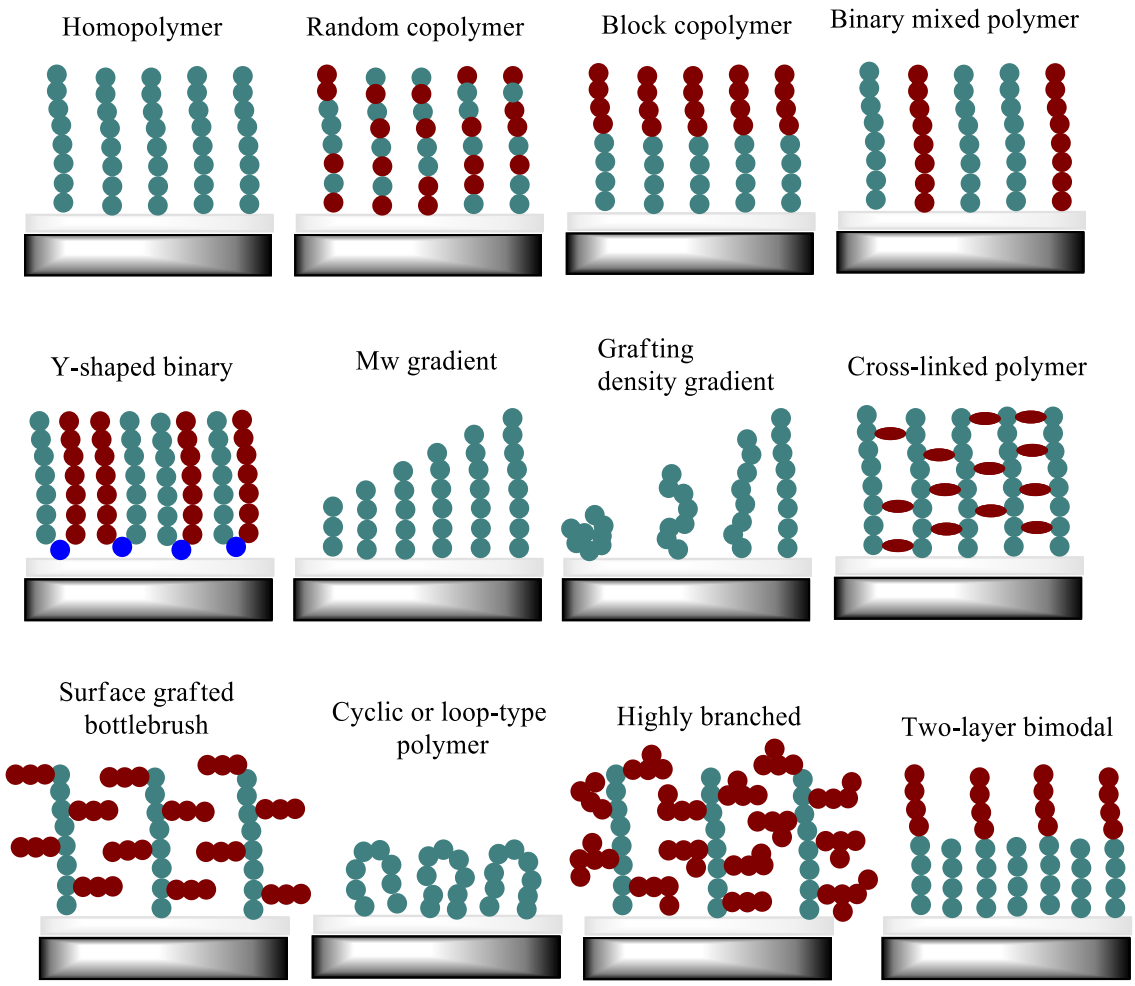


**Figure 1.11.** Schematic illustration of the different polymer brush architectures obtained by SI-CRPs. (a) homopolymer brushes, (b) random copolymer brushes, (c) block copolymer brushes, (d) binary mixed polymer brushes, (e) Y-shaped mixed copolymer brushes, (f) molecular weight gradient polymer brushes, (g) grafting density gradient polymer brushes, (h) cross-linked brushes, (i) surface grafted bottlebrush polymers, (j) cyclic or loop-type polymer brushes, (k) highly branched polymer brushes and (l) two-layer bimodal polymer brushes.[43]

### 1.1.4 Polymer brush architecture

A variety of polymer brush architectures with controlled composition, topology and functionality can be attained by the SI-ATRP method. In terms of their chemical

compositions, polymer brushes are divided into homopolymer, random- and block-copolymer, mixed polymer brushes and more sophisticated architectures such as gradient, y-shaped and (hyper)branched brushes. These examples of polymer brushes can be obtained by SI-ATRP or a contribution of several SI-CRP techniques. Figure 1.11 shows a schematic illustration of some examples of architectures of polymer brushes. Differences in architecture promote a better control of surface coverage, provide better access to certain functionalities and enable the formation of structured surfaces. Selected examples will be discussed in the following paragraphs.

#### 1.1.4.1 Homopolymer brushes

The most common architecture constitutes the end-anchored homopolymer chains, comprising one type of monomer repeat unit. The homopolymer brushes have been widely used in a plethora of scientific and technological fields. These systems can be further divided into neutral and charged polymer brushes. Figure 1.12 depicts the most commonly utilized chemical structures of polymer brushes for various applications based on (meth)acrylates and styrenes. Typically, neutral polymer brushes are based on hydrophilic polymers such as poly(2-hydroxyethyl methacrylate) (PHEMA), poly((polyethyleneglycol) methacrylate) (PPEGMA), poly(N-isopropylacrylamide) (PNIPAAm) and polyacrylamide (PAAm), nevertheless there are also many examples of hydrophobic polymer brushes based on PMMA, PS and PGMA, that give their distinct properties to the surface on which they are tethered, for use in several applications.

Charged homopolymer or polyelectrolyte (PEL) brushes have different properties compared to neutral brushes, and can undergo changes in their swelling and contraction in response to changes in the solution pH or ionic strength, rendering them excellent candidates for smart surfaces. PEL brushes consist of polymer chains containing ionizable groups along their backbone. The charge density of a polymer chain in a polar solvent depends on the type of polymer and the degree of dissociation of the ionizable groups. Based on the ionization constant of the polymer chains, PEL brushes are divided into (a) “strong” PEL brushes and (B) “weak” PEL brushes.[44]

Weak PEL brushes do not have permanent charges and the pH or ionic strength changes of their surrounding can tune their charge ratio and thus control their properties. Weak

polyanionic brushes accept protons at low pH and release them at neutral and high pH values when they become negatively charged. Weak polycationic brushes are deprotonated at high pH and become positively charged at neutral and low pH values. The structure and the properties of such polymer layers are dominated by electrostatic interactions. Due to the electrostatic interactions the polymer segments are strongly stretched and exhibit physical properties which are very different compared to neutral polymer brushes.[44] Poly(methacrylic acid) (PMAA) and poly(2-(dimethylamino)ethyl methacrylate) (PDMAEMA) brushes are the most widely studied weak PEL brushes. To understand the response of charged brushes to changes in the solution pH, the apparent dissociation constant, p$K_a$ of the polymer functional groups is essential.

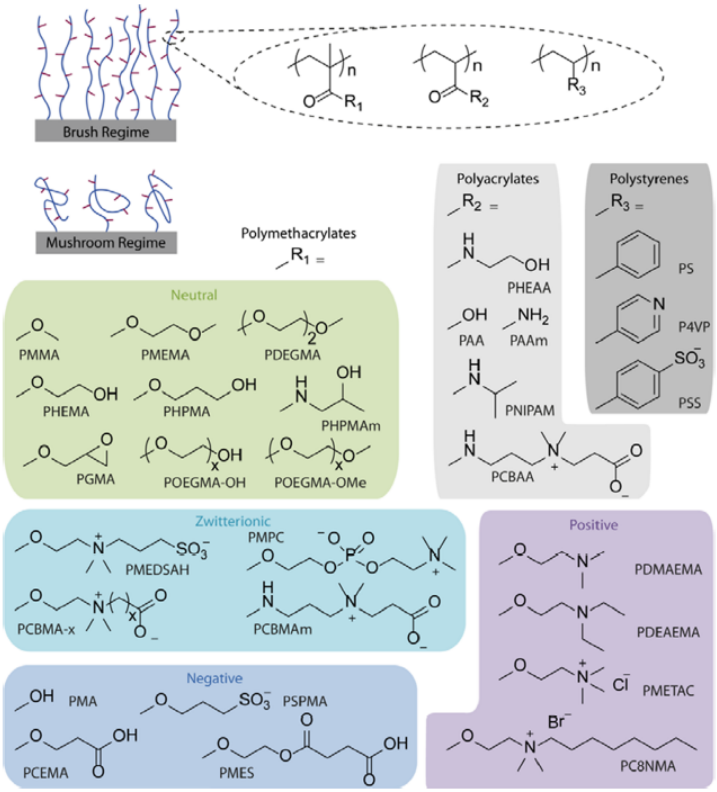


**Figure 1.12.** Chemical structures of the most commonly used end-grafted neutral and charged homopolymers.[45]

On the other hand, in strong PEL brushes, permanent charges are associated with strong acid or base groups, the degree of dissociation is not affected by the environment and as a consequence these brushes are insensitive to the local pH. The most commonly reported strong polybasic brush is poly(2-(methacrylolyloxy)ethyltrimethylammonium chloride) (PMETAC) (which is related to the substituted form of PDMAEMA with

methyl chloride), poly(methyl-4-vinylpyridinium) (PMePVP) and poly(vinylbenzyltrimethylammonium chloride) (PVBTMAC).

**Polyzwitterionic brushes.** Polyzwitterionic brushes is a type of end-grafted polyampholyte chains possessing both anionic and cationic groups within the one side group, and exhibits an anti-polyelectrolyte effect, due to attractive interchain/intrachain dipole-dipole interactions.[46] Therefore, polyzwitterionic brushes are usually weakly hydrated and have collapsed conformation at low salt concentrations, nevertheless they are strongly hydrated and adopt an extended conformation at high salt concentrations.[47] The most commonly reported brushes are poly(sulfo-betaine methacrylate) (PSBMA), poly(carboxy-betaine methacrylate) (PCBMA) and poly(phosphorylcholine methacrylate) (PPMC), which are mainly employed as coatings with ultra-low levels of hydrophilicity, fouling adsorption, friction, adhesion and so forth.

In general, homopolymer brushes possess interfacial physicochemical characteristics, that are determined by their chemical composition, grafting density, film thickness and solubility in the surrounding medium. More complex architectures give the opportunity of exploiting technologically relevant properties such as mechanical and thermal stability, viscoelasticity and low friction.

### 1.1.4.2 Copolymer brushes

#### 1.1.4.2.1 Block copolymer brushes

Compared to homopolymer brushes, which have a uniform chemical composition, the block copolymer brushes comprise different blocks which may present distinctive chemical properties. Block copolymer brushes were introduced to confirm the "living" character of the SI-CRP polymerization techniques on various substrates. Husseman et al. synthesized polystyrene-*b*-poly(styrene-co-methyl methacrylate) (PS-*b*-(PS-*co*-PMMA)) brushes on silica substrates using NMP.[48] The preparation of block copolymer brushes using SI-ATRP via the grafting-from technique was first accomplished by growing polystyrene-*b*-poly(*t*-butyl acrylate) (PS-*b*-P*t*BA) chains from silicon substrates.[35] Hydrolysis of these diblock copolymer brushes led to polystyrene-*b*-polyacrylic acid (PS-*b*-PAA) brushes. Since then, a vast number of researchers have

been using SI-ATRP for the preparation of diblock copolymer brushes via sequential block polymerization. Moreover, in order to evaluate the efficient sustain of the ATRP initiator at the end of the grafted polymer chains after SI-ATRP, Kim et al. prepared triblock copolymer brushes comprising poly(methyl acrylate) (PMA), PMMA and PHEMA.[49] Multi-block copolymer brushes can be prepared via SI-ATRP, nevertheless, the monomer reactivity and structure and the nature of the surface-attached initiator affect significantly this feasibility.[50]

Depending on the nature of the different blocks, responsive surface properties to several external stimuli can be obtained (see paragraph 1.2.1).

#### 1.1.4.2.2 Random copolymer brushes

Random copolymer brushes are assemblies of end-grafted polymer chains consisting of two or more monomer repeat units, which are randomly distributed along the anchored polymer chains and can be easily prepared by an one-step SI-CRP of a mixture of monomers.[51] Random copolymers combine the properties of each singular homopolymer, and are mainly prepared to tune the surface properties of materials and to induce responsiveness to external stimuli. However, due to the fact that, monomers often have different reactivities, the composition of the copolymer brushes may not be identical to that of the monomer feed. Ignatova et al. have prepared various random copolymer brushes on stainless steel substrates via SI-ATRP.[52] While most reported random copolymer brushes consist of linear polymer chains, more complex architectures, such as branched and cross-linked polymer brushes have been also prepared by SI-CRP techniques.[31]

### 1.1.4.3 Mixed homopolymer brushes

The profound interest on mixed brushes during the last decade has arisen by the stimuli-responsive nature of these surfaces. In general, mixed brushes comprise incompatible homopolymer chains that are randomly distributed along the polymer surface, thus the topography and morphology can be easily controlled though polymer-solvent interactions. Based on the SAM pre-functionalization of the surface, the mixed

homopolymer brushes can be divided into (a) binary mixed brushes and (b) Y-shaped binary mixed brushes.

#### 1.1.4.3.1 Mixed SAMs

Aside from single molecule type SAMs, that provide organic/inorganic hybrid initiators for the SI-ATRP of homopolymer and block copolymer brushes, mixed SAMs have been utilized to incorporate two types of molecules in one SAM, but typically the one type would preclude the other through steric hindrance. Feng et al. managed to prepare mixed SAMs by two methods: (a) co-adsorption and the (b) stepwise method.

Co-adsorption is the easiest procedure to obtain mixed SAMs, involving a mixture of the two molecules in a good solvent and immersion of the surfaces. Different affinities of the molecular head/anchor groups usually result to undesired mixed SAMs, therefore a "trial and error" procedure is required to address the concentration and molar ratios between the two molecules of the mixture.[53] For example, mixed SAMs of octyl- and dodecyl-tri-chlorosilane were prepared easily. However, the preparation of mixed SAMs using a tri-chlorosilane and a tri-ethoxysilane by co-adhesion was shown to be impossible, due to the fact that the faster binding of the tri-chlorosilane acted as a barrier for the assembly of the tri-ethoxysilanes. The stepwise method was used to evade this problem, by immersing a clean substrate in a solution of a first SAM for a predetermined length of time, followed by the immersion in a solution of a different molecule, which filled the gaps of the first monolayer deposition.[53-54] It was proposed that the larger head/anchor group should be utilized first as the smaller steric hindrance would allow the second molecules to fill the gaps that remained after the adsorption of the first larger molecule.

#### 1.1.4.3.2 Binary mixed homopolymer brushes

Mixed polymer brushes consist of two or more different homopolymers anchored randomly on a surface. Ionov et al. utilized the "grafting-to" technique to prepare binary mixed polymer brushes and study the effect of polymer composition and solvent selectivity for the two homopolymer chains.[55]

Studies on grafted-from mixed brushes began in 1999, when Sidorenko et al. synthesized binary mixed polymer brushes of PS and P2VP by a two-step conventional

free radical polymerization process.[56] Since then, a plethora of SI-CRP techniques have been employed for the synthesis and characterization of mixed brushes. Zhao was the first to prepare binary mixed brushes of PMMA/PS by the "grafting-from" method, using mixed SAMs of ATRP and NMP initiators.[57] In addition to mixed SAMs by solvent deposition, PMMA/PS brushes have been also synthesized by vapor deposition of an ATRP initiator followed by the vapor deposition of an NMP initiator. Nevertheless, phase separation of the initiator molecules is often observed, when the surface is modified with a mixture of orthogonal initiators,[58] which results to islands of one type of homopolymer chains, rather than a mixed polymer brush. Wang et al., prepared binary mixed PNIPAAm/PHEMA brushes via a two-step SI-ATRP. First SI-ATRP of NIPAAm was carried out from a spatially uniform initiator SAM on planar gold substrates, followed by electrochemical etching to partially remove the PNIPAM chains and backfilling with a ATRP initiator to grow the second PHEMA chains by SI-ATRP.[59] In 2011, Matyjaszewski et al. prepared binary mixed poly(butyl a acrylate)/poly(acrylic acid) PBA/PAA brushes via a two-step reverse ATRP, which involved a diazo-initiator on planar silicon surfaces.[60] Finally, Ionov et al. prepared mixed PS/PAA brushes via sequential SI-AGET-ATRP using a dehalogenation step between the polymerization procedures.[61]

#### 1.1.4.3.3 Y-shaped binary mixed brushes

In some cases, mixed initiators may not ensure uniform and well-distributed layers of the initiators if the one is preferably adsorbed onto the surface. This can result to the formation of islands of one type of the polymer brush, after the SI-CRP. To address this problem and avoid the phase separation of the mixed orthogonal initiators, one approach is to use a Y-shaped molecule with two different homopolymer chains linked to a focal point that can react with a site on the surface via "grafting-to".[62]

Zhao and He synthesized Y-shaped binary mixed brushes simply by employing a difunctional ATRP/NMP silane initiator (Y-silane), for the SI-CRP of mixed PS/PMMA brushes.[63] Nevertheless, the synthesis of the binary Y-initiator required a multiple-step protocol with low yield. Lately, other binary Y-silane initiators for ATRP/NMP and ATRP/RAFT brushes have been studied for the successful growth of Y-shaped binary mixed brushes.[64]

Mixed brushes are still under development and the ability to promptly control the phase separation of these systems has been mostly realized on curved surfaces. Thus, there is an unmet need to control these systems on planar surfaces.

#### 1.1.4.4 Other Complex Architectures

In addition to the linear polymer brushes, described above, other more complex architectures can be prepared by the SI-ATRP technique e.g. hyper-branched, bottle-brush, loop-type polymer brushes, etc. (see Figure 1.11). Details on these architectures are beyond the scope of this thesis and have been given in the remarkable reviews of Klok et al.[31, 43]

In conclusion, SI-ATRP constitutes a robust, versatile and reliable technique for the synthesis of polymer brushes. The good control over the brush composition and architecture, the reduced sensitivity to oxygen, moisture and impurities, the large variety of potential monomers, the commercial availability of catalysts and initiators and the facile immobilization of the latter on various substrates, constitute the main reasons for the use of SI-ATRP in the synthesis of polymer brushes.

### 1.1.5 Post-polymerization modification reactions

Post-polymerization modification (PPM) is a significant tool to introduce functionalities to polymer brushes which cannot be attained by SI-CRP techniques. There are several modifications that can be performed depended on the desired functional group and the application such as: (a) PPM to obtain ester side chain functionalized polymer brushes, (b) PPM to obtain acid side chain functionalized polymer brushes, (c) PPM of carboxylic acid side-chain functionalized polymer brushes, (d) PPM to obtain quaternized polymer brushes, (e) PPM of hydroxyl-side chain functionalized polymer brushes, (f) PPM of poly(glycidyl methacrylate) brushes, (g) PPM of other side-chain functional polymer brushes, and (h) selective chain-end PPM of the polymer brushes.[43]

The quaternization of PDMAEMA brushes has been widely explored mostly with the utilization of methyl iodide to form pendant quaternary ammonium salt moieties. Quaternization reactions have been employed to obtain polymer brushes with antibacterial properties. The cross-linking of the PDMAEMA brushes was achieved

using di-iodides. Finally, PQDMAEMA brushes have been shown (a) to possess tunable wettability based on the counterions, with nitrate counterions providing more hydrophilic brushes, whereas $Tf_2N^-$ counterions provide more hydrophobic brushes, (b) to bind femtomolar concentrations of DNA, (c) to resist protein adsorption and platelet adhesion.[43]

### 1.1.6 Theory of Polymer brushes

Theoretical descriptions can be used to interpret experimental observations and tailor the polymer brush properties. A plethora of theoretical mathematical models have been developed for the prediction of the conformation of the end-grafted polymer chains under different conditions of temperature, pressure, pH, solvent type and ionic strength. The following section describes some of these theoretical models.

#### 1.1.6.1 Neutral brushes

An analytical theoretical description of polymer brushes on planar surfaces was first introduced by Alexander.[65]

At very low grafting densities, the conformation that the adsorbed polymer chains adapt resembles more or less their random coil conformation. Nevertheless, at high grafting densities, the chains are stretched to avoid overlapping with neighboring chains and adopt a brush-type conformation. The distance between the anchoring points is lower than the polymer stretching distance, and induces dominant chain-chain interactions. Implementing the "Flory argument", Alexander derived the conformation of the brushes to be determined by the energy balance between the elastic free energy of the stretched polymer chain, $F_{el}$ and the energy of interaction between statistical segments (excluded volume repulsion), $F_{int}$ (see Equation 1.6).

$$F = F_{el} + F_{int} \tag{1.6}$$

The $F_{el}$ of ideal polymer chains increases quadratically with their end-to-end distance, which is represented by the brush thickness, h. The excluded volume stems from uniformly distributed monomer segments and is proportional to their volume fraction. The total free energy, F, of a single polymer chain in the brush can be transformed to:

$$F = k_B T \left( \frac{3h^2}{2Na^2} + \frac{wN^2\sigma}{h} \right) \tag{1.7}$$

Where, N is the degree of polymerization, w is the excluded volume, α is the monomer diameter and σ is the grafting density.

In a good solvent, the monomer-monomer interactions are governed by the monomer-solvent interactions and the thickness of the polymer brush can be obtained by minimizing the total free energy as follows:

$$h \sim N\alpha^{4/3}\sigma^{1/3} \tag{1.8}$$

Similarly, de Gennes addressed a simple scaling analysis, in which the polymer chain can be divided into a series of "blobs", and the steric interactions between the "blobs" determine the conformation of the brush. The analysis led to the correlation length of polymer chains in the brush to be the distance between anchoring points equal to $\sigma^{-1/2}$ and is similar to that by Alexander.[66] Based on these theories, the Alexander-de Gennes (AG) theory was described, which is the basic model for describing the properties of polymer brushes.

In a poor solvent, the interactions between monomer repeat units are attractive and thus the end-grafted chains are collapsed. In contrast to a free random walk polymer, for which the radius of gyration is scaling as $R_g \sim N^{3/5}$ in a good solvent and $R_g \sim N^{1/2}$ in a bad solvent, the thickness of the polymer brush is scaling linearly with N, implying a deformation of the densely-grafted polymer chains. In addition, the thickness of polymer brushes in poor and theta solvents can be calculated by equations 1.9 and 1.10, in which the power law dependence of the thickness, *v*, increases from 1/3 to 1/2 and 1, respectively.

$$h \sim N\sigma^{1/2} \tag{1.9}$$

$$h \sim N\sigma \tag{1.10}$$

On the contrary, the dependence on the molecular weight remains constant at N.

Other sophisticated models such as numerical and analytical self-consistent field (SCF) theories have been used to elucidate the structure of polymer brushes with quite different results.[67] A more accurate description of a polymer brush was introduced by Milner et al. based on the idea that the free chain-ends can be allocated anywhere within the brush.[3a, 67b, 68] The self-consistent field for equal length is a parabolic potential and

not stepwise as predicted by the AG theory, thus it is called the "parabolic field" approximation.

From the above, the key elements that define the conformation and features of polymer brushes is the grafting density and the surrounding medium. The grafting density is calculated based on the AG theory, which relates the dry thickness of the polymer brush with the distance between two anchoring points. If the grafting density is greater than the overlap density, steric interactions force the polymer chains into a stretched, extended conformation to relieve crowding locally. The balance between osmotic pressure, due to contact between segments, and the entropic elasticity, opposing the polymer stretching, defines the extension of a polymer brush.[66]

The effect of grafting density can be more pronounced due to solvent interactions, with highly swollen and collapsed states of the polymer brushes obtained after immersion in good and bad solvents, respectively. In the dry state, polymer brushes are in the collapsed state and behave in a similar way as in a poor solvent. The polymer brush conformation can be divided into four different regimes: (a) mushroom (b) pancake, (b) semi-dilute or moderate brush and (c) concentrated or high-density brush regime.[4] Figure 1.13a illustrates the scaling law and conformation of neutral brushes at different grafting densities and solvent conditions. In many cases, for simplicity, the term "polymer brush" is used for all end- grafted polymer chains, nevertheless it should be stressed that the term applies only under specific conditions when the behavior of the grafted polymer layer is defined by strong interactions between densely-grafted polymer chains.

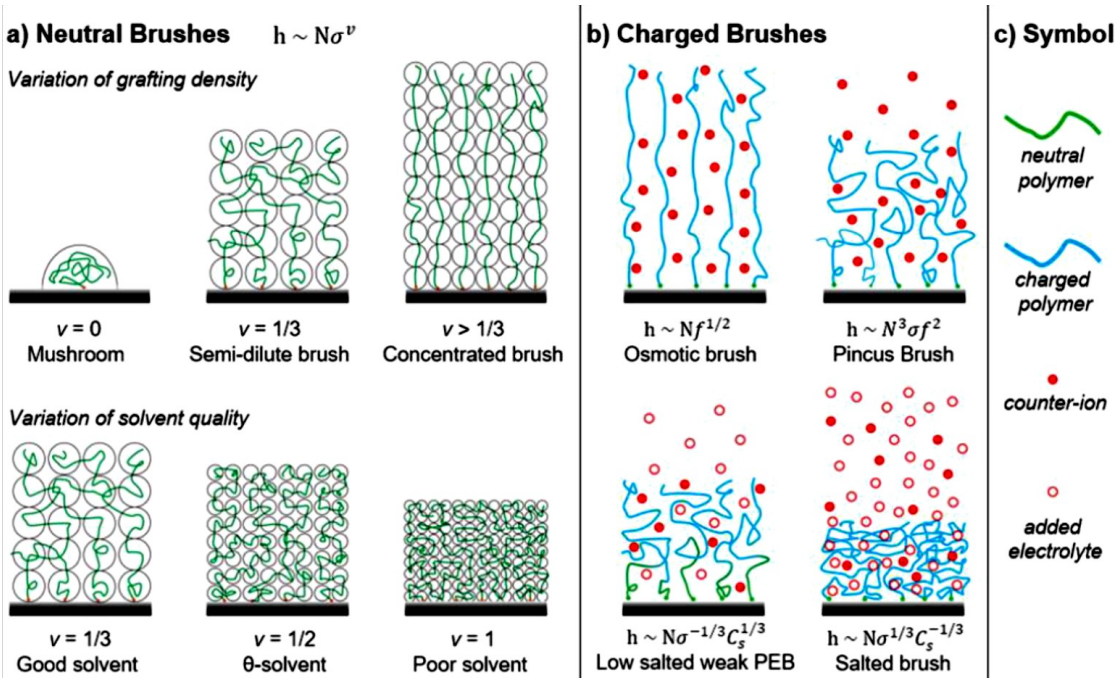


**Figure 1.13.** Schematic representation of the various regimes of (a) neutral and (b) charged polymer brushes, and their scaling laws depending on the grafting density and solvent quality. (c) Symbols used in the scheme.[69]

### 1.1.6.2 Charged brushes

In comparison to neutral brushes, charged brushes have different properties and additional considerations need to be considered. The complexity of the PEL brush structure increases, due to interactions by the presence of the charges, not only owing to the long-range electrostatic interactions between the charged groups, but also due to the counterions in solution.[70] These interactions are highly depended on changes of the surrounding environment, such as the ionic strength, pH value and the presence of counterions. In solution, polyelectrolytes carry charges that are screened by oppositively charged ions, namely counterions. The most commonly used surrounding medium is an electrolyte solution that alters the osmotic pressure and interactions between the polymer ions. Figure 1.13b illustrates the scaling laws and conformation of charged brushes of different grafting densities and at different solvent conditions.

Self-consistent field theories, which incorporate Poisson-Boltzmann equations, have described PEL brushes and reveal that the counterions are gathered in the PEL brush in order to minimize the free energy of the system, rendering the overall PEL brush

electroneutral. The electroneutrality plays a significant role in the theory of PEL brushes, since unscreened long-ranged electrostatic interactions do not exist.

**Strong PEL brushes.** A theoretical description of the behavior of strong PEL brushes on surfaces was first introduced by Pincus,[70a] and is expressed in equation 1.6, using a simple scaling model assuming a fraction of charged monomer units, $f$ that are always neutralized by counterions either inside the brush, comprising the "osmotic brush" regime or outside the brush entering the "Pincus brush" regime.

The wet thickness of a strong PEL brush is proportional to the molecular weight and the square root of the fraction of charged monomer repeat units, $f$, and independent of the grafting density.[69] The thickness scaling is caused by the balance between osmotic pressure and chain stretching and these systems are called "osmotic brushes", described by equation 1.11.

$$h \sim N f^{1/2} \tag{1.11}$$

The Pincus brush model was developed for low grafting density/extent of dissociation brushes, whose counterion cloud perturbs the brush region surroundings and cannot maintain its charge neutrality. Thus, under such conditions the osmotic pressure is weak due to the fact that the strong charge repulsion is dominant. The wet thickness is proportional to the grafting density, the molecular weight and the square root of the fraction of charged monomers, $f$ (Equation 1.12).

$$h \sim N^3 \sigma f^{1/2} \tag{1.12}$$

Lego et al. confirmed experimentally the Pincus brush theory using PAA brushes.[71]

**Weak PEL brushes.** Compared to strong PEL brushes, in weak PEL brushes the charges can be affected by the environmental conditions. i.e. pH, and thus the swelling of the brush varies. For example, increase of the pH results in the swelling of weak polyacid brushes, whereas weak polybasic brushes extent with the decrease of the pH. Studies on PMAA and PAA brushes have shown that the behavior of the wet brush thickness *vs* the grafting density is similar to neutral brushes with $\nu$ = 1/3, which opposes the mean-field theory prediction.[72] It was suggested that the similar behavior may originate by the low dissociation level for the polymers in brush, as predicted by

theory, which also contributes to an inhomogeneous ionization along the brush as observed experimentally by Ober et al.[73]

**Presence of salt ions.** The addition of electrolytes to both strong and weak PEL brushes transforms them to the so-called "salted" brushes, in which the charges are screened. The transformation occurs when the concentration of the electrolyte in the solution, $C_s$, is equal to its concentration inside the PEL brush. The osmotic pressure decreases by the entrance of the electrolyte ions in the brush and the scaling law of a salted brush can be described by the equation 1.13.

$$h \sim N C_s^{-1/3} \sigma^{1/3} \tag{1.13}$$

At high salt concentrations ($C_s$), the electrostatic interactions are vastly screened, the osmotic pressure within the system is reduced and the PEL brush behaves as a neutral brush, for which further increase of the electrolyte concentration does not affect the thickness of the brush.

Nevertheless, at low electrolyte concentrations, weak PEL brushes behave differently, with the thickness scaling being proportional to the added electrolyte, since the degree of dissociation increases with it. Zhulina et al. proposed the scaling law (equation 1.14) to describe the effect of dissociation.[72c]

$$h \sim N C_s^{1/3} \sigma^{-1/3} \tag{1.14}$$

At low electrolyte concentration, the sensitivity of the swelling change of weak PEL brushes decreases with the decrease of the grafting density. As the electrolyte concentration increases, charge screening becomes important and dominates at $C_{s,max}$, when the weak PEL brush reaches its maximum thickness.

## 1.2 Smart polymer brush surfaces and key applications

Smart coatings are in general all coatings that are capable of triggering a macroscopic response upon exposure to a stimulus, owing to the incorporation of stimiuli-responsive entities within the coatings. The modification of surfaces with polymer brushes is employed to tailor the surface properties such as hydrophilicity/phobicity, biocompatibility, fouling, antimicrobial properties, adhesion, adsorption, friction and corrosion resistance.[74] These responsive properties provide the basis for the development of "smart" surfaces. In particular, smart polymer brushes are

advantageous, due to their chemical versatility, which permits tuning the interfacial properties by a certain trigger such as temperature, pH, mechanical stress, solvent type, external electric field or light.[75]

The following paragraphs will focus on stimuli-responsive polymer brushes and on the applications of polymer surfaces with emphasis on their wettability, lubrication and antimicrobial properties.[76]

### 1.2.1 Stimuli-responsive brush surfaces

Relying on the chemical composition and architecture of the end-anchored polymer chains, environmental parameters such as solvent quality, pH, ionic strength, temperature, electromagnetic fields and the presence of specific electrolytes or molecules can affect the conformation and structure of polymer brushes and therefore introduce a responsive character on these systems, with tunable surface properties such as wettability, biocompatibility, biofouling, antimicrobial properties, adhesion, adsorption, corrosion resistance, lubrication and friction.[20, 74b, 74c] Three types of "smart" polymer brushes are typically utilized in designing stimuli-responsive surfaces (Figure 1.14). The responsive nature of homopolymer brushes stems from the property changes (swollen/collapsed) of the grafted polymer chains. Diblock copolymer brushes of two unlike polymer blocks, under external stimuli, can undergo phase segregation to lower the surface energy, which leads to the switching of the properties between the two polymers or to some intermediated state. Finally, mixed homopolymer brushes, comprising two different homopolymers, undergo phase segregation upon the application of an external stimulus, which determines their surface properties.[77] Some examples of the responsiveness of polymer brushes are given in the following, sorted by the type of stimulus which induces the responsive behavior of the brush.

#### 1.2.1.1 Solvent-induced responsiveness.

The solvent quality can profoundly affect the conformation of the polymer brush. In the presence of a good solvent, a typical behavior is that in which the grafted polymer chains are stretched away from the surface to enhance the solvent-polymer interactions, whereas, in a poor solvent the polymer chains collapse to these interactions.

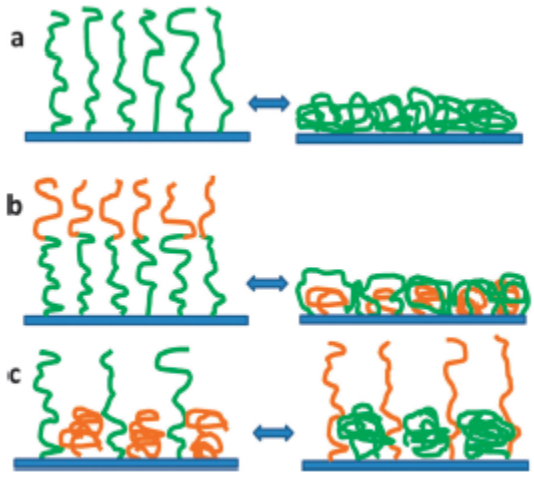


**Figure 1.14.** Schematic illustration of conformational changes of (a) homopolymer brushes, (b) diblock copolymer brushes and (c) mixed homopolymer brushes.[78]

**Homopolymer brushes.** The responsive behavior of the single-component homopolymer brushes are referred to changes of free energy of the brush in its environment due to the change of the solvent quality. A decrease in the layer thickness and reduction of the surface roughness was achieved upon immersion of PMMA brushes in water which is a poor solvent for the densely grafted homopolymer chains. Transition from the collapsed state to the swollen state was introduced by soaking the polymer brushes in tetrahydrofuran (THF), which is a good solvent.[79] Similar swelling and collapsed behavior was observed when PMMA brushes were exposed to various good (i.e. benzene, ethyl acetate) and poor (acetonitrile, isopropanol) solvents or solvent vapors.[80] A characteristic example of the application of solvent responsive homopolymer brushes was demonstrated for PBA or PAA brushes grafted on carbon nanotubes for gas sensors, with high sensitivities towards acetone, chloroform, toluene and methanol, organic vapors.[81] Humidity is considered as a solvent-responsive parameter for the responsiveness of hydrophilic polymer brushes. Characteristic examples are PDMAEMA or poly(4-vinyl pyridine) (P4VP) homopolymer brushes and their quaternized analogues, which are highly hydrophilic and the relative humidity has been shown to highly affect their degree of swelling.[82]

Solvent-responsive polymer brushes are primarily comprised of (a) diblock copolymer brushes or (b) mixed homopolymer brushes, which undergo solvent-induced phase segregation of the polymer chains and thus a reversible tuning of the surface properties

can be realized. This behavior is based on the morphological brush changes when the polymer brushes are immersed in a solvent with special affinity for one of the polymers.[83]

**Diblock copolymer brushes.** The solvent-responsive behavior of diblock copolymer brushes have been profoundly investigated and found that is more complicated than that of the homopolymer brushes. Figure 1.15a shows the schematic illustration of a solvent-responsive diblock copolymer brush. When the diblock brush is immersed in solvent B, that is a good solvent for both unlike polymer blocks of the end-grafted polymer chains, the system will be fully stretched. Nevertheless, after immersion in solvent A, that is poor solvent for the outer bocks and good solvent for the inner blocks, a simultaneous swelling of the inner blocks and a collapse of the outer blocks will result to penetration of the latter into the polymer phase towards the substrate in order to reduce the contact with the poor solvent. Micro- or nano-sized surface patterns may arise based on the interaction parameter of the two segments. Zhao et al. showed for the first time, via water contact angle (WCA) measurements and atomic force microscopy (AFM) that the selective collapse and swelling of PS-*b*-PMMA and PS-*b*-PMA blocks produced variable and switchable surface topologies. They observed that after treatment with different solvents, the two systems revealed either an unusual morphology or regular structure, which was attributed to the Flory-Huggins interaction parameter between PS and PMMA opposed to PS and PMA.[84] Baum and Brittain studied the rearrangement of PS-*b*-poly(N,N'-dimethylacrylamide) (PDMA) and PDMA-b-PMMA brushes upon exposure to selective solvents.[14b] The reversible behavior was examined by water contact angle measurements after treatment with the selective solvents and they found that samples had incomplete rearrangement as the contact angles achieved after treatment did not match with the characteristic contact angles of their PS or PDMA or PMMA analogues. Also, Boyes et al. employed AFM measurements on PS-*b*-PMMA brushes to demonstrate the morphological responsive behavior of the brushes after immersion in various selective solvents.[85] They found that these brushes reversibly rearrange upon treatment with selective solvents that result in the formation of unusual surface morphologies of either pinned micelles or dimple or ripple worm-like structures. Granville et al. studied the behavior of semi fluorinated diblock copolymer brushes treated with a good and a poor fluorinated solvent.[86] It was found that solvent-responsive rearrangements of the two blocks resulted in tuning of

the wetting properties of the diblock brushes, with the fluorine atoms playing some distinct role in their nearly full rearrangement. The AFM images of the diblock copolymer brushes upon selective solvent treatment suggested that the materials did not undergo the traditional rearrangement mechanism of PS-*b*-PMMA to form pinned micelles on the surface. The behavior of PS-*b*-PMMA brushes have been also shown to be affected by parameters such as the nature of the solvent used to wash the films and the annealing time.[87] Similar studies by different research groups were reported for different amphiphilic diblock copolymer brushes that their systems revealed almost fully reversible block rearrangements.[88]

Moreover, Xu et al. studied the influence of the individual block length on the solvent response of PnBA-*b*-PDMAEMA brushes, which was found to affect the surface responsive properties.[89] The bottom block of PBMA was held constant while the PDMAEMA block had a variable molecular mass. The responsive behavior and rearrangement of the PDMAEMA blocks exposed to water and hexane was monitored with water contact angle measurements, which indicated that shorter blocks of PDMAEMA compared to PBMA were able to fully rearrange in contrast to the thick PDMAEMA layer which suppressed any response from the PBMA block. Gao et al. observed that varying the length of the upper block of poly(oligo(ethylene glycol) methacrylate)-*b*-PMMA brushes resulted in various nanopatterns i.e. spherical aggregates, wormlike aggregates, line patterns, perforated layers and complete covered layers.[90] Yang et al. examined the solvent-responsive behavior of PDMS-*b*-PEG diblock copolymer brushes which exhibited various responses to different solvent treatments. When the samples were treated with selective solvents (water or toluene), the diblock copolymer brushes formed ‘‘onion-like’’ or pinned micelles structures at low grafting densities. When the brushes were treated with good solvents (DMF) for both blocks, the chains were more swollen and stretched to form a smooth surface.[91] One step further was taken by Santer and Ruhe, who utilized PMMA-*b*-PGMA brushes to move nanoobjects. By increasing the inner block length, upon exposure to selective solvents, different topological patterns were generated, e.g. ripple-like, worm-like and spherical, due to the switching of the chemical conformations and changes in the interfacial energy during phase transition. The nanoobjects tended to aggregate into islands during the morphological rearrangements and move along the surface.[88d, 92]

All the above-mentioned studies revealed that the assembly of block copolymer brushes represents a promising approach for designing surfaces with switchable topologies and properties. In addition, block copolymer brushes comprising multiple blocks with each block having distinct chemical properties have been shown to exhibit solvent-responsive properties.[93] An intriguing solvent responsive behavior has been shown for grafted oligomeric amphiphiles of PEG with short perfluorinated end-caps (f-PEGs) at low grafting densities that can be effectively applied as self-cleaning materials.[94]

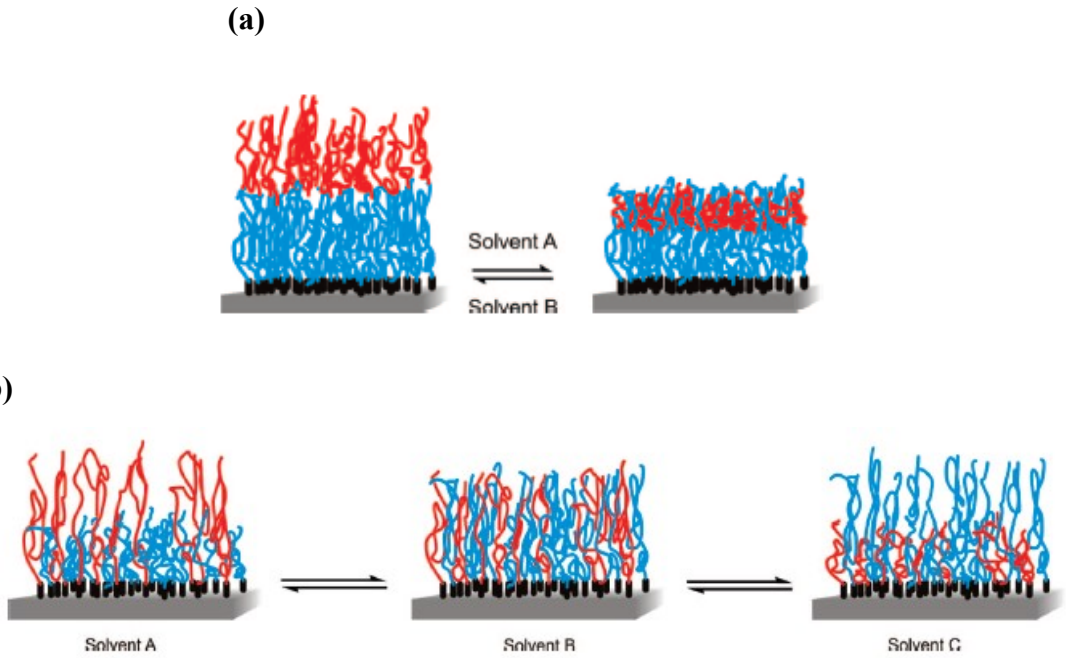


**Figure 1.15.** Structural changes in (A) a diblock copolymer brush upon variations in solvent quality; solvent A is a good solvent for the inner block (blue) but non solvent for the outer block (red), while solvent B is a good solvent for both segments and (B) mixed homopolymer brush solvent responsiveness; solvents A and C are selective solvents for each polymer (red and blue) and solvent B is a non-selective solvent.[31]

**Mixed homopolymer brushes.** The vast interest on mixed polymer brushes in the last decade has arisen due to the profound stimuli-responsive behavior of these films. Figure 1.15b shows a schematic illustration of a solvent-responsive mixed homopolymer brush. The topological and surface energy changes that occur in these systems are attributed to the selective solvation of one of the homopolymer chains anchored to the surface. The selective solvation of the two polymer segments of the mixed brushes can lead to a solvent-induced phase segregation of the brush that may result to reversible switching properties of the surfaces.

The solvent-induced topographical changes of PS/PMMA binary brushes have been studied by Santer et al. using AFM measurements. They found that microdomains are formed upon exposure to a selective solvent, toluene for PS and acetone for the PMMA chains, and possess a memory effect with the ability of the chains to recover to their initial state after repetitive cycles. Another example of solvent-induced switching is provided by Vyas et al., who utilized PS-P2VP and PS-PAA binary brushes that are able to switch between phase-segregated morphologies, that affect the chemical composition of the outer layer of the brush.[95]. The switching progress is controlled by tuning the solvent exposure, i.e. toluene and acidic water. In toluene the PS chains swell and stretch away from the surface, in order to occupy the outer part of the surface, while in the presence of acidic water, the P2VP brushes are solvated and stretch reaching the outermost polymer-solvent interface, overlapping the PS chains that are collapsed toward the substrate-polymer interface. Wang et. al. synthesized Y-shaped PS-PEO brushes on gold substrates to create an amphiphilic mixed brush system with different lateral and vertical microphase morphologies depending on the chain structure and the solvent treatment.[96] Ionov et al. presented a more facile "grafting-from" synthesis via SI-AGET-ATRP, as well as the pronounced switching properties of mixed polymer brushes comprising hydrophobic PS and hydrophilic PAA chains.[61] Lately, Uhlmann et al. synthesized amphiphilic poly((n-hexyl acrylate)-*co*-(4-tertbutylstyrene))-*b*-poly((n-hexylacrylate)-*co*-(4-tertbutylstyrene)-*co*-(N-acryloxy succinimide))-*b*-poly((N,N-dimethylacrylamide), P(nHa-*co*-tBS)-*b*-P(nHa-*co*-tBS-*co*-NAS)-*b*-PDMA triblock copolymer chains that comprise a central anchoring block. These amphiphilic triblocks can form binary mixed brushes on either flat surfaces or rough textile fabric, that can switch their conformations according to external stimuli during washing and laundering.[97]

#### 1.2.1.2 pH/ionic strength-induced responsiveness.

Systems that are sensitive to pH or ionic strength are basically homopolymer, block copolymer or mixed polymer brushes containing ionizable, weak polyacids such as carboxylic acid-functional poly(acrylic acid) (PAA) and PMAA, or weak polybases, such as tertiary amine-functional PDMAEMA and poly(2-(diethylamino)ethyl methacrylate) (PDEAEMA) or poly(4-vinylpyridine) (P4VP). The above mentioned PEL brushes exhibit remarkably high degree of swelling at their fully charged state,

ranging from 400% to 700%, due to the strong intra- and inter-chain repulsive forces from the charges and the associated osmotic pressure.[71, 98] At low ionic strength, the swelling of the PEL brushes is independent of the salt concentration, nevertheless at high ionic strength the swelling decreases with the salt concentration.[98] Yu et al. studied the structural conformation of polystyrene sulfonate (PSS) brushes in the presence of mono-, di- and tri-valent counterions. By altering the surrounding salt environment from monovalent counterions of the PEL chains to trivalent cations, the structure of the brushes changes from an extended conformation to a pinned-micelle structure and is reversed back to an extended structure by increasing the monovalent cation concentration.[99] Strong polybasic PMETAC brushes have been shown to reveal electrolyte responsive behavior, with the swollen state in aqueous solution to be changed to a collapsed stated upon immersion in 1M NaCl aqueous solution and the subsequent reversal of this collapse by exposure to pure water.[100]

The pH-response of weak polybasic brushes such as PDMAEMA is governed by the association and dissociation of protons with the monomer repeat units. Brush charge is high at pH values below the apparent brush p$K_\alpha$ and the polymer chains swell via counterion and solvent uptake. Above the p$K_\alpha$, the brush becomes deprotonated and the system collapses, due to dominant hydrophobic-hydrophobic interactions. The pH-response of PDMAEMA brushes has been well-studied. The p$K_\alpha$ value of the brushes is around 7.0, which renders the brushes desolvated and collapsed at high pH and more extended and swollen at low pH.[101] The same behavior stems for the weak polyacid brushes, however above the p$K_\alpha$ the opposite phenomenon arises and the chains are charged.

Yu and Han studied the responsive behavior of PAA-*b*-P2VP and P2VP-*b*-PAA diblock brushes with different block lengths at various pH regions. In neutral pH, both sets of block brushes possessed similar behavior attributed to electrostatic interactions between the oppositely charged groups.[102] Basic pH conditions showed a small degree of rearrangement, while decreasing the pH to acidic values and increasing the length of the PAA block in the PAA-*b*-P2VP brushes resulted to the looping back of the P2VP segments towards the PAA block. Motornov et al. grafted amino-terminated poly(dimethylsiloxane) (PDMS-$NH_2$) and carboxy-terminated poly(2-vinylpyridine) (P2VP-COOH) onto an epoxy-functionalized electrode surface to create mixed

homopolymer brushes featuring morphological transitions that could be regulated via changes in pH.[103]

#### 1.2.1.3 Temperature-induced responsiveness

Thermo-responsive polymer brushes constitute a category of polymer brushes whose properties can be affected by changes in temperature. The most widespread studied thermo-responsive polymer brushes are poly(N-isopropylacrylamide) (PNiPAAm) brushes, displaying a lower critical solution temperature, LCST, of ~32-33 ºC and undergoing a reversible phase transition in aqueous solution, due to changes in temperature.[104] PNiPAAm chains exhibit a hydrogen bonding network between the amide groups and water molecules. Below the LCST, the polymer brushes are in an extended and swollen conformation, nevertheless increasing the temperature above the LCST, a phase transition into a collapsed morphology is induced, because the hydrogen bonding is disrupting and the water is forced out. The PNiPAAm end-grafted chains do not form aggregates and phase separation, however the conformation transitions from the hydrophilic swollen state to the hydrophobic collapsed state, provides a thermally controlled wettability and thickness.[104] The reversible volume phase transition of PNiPAAm brushes has been thoroughly used in thermo-responsive cell culture media. Other thermo-responsive polymer brushes comprising poly(oligo(ethylene glycol) methacrylate) (POEGMA) or poly(bis(ethylene glycol) methyl ether methacrylate) (PDEGMA) chains have been obtained to allow precise control of the position of the LCST in a wide range of temperatures.[105] Finally, some polyzwitterionic brushes, such as poly(2-(methacryloyloxy)ethyl dimethyl(3-sulfopropyl)ammonium hydroxide) (PMEDSAH) exhibit an upper critical solution temperature, UCST, in aqueous solutions in which the opposite phenomenon, compared to LCST, occurs, meaning that above this temperature the polymer chains are in a swollen state.[47, 106]

#### 1.2.1.4 Photo-induced responsiveness

The utilization of light as an external trigger is intriguing since it allows facile operation with limited chemical contamination. Photo-responsive polymer brushes that can be tuned by light are mainly comprising spiropyran derivatives and/or azobenzene molecules. Spiropyran-containing polymers can be transformed from a ring-closed nonpolar spiro conformation state to a ring-opened polar zwitterionic merocyanine

isomer, under UV light and then reversibly change back to the spiro conformation by visible light.[107] Polymer brushes that contain a cationic azobenzene surfactant were studied for their light-induced changes in thickness and surface roughness.[108] Azobenzene surfactants under UV light can change from the stable trans form to the cis form and the isomerization can be reversed via visible blue light. The isomerisation of these systems results to UV/light-responsive surface properties including hydrophilicity and cell adhesion. A characteristic example is given by Locklin et al., who studied the responsive photocontrol of the morphological changes, color and wetting behavior of poly(spiropyran methacrylate-*co*-methyl methacrylate) brushes on oxide surfaces.[109]

### 1.2.2 Surface Wettability

#### 1.2.2.1 Introduction to wetting properties

Wetting is a phenomenon during which liquid contacts with a solid material, and the interface of the latter is transformed from a solid-air interface to a solid-liquid interface. It is very close to the adsorption phenomenon, since both are due to interactions among molecules of different substances.[110]

The chemical functionality of the surface and the surface morphology, primarily determine the wettability of a material, which is one of the most important and fundamental properties of solid surfaces.[111] A frequently utilized parameter for the quantitative measure of the wetting phenomena is the contact angle (CA), θ, between a solid surface and a liquid. If liquid molecules interact strongly with the surface, then the liquid will spread on the solid surface which describes the wetting phenomenon. Thermodynamically, two prime regimes occur in equilibrium, namely complete wetting and partial wetting. In the case of complete wetting, the free energy of the system is decreased and the equilibrium CA between the flat solid surface and the liquid is zero ($\theta_{eq} = 0^o$). If the liquid is dropped on a smooth solid surface and forms a finite CA then partial wetting occurs ($\theta_{eq} > 0^o$). When the $\theta_{eq}$ exceeds a CA value of 90º, then it is called non-wetting situation, the free energy is high, and the water molecules can be easily removed from the surface.

Partial wetting represents three interfaces of the liquid droplet perimeter, the solid (S), liquid (L) and gas or vapor (G), with three interfacial tensions: the solid/liquid interfacial surface tension, $\gamma_{SL}$, the surface tension of the liquid, $\gamma_L$, (or liquid/gas surface tension, $\gamma_{LG}$) and the surface free energy of the solid, $\gamma_S$, (or the solid/gas surface tension, $\gamma_{SG}$). The equilibrium of the three-phase contact boundaries determines the value of CA, based on Young-Laplace equation for the equilibrium conditions in an ideal smooth surface (Figure 1.16a):[112]

$$cos\theta_Y = \frac{\gamma_{SG}-\gamma_{SL}}{\gamma_{LG}} \quad (1.15)$$

The CA of a liquid determines both the surface energy and the surface tension.[113]

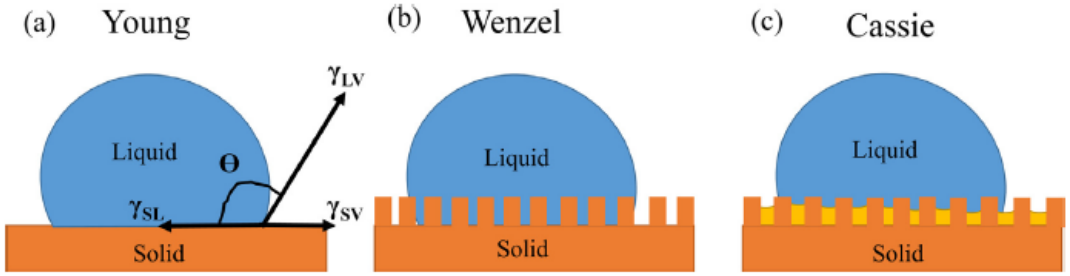


**Figure 1.16.** (a) Young's model, describing forces acting at the three phase contact line of a liquid on a smooth solid surface, (b) Wenzel's model for the interpretation of surface roughness and (c) Cassie's-Baxter model for the interpretation of surface roughness and trapped gas inside the nanostructures, with the apparent CA.[114]

The terms hydrophilic surface and hydrophobic surface have been extensively used to describe opposite effects of the behavior of water molecules on a solid surface. Strong affinity between water molecules and a surface leads to hydrophilic surfaces, whereas hydrophobic surfaces repel water.[115] According to the measured WCA the wettability of surface can be: (a) hydrophilic and (b) hydrophobic with WCAs in the range of 10º $< \theta_Y <$ 90º and 90º $< \theta_Y <$ 150º, respectively, and (c) superhydrophilic and (d) superhydrophobic, for wetting behavior in the range of 0º $< \theta_Y <$ 10º and 150º $< \theta_Y <$ 180º respectively. The higher the WCA, the bigger the strength of the liquid-liquid interaction becomes, making the material more hydrophobic. This state is exemplified by poor wetting and a low free energy of the solid surface. On the other hand, hydrophilicity is characterized by high surface energy. Figure 1.17 shows the contact angle range for the different wetting phenomena. The CA gives important indications

on the wetting properties of a surface, nevertheless it depends on the quality of the liquid being measured.

It is noteworthy that particularly for biomaterial surfaces, a threshold of $\theta_Y$ = 65º rather than 90º, is proposed for the division from hydrophilicity to hydrophilicity.[116] Values below that "Berg threshold" are referred to polymer surfaces with a dense layer of water molecules capable to exclude hydrophobic interactions with proteins or foulants in the absence of charges.

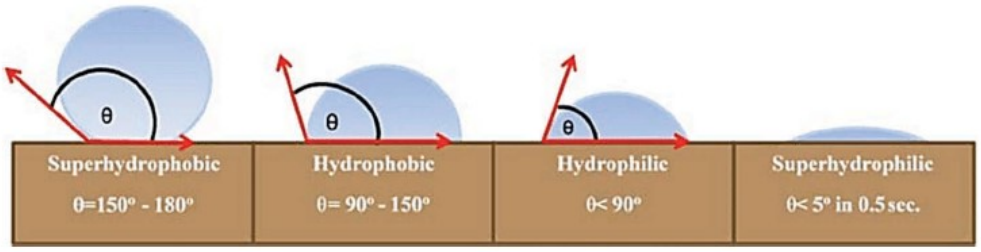


**Figure 1.17.** Schematic illustration of WCA droplets and various wettability phenomena on surfaces.[117]

Nevertheless, non-ideal conditions, due to surface roughness and morphology lead to deviations from the Young's equation. Two key theories are commonly utilized to correlate the surface roughness with the CA of a liquid droplet on a surface, namely the Wenzel model and the Cassie-Baxter model (Figure 1.17b,c). In the Wenzel model, the probing liquid drop fills the asperities of the rough surface after contact, so that the surface roughness contributes to the wetting behavior, denoted as the roughness factor r. The CA is determined by the equation:

$$cos\theta_w = r\ cos\theta_{eq} \tag{1.16}$$

where r denotes the true surface area, divided by the planar surface area and $\theta_{eq}$ is the CA value of a smooth and flat surface of the same material. When $\theta_{eq}$<90º, the increase in the surface roughness results to a decrease in the value of $\theta_w$, whereas when $\theta_{eq}$>90º $\theta_w$ is increased.

In the Cassie-Baxter model the gas is trapped in the nanoholes between the surface underneath and the water droplet, which results to the formation of a sphere that resides on the top. The Cassie-Baxter CA, $\theta_C$, can be calculated by the equation:[118]

$$cos\theta_C = \varphi_S\, cos\theta_S + \varphi_G\, cos\theta_G \quad (1.17)$$

where $\varphi_S$ is the area fraction of the solid phase and $\varphi_G$ is the area fraction of the gas phase on the surface. Figure 1.16a-c illustrates the different wetting models.

There are plenty experimental techniques to determine the CA, including tensiometry, the compressed droplets method, Wilhelmy technique, captive bubble method, capillary bridge method and drop shape analysis (DSA) amongst others.[113] The most facile and commonly attained method is DSA, in which the CA is determined by a shadow image of a static sessile drop and the surface tension or interfacial tension from the shadow image of a pendant drop. The liquid drop is deposited on the surface using a syringe and the CA is measured using a goniometer.

#### 1.2.2.2 Surface energy and surface tension

One of the significant applications of the CA measurements is the assessment of surface free energy, γ, of the solid surface. It has been confirmed that surface free energy has a major impact on the wettability of the surface: low free energy surfaces are hydrophobic and high free energy surfaces are hydrophilic. The surface energy is dimensionally equivalent to surface tension of the liquid, which are both work divided by a unit area ($J/m^2$ or $g/s^2$) and force divided by a unit length (N/m or $g/s^2$). A clean metal or metal oxide usually have high surface energies. If a liquid, an adhesive or a polymer blend has surface tension lower than the high-energy solid, then after deposition it will spontaneously coat the surface.

In general, when the surface energy of a specific surface is high enough, the surface can be easily wetted by a liquid droplet and behaves lyophilic. Otherwise, the surface cannot be wetted by the liquid droplet, exhibiting lyophobic property. The surface energy is commonly determined by the outer atoms or groups on the surface, i.e., surface chemistry. To obtain interfaces with variable bonding chemistry, organic coating using silane chemistry between silicon-based surfaces and silane coupling agents or polymer chemistry by grafting polymer chains on materials is utilized.[119]

The surface tension of a liquid or a polymer solution can be measured directly by a tensiometer. Surface energy is a relative value that cannot be directly measured, nevertheless it can be estimated by applying a set of liquid/solid CA's with liquids of a

known surface tension.[120] Zisman developed a one-parameter theory to determine the surface energy of a smooth flat surface by studying the CA behavior of probe liquids of varying surface tension, however it often leads to incorrect results.[121] Fowkes suggested that the surface energy of a solid or a liquid comprises a sum of independent components associated with specific polar interactions, along with non-polar interactions.[122] Non-polar interactions are attributed to dispersive forces (van der Waals forces) and non-specific forces (hydrophobic interactions) while the polar interactions are due to functional groups such as amides, hydroxyl carbonyl and nitrate moieties. Fowkes idea was continued by Owen and Wendt, who stated that the interfacial interactions depend on the properties of both the solid and the liquid, and $\gamma_{SL}$ results from the equation:[123]

$$\gamma_{SL} = \gamma_S + \gamma_L - 2\left[\left(\gamma_S^d \gamma_L^d\right)^{1/2} + \left(\gamma_S^p \gamma_L^p\right)^{1/2}\right] \quad (1.18)$$

with $\gamma_S^d \gamma_L^d$ and $\gamma_S^p \gamma_L^p$ being the dispersion and polar components, respectively. Interpretation of Youngs equation results to the OWRK equation:

$$\gamma_L(1 + cos\theta) = 2\left[\left(\gamma_S^d \gamma_L^d\right)^{1/2} + \left(\gamma_S^p \gamma_L^p\right)^{1/2}\right] \quad (1.19)$$

By measuring the CA of at least two liquids with known dispersive (diiodomethane) and polar (water) components, the $\gamma_S^d$ and $\gamma_S^p$ unknown values of the solid can be calculated.

Another theory expressed by van Oss describing a combination of three components, due to the fact that the polar component is divided to acid and base components, and thus the surface energy of a polymer brush is determined only when three liquids of known values of $\gamma_L^d$, $\gamma_L^+, \gamma_L^-$, two polar and one apolar ($\gamma_L = \gamma_L^d$ ) are applied to the following vOCG equation:[124]

$$\gamma_L(1 - cos\theta) = 2\left[\left(\gamma_S^d \gamma_L^d\right)^{1/2} + (\gamma_S^- \gamma_L^+)^{1/2} + (\gamma_S^+ \gamma_L^-)^{1/2}\right] \quad (1.20)$$

where $\gamma^-$ and $\gamma^+$ are the electron- donor and acceptor parameters of $\gamma$. To determine the components of $\gamma_S$ of a polymer brush, pairs of polar solvents such as water/glycerol, water/ethylene glycol or water/formamide are employed, while diiodomethane or a-bromonapthalene is used as an apolar liquid. The unknown value of $\gamma_S$ ($\gamma_S^d, \gamma_S^+, \gamma_S^-$) is determined by solving simultaneously three equations derived from 1.19 and 1.20. The

CA of the three liquids water, diiodomethane and glycerol give the known values of $\gamma_L^d, \gamma_L^+, \gamma_L^-$.

As mentioned above for the CA, the surface energy value of the solid varies on the quality of the liquid and comparison among measurements from different methodologies is not safe.

#### 1.2.2.3 Wettability of polymer brushes

Controlling the wettability of a surface is of considerable importance in a plethora of applications such as biological interfaces, agricultural applications and daily life and industrial processes.[76] Recently, the swift developments in the field of smart polymer coatings, have prompted the research community to consider systems with incorporated responsive moieties that exhibit hydrophobic behavior in the designing of surfaces for potential application in waste-water, oil-water separation, removal of heavy metal ions from drinking water, etc. Considering the potential applications of special wettable polymer coating surfaces, two aspects should be addressed. The first is the modification of functional moieties and second the reversibility of the transitions.

Based on the chemical modification of surfaces, polymer brush coatings have been utilized as robust nanocoatings for tailoring the wettability of surfaces. Polymer brushes incorporating neutral hydrophilic/hydrophobic polymers, charged PEL chains and even extremely hydrophobic perfluorinated polymers have been explored in this regard. It is widely known that the surface properties of the polymer brushes are vastly diverse compared to their bulk polymer properties.

An effective way to enhance the hydrophobicity of a solid surface, is by the use of low-surface-tension materials, such as fluorinated polymers. Fluorinated polymers are outstanding polymer materials with a variety of special physical properties that are mainly attributed to the low polarizability and the strong electronegativity of their fluorine atoms. Owing to low polarizability, the fluorinated polymers possess low susceptibility to dispersion forces, therefore exhibit weak adhesive and intermolecular forces. Poly(tetrafluoroethylene) (PTFE) as the benchmark low surface energy material has limitations due to its microcrystalline surface structure. Many fluorinated polymers with good film-forming properties, such as fluorinated polyacrylates, polymethacrylates, and polysiloxanes, have been synthesized, and most of the polymer

films fabricated by spin-coating solutions of these polymers on the solid surfaces exhibited high water contact angle values (> 120º) and ultralow surface energies (less than 12 mJ $m^2$). However, these films have weak adhesion to surfaces, which thereby causes poor stability and consequently limits their applications.[125] The development of surface-grafted fluorinated brushes have been shown to overcome such problems.[126]

Finally, by grafting polymer brushes onto rough, micro/nanostructured surfaces, the wettability is enhanced compared to that of flat surfaces. Grafting hydrophilic polymer chains onto rough surfaces results in superhydrophilic surfaces, while grafting hydrophobic polymer chains produces superhydrophobic surfaces.[127]

Reversibility is a crucial trait of stimuli-responsive polymer brushes, which undergo vast surface energy changes, mainly due to dynamic conformation transitions of the polymer chains upon the application of an external stimulus, which change the surface free energy, and thus allows to control the switching of the surface wetting properties.[128] Among various kinds of smart surfaces, responsive surfaces with switchable wettability have drawn attention for use in a plethora of applications, i.e. oil/water separation sensors, microfluidics, drug delivery and so on.

As explained above (1.2.1), stimuli-responsive polymer brushes can be triggered by various external stimuli to alter their surface properties, including their wetting properties. Sun et al. showed that PNiPAAm brushes on silicon substrates can be employed for constructing thermally responsive functional surfaces, in which the wettability can be tuned reversibly below and above the LCST.[104] The switchable mechanism is attributed to interactions between the PNiPAAm chains and water molecules. Based on this thermo-responsive behavior of PNiPAAm a lot of research has been carried out on grafting polymer brushes onto micro/nanostructured surfaces to alter the wettability from the superhydrophilic to the superhydrophobic state.[104, 129] pH-responsive polymer brushes containing either weak acid or base moieties with certain p$K_\alpha$ values can accept or donate protons in response to pH and along with the abovementioned conformational changes result in changes of the surface wettability. Photo-responsive polymer brushes allow to dynamically change the surface wettability by generating different forms of specific conjugated molecules upon irradiation with visible or UV light. The solvent-responsive wettability of a smart polymer brush is sensitive to the surrounding media properties, and is based on interfacial free energy

driven by the configuration change of the end-grafted polymer chains, that is governed by the interactions of the chains with the solvent. Upon solvent switching, the wettability of the polymer brushes can be tuned. A similar design strategy is followed for the surface grafting of other stimuli-responsive polymer brushes onto substrates to allow changing the surface wettability.[110]

### 1.2.3 Lubricant surfaces

In the past years, many studies have indicated that the surface modification of materials with polymer coatings can effectively lead to an improvement of the tribological properties of the materials.[130] The fundamentals of tribology are based on mechanics, surface physics, and chemistry. The science of tribology (Greek *tribo*: rubbing) concentrates on contact mechanics of moving interfaces that involve energy dissipations. For that reason, the tribological properties of materials deal with adhesion, friction, scratch resistance and wear, which determine the utility of the materials for a particular application. Over the last few decades, the field of tribology, which includes the study of adhesion and friction between surfaces, has received vast attention mainly due to industrial energy losses. Nevertheless, tribology is also critical to the function of many biological systems.

The determination of the micro- and nano-tribological properties of materials such as metals, polymers, ceramics, organic monolayers and biomaterials was optimized by the development of the surface force apparatus (SFA) and atomic force microscopy (AFM) techniques, under controlled conditions (ambient, liquid, vacuum, etc.).[130a] AFM assesses the forces between a sample surface and an AFM tip mounted on a flexible cantilever, by the optical deflection of the latter after their contact. Deflection of the cantilever in the vertical direction gives information about adhesive and repulsive forces, while the lateral cantilever bending monitors the frictional forces. A basic introduction to adhesion and friction and a review on polymer brushes used to reduce these properties follows next.

#### 1.2.3.1 Introduction to tribological properties

**Adhesion**. The term Adhesion refers to attraction of two surfaces that are brought into contact. The adhesion force is defined as the maximum force required for separating two contacting solid surfaces. Two solid surfaces that come into contact, are physically

bonded across the interface. The interaction between two materials 1 and 2 is often described as the work of adhesion ($W_a$), which is proportional to the specific surface energy given by the following Dupre formula:

$$W_a = \gamma_1 + \gamma_2 - \gamma_{12} \quad (1.21)$$

Where, $\gamma_1$ and $\gamma_2$ are free surface energies of the materials 1 and 2 and $\gamma_{12}$ is the interfacial free energy. Nevertheless, experimental values of $\gamma$ for solids are difficult to attain.

Opposing surfaces that comprise low roughness and flexible interface materials demonstrate strong adhesion forces. Increasing the normal load between surfaces results to deformation of the material roughness and thus should be considered.[131] There are mainly four identified contributions to adhesion interactions: molecular bonding, electrostatic forces, capillary forces and forces between excess charges.[132] Molecular bonding influences the least, followed by electrostatic attraction, capillary forces and attraction forces due to excess charges.

Molecular bonding in contacting polymer surfaces, can occur at very short distances, by either neighboring neutral particles or physisorption of polymer chains onto the opposing surface, with form molecular bonds owing to the existence of energy instability on the contact interface. In non-polar particles, van der Waals interactions result by quantum fluctuations in the electronic structures, which lead to dipole mutual attraction, whereas in polar polymer molecules, containing OH, COOH, NHCO, etc., hydrogen bonding and dipole-dipole interactions are responsible for molecular attraction.[133]

At higher distances, Coulomb interactions due to the excess charges on the surface and electrostatic contact potential between the charges, contribute to the forces. Capillary bridges are usually formed, when water molecules are present in pores or slits on both surfaces, that are in close proximity, which result in an increase of the normal force. The adhesive properties are significantly sensitive to the presence of even trace amounts of vapor in the atmosphere. For example, capillary condensation of water around surface contact areas has been shown to have a profound effect on the adhesion forces between mica surfaces in various liquids.[134]

Adhesive forces can be measured typically by AFM measurements, by detecting the optical deflection during approach and retraction of a tip mounted on a flexible cantilever and a surface. The force that is required to pull-out the cantilever from the surface is the adhesive force. Typical force-distance curves are presented in Figure 1.18 (left). At initial stages the tip is approaching the sample surface and thus no forces are detected (A). When the cantilever is in close proximity with the surface, the tip experiences a bending due to an adhesive force based on van der Waals or electrostatic interactions (B). Under a normal applied load, the cantilever is bending to the opposite direction where repulsive forces are developed on the tip (C). During retraction, the tip stays in contact with the sample surface until the cantilever overcomes the attractive forces (D), and finally the tip is detached, going back to the equilibrium state (E).

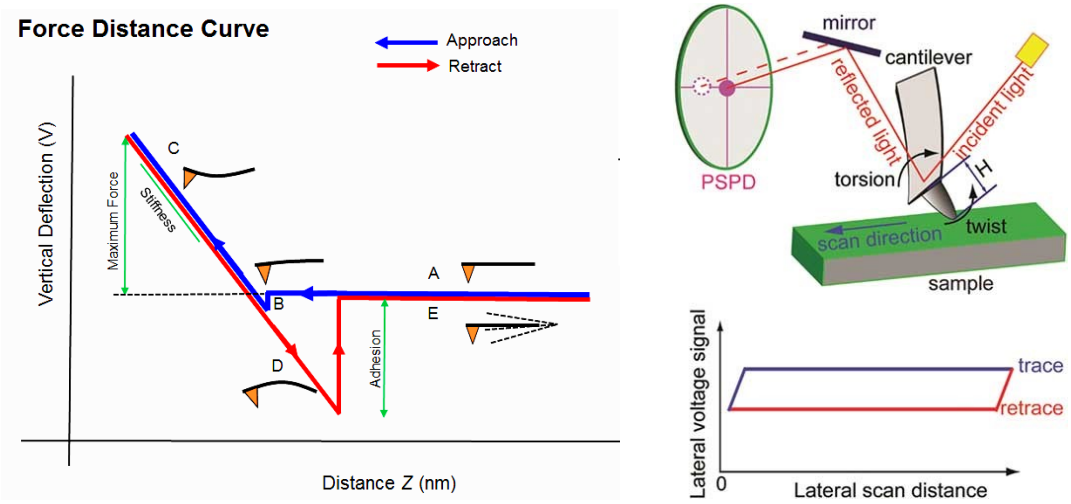


**Figure 1.18.** A typical force distance curve showing the probe approach and retraction cycle during adhesion measurements (left) The curve picture figure was adopted from the website https://wiki.anton-paar.com. Schematic representation of the LFM measurement using a beam-deflection scanning probe and a sample and the detected lateral voltage signal against the scan distance in parallel to the sample (right).[135]

**Friction**. Friction can be defined as the tangential force of resistance to the relative motion of two sliding surfaces in opposite directions, including solid-solid, solid-liquid, solid-air, liquid-air and even liquid-liquid interfaces. In real life, friction is vastly desirable since it is necessary for example in the hip and knee joints when we are walking. Thus, when it comes to loss of energy amounts, or durability of commonly

used materials and the painless movement of human bodies, the reduction or elimination of friction is critical.

Friction force (F) between two surfaces one of which is static and the other is sliding laterally with certain velocity is proportional to the sum of the normal applied load (N) and the adhesion (A) amongst them, based on the Amonton's law of friction at the nanoscale:[136]

$$F = \mu(N+\mathrm{A}) \tag{1.22}$$

Where, μ (or COF) represents the friction coefficient of the contacting materials and is the quantitively expression of friction. Although future versions of this model could accommodate alternative friction laws, this assumption often holds at the nanoscale. The normal load, sliding velocity, temperature, moisture, flexibility and roughness of the materials are among the factors that influence the COF. Considering the crucial role of adhesion for the friction characteristic it should also be kept in mind that the environmental conditions have a great influence on adhesion.[137]

Lateral force microscopy (LFM) also known as friction force microscopy (FFM) is an AFM-based technique used to make friction measurements in the micro and nanoscale. In traditional AFM, in contact mode, the topography is observed by the vertical deflection of the cantilever, whereas in LFM, the twisting or lateral deflection of the cantilever is observed, and provides information about the friction between the tip and the surface.

Lateral scanning of the sample surface results in the torsion of the cantilever. This is detected as the lateral voltage signal, by a position-sensitive photodetector (PSPD). *H* is the torsional moment arm, i.e., the distance from the mid-plane of the centre of the cantilever to the contact point of the tip. The detected lateral voltage signal is plotted against the lateral scan distance for the forward scan direction (trace, indicated by the blue line) and backward scan direction (retrace, indicated by the red line). The lateral voltage signal formed as a hysteretic friction loop, can be converted to friction force at the interface, using a conversion/calibration factor.

The primary issue of this technique is the difficulty in calibrating the cantilever and tip in order to obtain quantitative data.[135-136] The interpretation of LFM results recorded under ambient conditions has to include the dominant role of capillary forces, which

significantly increase adhesion. A humid environment results in higher adsorption of water on hydrophilic surfaces, which contributes to an increase in the friction forces due to capillary bridging.

#### 1.2.3.2 Polymer-brush based lubrication

Frictional resistance is wide-spread in many fields ranging from daily life to industrial manufacturing. For example, biological interfaces such as, the arthrosis surfaces, always exhibit an extremely low frictional coefficient (0.001 to 0.03), in which biological lubricants play an important part.[138] Typically, one strategy to reduce friction at solid-solid interactions is to introduce a thin layer of a viscous fluid between the contacting surfaces, which supports the normal load and prevents direct contact.[139] This method is known as lubrication, nevertheless it is susceptible to wear and damage of the materials in the frictional area. The desire of creating lubrication solutions for reducing friction has resulted to the utilization of SAMs, nevertheless the durability of these ultrathin layers has been a concern. An intriguing class of thin, polymer-based lubrication layers, which resemble some of the structural features of the brush-like biomacromolecules that lubricate the articular cartilage surfaces in human body, are polymer brushes.[140] Important practical applications include lubrication of mechanical engines (pumps, reservoir engines), micro/nano-electromechanical systems (MEMs/NEMs), biomedical implants for prosthetic applications (hips, knees), and others, such as catheters, contact lenses, etc.[141] Decorating flat surfaces with polymer brushes has been shown to allow the reduction of the adhesion force and kinetic friction coefficient by several orders of magnitude, as compared to bare or oil-lubricated surfaces.[140b]

The profound lubrication properties of polymer brushes arise from their unique architecture and the selection of a good solvent for facilitating swelling. In the presence of a good solvent, solvation repulsion effects result in swelling of the polymer chains normal to the surface. When two surfaces, having the solvated stretched polymer chains at the interface, are sliding, low adhesion, low friction and significant lubrication are presented. The mechanism by which solvated polymer brushes lubricate is thought to be as follows:[2]

1. The resistance to rearrangement of the grafted chains due to the repulsive nature of the brushes
2. Lubricant entrapment in the polymer brushes
3. High concentrations of lubricant in the outer polymer brush creates a low shear area protecting the brush system.

Nevertheless, due to the complexity and the influence of different phenomena in friction and adhesion forces, the understanding of the tribological properties at molecular level is still a challenge and properties such as the grafting density of the polymer brushes, the bulk density, the swelling properties in various solvents, environmental conditions and others, need to be considered.[142]

The majority of polymer brush lubricants are hydrophilic, inspired by nature, where some biological surfaces (i.e. joint system in the human body, eyes) possess extremely low-friction based on the hydration lubrication mechanism. Densely grafted hydrophilic polymer chains have been shown to be an efficient boundary lubricant and wet layer at moderate normal loads and shear velocities in aqueous media, due to the combination of osmotic forces and conformational entropy.[143] There are three primary types of hydrophilic brush-lubricants, namely (a) neutral, (b) polyanionic/cationic and (c) polyzwitterionic hydrophilic brushes. The grafted brushes can be also oil-soluble to improve the oil-based lubrication systems.[144] Figure 1.19 illustrates the classes of low frictional brushes.

**Neutral hydrophilic brush lubricants** comprise polar polymer chains that interact with water molecules by hydrogen bonding, i.e. poly(oligo(ethylene glycol) methacrylate) (POEGMA), poly(ethylene glycol) (PEG), PHEMA and poly(acrylamide) (PAAm).[145] Under low pressures, the water molecules provide a hydration layer on the hydrophilic surfaces that acts as thr lubricant. POEGMA brushes have been tested on crosslinked polyethylene orthopedic bearings, mimicking conditions of natural joint lubrication, and exhibited low COF of 0.03 at 29 MPa applied pressure.[146]

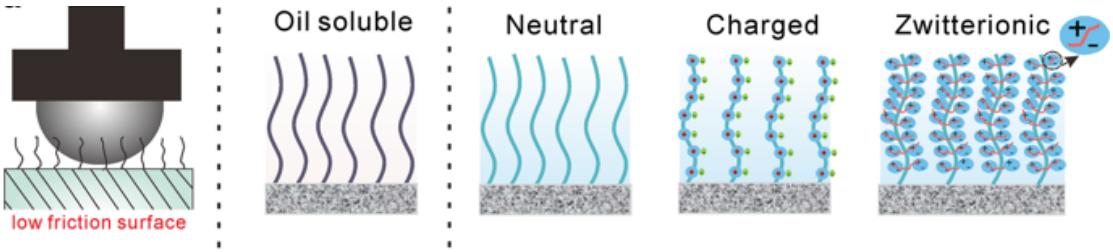


**Figure 1.19.** Schematic illustration of the classes of polymer brushes that can be grafted on solid surfaces to realize low friction.[144]

**Polyanionic/polycationic brush lubricants** are more robust than the neutral ones and can undertake higher pressures up to 45 MPa, when sliding. This is attributed to the stronger ion-dipole interactions between charged polymer chains and water molecules and due to their higher swelling resulting from inter and intra-molecular repulsions. Osmotic pressure within the brushes and steric repulsion upon compression contribute to their exceptional lubrication characteristics. A vast advantage in these systems is that the lubrication characteristics can be tuned by varying the pH, the counterions or the chemical composition of the brush. Examples of polyanionic/polycationic brushes are PMAA, PMETAC, PDMAEMA, poly(3-sulfopropyl methacrylate) (PSPMA), poly(sulfonated glycidyl methacrylate) (PSGMA) and poly(2-methacryloxyethyl phosphate) (PMPA).[145b] PDMAEMA brushes have been tested for applications in prosthetics with COF around 0.05 in an acellular simulated body fluid, whereas for bovine serum (BS) the COF was 0.13.[146] The authors suggested that the positively charged tertiary amine groups of the PDMAEMA chains attract negatively charged proteins e.g. albumin that are present in BS and faclitates the sliding of the surfaces.

**Polyzwitterionic brush lubricants** are the most recent class of polymer brush lubricants, which are based on the hydration lubrication mechanism, since they have no net charge and thus are insensitive to environmental factors, including pH or mobile counterions. Each zwitterionic monomer repeat unit is capable of strongly binding around 15 water molecules and therefore this high hydration defines them as efficient hydrophilic lubricants even at high pressures.[147] Poly(sulfobetaine methacrylate) (PSBMA) and poly(2-methacryloylethyl phosphorylcholine) (PMPC) brushes are the most extensively studied in the literature with extremely low COF of $10^{-5}$ to $10^{-4}$ at pressures of 15 MPa, while possessing high stability even at pressures as high as 139 MPa (with COF of 0.08 – 0.13).[148] Recently, a less explored polyzwitterionic brush,

poly(3-(1-(4-vinylbenzyl)-1H-imidazol-3-ium-3-yl)propane-1-sulfonate) (PVBIPS) was shown to confer unique ionic-strength-dependent swelling properties with low COF upon exposure to high-ionic-strength solutions.[149]

**Hydrophobic brush lubricants.** Apart from hydrophilic polymer brushes that act as hydrodynamic lubricants, hydrophobic polymer brushes can be utilized as boundary lubricants and combine the lubrication properties of the brushes with the rheology and high temperature advantages of oil. The first hydrophobic polymer brush lubricant reported was a polystyrene brush grafted on mica via zwitterionic chain ends.[150] This system was found to decrease the COF in toluene to below 0.001 for contact pressure up to 1 MPa. A number of reports since then have utilized PMMA, poly(ethyl methacrylate) (PEMA), poly(butyl acrylate) (PBA), poly(hexyl methacrylate) (P6MA), poly(dodecyl methacrylate) (P12MA) and poly(octadecyl methacrylate) (P18MA) brushes.[145b] All these studies suggested that the presence of a good solvent is crucial to obtain polymer brushes with ultra-low friction (COF = 0.002). Interestingly, thick P12MA brushes in hexadecane, were found to exhibit a low COF (0.02-0.12) under normal loads up to 460 MPa.[151]

In this category of hydrophobic/oleophilic polymer coatings, fluorinated polymers constitute distinct materials with significant properties such as thermal stability, water repellency, chemical resistance, non-adhesion and low friction. The high binding energy and low polarizability of the C-F groups are responsible for these properties. So far, physisorbed PTFE thin coatings are employed to reduce the adhesion and friction forces on these devices, nevertheless these coatings possess long term mechanical instability and low wear resistance.[152] Lately, Zuilhof's group has examined the lubrication properties of fluorinated polymer brushes prepared by SI-ATRP with low COF values of 0.004-0.006 in fluorocarbon solvents and hexadecane.[126c] A significant outcome is that fluorinated polymer brushes can serve as solid lubricants in micro/nano-electromechanical systems (MEMs/NEMs) or in applications where liquids cannot be used. Despite the fact that the reduction the surface friction of materials has been studied extensively, only few studies are available on the tribological properties of polymer brushes in the dry state.[95, 126b, 126c, 153] The dry friction between a sample surface and the AFM probe is closely related to the interactions among them which are dominated by van der Waals forces.

#### 1.2.3.3 Switchable friction

The interfacial adhesion and friction properties of stimuli-sensitive polymer brushes can be tuned by varying the polymer chemistry, topography, hydration state and interface charge. There is a clear distinction between the switching adhesion and friction of two similar polymer brush surfaces and a polymer brush surface with a different surface.

**Adhesion and friction between two opposing polymer brushes.** Both the adhesion and friction are highly dependent on the solvent quality. In a good solvent, the polymer-polymer interactions are screened by the solvent and thus the brush is in a repulsive state. After the compression of the surfaces at low normal loads, the solvent remains in contact with the brush and the adhesion and friction are kept low. Nevertheless, in poor a solvent, the interactions between the polymer chains are favored in contrast to those between the polymer and the solvent, and thus the adhesion and the friction values are higher. Therefore, by altering the external stimuli, which in many cases is the exchange from poor to good solvent, the adhesion and friction of these systems can be tuned from high to low. Co-nonsolvency, temperature, nature of the counterions, electric field and UV are among the different external stimuli that have been employed to control the solvent conditions and switch the adhesive and frictional behavior between two chemically similar polymer surfaces in a face-to-face mode.[154]

When the normal applied load is higher than the osmotic pressure, then entanglements between the polymer chains can occur upon compression or sliding which result in an increase in the adhesion and friction, respectively and respond oppositely to the external stimulus.

**Adhesion and friction between polymer brushes and different opposing surfaces**. The adhesion and friction between polymer brushes and solid surfaces are determined by their interactions within the solvent medium. In the presence of good solvent, if the polymer brush-solvent interaction is higher than the interaction between the polymer brush and the opposing surface, then the friction is low. Variations again in the solvent quality from good to poor, results in tuning the friction properties. In the case that the interactions between the polymer brush and the opposing surface are higher than the solvent-polymer brush and solvent-surface interactions, then the switching is dependent on changes in the area of contact of the two surfaces. Finally, a method to produce

switchable friction properties is by compressing opposing surfaces grafted with two different polymer chains. In a selective solvent for each polymer brush, the solvation is kept either in the one or the other and thus the friction can be switched.[155]

Hydrophilic PEL brush-based boundary lubricants are mainly used for the design of smart surfaces whose friction can respond to a range of stimuli. The switching to low adhesive and frictional properties can be achieved only under certain environmental conditions. Nordgren et al. have studied PDMAEMA brushes grafted from gold substrates using AFM, and they found that the nanotribological properties of the films reflect the brush conformation which can be controlled by both temperature and pH.[156] An example of the switching friction between two chemically different surfaces brought in contact, was studied by Zhang et al., who measured the friction properties between a PMPC brush and a Au cantilever in ethanol/water mixtures.[157] By employing lateral force microscopy (LFM) studies, they found that the brushes exhibited low frictional properties at low EtOH/water volume ratios, and the friction increased above 70% EtOH in water, in which the PMPC brushes were in the collapsed state. Wei et al. found that tunable friction, from superior lubrication (COF=$10^{-3}$) to ultrahigh friction (COF>1), can be achieved by counterion driven interactions on polycationic brushes and surfactant driven interactions on polyanionic brushes.[158] The mechanism of tunable friction was attributed to the lubrication of highly hydrated and swollen polymer brushes, the moderate lubrication of partially collapsed polymer chains and the high friction of completely dehydrated and collapsed chains. Ma et al. reported switchable adhesion and friction between a PDMS surface and nanofibrillar PSPMA or PMAA brush surfaces, by varying the humidity or the pH, respectively.[159] Lately, a less explored polyzwitterionic brush, PVBIPS was shown to change its conformational properties upon exposure to high-ionic-strength solutions which led to ultralow COF.[149]

The solvent-responsive adhesion and frictional properties of PS/P2VP and PS/PAA binary polymer brushes was reported by Vyas.[95] The topological changes that occur in these systems were attributed to the selective solvation of one of the homopolymer chains anchored onto the surface, which lead to conformational changes that induce reversible adhesion and friction. So far, there are only very few reports on the responsive tribological properties of mixed polymer brushes under dry conditions.[95]

### 1.2.4 Stability of brush coatings

Stability, that is the capacity of a coating to maintain its properties over time, constitutes one of the most crucial factors, determining the suitability of a surface for use in several applications. Highly solvated polymer brushes are subjected to osmotic forces that can contribute to the acceleration or the catalysis of the degrafting of the hydrophilic polymer chains from the surfaces, due to hydrolysis or the chemical degradation of the anchored initiator molecules. This can be more intense under harsh environments such as water with high salt concentration.

To improve the stability of polymer brushes under aggressive media, many groups examined the synthesis of diblock copolymer brushes, comprising a hydrophobic layer at the interface between the substrate and the polymer chains, that will hinder the penetration of the aqueous solvent to the grafting points and thus will prevent hydrolysis, rendering these surfaces stable for prolonged periods of time. PS, poly(2-ethylhexyl methacrylate) (PEHMA) and PMMA blocks have been used so far as protecting layers of hydrophilic polymer brushes i.e. PMAA and PSBMA.[160] Nevertheless, it has been shown lately that even in the presence of a PMMA inner block, degrafting can occur, even though the rate is significantly reduced, meaning that these moderate hydrophobic protecting layers eventually become permeable by the solvent.[160c] A study of hydrophobic polymer brushes in organic media in the presence of ppm of water resulted to the hypothesis that the degrafting of the polymer brushes is driven by an amplification of the tension at the polymer brush-substrate interface, that is a consequence of the swelling of the polymer brushes, and the presence of an appropriate hydrolysis agent (i.e. water).[161]

## 1.3 Antimicrobial polymer coatings

### 1.3.1 Microorganisms and pathogens

Microorganisms or microbes constitute the oldest form of life on this planet and over the passage of millions of years they have developed versatile adaptive mechanisms to retain their existence.[162] Microbes are divided into five prime classifications: bacteria, fungi, viruses, algae and protozoa.

Bacteria are primarily prokaryotic, unicellular microorganisms without a nucleus and their size ranges from 1-5 μm, which is much lower than the size of a typical eukaryotic

cell (10-100 μm). The plasma membrane of the bacteria comprises a phospholipid bilayer with similar characteristics to the plasma membranes found in mammalian cells. Based on their outer cell membrane and their gram staining, bacteria strains are classified into two main groups, namely gram-positive (stained dark purple-violet) and gram-negative (stained red-pink). Gram-positive bacteria are surrounded by a cytoplasmic membrane and a cell wall around 20 - 80 nm thick containing peptidoglycans (polymer consisting of sugar moieties and amino acids) linked to lipoteichoic acids. On the other hand, gram-negative bacteria have an inner plasma membrane consisting of phospholipids, the periplasm which is a thinner peptidoglycan wall around 6 - 10 nm thick and is surrounded by an outer lipid membrane connected with a leaflet of lipopolysaccharides. Phospholipids comprise two long alkyl chains of 18 carbons connected through phosphoric acid. In principal, this outer membrane feature offers to the gram-negative strains further resilience compared to the less protected gram-positive strains. The main difference between the plasma membranes of mammalian and bacterial cells is their composition. In mammalian cells the negative charges are distributed in the inner part of the phospholipid membrane, whereas in bacterial cells the negative charges are distributed in both sides of the membrane. Moreover, the bacterial cell membranes possess improved mechanical stability against physical deformation compared to the mammalian cells (see Figure 1.20).

Protozoa are eukaryotic unicellular microorganisms, while fungi and algae are eukaryotic, unicellular and multicellular forms of microorganisms with genuine nuclei.[163] Viruses are usually exploiting host cells, as they represent a non-independent form of life and therefore, are forced to act as intracellular parasites.

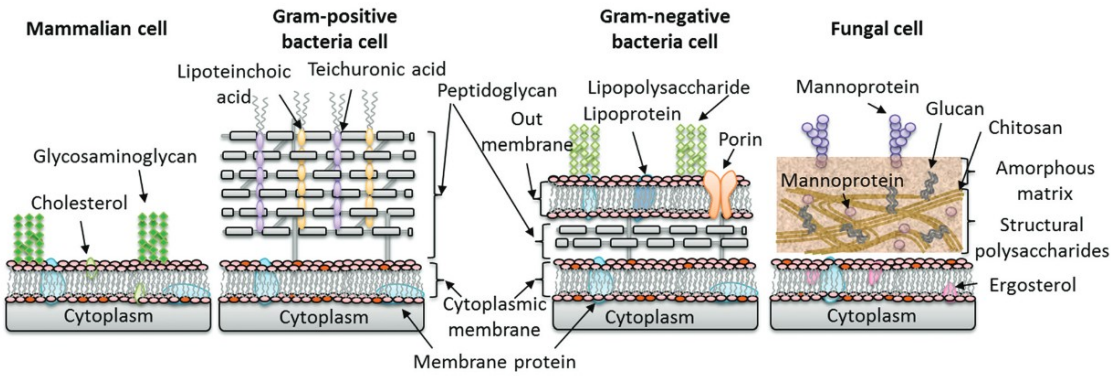


**Figure 1.20.** Cross-section and structural analysis of the cell envelope of mammalian and various microbial cells. [164]

Microbial infections affect animals, plants and human beings and pose a major challenge to human health worldwide. The discovery that numerous germs, such as bacteria, viruses, protozoa and fungi are primarily responsible for elevated human morbidity and mortality (over one-fourth of global deaths annually) has led to a vital seek for the prevention of microbial infections. Since the introduction of penicillin in 1940s, as an antibiotic that intervenes with the bacterial growth and prevents bacterial infections, a majority of low molecular weight antibiotics, such as streptomycin (aminoglycosides), tetracycline (tetracyclines), erythromycin (macrolides), vancomycin (glycopeptides), and cipro-floxacin (quinolones), that target specifically either the DNA replication, the cell wall or the protein synthesis of bacteria, were used for the prevention of pathogenesis. This period was called the "Golden Age of antibiotics".[165] Nevertheless, the widespread and injudicious use of antibiotics induced the phenomenon of bacterial antibiotic-resistance which stems from the adaptive mechanisms of bacteria. In addition, the two diverse types of bacteria, gram-positive and gram-negative, react differently to antibiotics, so treating multiple bacterial infections requires different antibiotics. The need of alternative antimicrobial agents to prevent antibiotic-resistance led to the development of natural or synthetic low molecular weight antimicrobial agents.

Low molecular weight antimicrobial compounds or bactericides have been used extensively in industrial and biomedical applications in the past decades. Compared to antibiotics that target specific routes of bacterial growth, bactericides can kill bacteria in a non-specific manner related to membrane damage, oxidative stress and interaction with the genetic material and proteins, thus they are less susceptible in resulting in the resistance of microbes to these agents. During the last decade, the use of quaternary ammonium salts (QAS) has shown great potential for the aforementioned applications. Most QAS are cationic moieties comprising a nitrogen atom ($N^+$) attached by covalent bonds to four different alkyl groups (R) or alkyl groups substituted with other functionalities, and a halide anion ($X^-$) which is usually a chlorine, bromine or iodine atom. Their high potency has been proven when the positive charge is supported by a hydrophobic moiety, typically in the form of long alkyl chains. It is proposed that the electrostatic interactions between the negatively charged bacterial membrane and positively charged QAS involves the intercalation of hydrophobic alkyl functionalities of QAS into the phospholipid hydrocarbon core which can denaturate structural

proteins and enzymes. Definitive killing is caused via disruption of the bilayer organization, and consequently formation of holes in the membrane, leading to cell lysis. Nevertheless, eventually the majority of the bactericides have proven to be detrimental, due to high levels of environmental pollution, human toxicity and in some cases resistance against them. In contrast, antimicrobial polymers can surpass these problems by establishing bactericidal activity with reduced cytotoxicity, low propensity for resistance development, higher chemical stability and non-volatility, and potent long-term efficacy (Figure 1.21). Besides that, polymeric materials offer the possibility of antibacterial coatings.

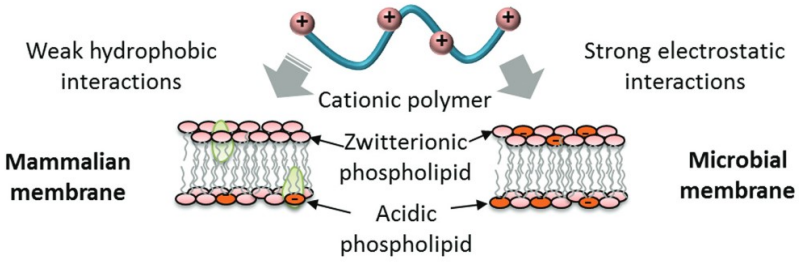


**Figure 1.21.** Schematic illustration of selective interactions of cationic polymers with mammalian and microbial membranes.[164]

### 1.3.2 Introduction to the concept of antimicrobial polymers

Antimicrobial polymers or polymeric disinfectants or antibiotic polymers have gained a profound interest as novel antimicrobial systems, due to their intrinsic properties, variable functionalities and great biocidal activities against a variety of bacteria. Due to the negative charge of the bacterial cell surface derived either from teichoic acids or phospholipids in gram-positive and gram-negative bacteria, it is believed that the best antimicrobial candidates would be amphiphilic polymers bearing cationic sites among other functionalities. The hydrophilic parts are mostly cationic pendant groups linked to a monomer repeat unit or parts of the polymer backbone if they are supported by long alkyl side chains that assure sufficient hydrophobicity to the polymeric system.[166] The electrostatic interactions of the bacteria with the antimicrobial cationic polymers is considered crucial to fight the problem of microbial resistance. Lengthening the alkyl side chain can result in more hydrophobic structures that can interact more strongly with the lipid bilayer of the microbial membranes. Nevertheless, excessive increase of

the chain length, may result to intense aggregation of the polymer chains and increased hemolytic activity, thus lead to a weaker bactericidal activity.

According to Katsumi, antimicrobial polymers should:

- have sufficient contact with the microorganisms
- have sufficient cationic charge to provoke adhesion to the microbial cell membrane
- have hydrophobic moieties that will integrate in the cell membrane
- be non-toxic to mammalian cells.

They can be grouped into two main categories: (a) polymers with inherent antimicrobial activity, and (b) chemically modified polymers to confer antimicrobial activity.[167]

Polymers with inherent antimicrobial activity comprise (a) natural polymers, such as chitosan (CS), poly-ε-lysine (ε-PL) and natural antimicrobial peptides (AMPs), (b) synthetic polymers that contain nitrogen moieties e.g. linear quaternary ammonium salt polymers, polymers with quaternary pyridinium compounds, polyethylenimines, polyguanides, poly(ionic liquid)s, (c) synthetic polymers that contain halogen compounds, i.e. poly (n-halamines), fluorine/chlorine containing cationic polymers and (d) polymers mimicking natural peptides.[168]

Polymers that are not able to confer any - or possess negligible - antimicrobial activity are a class of antimicrobial polymers that need to be chemically modified with an active antimicrobial agent. These polymers can be divided to (i) polymers containing active pendant groups e.g. quaternary ammonium, phosphonium or sulfonium salt groups and hydroxyl group-containing organic acids, (ii) polymers with attached antimicrobial organic agents and (iii) polymers linked with inorganic agents.[168] Among them, inherent antimicrobial polymers based on QAS and chemically modified polymers bearing QAS are the most widely studied antimicrobial polymers.[166] Studies on QAS with several alkyl chain length functionalities showed different results owing to changes in the solubility of the polymers in water, that limits the availability and possibility of polymer penetration to the bacterial cell wall.[169]

### 1.3.3 Bacterial adhesion and biofilm formation on surfaces

Besides their resistance mechanisms, bacteria can adhere to surfaces and form communities that alleviate the burden of diseases. Bacterial contamination of surfaces constitute a prime threat in a plethora of fields, predominantly in medical devices, drugs, hospital surfaces, dental restoration and surgery equipment, health care products and hygienic applications, water purification systems, textiles, food packaging and storage, major or domestic appliances, aeronautic, marine, etc.[167] Microorganisms and in particular bacteria have the tendency to contaminate any type of surface under a moist environment and lead to a biofilm formation through a multistep fouling process, which is similar for almost all microbial species. Briefly, when a surface is immersed into a biological fluid, the fouling process involves initial adhesion of ions and proteins within seconds to form a conditioning layer. Then adhesion of planktonic bacteria to the conditioning film is endorsed, through Brownian motion, van der Waals attraction, gravitation forces, electrostatic charges and hydrophobic interactions.[170] Initially the adhesion process is reversible until the time of the biofilm formation in which the attachment of bacteria is permanent. A bacterial biofilm is a complex assembly of multi-layers of bacterial aggregates encased in an exopolysaccharide matrix excreted by the adhered bacteria and this construction affords the microbial cells the necessary protection against flow detachment, host defenses and hostile antimicrobial molecules, making the cells less vulnerable compared to unprotected microbial cells.[171] Biofilms, due to the increased pressure of further proliferation and maturation can be ruptured and act as reservoirs of microbes, which detach from the matrix and contribute to the epidemiology of the infection through air, water, soil, etc.[172] A schematic representation of the fouling process and biofilm formation is shown in Figure 1.22.

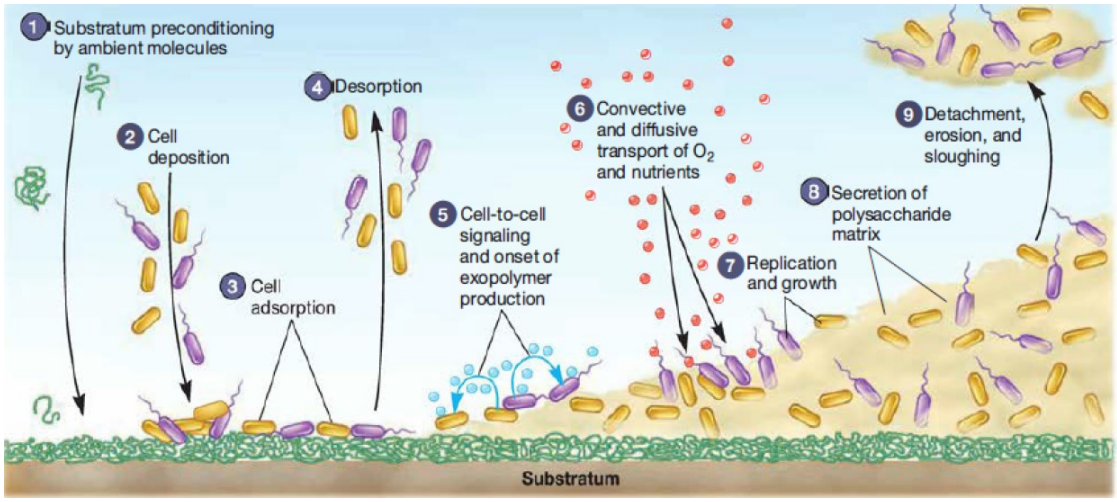


**Figure 1.22.** Schematic illustration of biofilm formation often facilitated by (1) fouling of proteins (conditioning film). The process of biofilm formation begins with the reversible (2) deposition, (3) attachment and (4) desorption of planktonic bacteria, followed by the (5) bacteria change of gene expression patterns and production of the extracellular polymeric matrix, (6-7) microcolonies of bacteria, which are formed inside the matrix, (8) further maturation, and finally (9) the mature biofilm, that can disperse planktonic bacteria to new clean surfaces.[173]

Contamination can occur either by airborne bacteria in the dry state or by the direct contact with biological fluids in the wet state i.e. blood, serum, protein solutions. Ideally, infections can be prevented by assuring aseptic conditions on surfaces, however this can be applied only in airborne bacteria, while further treatments are needed to be deployed in order to maintain such conditions.

Global epidemiology situations, nosocomial infection risks and high operational and maintenance costs e.g. for shipping companies have given rise to the development and excessive usage of antimicrobial agents such as (a) antibiotics (penicillins, rifampin, oxazolidones, polymixins), which abolish microorganisms within the body, (b) disinfectants ("nonselective antimicrobials" such as silver salts, hypochlorite, reactive oxygen species, alcohols, essential oils and quaternary ammonium salts), which are applied on non-living surfaces and (c) antiseptics (applied to living tissue to reduce infection, such as alcohols, iodine, hydrogen peroxide) against bacterial infection.

The widespread and injudicious use of antimicrobial agents to prevent the growth of bacteria on surfaces, implants, etc. has resulted in the formation of resistant microorganisms, that promptly and simply modify their cell envelope or mutate their

genes, making their effective eradication difficult.[174] Furthermore, most of the bacteria in a biofilm are in a stationary-growth phase with low metabolism and expression of genes, compared to the growth phase of their planktonic counterparts, which renders them less susceptible to antimicrobial therapy.[175] Reciprocally, the continuous utilization of antimicrobial agents can induce a biofilm stabilization. It should be noted that once the initial attachment occurs, the biofilm formation is irreversible and conventional methods to prevent the biofilm formation may result to further contamination.[176] Sterilization methods such as UV irradiation and autoclaving are effective against biofilm formation, however continuous operation is not possible and energy consuming. Hence, it is vital that material scientists develop novel antimicrobial surfaces or modify the performance of existing antimicrobial surfaces to counteract this profound issue and prevent permanently the adhesion before the development of biofilms. Since initial adhesion is the key step for biofilm formation, strategies have focused on utilizing the physicochemical properties of surfaces.

### 1.3.4 Current strategies to control biofilm formation

A promising approach to combat the bacterial cross-infection is the usage of specific antimicrobial polymer coatings either physisorbed or covalently linked on the surface that effectively prevent or resist the initial adhesion of microorganisms by overlooking the conditioning layer for long-lasting sterilization. This can be attained by either repelling or killing the pathogen microbes.[166]

Antimicrobial polymer coatings can be classified into (i) antifouling coatings, intended to repel protein and bacterial adhesion through non-favorable interactions, such as exclusion steric repulsion, electrostatic repulsion and low surface energy modification, and (ii) bactericidal coatings, which exert the killing of the bacteria by inactivation of the bacteria cells after contact with chemical agents that are either released from a matrix or covalently tethered to the polymer surface (Figure 1.23).[177] From the applications perspective, an ideal antimicrobial surface for the retardation of microorganism colonization for biomedical implants, marine equipment and water treatment membranes should provide both antifouling and bactericidal characteristics against different types of foulants.

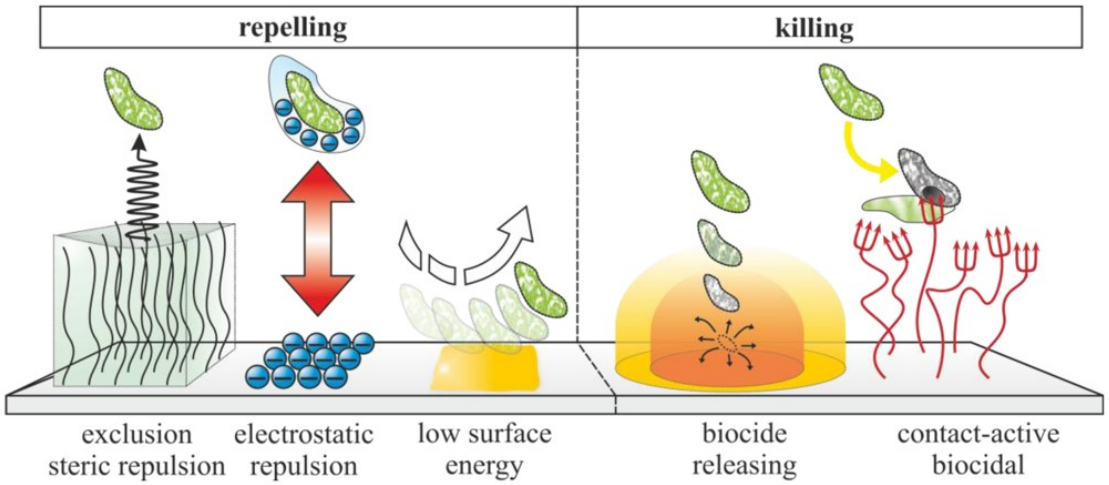


**Figure 1.23.** Classification of the approaches used to fabricate antifouling (repelling) or bactericidal (killing) surfaces for biofilm management.[166]

### 1.3.5 Antifouling polymer coatings

Antifouling polymer coatings also known as anti-adhesive or bio-passive polymer coatings comprise an important class of antimicrobial surfaces that are proficient of lessening the extent of bacterial contamination and further biofilm formation.[178] The concept of antifouling implies the repellence or removal of bacterial fouling, as well as of protein adsorption and the adhesion of mammalian cells or marine foulants on surfaces through unfavorable interactions.[177a, 179] A significant aspect is that antifouling polymer coatings have the ability to prevent biofilm formation on the surfaces, but do not kill the microorganisms. Researchers have discovered that by tailoring the surface properties of a biomaterial, e.g. hydrophilicity, surface roughness or topology, electrostatic interactions and surface compliance, can significantly reduce the rate of bacterial attachment via minimizing the adhesive forces between the surface and invading proteins and bacteria.[180] The two main strategies for an antifouling action is the use of (a) bacteria-repellent coatings, consisting of hydrophilic polymers that prevent bacteria adhesion due to their low interfacial energy with water and (b) bacteria-release coatings, comprising hydrophobic polymers which allow to remove the fouling using low shearing stresses, thus low amount of energy (Figure 1.24).

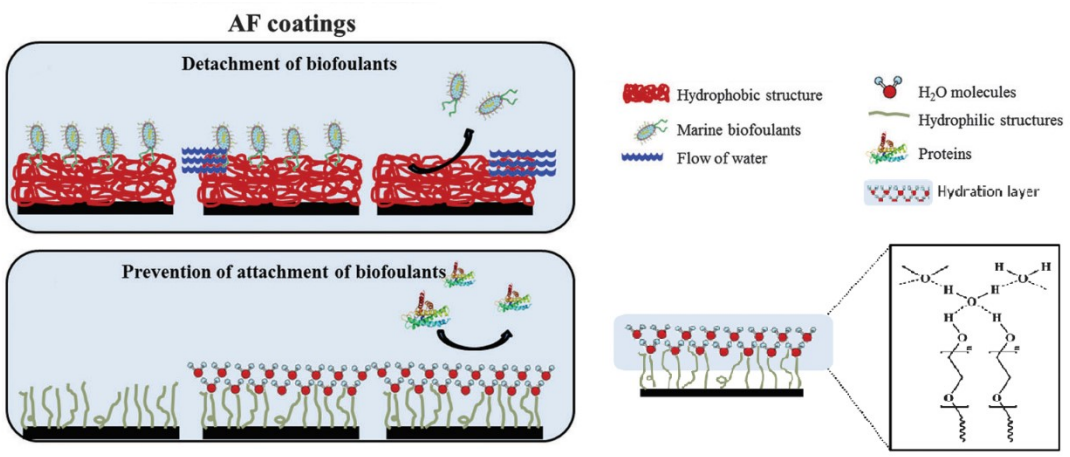


**Figure 1.24.** Schematic illustration of antifouling surfaces: bacteria-release (top left) and bacteria-repellent surfaces (bottom left).[181]

### 1.3.5.1 Bacteria-repellent coatings

As mentioned above, the initial adhesion of bacteria on the surfaces is facilitated by a layer of adsorbed proteins that forms a conditioning film for the bacteria to grow. Hence, designing surfaces that can reduce or prevent protein adsorption was hypothesized to be beneficial for bacterial resistance. These types of surfaces are usually prepared from hydrophilic or charged polymer coatings, which possess profound antifouling properties. In theory, these features are based on a surface hydration layer, which is formed near the polymer coating in the aqueous environment and serves as an energetic repellent barrier for protein and subsequent bacterial adhesion on the surface. The attachment of bacteria cells on a surface, that has low interfacial energy with water, results in low enthalpy gain of adhesion, loss of enthalpy and thus an unfavorable change in free energy. Aside from hydration, polymer chain flexibility also plays a significant role, since the compression of the polymer chains by the protein molecules or bacteria cells, results in enhanced steric repulsion forces or steric hindrance and an unfavorable decrease in entropy (see Figure 1.25).[69, 182]

Dense physisorbed polymer layers or polymer brushes based on (a) neutral hydrophilic polymers, and (b) zwitterionic hydrophilic polymers have been employed for the fabrication of highly hydrated and steric repulsive bacteria-repellent surfaces. Hydrophilic polymer coatings need to be grafted on surfaces, when immersed in aqueous environments, due to the detachment of these soluble films.

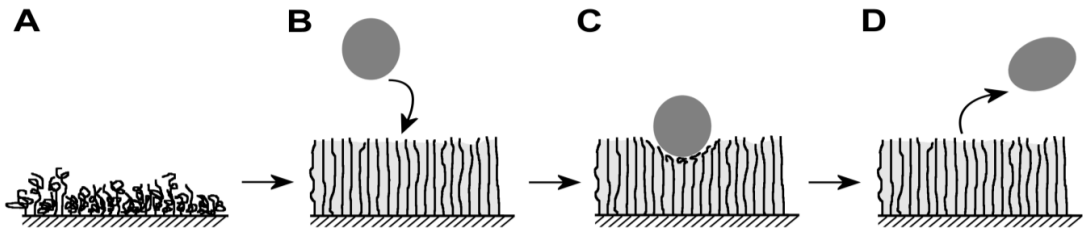


**Figure 1.25.** Antifouling hydrophilic polymer brush surfaces: (A) polymer brushes in the dry state, (B) tightly packed hydrated brushes in aqueous environment, (C, D) repulsion of microorganisms or proteins by steric hindrance due to the layer of water and the elasticity of the polymer chains.[172b]

#### 1.3.5.1.1 Poly-hydrophilic brush surfaces

A variety of neutral hydrophilic polymers have been introduced as bacterial antifouling coatings, with the most common neutral systems being based on polymers such as poly(2-hydroxyethyl methacrylate) (PHEMA), 2-methyl-2-oxazoline (PMOXA), polyacrylamide (PAAm), and poly(poly(ethylene glycol) methacrylate) (PPEGMA), due to their similar behavior with PEG and their capability for further modification of their hydroxyl end groups to more complex systems. PEG or PEO represent perhaps the most prevalent class of biopolymers in the literature for inhibiting protein and cell adhesion on surfaces and thus PEG-based polymers are often termed as "gold standard materials" for antifouling surfaces.[183] PEG-based polymer brushes are intriguing due to their exquisite water solubility or hydrophilicity, because they are excellent hydrogen-bond acceptors, and the ability to deviate the interactions among proteins, bacteria and water which renders them very promising for biological applications. Although PEG-based brush surfaces exhibit high protein and bacteria repellence, the utility of PEG chains is compromised due to their instability because they undergo metal ionization and oxidative degradation *in vivo*, which could lead to the destruction of the hydration layer.[184] Resembling PEG-based coatings, hydrophilic PHEMA coatings exhibit high antifouling efficacies, due to the fact that the PHEMA chains are stretched promptly and oriented causing the physical exclusion of proteins and cells in aqueous environments.[185] An alternative to synthetic hydrophilic polymers are polysaccharides, such as alginic acid (AA) and hyaluronic acid (HA), which are natural macromolecules with fouling-resistant properties.

To date, the majority of antifouling polymer brushes that have been used are hydrophilic, with contact angles below the Berg threshold of 65°.[116] Values below that threshold are referred to polymer surfaces with a dense layer of water molecules capable to exclude hydrophobic interactions with proteins or foulants. However, if electrostatic attractions are present in the polymer system or when the surface hydration is compromised, protein adhesion is inevitable to occur. Even though highly hydrophilic polymer coatings have high surface energies (e.g. PEG > 43 mN / m), the possible reasons for their protein resistance and cell adhesion is explained based on (a) the cruciality of the interfacial energy between the polymer coating and water, which in highly hydrophilic surfaces is extremely low (for PEG it is 5 mJ / $m^2$), (b) the repulsive forces generated from the compression of the elastic stretched polymer chains by the invaded proteins and bacteria, and (c) the thermodynamic osmotic stress, which means that the energetic and kinetic penalty for the removal of water molecules, during a protein or bacteria invasion in highly hydrated polymeric surfaces, is extremely high.[186] The repellent performance of highly hydrophilic neutral brushes is effective against both positive and negative biomolecules under long-term experiments, classifying them as standardized bacteria-repellent surfaces.[45]

In all cases, the optimization of the thickness, grafting density and chain flexibility of the grafted polymer chains seems to play a pivotal role in the overall antifouling efficiency of the polymer brushes. As a matter of fact, an increase in the thickness of the hydrophilic polymer brush generates high hydration capacity and repellent activity, until an optimum range. Above this range, a decrease in the antifouling behavior may be ascribed to chain entanglements or crowding in the film.[187] Moreover, fully stretched polymer chains in highly dense polymer brushes were shown to be ideal repellent surfaces compared to low-density grafted polymer chains in the mushroom regime, where the films promote adsorption of proteins and microorganisms.[69, 188] Finally, studies on the effect of the grafting density have revealed a hindering of the polymer chain flexibility with the grafting density, which resulted in an increase in protein adsorption.

#### 1.3.5.1.2 Polyzwitterionic brush surfaces

As an alternative to neutral hydrophilic brush surfaces, polyzwitterionic hydrophilic brush surfaces have been shown to possess effective antifouling characteristics, through

the same principle of highly-hydrated polymer surfaces with high hydrolytic and oxidative stability. Zwitterionic polymer coatings are electrically neutral coatings and can be classified into two main categories (i) polybetaines, carrying a positive and negative charge on the same monomer repeat unit, and (ii) polyampholyte copolymers, with 1:1 positive and negative charge on two different monomer units.[182] Based on their negatively charge moiety, polybetaines can be classified as polysulfobetaines (PSB), polycarboxybetaines (PCB) and polyphosphonobetaines (PPB). The electrostatically driven hydration in polyzwitterionic brushes includes strong binding of water molecules compared to the weak hydrogen bonding in neutral hydrophilic polymer brushes which makes the hydration layer even more robust and stable.[189] Polyampholytes are synthetic analogues of biomolecules such as proteins and constitute an important group of antifouling coatings due to their strong hydration via ionic solvation. Several examples of hydrophilic zwitterionic polymer brushes based on sulfobetaine methacrylate (SBMA) and carboxybetaine methacrylate (CBMA) have been utilized for the prevention of protein and bacterial adhesion in biomedical applications.[190] It is suggested that a nanoscale homogenous mixture of balanced charged moieties from polyzwitterionic materials is the key to control the antifouling properties.[182] Due to their synthetic flexibility, polyzwitterionic surfaces are considered the next generation of antifouling surfaces in several applications.

#### 1.3.5.1.3 Negatively-charged brush surfaces

Polymer brushes that display a negative charge have been shown to induce bacteria-repellent properties and reduction of the mass of biofilm formed during longer periods of time. Characteristic examples are the PSPMA and PGMA brushes functionalized with sulfonate groups. It was observed that the biofilm structures formed on negatively charged surfaces could be removed more easily at higher shear stress compared to the more homogeneous flat biofilm formed on a polycationic surface. Nevertheless, it has been observed that positively charged proteins such as lysozymes affect the repelling properties of negatively-charged surfaces.[45]

### 1.3.5.2 Bacteria-release polymer coatings

In principal, in antifouling surfaces the intermolecular forces between the surface and extracellular biomolecules are deteriorated. It is well known that the surface energy (γ)

is related to the intensity of microbial adhesion and growth on surfaces.[191] Hydrophilic polymers with high surface energies tend to retain a layer of water on top of them that limits the interactions of proteins with the surfaces, due to the thermodynamically unfavorable process of water rearrangement, which is required for protein adhesion.

On the contrary, the concept of bacteria-release surfaces does not prevent the attachment of microorganisms, however it relies on minimizing the initial adhesion strength of biomolecules on the surface followed by release under low shear stresses, usually a water flow.[186, 192] Hydrophobic polymers with very low surface energy and high interfacial energy with water, offer very weak protein or bacterial adhesion which can be detached by replacement with water molecules under low applied frictional forces (Figure 1.24). Common hydrophobic polymer coatings such as PS, PMMA, etc. are not antifouling and further treatment is necessary to introduce antifouling properties. Therefore, hydrophobic polymer coatings with low surface energies, usually below 20 mN / m and high interfacial energies with water, around 50 mJ / $m^2$ are named fouling-release coatings.[193] Bacteria-releasing polymer coatings can be obtained by either physical modification or chemical immobilization since the polymers have great stability under an aqueous environment.

Apart from, surface hydrophobicity and low surface energy, other parameters that influence the bacteria-release properties of a surface is the film thickness, the surface roughness and the elastic modulus of the material. Low surface energy polymer coatings, based on their chemical structure, are divided into silicones, such as polydimethylsiloxane (PDMS), and fluorinated polymers, such as poly(tetrafluoroethylene) (PTFE), which are widely explored, due to their low adhesion strength, good mechanical properties and bio-inertness.[194] According to the Baier curve (Figure 1.26), surfaces with intermediate WCA and high surface energy values are more prone to microbial fouling, whereas low surface energy and hydrophobic surfaces are less susceptible to fouling.[195]

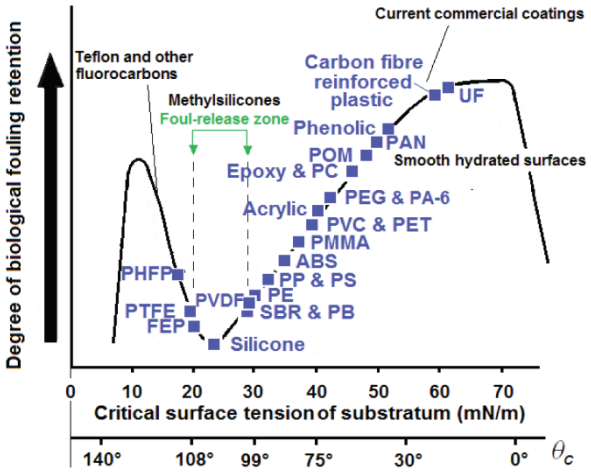


**Figure 1.26.** Baier curve of self-cleaning surfaces against biofilm formation.[196]

PDMS elastomers are known to reduce the adhesion of microorganisms due to their low critical surface energy (10-20 mN/m), low modulus, low micro-roughness and low glass transition temperature. The fundamental properties of PDMS originate by the siloxane bonds, which comprise a flexible backbone with low energy side groups. However, the major disadvantage of these materials is their poor adhesion when being coated on substrates.

Fluorinated polymer films are known for their non-polar nature and their ultra-low surface energy (<13 mN/m), high hydrophobicity and non-sticking characteristics. The low adhesion strength on fluoropolymers stems from the organized ordered structures of $-CF_3$ and $-CF_2$ moieties, which are exposed densely on the interface and minimize the surface energy and the surface molecular diffusion. PTFE is the most known commercial fluoropolymer for self-cleaning applications, however its crystallinity and complete insolubility in common organic solvents hinders its usage in more advanced applications. Extended research has been preferably focused on fluoropolymer coatings comprising fluorinated (meth-)acrylates, perfluoropolyethers and PEG modified fluoropolymers that offer smooth film structures with antifouling properties. Fluoropolymer coatings are shown to exhibit better antifouling properties than PDMS coatings, yet these materials undergo a reconstruction when immersed in water and thus lose their low surface energy and thus their long-term antifouling characteristics.[197] The increase of the fluorinated chain can result to lower surface energy values, nevertheless it poses the risk of releasing persistent organic pollutants. Thus, there is a need of a

minimum possible amount of fluorination to achieve lower surface energy. Compared to polyzwitterionic and polyhydrophilic brush surfaces, polymer brushes comprising low surface energy polymer chains have not been studied extensively against the fouling process of bacteria.

Nanostructured surfaces are also important, since effective air entrapment in their 3-D nanomorphology (spikes, pillars) renders them non-adhesive and slippery. The immobilization of polymer brushes on a nanostructured surface can enhance its superhydrophilicity/superhydrophobicity, thus reducing further the adhesion forces of bacteria.

### 1.3.6 Bactericidal polymer coatings

In contrast to antifouling polymers which are passive, and their action is restrained only as non-fouling coatings, antimicrobial polymers can either act similar to antibacterial agents in solution by inactivating the bacteria cells, or when they are anchored on surfaces, can as well promote bactericidal action after contact between the surfaces and the bacteria and degrade or kill the bacteria cells.

Based on their inactivation principle, bactericidal surfaces can be grouped into two prime categories: (a) surfaces with entrapped antibacterial agents that can be eluted upon interaction with an operational environment or (b) surfaces with immobilized polymeric antibacterial moieties that kill the adhered cells after contact. Polymer surfaces are considered as bactericidal materials, if they realize a reduction of colony forming units (CFU) greater than 2-log.[196]

#### 1.3.6.1 Bactericide-release coatings

Most commonly and adapted by living forms in nature, i.e. animals, plants, fungi, is the release of antimicrobial compounds, such as peptides and antibiotics for the simple purpose of preventing surfaces from fouling. The oldest approach for preventing bacterial biofilm formation is based on polymer coatings that dynamically release water soluble antibacterial agents or antibiotics in some predefined fashion. To date, leaching polymer surfaces are designed to carry biocides by physical adsorption, impregnation in the polymer matrix, complexation or conjugation, that can be released slowly locally and in vast amounts, in order to counteract the initial bacterial attachment. In these

systems, polymers are usually degradable or non-degradable biomaterials, that do not provide antimicrobial activity, thus their role is the active release of the antimicrobial agents. The leached bactericides typically form an outer inhibition zone and an inner kill zone that destroys microbes in the vicinity of the surface. Their performance is significantly influenced by the polymer surface, which determines the release rate of the bactericides.

The widely used categories of bactericide-release coatings in literature are classified based on their biocides and disinfectants i.e. antibiotic-releasing, metal-releasing, nitric oxide (NO)-releasing, QAS-releasing coatings, etc.[198] Since surfaces are leaching antimicrobial agents, the drawback of deposition of bacterial debris and intramolecular substances after killing is less possible, which comprise a major issue in contact-active bactericidal surfaces (see next paragraph).

Metal- and metal oxide-releasing bactericidal surfaces are the most employed surfaces that comprise designs of metal-doped, coated, metal-containing polymers, metal nanoparticles or metal thin films.[172b] Primarily, coatings containing silver nanoparticles, silver salts and silver sulfadiazine, which are capable of releasing silver ions ($Ag+$ ions) at the implementation site have been thoroughly designed. The bactericidal ability of these surfaces results from a multiple mechanism of action comprising oxidative stress induction, diffusion of metal ions from the surfaces and non-oxidative modes presented by a membrane disruption, penetration and interaction with DNA and proteins (binding with thiol groups, which are present on proteins and enzymes, and thus inactivating them). In addition, this multiple mechanism requires a plethora of different gene expressions, which is complicated for the bacteria to adapt and to develop resistance.[199] Silver, tin, zinc, gallium, selenium and copper are among the most employed bactericidal compounds for biomedical, domestic and marine applications, respectively. Nevertheless, the excessive usage of metals in deodorants, washing procedures etc. has resulted in waste water pollution and resistance to metals, while several have been ascribed as hazardous to sea life form and thus have been abandoned. Same issue stands for halogen (chlorine, iodine) containing compounds, phenols, quaternary ammonium salts, etc. This means that it is imperative that scientists design coatings that maintain the sufficient concentration range of the released agent for bacterial killing under a predetermined period of application with respect to the

applied environment, e.g. low cytotoxicity *in vivo*, contamination and accumulation in nature.[200]

Alternatives, such as antibiotic-release coatings based on aminoglycosides (gentamycin, tobramycin), penicillins (ampicillin), rifamicyns (rifampin), quinolones (ciprofaxin), tetracyclines (minocycline) and glycopeptides (vancomycin) or enzymes (lysozyme, acylase) and organic cationic-, non-cationic- and non-organic-releasing coatings i.e. QAS, chlorhexidine, cationic surfactants (CTAB), chitosan, NO, triclosan and furanones, have been applied within coatings for prevention of biofilm formation on medical devices (catheters and implants).[201] Nevertheless, a major limitation of these overall bactericidal release-based coatings arise from the difficulty to control the release rate and the concentration of the biocidal agents. Thus, either sub-lethal concentration release of antimicrobial agents induces antibiotic-resistance and enhancement of biofilm formation, or the reservoir of antimicrobial agents becomes exhausted and the bactericidal surface fails. Lately, antimicrobial coatings based on titanium dioxide, that produce unlimited antimicrobial reactive oxygen species (ROS) have been described as an alternative, but required activation by UV-light.[202]

**Polymer brushes.** Release-based bactericidal polymer brushes are less exploited due to the minority of antimicrobial agents that are appropriate for immobilization and controlled release from these coatings.[203] An example was given by Hu et al., with the incorporation of $Ag+$ ions in poly(3-sulfopropyl methacrylate) (PSPM) brushes grown from silicon and gold substrates. These systems were shown to completely inhibit the biofilm formation of *S. aureus* and *P. aeruginosa* bacterial strains, compared to PSPM brushes without silver ions, with slow leaching of the $Ag+$ ions under water and NaCl media.[203a] Lately, PCBMA brushes grown from gold substrates were loaded with silver ions, to provide surfaces with high bactericidal activity, due to the $Ag+$ ions, and potent antifouling activity, due to the PCBMA chains, against *E. coli* bacterial strain.[204]

### 1.3.6.2 Contact-killing coatings

To evade the reservoir exhaustion of release-based antimicrobial surfaces, contact-killing surfaces of immobilized polymer coatings, e.g. polymer brushes, possessing antimicrobial activity have been developed featuring monomeric antimicrobial compounds which are covalently attached to a polymer backbone and are capable of

leading to bacterial death.[205] In this approach, killing of microbes is furnished upon contact. The bactericidal action is derived from the whole structure of the antimicrobial polymer and not from the antimicrobial compound itself.

The main advantages of contact-killing compare to release-killing is that they: (a) offer an improved and prolonged antimicrobial activity, (b) are not likely to result in the development of antibiotic resistant strains -compared to antibiotics- due to the different mode of action, which involves physical damage of the bacterial cell walls/membranes and viral envelopes,[206] (c) provoke no undesirable effects on the physicochemical properties of the materials, and (d) possess non-toxic properties that do not affect the host tissues or immune systems in case of implants.[207]

Contact-killing coatings can be prepared either by (a) chemical immobilization methods, such as "grafting-to", "grafting-from", crosslinking polymerization and hydrogels or by (b) physical immobilization methods, e.g. physical adsorption using spin or dip coating and layer by layer deposition. Important aspect of these methods is to develop well-defined polymer structures with dense antimicrobial compounds that can afford high biocidal activity. In the literature, the most widely exploited substrates that have been coated with bactericidal polymers to study their efficacy as bactericidal surfaces are silicon, glass, gold, PET, wool, nylon etc.[69] The pendant antimicrobial compounds vary between (a) natural molecules, such as chitosan and its derivatives, photoactive metal and metal oxide nanoparticles (e.g. AgNPs), antimicrobial enzymes (AMEs) and peptides (AMPs) and (b) synthetic chemicals, such as quaternary ammonium salts (QAS), quaternary phosphonium salts (QPS), pyridinium and quanidinium moieties, n-halamines and antibiotics. The type of the polymer backbone also varies, with the most commonly attained being poly(meth)acrylates, poly(meth)acrylamides and polystyrenes.[208]

Coatings with polymeric antibiotics such as PEG/penicillin modified PTFE surfaces, have been used to obtain bactericidal surfaces with low toxicity. However a major drawback of this strategy is the induction of resistance and in many cases, the surfaces performed inhibited activity compared to the highly effective low molecular weight antibiotic analogues in solution, which means that the mechanism of their antimicrobial activity is hindered once they are attached on the surface.[201, 209] AMPs are produced by organisms such as plants, insects and are considered also as promising antibacterial

coatings having similar problems, as studies highlight the importance of providing the conjugated peptide with lateral mobility and appropriate orientation for its bactericidal efficacy.[200]

The hindering of the antimicrobial action of bactericides on surfaces compared to solution constitutes a major drawback of almost all surface bound immobile antimicrobial compounds. The significant aspect of polymer brushes is that they provide an anchor for the antimicrobial compounds through a flexible covalently bound polymer chain, which makes them still able to reach the site of action and eventually interact with the bacteria. Polycations bearing QAS or alkyl pyridinium moieties are the most extensively exploited antimicrobial polymers for the study of contact-killing polymer coatings. Bacteria adhere strongly on cationic surfaces, thus the strategy of constructing bactericidal surfaces using QAS groups is effective. Polymer brushes have been shown to be effective for anchoring QAS.[74a, 210] Quaternized forms of P4VP, polyethylene imine (PEI) and PDMAEMA are typical bactericidal polymers. A pioneer study of Klibanov et. al reported the grafting of poly(vinyl-N-hexylpyridinium) chains on HDPE, LDPE, nylon, PP and PET synthetic polymer surfaces using different alkyl bromides, to achieve 2-log reduction of gram-positive and gram-negative bacteria.[211] The non-leaching character of these systems was supported by zone of inhibition experiments and it was suggested that only long-polycationic end-grafted chains can act as bactericidal surfaces. Matyjaszewski's group employed the SI-ATRP technique to obtain PDMAEMA brushes bearing QAS groups with charge densities above $1\times10^{15}$ accessible quaternary amine units per $cm^2$, which was found important for surfaces with high bactericidal efficacy.[74a, 212] Quaternized chitosan was also modified with PHEMA brushes conferring bactericidal action on stainless steel surfaces.[213]

Polymer brushes with QAS are fabricated using two methods: (a) post-polymerization quaternization of functional polymer surfaces and (b) polymerization of monomers containing the quaternary ammonium moieties, coined as quaternary ammonium monomers. The drawback in these approaches is the poor molecular characterization of the polymer surfaces and the low polymerization yields, respectively.[207] The role of the charges is to attract and capture bacteria cells on the cationic polymer surfaces and further promote the interaction between the surface and the cell envelope. As mentioned by Charnley et al, the efficiency of these surfaces stems from the mobility of the cationic group, which is ensured by the binding to the surface through a polymeric spacer.[214]

However, the precise mechanism of action is yet under debate (see paragraph 1.3.6.2.1). Overall, polymer brushes bearing QAS groups have not found their use *in vivo* yet and further research is required in this direction.

#### 1.3.6.2.1 Mechanisms of bactericidal action of contact-killing coatings

##### 1.3.6.2.1.1 Mode of action of antimicrobial polymers in solution

Antimicrobial polymers are usually polycations resembling the architecture of amphiphilic surfactants, with the cationic groups acting as the hydrophilic parts that interact with the negatively charged phospholipid membrane of the bacteria and the alkyl chain aligned with the hydrophobic core of the phospholipid bilayer.

The mechanism of action of antimicrobial polymers was proposed by Ikeda et al. According to this concept, the positively charged antimicrobial polymers are attracted by the negatively charged outer membrane of i.e. gram-negative bacteria and are adsorbed through electrostatic interactions. The membrane's selective permeability and functionalities are misplaced, and the membrane is disrupted by hydrophobic interactions. Next, the antimicrobial polymers diffuse through the thin peptidoglycan wall and the inner cytoplasmic membrane is disoriented similarly to the outer membrane. For gram-positive bacteria, the absence of the outer membrane is camouflaged by a thicker cell wall, through which the polymers must diffuse in order to disrupt the plasmic membrane.

The interactions of bactericidal polymers in solution with bacterial cells have been explored by several groups, using molecular dynamic simulations, which have elucidated and strengthened the bactericidal mechanism. A putative model was proposed by Kuroda et al., in which the amphiphilic character of the polymers is highlighted, using poly-QAS statistical copolymers. The mode of action was based on the initial binding of the bactericidal polymers on specific sites of the cell surface and the formation of polymer-phospholipid complexes that cause instability and disruption of the phospholipid membrane (Figure 1.27). It was realized that in the aqueous solution, micelles are formed from the cationic polymers which are attracted through electrostatic attraction onto the negatively charged surface of the bacteria. The hydrophobic alkyl chains insert into the phospholipid bilayer causing damage, while the cationic moieties remain outside. According to this mechanism, any factor that

strengthens the interactions between the polymers and the bacteria affects the overall bactericidal activity. Unfortunately, a similar mechanism provokes mammalian cell toxicity. However, it is possible to control the cytotoxicity by employing optimized architectures and chemical structures. The immobilization of polycations on surfaces is considered to be the most effective approach to combine high biocidal activity with low cytotoxicity.

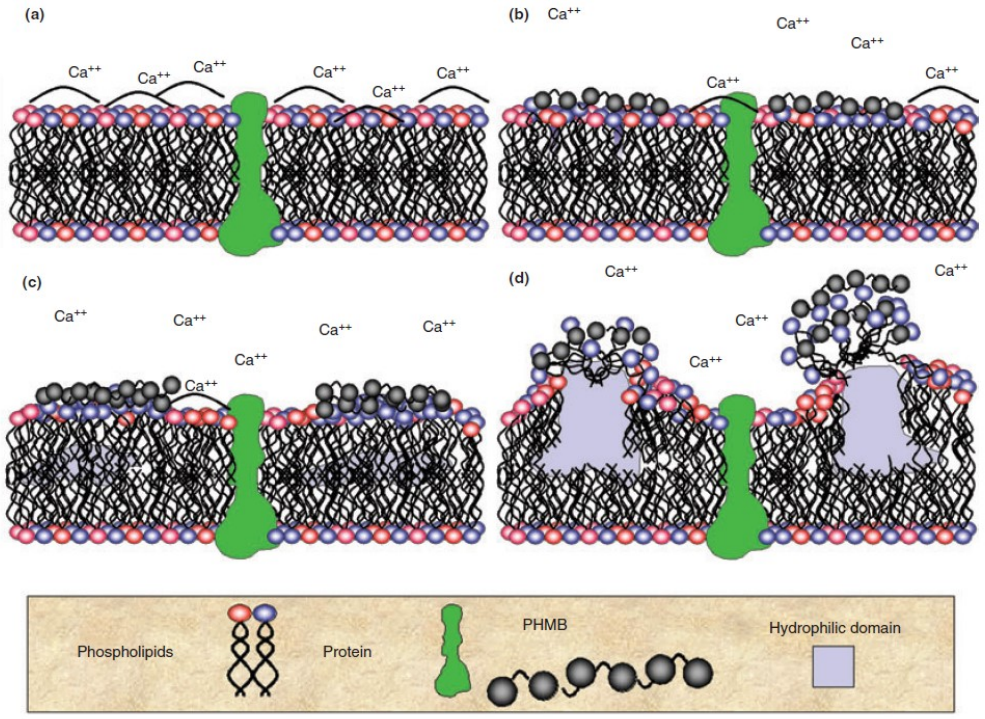


**Figure 1.27.** Schematic illustration of the mechanism of action of a cationic polymer against a bacterial cytoplasmic membrane.[215]

#### 1.3.6.2.1.2 Factors affecting bactericidal performance

The functional parameters that have a profound impact on the bactericidal efficiency of the polycations in solution are: (a) the molecular weight, and (b) hydrophilic/hydrophobic balance, which is related to (i) the polycation charge density, (ii) the N-alkyl chain length of the QAS and (iii) the counterion.

Molecular weight plays a key role in the physicochemical properties of polymers, and also influences the bactericidal activity of cationic polymers. Variation of the $M_w$ results in alteration of the length of the polymer backbone, the number of charged moieties and the overall hydrophobicity, and thus the interaction between bacteria cells

and the polymer. Selectivity and antimicrobial activity are enhanced with high $M_w$ cationic polymers, which provide higher electrostatic attraction and hydrophobic interactions. Ikeda et al. have found that the $M_w$ is the major factor in controlling the bactericidal activity of polycations following a bell-like shape dependence. It was claimed that the adsorption ability and capability of polymer molecules to diffuse and penetrate within the bacterial membrane increased with the $M_w$, whereas after an optimum value the bactericidal activity is concealed due to solubility and diffusion constrains. Several studies were carried out to understand the relationship of the $M_w$ with the bactericidal performance of polymers. In conclusion, an average $M_w$ is required for cationic polymers to possess biocidal activity, while a "sieving effect" is observed at high $M_w$'s, which describes the blocking of the polymers by the dense peptidoglycan cell-wall of gram-positive bacteria. Nevertheless, there are also dismissive studies about the effect of the $M_w$ on the antimicrobial activities of cationic polymers.[216]

Amphiphilicity or hydrophilic/hydrophobic balance is known to be the most crucial factor affecting the efficiency and selectivity of polymers towards microorganisms. In bactericidal polymers hydrophilicity is expressed by the presence of cationic groups alongside the polymer chain. These groups can be either permanent charges i.e. quaternized amines, or reversible charges i.e. primary, secondary and tertiary amines. Highly-charged hydrophilic polycations can attach on the negatively charged membranes of the bacteria, however the disruption of the membrane is not favorable in the absence of hydrophobic groups, which are typically alkyl groups, that can permeate through the cell membrane and afford lysis. The hydrophobic alkyl chains could be either a polymer backbone with a hydrophobic character or hydrophobic side chains attached to a hydrophilic polymer backbone.[166] Highly hydrophobic polymers have been found to be cytotoxic and hemolytic to all types of cells, as a result their selectivity and solubility in aqueous biological conditions and the overall biocidal performance is compromised. Thus, it is vital that the hydrophilic/hydrophobic ratio is kept at a certain balance to accomplish the desirable killing activity. The structural parameters that affect the amphiphilicity are the length of the substituted alkyl chains (ACLs), the polymer composition and the counterions.

It has been shown that an increase in the ACL of the side QAS group of the polymer chain, results in variation of the antibacterial activities. During bacteria invasion by polymer chains, the alkyl side chains align with the lipid molecules within the bacterial

membrane and affect its integrity. QAS can be grouped into short-chained and long chained below and above a threshold of 6 carbon atoms, respectively.[217] It has been shown that QAS groups, which bear long alkyl chains, between 12 and 14 carbon atoms, possess optimal bactericidal activity,.[218] Positive charges provide better electrostatic interaction of the surfaces with the negatively charged bacteria cells. Thus, it is obvious that the higher the charge density of a surface the more enhanced the electrostatic interactions and the antimicrobial activity. In addition, the counterions have been shown to affect the solubility of the QAS. If the counterions introduce high hydrophobicity, the solubility will be reduced in a polar environment. Moreover, when the counter anions are strongly bound onto the polymeric cations, an undesirable protection of the cations occurs, which affects the electrostatic attraction of the polymer by the bacterial membrane. There are conflicting reports in the literature on the effect of $Cl^-$, $Br^-$ and $I^-$ ions on the bactericidal behavior of polycations.[219] Additional parameters that affect the bactericidal activity of the polymers in solution are: (a) the type of the cationic group, (b) the position of the charge in the side chain, (c) the architecture of the polymer chains (statistical or block copolymers, polyzwitterions, etc.) and (d) the structure of the cationic groups (primary, tertiary, quaternary amines).

#### 1.3.6.2.1.3 Mechanism of contact-killing polymer coatings

Coatings of grafted bactericidal polymers are mostly cationic and kill after contact, upon microbial invasion on the surfaces. In contrast to cationic polymers in solution, the diffusion and binding of antimicrobial polymers on the bacterial cell membrane is disabled, due to the immobilization of the polymer chains on the surfaces.

Major key factors, affecting the antimicrobial efficiency of these surface immobilized polymers, have been claimed to be, either the polymer charge density (CD) or the alkyl chain length (ACL) of the cationic moieties, or both. The $M_w$ of the polymer and the film thickness have been also found crucial, only when they affect the coverage of the surface. The charge acts as a “fishing rod” that pulls negatively charged bacteria, for further interaction between the contact killing surface and the bacteria. The higher the CD of a surface the more enhanced the electrostatic interactions and thus the antimicrobial activity. Previous studies have shown that the optimum range of CDs should be above a critical threshold of $1\times10^{14}$ $N^+$ $cm^{-2}$ and surface charge densities

(SCDs) above $1\times10^{13}$ $N^{+}$ $cm^{-2}$ are required for an antibacterial active surface against gram-positive and gram-negative bacteria in high division conditions.[74a, 220]

Despite the fact that the role of cationic charges on the bacterial death is not doubted, the ACL effect is not yet fully understood, since the permeation of the cell wall membranes is questioned, due to the lack of degrees of freedom in the polymer chains that are attached on surfaces, compared to the respective polymer chains in solution, which results in discrete interactions with the bacterial cells.[221] In fact, the exact mechanism of antimicrobial immobilized QAS is under debate and investigations have revealed that they may act differently than the free and solvated QAS in solution.[166] In recent studies Klibanov et al. have shown that some bacteria that are immune to QAS in solution are prone and do not develop resistance when the QAS are surface bound as polymer coatings, which enhances the different mode of action.[222] So far, three different mechanisms are dominant in the literature, however is not certain yet that one of them can be considered as the primary concept for all polymeric bactericidal surfaces.

The first model describing the bactericidal action on surfaces was proposed in 2001 by Tiller and was considered to be analogous to the mode of action of antimicrobial polymers in solution. It described an insertion of the polymer chains into the core of the cell membrane. This early work, known as the "polymeric spacer effect" suggests that the penetration of cationic polymer chains into the bacterial cell membranes causes definitive killing via disruption of the outer cell-membrane for gram-negative bacteria or the cell wall and plasmic membrane for gram-positive bacteria, leading to cell lysis (Figure 1.28b). It was suggested that high $M_w$ alkylated P4VP grafted chains on surfaces with short alkyl chain lengths on the pyridinium ring, acting as a long-distance spacer carrying an antimicrobial agent, are capable of creating a hole on the bacterial cell wall with high bactericidal activities. Remarkably, the same polymer chains were not bactericidal in solution, while surfaces with low $M_w$ or alkylated with high chain lengths formed agglomerates and were not bactericidal as well. Experiments indicated that the immobilized polymeric chains must exist as individual entities (not entangled-agglomerates) to ensure antimicrobial activity. Many researchers found this assumption sensible and assessed the bactericidal activity of their systems by the penetration of flexible and long antimicrobial polymer chains in the bacterial membranes.

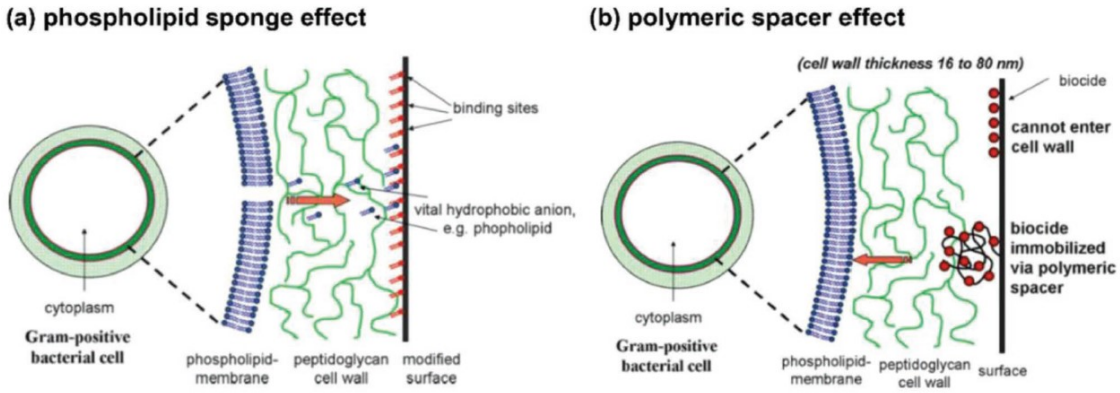


**Figure 1.28.** Mechanisms of contact-killing of polymer coatings based on the (a) phospholipid sponge effect and the (b) polymeric spacer effect.[223]

Several studies have been questioning whether the polymeric spacer model is the working mechanism for contact-active bactericidal surfaces based on QAS. Murata et al. employed quaternized PDMAEMA brushes with short alkyl chain lengths and reported a linear dependence of the biocidal activity with the charge density of the film, while the bactericidal activity did not seem to be related with the polymer chain length and the $M_w$.[74a] Similar to these results, many studies did not regard the polymeric spacer effect to be the mode of action of cationic polymer coatings.[212b] Thereafter, the "ion exchange model" was proposed by Kugler et al., which referred to a bacterial killing mechanism that involves an "ion exchange" between divalent cationic species, $Ca^{2+}$ and $Mg^{2+}$ present in the outer cell membrane of the bacteria with cations from the charged polymer surface.[220a] The role of the divalent cations is to neutralize the negatively charged phospholipid membrane and prevent the phospholipids from repelling each other causing instability to the membrane. It was proposed that during the bacteria invasion on surfaces, the divalent cations are released, and the membrane of the bacteria is disintegrated, which results to cell death. P4VP brushes were densely grafted on surfaces at lower film thicknesses than the thickness of a cell membrane or the cell wall of bacteria. In this manner, they proved that the only plausible action was due to electrostatic interactions between the polymer coatings and the bacterial cells and independent of the $M_w$. Towards this hypothesis, many researchers have based their work on the correlation between the charge density and the bactericidal activity.

In synopsis, during the past decade two mechanisms were favored as dominant mode of actions, based on either damaging the cell membranes through poking of long

cationic polymer chains that are grafted on surfaces (a) or on an exchange of divalent cations between highly charged surfaces, above a charge density threshold, and the bacteria (b). Lately, a third mechanism the "phospholipid sponge effect" was introduced, by Bieser and Tiller which involves the selective attraction and subsequent adsorption of anionic phospholipids from the bacterial cell membrane towards a cationic polymer coating.[224] This immigration of the negative charged liposomes toward the polymer "sponge" coating could result in disintegration and formation of holes on the membrane of bacteria (Figure 1.28a). Moreover, it was shown that the bactericidal activity is highly affected by two factors, the charge density and the hydrophilicity/hydrophobicity of the surface. The phospholipid sponge effect has been evidenced by several researchers.[225] A relatively similar mechanism, that applies only to bactericidal polymer brushes or surface grafted coatings was proposed by Asri et al. and suggests that, locally enhanced attractive forces exist between the anionic lipids of the bacteria envelope and the positively charged quaternary ammonium salt species of the polymer.[221] The adhesive forces are orders of magnitude higher than the typical forces that the bacteria receive, and compromise their growth.

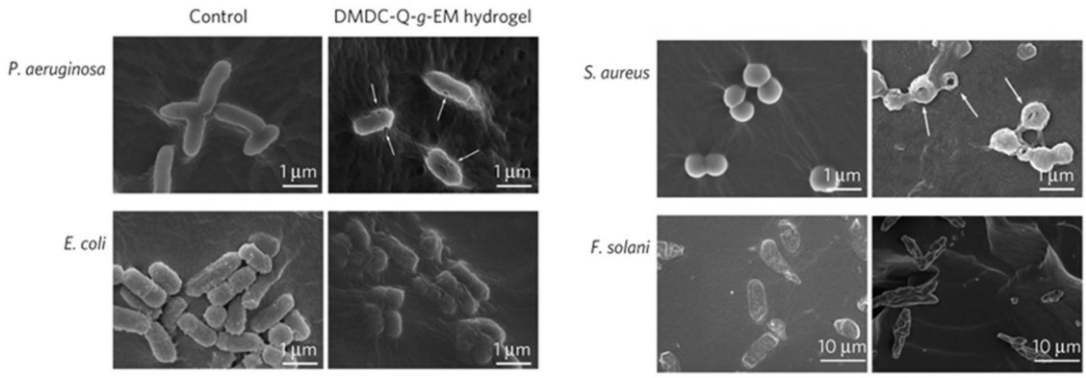


**Figure 1.29.** SEM of different bacteria species on a control sample (left) and on a QAS-based surface (right). Either hole formation or cell membrane deformation is visible after contact with the antimicrobial surfaces.[222]

The common outcome from all these mechanisms is the bacteria cell wall/membrane disruption, which was proved by the formation of holes observed by scanning electron microscopy (SEM), through the attraction and capture of negatively charged bacteria on the charged QAS-based polymer surfaces (Figure 1.29).[226] Nevertheless, that does not indicate how it occurs and it is possible that a combination or all the proposed mechanisms take place depending on the surface.[222]

### 1.3.7 Dual-function antimicrobial surfaces

The drawback of antifouling surfaces remains their incompetence to impact on the mortality of pathogenic microbes; thus, the non-attached microorganisms can still contaminate other surfaces. For the application of bactericidal contact-killing polymer surfaces, long term exposure of the bactericidal groups to the biological environment results in a decrease of the killing efficiency and an increase of the toxicity to normal cells or tissues, whereas, coatings based on the bactericide-releasing mechanism may suffer of premature depletion of bactericides, emergence of resistance or other undesired side effects. In simple words, the major problem of the existing antimicrobial and antifouling surfaces is the loss of effectiveness over time. Zou et al. poetically stated that "It takes walls and knights to defend a castle" referring to antimicrobial and antifouling surfaces.[227] Thereby, it is promising to endow a combination of antifouling and bactericidal surface properties by a "kill-and-release" strategy of smart antibacterial coatings.

#### 1.3.7.1 Bacteria-repelling and bacteria-releasing antifouling surfaces

This class of dual function surfaces are not bactericidal surfaces and are commonly attained for marine applications, due to the fact that these surfaces can inhibit the multistep fouling process of microorganisms and/or reduce the adhesion forces between the surface and the attached bacteria, which results in the removal of the latter under certain conditions. Cheng et al. studied the antifouling properties of carboxybetaine-functionalized polysiloxane (PDMS-g-CB) blend films on polydimethylsiloxane (PDMS) elastomers, which were found to inhibit the adhesion of *E. coli* compared to untreated PDMS, while it did not exhibit any bactericidal activity, skin irritation and toxicity.[228] Yeh et al. developed a stable superhydrophilic zwitterionic interface on a PDMS elastomer by covalent silanization of sulfobetaine silane (SBSi) to resist nonspecific adsorption of bacteria, proteins, and lipids with high stability and no cytotoxicity.[229]

#### 1.3.7.2 Bactericide-releasing and contact-killing bactericidal surfaces.

Contact-killing and bactericide-releasing antibacterial surfaces comprise both bactericidal units and bactericide-releasing units to realize both specific functions against pathogens. These surfaces are significantly interesting, due to the fact that they

can minimize the selection and proliferation of resistant bacteria strains, providing prolonged bactericidal efficacy. Li et al. designed coatings with both bactericide-release and contact-killing capabilities. They combined LbL-deposited reservoir of PAH and PAA bilayers incorporated silver under a NP surface cap with immobilized QAS groups. The silver release provided strong initial bactericidal effect, whereas upon exhaustion the QAS moieties retained the bactericidal activity.[230] Since then, a variety combinations have been attained.[231] Lately Yin et al, showed that the incorporation of silver NPs in PQDMAEMA brushes, quaternized with ethyl and hexyl bromides, resulted in bifunctional antimicrobial surfaces against gram-positive and gram-negative bacteria strains.[232] A similar bactericidal activity was observed by Sambhy et al., when coating surfaces with a cationic polymer and silver bromide NPs. The coatings were capable of killing both gram-negative and gram-positive bacteria on surfaces and in solution.[233]

#### 1.3.7.3 Bactericidal and bacteria-repelling antibacterial surfaces

This strategy relies on the combination of contact-killing or bactericide-release surface bearing antifouling moieties.

**Bactericide-release and bacteria-repelling/releasing surfaces.** This class of dual function surfaces includes the use of an inherent low adhesive polymer incorporating active moieties. These coatings can inhibit the attachment of bacteria by killing, followed by their ability to repel the debris. Examples of this approach include the use of poly(vinyl alcohol) (PVA), PEG-based copolymers or PAA-based hydrogel coatings, that exhibit high bacteria-repelling properties, and at the same time, are loaded with antibiotics or other bactericides, which are released locally. Tiller et al. prepared antimicrobial surfaces with a rather complex network structure using PHEA with PEI cross-link points. The network was capable of creating complexes with silver ions from solution.[234] The introduction of an outer PEG layer on these networks, provided polymeric networks with high bactericidal efficacy against gram-positive bacteria, that are repelled after the exhaustion of the silver ion reservoir. Yin et al, prepared a LbL-deposited coating of PEI and PAA, loaded with silver NPs, and modified with a fluorinated layer to endow the surface an antifouling character. The release of $Ag^+$ was prolonged compared to the unmodified coatings and the surface wettability switched to the superhydrophobic state, introducing an antifouling character to the surface.[235]

**Contact killing and bacteria-repelling surfaces.** Another approach combines contact-killing bactericidal polymer chains with bacteria-repelling properties in order to retain the antimicrobial efficacy of the surfaces. Yang et. al, prepared PHEMA polymer brushes on stainless steel via SI-ATRP, followed by coupling of CS to introduce a dual-functional surface. The PHEMA chains offered a superhydrophilic bacteria-repelling activity, while CS provided the ammonium charges for bacteria killing.[213] Lately, Yan et al., prepared polymer brushes comprising an inner antifouling PEGMA layer and a low density-grafted PQDMAEMA-C2 outer bactericidal layer for an effective long-term antibacterial action underwater (Figure 1.30).[236]

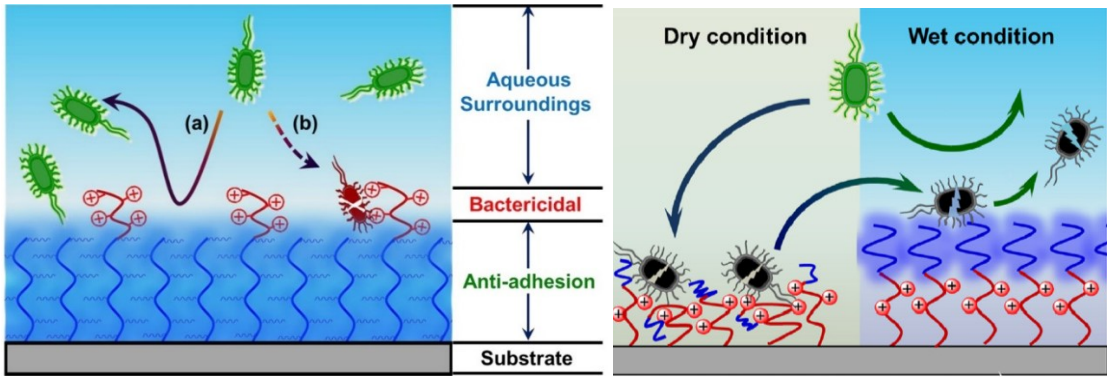


**Figure 1.30.** Schematic Illustrations of the surface with integrated antifouling and bactericidal capabilities. On the left the surface consists of two functional layers, namely a highly dense PEG bottom layer for bacterial repellence and a loose QAC top layer for bactericidal action. [236] On the right, under dry conditions a zwitterionic PSBMA outer layer is collapsed and the PQDMAEMA layer acts as the contact-killing layer, whereas under wet conditions the highly hydrated PSBMA layer swells transforming the surface to bacteria-repellent and bacteria-releasing.

### 1.3.7.4 Smart switchable antibacterial coatings.

Lately, several studies have focused on developing smart antibacterial coatings that can switch their antibacterial properties in the presence of an external stimulus such as pH or temperature. This was mostly deprived by the demand of combining bactericidal and antifouling properties at will. A pioneer work of Laloyaux et. al., was the development of novel smart coatings that can switch reversibly between bactericidal and bacteria repellent, mediated by an external thermal stimulus.[237] A thermo-sensitive copolymer comprising 2-(2-methoxyehoxy)ethyl methacrylate ($MEO_2MA$), OEGMA and HEMA was grown from silicon substrates to form polymer brushes, followed by the grafting

of AMP magainin-I on the polymer. At temperatures slightly above the characteristic collapse transition temperature $T_{coll}$ of the polymer, the end-grafted polymer chains are in a collapsed state, with the OEGMA exposed segments acting as bacteria-repellent surfaces. Decreasing the temperature below $T_{coll}$, the polymer chains swell gradually, and the solvated polymer brushes promote the lethal contact of AMP with bacteria, which results to contact killing bactericidal surfaces. Similarly, thermoresponsive copolymer brushes based on PNiPAam were prepared to switch the antibacterial properties of the surfaces above and below the LCST.[238]

Another category of switchable antibacterial coatings are those developed by Jiang's team that can alter their chemical structure from a cationic form to a zwitterionic form by changing the solution pH.[239] Polymer brushes based on poly(2-((2-hydroxy-3-(methacryloyloxy)propyl)dimethylammino)acetate) (PCBOH), were shown to possess bactericidal properties upon treatment with TFA, by forming brushes with a ring structure bearing QAS groups, and bacteria-repelling properties, after hydrolysis in a weak base, due to the formation of zwitterionic groups.

Finally, antibacterial coatings based on moisture switching under dry and wet conditions have been studied. For example, hierarchical brushes with a zwitterionic PSBMA outer layer and a cationic bactericidal inner layer (PQDMAEMA) were prepared via SI-PIMP.[240] In dry conditions the PSBMA brush collapses to facilitate bacteria adhesion and contact killing. In wet conditions, strong hydration causes PSBMA to swell and the hydration layer promotes bacteria repelling and dead bacteria release (Figure 1.30). These surfaces exhibit a switchable antibacterial mechanism that kills airborne bacteria on the surface during dry storage and releases dead bacteria while repelling further attachment of planktonic bacteria in aqueous environments, rendering them extremely promising for applications in medical devices.

## 1.4 Aim of this work

This thesis presents the synthesis and characterization of novel, well-defined polymer brushes, bearing desirable functionalities, via SI-ATRP. The surface properties and the antimicrobial performance of the brushes were studied rendering them attractive for use as lubricants and/or antimicrobial surfaces in the solid state. The thesis is organized as

following: after, a general introduction to the field of polymer brushes, their synthesis and properties (Chapter 1), Chapter 2 presents the experimental part of the work used for the synthesis of homopolymer, diblock copolymer and binary mixed polymer brushes and their physicochemical and antimicrobial characterization.

Chapter 3 discusses the influence of the different polymer brush functionalities on the surface properties of the films. Homopolymer brushes based on poly(2-(dimethylamino)ethyl methacrylate) (PDMAEMA) or fluorinated methacrylates, were synthesized, via surface-initiated atom transfer radical polymerization (SI-ATRP), on glass and silicon substrates. Three different fluorinated methacrylates, with fluorinated alkyl chain lengths (FCLs = 1 4 and 6 fluorocarbon atoms) in the side-groups, referred to as TFEMA, OFPMA and TDFOMA, respectively, were utilized for the synthesis of semi-fluorinated brushes. The tertiary amine groups of the PDMAEMA brushes were modified via a quaternization reaction, using different alkyl halides, to obtain quaternized PDMAEMA (PQDMAEMA) cationic brushes. Variations in the hydrophilicity/hydrophobicity and the surface free energy of the brush, as a function of the FCL and the ACL of the quaternization agent, were determined by static contact angle (CA) measurements. A hydrophilic to hydrophobic transition of the surfaces and a significant decrease of the degree of quaternization of the DMAEMA moieties was found upon increasing the ACL of the quaternization agent above six carbon atoms, allowing to tune the wettability, the thickness and the pH-response of the brushes via a facile post-polymerization, quaternization reaction. AFM silicon nitride tips were used to examine the adhesion and friction properties of the homopolymer brushes against sliding inorganic surfaces. Finally, the hydrophilic, PDMAEMA and PQDMAEMA, brushes suffered from high instability and degrafting of the polymer chains in water, due to the hydrolysis of the labile, ester or siloxane bonds of the surface-bound initiator, that is mechanically driven by the tension on the chains, whereas, all fluorinated brushes were stable due to the inhibition of the penetration of water molecules at the polymer-substrate interphase.

In Chapter 4, novel diblock copolymer brushes, PDMAEMA-*b*-PTFEMA, PDMAEMA-*b*-POFPMA and PDMAEMA-*b*-PTDFOMA, were synthesized via sequential SI-ATRP. Two families of brushes were prepared, the first comprising a lower content of the fluorocarbon block and the second comprising an almost symmetric amphiphilic diblock copolymer. The reorganization of the amphiphilic

diblock copolymer chains and the switching of the film wettability, upon exposure to selective solvents for the two blocks, were observed and were influenced by the ratio of the two blocks. Quaternization of the DMAEMA groups, deteriorated the responsive behavior of the brushes, owing to the large $\chi$ value between the two very dissimilar blocks (charged PQDMAEMA and semi-fluorinated polymethacrylates). Nevertheless, evidence of unwanted chain degrafting was found again, attributed to hydrolysis, after exposure of the brushes in aqueous media for prolonged time periods.

In Chapter 5, the synthesis of amphiphilic binary mixed polymer brushes, comprising functional PDMAEMA chains and low-surface energy PTFEMA, POFPMA or PTDFOMA chains, is presented. Two different methods for the preparation of the mixed ATRP initiator SAMs were studied to find the optimal conditions for the mixed brush formation. Next, semi-fluorinated homopolymer chains were grafted from the silicon substrates, followed by the growth of the PDMAEMA chains, via a two-step SI-ATRP process. The surface properties (wettability, surface energy and friction of the mixed brushes, upon treatment with selective solvents for the two polymers, were investigated by contact angle measurements, AFM and LFM studies. These surfaces exhibited tunable wettability, friction and surface energies, in response to external stimuli, which renders them attractive for use as "smart" responsive surfaces in the dry state. Quaternization of PDMAEMA affected significantly the responsive behavior of these brushes, similar to the diblock copolymer brushes discussed in Chapter 4. Finally, the amphiphilic mixed polymer brushes exhibited a remarkable stability in aqueous media with the fluorinated polymer acting as a carpet to shield the labile initiator bonds from hydrolysis.

The last chapter (Chapter 6) deals with the antimicrobial activity of the prepared polymer brushes. Antimicrobial polymer coatings provide an effective approach for the long-lasting sterilization of surfaces against biofilm formation. The effect of the ACL of the PQDMAEMA brushes, was investigated. Antimicrobial tests revealed that the hydrophilic polymer brushes exhibited enhanced bactericidal activity against *Escherichia coli* (*E. coli*) and *Bacillus cereus* (*B. cereus)*, whereas the hydrophobic surfaces showed a significant deterioration of the *in vitro* bactericidal performance. In another approach, the antifouling activity (bacterial-releasing properties) of the semi-fluorinated homopolymer brushes, bearing different FCLs on the polymer side groups, was found to increase with the number of fluorocarbon atoms. These results elucidate

the antimicrobial action of quaternized polymer brushes and low-surface energy fluorinated brushes, dictating the appropriate choice of the ACL or the FCL, for the development of coatings that effectively inhibit biofilm formation on surfaces either by killing or by releasing the bacteria. Finally, dual functional coatings, comprising the bacterial-releasing fluorinated chains, PTFEMA, POFPMA or PTDFOMA, and the bactericidal PQDMAEMA chains, in binary mixed polymer brushes, were shown to possess significantly improved antimicrobial performance, against both *E. coli* and *B. cereus*, due to their combined antifouling and bacteria killing action.

## 1.5 References

1. (a) Sagiv, J., Organized Monolayers by Adsorption .1. Formation and Structure of Oleophobic Mixed Monolayers on Solid-Surfaces. *J Am Chem Soc* **1980,** *102* (1), 92-98; (b) Nuzzo, R. G.; Allara, D. L., Adsorption of Bifunctional Organic Disulfides on Gold Surfaces. *J Am Chem Soc* **1983,** *105* (13), 4481-4483.
2. Watson, S.; Nie, M.; Wang, L.; Stokes, K., Challenges and developments of self-assembled monolayers and polymer brushes as a green lubrication solution for tribological applications. *Rsc Adv* **2015,** *5* (109), 89698-89730.
3. (a) Milner, S., Polymer brushes. *Science* **1991,** *251* (4996), 905-914; (b) Zhao, B.; Brittain, W. J., Polymer brushes: surface-immobilized macromolecules. *Prog Polym Sci* **2000,** *25* (5), 677-710.
4. (a) Egorov, S. A.; Hsu, H. P.; Milchev, A.; Binder, K., Semiflexible polymer brushes and the brush-mushroom crossover. *Soft Matter* **2015,** *11* (13), 2604-16; (b) Moh, L. C.; Losego, M. D.; Braun, P. V., Solvent quality effects on scaling behavior of poly(methyl methacrylate) brushes in the moderate- and high-density regimes. *Langmuir* **2011,** *27* (7), 3698-702; (c) Zhou, F.; Huck, W. T., Surface grafted polymer brushes as ideal building blocks for "smart" surfaces. *Phys Chem Chem Phys* **2006,** *8* (33), 3815-23.
5. Matyjaszewski, K.; Spanswick, J., Atom Transfer Radical Polymerization (ATRP). In *Reference Module in Materials Science and Materials Engineering*, Elsevier: 2016.
6. Hadziioannou, G.; Patel, S.; Granick, S.; Tirrell, M., Forces between surfaces of block copolymers adsorbed on mica. *J Am Chem Soc* **1986,** *108* (11), 2869-2876.
7. Luzinov, I.; Julthongpiput, D.; Malz, H.; Pionteck, J.; Tsukruk, V. V., Polystyrene layers grafted to epoxy-modified silicon surfaces. *Macromolecules* **2000,** *33* (3), 1043-1048.
8. Lukas, M.; Leonie, B.; Christopher, B.-K., Polymer on Top: Current Limits and Future Perspectives of Quantitatively Evaluating Surface Grafting. *Adv Mater* **2018,** *30* (21), 1706321.
9. Jennings, G. K.; Brantley, E. L., Physicochemical properties of surface-initiated polymer films in the modification and processing of materials. *Adv Mater* **2004,** *16* (22), 1983-1994.
10. Klok, H. A.; Genzer, J., Expanding the Polymer Mechanochemistry Toolbox through Surface-Initiated Polymerization. *Acs Macro Lett* **2015,** *4* (6), 636-639.

11. Kang, C.; Crockett, R.; Spencer, N. D., The influence of surface grafting on the growth rate of polymer chains. *Polym Chem-Uk* **2016,** *7* (2), 302-309.
12. Datta, P.; Genzer, J., "Grafting through" polymerization involving surface-bound monomers. *Journal of Polymer Science Part A: Polymer Chemistry* **2016,** *54* (2), 263-274.
13. Das, S.; Banik, M.; Chen, G.; Sinha, S.; Mukherjee, R., Polyelectrolyte brushes: theory, modelling, synthesis and applications. *Soft Matter* **2015,** *11* (44), 8550-8583.
14. (a) Pyun, J.; Kowalewski, T.; Matyjaszewski, K., Synthesis of Polymer Brushes Using Atom Transfer Radical Polymerization. *Macromol Rapid Comm* **2003,** *24* (18), 1043-1059; (b) Baum, M.; Brittain, W. J., Synthesis of Polymer Brushes on Silicate Substrates via Reversible Addition Fragmentation Chain Transfer Technique. *Macromolecules* **2002,** *35* (3), 610-615; (c) Brinks, M. K.; Studer, A., Polymer Brushes by Nitroxide-Mediated Polymerization. *Macromol Rapid Comm* **2009,** *30* (13), 1043-1057.
15. (a) Wang, J. S.; Matyjaszewski, K., Controlled Living Radical Polymerization - Atom-Transfer Radical Polymerization in the Presence of Transition-Metal Complexes. *J Am Chem Soc* **1995,** *117* (20), 5614-5615; (b) Kato, M.; Kamigaito, M.; Sawamoto, M.; Higashimura, T., Polymerization of Methyl-Methacrylate with the Carbon-Tetrachloride Dichlorotris(Triphenylphosphine)Ruthenium(Ii) Methylaluminum Bis(2,6-Di-Tert-Butylphenoxide) Initiating System - Possibility of Living Radical Polymerization. *Macromolecules* **1995,** *28* (5), 1721-1723.
16. Curran, D. P., The Design and Application of Free Radical Chain Reactions in Organic Synthesis. Part 2. *Synthesis* **1988,** *1988* (07), 489-513.
17. Pintauer, T.; Matyjaszewski, K., Structural aspects of copper catalyzed atom transfer radical polymerization. *Coordination Chemistry Reviews* **2005,** *249* (11), 1155-1184.
18. Matyjaszewski, K.; Xia, J. H., Atom transfer radical polymerization. *Chemical Reviews* **2001,** *101* (9), 2921-2990.
19. (a) Matyjaszewski, K., Introduction to Living Polymerization, Living and/or Controlled Polymerization. *J Phys Org Chem* **1995,** *8* (4), 197-207; (b) Matyjaszewski, K.; Gaynor, S.; Greszta, D.; Mardare, D.; Shigemoto, T., Living and Controlled Radical Polymerization. *J Phys Org Chem* **1995,** *8* (4), 306-315.
20. Matyjaszewski, K., Advanced Materials by Atom Transfer Radical Polymerization. *Adv Mater* **2018,** *30* (23), 1706441.
21. (a) Matyjaszewski, K.; Paik, H. J.; Zhou, P.; Diamanti, S. J., Determination of activation and deactivation rate constants of model compounds in atom transfer radical polymerization. *Macromolecules* **2001,** *34* (15), 5125-5131; (b) Tang, W.; Matyjaszewski, K., Effect of ligand structure on activation rate constants in ATRP. *Macromolecules* **2006,** *39* (15), 4953-4959; (c) Tang, W.; Tsarevsky, N. V.; Matyjaszewski, K., Determination of equilibrium constants for atom transfer radical polymerization. *J Am Chem Soc* **2006,** *128* (5), 1598-1604; (d) Tang, W.; Kwak, Y.; Braunecker, W.; Tsarevsky, N. V.; Coote, M. L.; Matyjaszewski, K., Understanding atom transfer radical polymerization: Effect of ligand and initiator structures on the equilibrium constants. *J Am Chem Soc* **2008,** *130* (32), 10702-10713.
22. Wang, T.-L.; Liu, Y.-Z.; Jeng, B.-C.; Cai, Y.-C., The Effect of Initiators and Reaction Conditions on the Polymer Syntheses by Atom Transfer Radical Polymerization. *J Polym Res* **2005,** *12* (2), 67-75.
23. Tang, W.; Matyjaszewski, K., Effects of Initiator Structure on Activation Rate Constants in ATRP. *Macromolecules* **2007,** *40* (6), 1858-1863.

24. di Lena, F.; Matyjaszewski, K., Transition metal catalysts for controlled radical polymerization. *Prog Polym Sci* **2010,** *35* (8), 959-1021.
25. (a) Tsarevsky, N. V.; Matyjaszewski, K., "Green" Atom Transfer Radical Polymerization: From Process Design to Preparation of Well-Defined Environmentally Friendly Polymeric Materials. *Chemical Reviews* **2007,** *107* (6), 2270-2299; (b) Xia, J.; Johnson, T.; Gaynor, S. G.; Matyjaszewski, K.; DeSimone, J., Atom Transfer Radical Polymerization in Supercritical Carbon Dioxide. *Macromolecules* **1999,** *32* (15), 4802-4805; (c) Simakova, A.; Averick, S. E.; Konkolewicz, D.; Matyjaszewski, K., Aqueous ARGET ATRP. *Macromolecules* **2012,** *45* (16), 6371-6379; (d) Coca, S.; Jasieczek, C. B.; Beers, K. L.; Matyjaszewski, K., Polymerization of acrylates by atom transfer radical polymerization. Homopolymerization of 2-hydroxyethyl acrylate. *Journal of Polymer Science Part A: Polymer Chemistry* **1998,** *36* (9), 1417-1424; (e) Duxbury, C. J.; Wang, W.; de Geus, M.; Heise, A.; Howdle, S. M., Can Block Copolymers Be Synthesized by a Single-Step Chemoenzymatic Route in Supercritical Carbon Dioxide? *J Am Chem Soc* **2005,** *127* (8), 2384-2385; (f) Biedroń, T.; Kubisa, P., Ionic liquids as reaction media for polymerization processes: atom transfer radical polymerization (ATRP) of acrylates in ionic liquids. *Polym Int* **2003,** *52* (10), 1584-1588; (g) Perrier, S.; Gemici, H.; Li, S., Poly(ethylene glycol) as solvent for transition metal mediated living radical polymerisation. *Chem Commun* **2004,** (5), 604-605.
26. (a) Braunecker, W. A.; Tsarevsky, N. V.; Gennaro, A.; Matyjaszewski, K., Thermodynamic Components of the Atom Transfer Radical Polymerization Equilibrium: Quantifying Solvent Effects. *Macromolecules* **2009,** *42* (17), 6348-6360; (b) Seeliger, F.; Matyjaszewski, K., Temperature Effect on Activation Rate Constants in ATRP: New Mechanistic Insights into the Activation Process. *Macromolecules* **2009,** *42* (16), 6050-6055; (c) Kwiatkowski, P.; Jurczak, J.; Pietrasik, J.; Jakubowski, W.; Mueller, L.; Matyjaszewski, K., High Molecular Weight Polymethacrylates by AGET ATRP under High Pressure. *Macromolecules* **2008,** *41* (4), 1067-1069.
27. Tsarevsky, N. V.; Braunecker, W. A.; Vacca, A.; Gans, P.; Matyjaszewski, K., Competitive Equilibria in Atom Transfer Radical Polymerization. *Macromol Symp* **2007,** *248* (1), 60-70.
28. Chmielarz, P.; Fantin, M.; Park, S.; Isse, A. A.; Gennaro, A.; Magenau, A. J. D.; Sobkowiak, A.; Matyjaszewski, K., Electrochemically mediated atom transfer radical polymerization (eATRP). *Prog Polym Sci* **2017,** *69*, 47-78.
29. (a) Matyjaszewski, K.; Miller, P. J.; Shukla, N.; Immaraporn, B.; Gelman, A.; Luokala, B. B.; Siclovan, T. M.; Kickelbick, G.; Vallant, T.; Hoffmann, H.; Pakula, T., Polymers at Interfaces: Using Atom Transfer Radical Polymerization in the Controlled Growth of Homopolymers and Block Copolymers from Silicon Surfaces in the Absence of Untethered Sacrificial Initiator. *Macromolecules* **1999,** *32* (26), 8716-8724; (b) Hui, C. M.; Pietrasik, J.; Schmitt, M.; Mahoney, C.; Choi, J.; Bockstaller, M. R.; Matyjaszewski, K., Surface-Initiated Polymerization as an Enabling Tool for Multifunctional (Nano-)Engineered Hybrid Materials. *Chem Mater* **2014,** *26* (1), 745-762; (c) Kruk, M.; Dufour, B.; Celer, E. B.; Kowalewski, T.; Jaroniec, M.; Matyjaszewski, K., Grafting Monodisperse Polymer Chains from Concave Surfaces of Ordered Mesoporous Silicas. *Macromolecules* **2008,** *41* (22), 8584-8591.
30. (a) Ejaz, M.; Yamamoto, S.; Ohno, K.; Tsujii, Y.; Fukuda, T., Controlled graft polymerization of methyl methacrylate on silicon substrate by the combined use of the Langmuir-Blodgett and atom transfer radical polymerization techniques. *Macromolecules* **1998,** *31* (17), 5934-5936; (b) Huang, X. Y.; Wirth, M. J., Surface-initiated radical polymerization on porous silica. *Anal Chem* **1997,** *69* (22), 4577-4580.

31. Barbey, R.; Lavanant, L.; Paripovic, D.; Schüwer, N.; Sugnaux, C.; Tugulu, S.; Klok, H.-A., Polymer Brushes via Surface-Initiated Controlled Radical Polymerization: Synthesis, Characterization, Properties, and Applications. *Chemical Reviews* **2009,** *109* (11), 5437-5527.
32. Yamamoto, S.; Ejaz, M.; Tsujii, Y.; Fukuda, T., Surface Interaction Forces of Well-Defined, High-Density Polymer Brushes Studied by Atomic Force Microscopy. 2. Effect of Graft Density. *Macromolecules* **2000,** *33* (15), 5608-5612.
33. Tugulu, S.; Klok, H.-A., Stability and Nonfouling Properties of Poly(poly(ethylene glycol) methacrylate) Brushes under Cell Culture Conditions. *Biomacromolecules* **2008,** *9* (3), 906-912.
34. Huang, C.; Tassone, T.; Woodberry, K.; Sunday, D.; Green, D. L., Impact of ATRP Initiator Spacer Length on Grafting Poly(methyl methacrylate) from Silica Nanoparticles. *Langmuir* **2009,** *25* (23), 13351-13360.
35. Matyjaszewski, K.; Miller, P. J.; Shukla, N.; Immaraporn, B.; Gelman, A.; Luokala, B. B.; Siclovan, T. M.; Kickelbick, G.; Vallant, T.; Hoffmann, H.; Pakula, T., Polymers at interfaces: Using atom transfer radical polymerization in the controlled growth of homopolymers and block copolymers from silicon surfaces in the absence of untethered sacrificial initiator. *Macromolecules* **1999,** *32* (26), 8716-8724.
36. Edmondson, S.; Vo, C.-D.; Armes, S. P.; Unali, G.-F., Surface Polymerization from Planar Surfaces by Atom Transfer Radical Polymerization Using Polyelectrolytic Macroinitiators. *Macromolecules* **2007,** *40* (15), 5271-5278.
37. (a) Gao, X.; Feng, W.; Zhu, S.; Sheardown, H.; Brash, J. L., Kinetic Modeling of Surface-Initiated Atom Transfer Radical Polymerization. *Macromolecular Reaction Engineering* **2010,** *4* (3-4), 235-250; (b) Xiao, D.; Wirth, M. J., Kinetics of Surface-Initiated Atom Transfer Radical Polymerization of Acrylamide on Silica. *Macromolecules* **2002,** *35* (8), 2919-2925.
38. Yamamoto, S.; Ejaz, M.; Tsujii, Y.; Matsumoto, M.; Fukuda, T., Surface Interaction Forces of Well-Defined, High-Density Polymer Brushes Studied by Atomic Force Microscopy. 1. Effect of Chain Length. *Macromolecules* **2000,** *33* (15), 5602-5607.
39. Pyun, J.; Matyjaszewski, K., Synthesis of Nanocomposite Organic/Inorganic Hybrid Materials Using Controlled/"Living" Radical Polymerization. *Chem Mater* **2001,** *13* (10), 3436-3448.
40. Jeyaprakash, J. D.; Samuel, S.; Dhamodharan, R.; Rühe, J., Polymer Brushes via ATRP: Role of Activator and Deactivator in the Surface-Initiated ATRP of Styrene on Planar Substrates. *Macromol Rapid Comm* **2002,** *23* (4), 277-281.
41. Zhou, D.; Gao, X.; Wang, W.-j.; Zhu, S., Termination of Surface Radicals and Kinetic Modeling of ATRP Grafting from Flat Surfaces by Addition of Deactivator. *Macromolecules* **2012,** *45* (3), 1198-1207.
42. (a) Gorman, C. B.; Petrie, R. J.; Genzer, J., Effect of Substrate Geometry on Polymer Molecular Weight and Polydispersity during Surface-Initiated Polymerization. *Macromolecules* **2008,** *41* (13), 4856-4865; (b) Bombalski, L.; Min, K.; Dong, H.; Tang, C.; Matyjaszewski, K., Preparation of Well-Defined Hybrid Materials by ATRP in Miniemulsion. *Macromolecules* **2007,** *40* (21), 7429-7432.
43. Zoppe, J. O.; Ataman, N. C.; Mocny, P.; Wang, J.; Moraes, J.; Klok, H.-A., Surface-Initiated Controlled Radical Polymerization: State-of-the-Art, Opportunities, and Challenges in Surface and Interface Engineering with Polymer Brushes. *Chemical Reviews* **2017,** *117* (3), 1105-1318.
44. Rühe, J.; Ballauff, M.; Biesalski, M.; Dziezok, P.; Gröhn, F.; Johannsmann, D.; Houbenov, N.; Hugenberg, N.; Konradi, R.; Minko, S.; Motornov, M.; Netz, R. R.;

Schmidt, M.; Seidel, C.; Stamm, M.; Stephan, T.; Usov, D.; Zhang, H., Polyelectrolyte Brushes. In *Polyelectrolytes with Defined Molecular Architecture I*, Schmidt, M., Ed. Springer Berlin Heidelberg: Berlin, Heidelberg, 2004; pp 79-150.
45. Krishnamoorthy, M.; Hakobyan, S.; Ramstedt, M.; Gautrot, J. E., Surface-initiated polymer brushes in the biomedical field: applications in membrane science, biosensing, cell culture, regenerative medicine and antibacterial coatings. *Chem Rev* **2014,** *114* (21), 10976-1026.
46. Lowe, A. B.; McCormick, C. L., Synthesis and Solution Properties of Zwitterionic Polymers. *Chemical Reviews* **2002,** *102* (11), 4177-4190.
47. Cheng, N.; Brown, A. A.; Azzaroni, O.; Huck, W. T. S., Thickness-Dependent Properties of Polyzwitterionic Brushes. *Macromolecules* **2008,** *41* (17), 6317-6321.
48. Husseman, M.; Malmström, E. E.; McNamara, M.; Mate, M.; Mecerreyes, D.; Benoit, D. G.; Hedrick, J. L.; Mansky, P.; Huang, E.; Russell, T. P.; Hawker, C. J., Controlled Synthesis of Polymer Brushes by "Living" Free Radical Polymerization Techniques. *Macromolecules* **1999,** *32* (5), 1424-1431.
49. Kim, J.-B.; Huang, W.; Bruening, M. L.; Baker, G. L., Synthesis of Triblock Copolymer Brushes by Surface-Initiated Atom Transfer Radical Polymerization. *Macromolecules* **2002,** *35* (14), 5410-5416.
50. Tomlinson, M. R.; Efimenko, K.; Genzer, J., Study of Kinetics and Macroinitiator Efficiency in Surface-Initiated Atom-Transfer Radical Polymerization. *Macromolecules* **2006,** *39* (26), 9049-9056.
51. Mansky, P.; Liu, Y.; Huang, E.; Russell, T.; Hawker, C., Controlling polymer-surface interactions with random copolymer brushes. *Science* **1997,** *275* (5305), 1458-1460.
52. Ignatova, M.; Voccia, S.; Gilbert, B.; Markova, N.; Cossement, D.; Gouttebaron, R.; Jérôme, R.; Jérôme, C., Combination of Electrografting and Atom-Transfer Radical Polymerization for Making the Stainless Steel Surface Antibacterial and Protein Antiadhesive. *Langmuir* **2006,** *22* (1), 255-262.
53. Feng, J.; Xu, G. H.; An, Y.; Zeng, X., Construction of the homogeneously mixed SAM composed of octyltriethoxysilane and octadecyltrichlorosilane by taking advantage of the molecular steric restriction. *Colloids and Surfaces A: Physicochemical and Engineering Aspects* **2008,** *316* (1), 194-201.
54. Choi, I.; Kim, Y.; Kang, S. K.; Lee, J.; Yi, J., Phase Separation of a Mixed Self-Assembled Monolayer Prepared via a Stepwise Method. *Langmuir* **2006,** *22* (11), 4885-4889.
55. Ionov, L.; Sidorenko, A.; Stamm, M.; Minko, S.; Zdyrko, B.; Klep, V.; Luzinov, I., Gradient Mixed Brushes: "Grafting To" Approach. *Macromolecules* **2004,** *37* (19), 7421-7423.
56. Sidorenko, A.; Minko, S.; Schenk-Meuser, K.; Duschner, H.; Stamm, M., Switching of Polymer Brushes. *Langmuir* **1999,** *15* (24), 8349-8355.
57. Zhao, B., Synthesis of binary mixed homopolymer brushes by combining atom transfer radical polymerization and nitroxide-mediated radical polymerization. *Polymer* **2003,** *44* (15), 4079-4083.
58. Ajioka, N.; Suzuki, Y.; Yokoyama, A.; Yokozawa, T., Synthesis of well-defined polystyrene-b-aromatic polyether using an orthogonal initiator for atom transfer radical polymerization and chain-growth condensation polymerization. *Macromolecules* **2007,** *40* (15), 5294-5300.
59. Wang, X. J.; Bohn, P. W., Spatiotemporally Controlled Formation of Two-Component Counterpropagating Lateral Graft Density Gradients of Mixed Polymer Brushes on Planar Au Surfaces. *Adv Mater* **2007,** *19* (4), 515-520.

60. Ye, P. L.; Dong, H. C.; Zhong, M. J.; Matyjaszewski, K., Synthesis of Binary Polymer Brushes via Two-Step Reverse Atom Transfer Radical Polymerization. *Macromolecules* **2011,** *44* (7), 2253-2260.
61. Ionov, L.; Minko, S., Mixed Polymer Brushes with Locking Switching. *Acs Appl Mater Inter* **2012,** *4* (1), 483-489.
62. Julthongpiput, D.; Lin, Y.-H.; Teng, J.; Zubarev, E. R.; Tsukruk, V. V., Y-Shaped Polymer Brushes: Nanoscale Switchable Surfaces. *Langmuir* **2003,** *19* (19), 7832-7836.
63. Zhao, B.; He, T., Synthesis of Well-Defined Mixed Poly(methyl methacrylate)/Polystyrene Brushes from an Asymmetric Difunctional Initiator-Terminated Self-Assembled Monolayer. *Macromolecules* **2003,** *36* (23), 8599-8602.
64. (a) Huang, X.; Hauptmann, N.; Appelhans, D.; Formanek, P.; Frank, S.; Kaskel, S.; Temme, A.; Voit, B., Synthesis of Hetero-Polymer Functionalized Nanocarriers by Combining Surface-Initiated ATRP and RAFT Polymerization. *Small* **2012,** *8* (23), 3579-3583; (b) Calabrese, D. R.; Ditter, D.; Liedel, C.; Blumfield, A.; Zentel, R.; Ober, C. K., Design, Synthesis, and Use of Y-Shaped ATRP/NMP Surface Tethered Initiator. *Acs Macro Lett* **2015,** *4* (6), 606-610.
65. Alexander, S., Adsorption of Chain Molecules with a Polar Head a-Scaling Description. *J Phys-Paris* **1977,** *38* (8), 983-987.
66. de Gennes, P. G., Conformations of Polymers Attached to an Interface. *Macromolecules* **1980,** *13* (5), 1069-1075.
67. (a) Zhulina, E. B.; Borisov, O. V.; Pryamitsyn, V. A.; Birshtein, T. M., Coil Globule Type Transitions in Polymers .1. Collapse of Layers of Grafted Polymer-Chains. *Macromolecules* **1991,** *24* (1), 140-149; (b) Milner, S. T.; Witten, T. A.; Cates, M. E., Theory of the Grafted Polymer Brush. *Macromolecules* **1988,** *21* (8), 2610-2619; (c) Cosgrove, T.; Heath, T.; Vanlent, B.; Leermakers, F.; Scheutjens, J., Configuration of Terminally Attached Chains at the Solid Solvent Interface - Self-Consistent Field-Theory and a Monte-Carlo Model. *Macromolecules* **1987,** *20* (7), 1692-1696.
68. Milner, S. T.; Witten, T. A.; Cates, M. E., A Parabolic Density Profile for Grafted Polymers. *Europhys Lett* **1988,** *5* (5), 413-418.
69. Chen, W.-L.; Cordero, R.; Tran, H.; Ober, C. K., 50th Anniversary Perspective: Polymer Brushes: Novel Surfaces for Future Materials. *Macromolecules* **2017,** *50* (11), 4089-4113.
70. (a) Pincus, P., Colloid stabilization with grafted polyelectrolytes. *Macromolecules* **1991,** *24* (10), 2912-2919; (b) Borisov, O. V.; Birshtein, T. M.; Zhulina, E. B., Collapse of Grafted Polyelectrolyte Layer. *J Phys Ii* **1991,** *1* (5), 521-526.
71. Lego, B.; Skene, W. G.; Giasson, S., Swelling Study of Responsive Polyelectrolyte Brushes Grafted from Mica Substrates: Effect of pH, Salt, and Grafting Density. *Macromolecules* **2010,** *43* (9), 4384-4393.
72. (a) Gong, P.; Wu, T.; Genzer, J.; Szleifer, I., Behavior of Surface-Anchored Poly(acrylic acid) Brushes with Grafting Density Gradients on Solid Substrates: 2. Theory. *Macromolecules* **2007,** *40* (24), 8765-8773; (b) Biesalski, M.; Johannsmann, D.; Rühe, J., Synthesis and swelling behavior of a weak polyacid brush. *The Journal of Chemical Physics* **2002,** *117* (10), 4988-4994; (c) Zhulina, E. B.; Birshtein, T. M.; Borisov, O. V., Theory of Ionizable Polymer Brushes. *Macromolecules* **1995,** *28* (5), 1491-1499.
73. (a) Dong, R.; Lindau, M.; Ober, C. K., Dissociation Behavior of Weak Polyelectrolyte Brushes on a Planar Surface. *Langmuir* **2009,** *25* (8), 4774-4779; (b) Wu, T.; Gong, P.; Szleifer, I.; Vlček, P.; Šubr, V.; Genzer, J., Behavior of Surface-

Anchored Poly(acrylic acid) Brushes with Grafting Density Gradients on Solid Substrates: 1. Experiment. *Macromolecules* **2007,** *40* (24), 8756-8764.
74. (a) Murata, H.; Koepsel, R. R.; Matyjaszewski, K.; Russell, A. J., Permanent, non-leaching antibacterial surfaces—2: How high density cationic surfaces kill bacterial cells. *Biomaterials* **2007,** *28* (32), 4870-4879; (b) Tsujii, Y.; Ohno, K.; Yamamoto, S.; Goto, A.; Fukuda, T., Structure and Properties of High-Density Polymer Brushes Prepared by Surface-InitiatedLiving Radical Polymerization. In *Surface-Initiated Polymerization I*, Jordan, R., Ed. Springer Berlin Heidelberg: Berlin, Heidelberg, 2006; pp 1-45; (c) Park, S.; Cho, H. Y.; Yoon, J. A.; Kwak, Y.; Srinivasan, A.; Hollinger, J. O.; Paik, H.-j.; Matyjaszewski, K., Photo-Cross-Linkable Thermoresponsive Star Polymers Designed for Control of Cell-Surface Interactions. *Biomacromolecules* **2010,** *11* (10), 2647-2652.
75. Gao, Y. F.; Wei, M. L.; Li, X.; Xu, W. W.; Ahiabu, A.; Perdiz, J.; Liu, Z. N.; Serpe, M. J., Stimuli-responsive polymers: Fundamental considerations and applications. *Macromol Res* **2017,** *25* (6), 513-527.
76. Anastasiadis, S. H., Development of Functional Polymer Surfaces with Controlled Wettability. *Langmuir* **2013,** *29* (30), 9277-9290.
77. Stuart, M. A. C.; Huck, W. T. S.; Genzer, J.; Muller, M.; Ober, C.; Stamm, M.; Sukhorukov, G. B.; Szleifer, I.; Tsukruk, V. V.; Urban, M.; Winnik, F.; Zauscher, S.; Luzinov, I.; Minko, S., Emerging applications of stimuli-responsive polymer materials. *Nat Mater* **2010,** *9* (2), 101-113.
78. Zhai, L., Stimuli-responsive polymer films. *Chemical Society Reviews* **2013,** *42* (17), 7148.
79. Chen, J.-K.; Hsieh, C.-Y.; Huang, C.-F.; Li, P. M.; Kuo, S.-W.; Chang, F.-C., Using Solvent Immersion to Fabricate Variably Patterned Poly(methyl methacrylate) Brushes on Silicon Surfaces. *Macromolecules* **2008,** *41* (22), 8729-8736.
80. (a) Aoki, H.; Kitamura, M.; Ito, S., Nanosecond Dynamics of Poly(methyl methacrylate) Brushes in Solvents Studied by Fluorescence Depolarization Method. *Macromolecules* **2008,** *41* (2), 285-287; (b) Bumbu, G.-G.; Wolkenhauer, M.; Kircher, G.; Gutmann, J. S.; Berger, R., Micromechanical Cantilever Technique: A Tool for Investigating the Swelling of Polymer Brushes. *Langmuir* **2007,** *23* (4), 2203-2207; (c) Wolkenhauer, M.; Bumbu, G.-G.; Cheng, Y.; Roth, S. V.; Gutmann, J. S., Investigation of micromechanical cantilever sensors with microfocus grazing incidence small-angle x-ray scattering. *Applied Physics Letters* **2006,** *89* (5), 054101.
81. Zhang, J.; Liu, X.; Neri, G.; Pinna, N., Nanostructured Materials for Room-Temperature Gas Sensors. *Adv Mater* **2016,** *28*, 795–831.
82. (a) Biesalski, M.; Rühe, J., Swelling of a Polyelectrolyte Brush in Humid Air. *Langmuir* **1999,** *16*; (b) Galvin, C.; Genzer, J., Vapor Swelling of Hydrophilic Polymer Brushes: for Materials Science and Biotechnology 2 Volume Set. 2017; pp 243-266.
83. Zhao, B.; Haasch, R. T.; MacLaren, S., Solvent-Induced Self-Assembly of Mixed Poly(methyl methacrylate)/Polystyrene Brushes on Planar Silica Substrates: Molecular Weight Effect. *J Am Chem Soc* **2004,** *126* (19), 6124-6134.
84. (a) Zhao, B.; Brittain, W. J., Synthesis, Characterization, and Properties of Tethered Polystyrene-b-polyacrylate Brushes on Flat Silicate Substrates. *Macromolecules* **2000,** *33* (23), 8813-8820; (b) Zhao, B.; Brittain, W. J.; Zhou, W.; Cheng, S. Z. D., Nanopattern Formation from Tethered PS-b-PMMA Brushes upon Treatment with Selective Solvents. *J Am Chem Soc* **2000,** *122* (10), 2407-2408.
85. Boyes, S. G.; Akgun, B.; Brittain, W. J.; Foster, M. D., Synthesis, Characterization, and Properties of Polyelectrolyte Block Copolymer Brushes Prepared

by Atom Transfer Radical Polymerization and Their Use in the Synthesis of Metal Nanoparticles. *Macromolecules* **2003,** *36* (25), 9539-9548.
86. Granville, A. M.; Boyes, S. G.; Akgun, B.; Foster, M. D.; Brittain, W. J., Synthesis and Characterization of Stimuli-Responsive Semifluorinated Polymer Brushes Prepared by Atom Transfer Radical Polymerization. *Macromolecules* **2004,** *37* (8), 2790-2796.
87. O'Driscoll, B. M. D.; Griffiths, G. H.; Matsen, M. W.; Perrier, S.; Ladmiral, V.; Hamley, I. W., Lateral Phase Separation in Grafted Diblock Copolymer Films. *Macromolecules* **2010,** *43* (19), 8177-8184.
88. (a) Rowe, M. D.; Hammer, B. A. G.; Boyes, S. G., Synthesis of Surface-Initiated Stimuli-Responsive Diblock Copolymer Brushes Utilizing a Combination of ATRP and RAFT Polymerization Techniques. *Macromolecules* **2008,** *41* (12), 4147-4157; (b) Tomlinson, M.; Genzer, J., Formation and properties of multivariant assemblies of surface-tethered diblock and triblock copolymers. *Polymer* **2008,** *49*; (c) Tomlinson, M. R.; Genzer, J., Evolution of Surface Morphologies in Multivariant Assemblies of Surface-Tethered Diblock Copolymers after Selective Solvent Treatment. *Langmuir* **2005,** *21* (25), 11552-11555; (d) Yu, K.; Wang, H.; Xue, L.; Han, Y., Stimuli-Responsive Polyelectrolyte Block Copolymer Brushes Synthesized from the Si Wafer via Atom-Transfer Radical Polymerization. *Langmuir* **2007,** *23* (3), 1443-1452; (e) Kong, B.; Lee, J. K.; Choi, I. S., Surface-Initiated, Ring-Opening Metathesis Polymerization: Formation of Diblock Copolymer Brushes and Solvent-Dependent Morphological Changes. *Langmuir* **2007,** *23* (12), 6761-6765.
89. Xu, C.; Wu, T.; Drain, C. M.; Batteas, J. D.; Fasolka, M. J.; Beers, K. L., Effect of Block Length on Solvent Response of Block Copolymer Brushes: Combinatorial Study with Block Copolymer Brush Gradients. *Macromolecules* **2006,** *39* (9), 3359-3364.
90. Gao, X.; Feng, W.; Zhu, S.; Sheardown, H.; Brash, J. L., A Facile Method of Forming Nanoscale Patterns on Poly(ethylene glycol)-Based Surfaces by Self-Assembly of Randomly Grafted Block Copolymer Brushes. *Langmuir* **2008,** *24* (15), 8303-8308.
91. Yang, M.; Mao, J.; Nie, W.; Dong, Z.; Wang, D.; Zhao, Z.; Ji, X., Facile synthesis and responsive behavior of PDMS-b-PEG diblock copolymer brushes via photoinitiated "thiol-ene" click reaction. *Journal of Polymer Science Part A: Polymer Chemistry* **2012,** *50* (10), 2075-2083.
92. Santer, S.; Rühe, J., Motion of nano-objects on polymer brushes. *Polymer* **2004,** *45* (25), 8279-8297.
93. (a) Boyes, S. G.; Brittain, W. J.; Weng, X.; Cheng, S. Z. D., Synthesis, Characterization, and Properties of ABA Type Triblock Copolymer Brushes of Styrene and Methyl Acrylate Prepared by Atom Transfer Radical Polymerization. *Macromolecules* **2002,** *35* (13), 4960-4967; (b) Ramakrishna, S. N.; Cirelli, M.; Kooij, E. S.; Klein Gunnewiek, M.; Benetti, E. M., Amplified Responsiveness of Multilayered Polymer Grafts: Synergy between Brushes and Hydrogels. *Macromolecules* **2015,** *48* (19), 7106-7116.
94. Howarter, J. A.; Youngblood, J. P., Self-Cleaning and Anti-Fog Surfaces via Stimuli-Responsive Polymer Brushes. *Adv Mater* **2007,** *19* (22), 3838-3843.
95. Vyas, M. K.; Schneider, K.; Nandan, B.; Stamm, M., Switching of friction by binary polymer brushes. *Soft Matter* **2008,** *4* (5), 1024-1032.
96. Wang, Z.-L.; Xu, J.-T.; Du, B.-Y.; Fan, Z.-Q., Preparation and characterization of V-shaped PS-b-PEO brushes anchored on planar gold substrate through the trithiocarbonate junction group. *J Colloid Interf Sci* **2012,** *384* (1), 29-37.

97. Messerschmidt, M.; Janke, A.; Simon, F.; Hanzelmann, C.; Riske, T.; Stamm, M.; Raether, B.; da Costa e Silva, O.; Uhlmann, P., Fluorocarbon-Free Dual-Action Textile Finishes Based on Covalently Attached Thermoresponsive Block Copolymer Brush Coatings. *Acs Appl Mater Inter* **2018,** *10* (46), 40088-40099.
98. Sanjuan, S.; Perrin, P.; Pantoustier, N.; Tran, Y., Synthesis and Swelling Behavior of pH-Responsive Polybase Brushes. *Langmuir* **2007,** *23* (10), 5769-5778.
99. Yu, J.; Mao, J.; Yuan, G.; Satija, S.; Jiang, Z.; Chen, W.; Tirrell, M., Structure of Polyelectrolyte Brushes in the Presence of Multivalent Counterions. *Macromolecules* **2016,** *49* (15), 5609-5617.
100. Moya, S.; Azzaroni, O.; Farhan, T.; Osborne, V. L.; Huck, W. T. S., Locking and Unlocking of Polyelectrolyte Brushes: Toward the Fabrication of Chemically Controlled Nanoactuators. *Angewandte Chemie International Edition* **2005,** *44* (29), 4578-4581.
101. Willott, J. D.; Humphreys, B. A.; Murdoch, T. J.; Edmondson, S.; Webber, G. B.; Wanless, E. J., Hydrophobic effects within the dynamic pH-response of polybasic tertiary amine methacrylate brushes. *Physical Chemistry Chemical Physics* **2015,** *17* (5), 3880-3890.
102. Yu, K.; Han, Y., Effect of block sequence and block length on the stimuli-responsive behavior of polyampholyte brushes: hydrogen bonding and electrostatic interaction as the driving force for surface rearrangement. *Soft Matter* **2009,** *5* (4), 759-768.
103. Motornov, M.; Sheparovych, R.; Katz, E.; Minko, S., Chemical Gating with Nanostructured Responsive Polymer Brushes: Mixed BrushversusHomopolymer Brush. *ACS Nano* **2007,** *2* (1), 41-52.
104. Sun, T.; Wang, G.; Feng, L.; Liu, B.; Ma, Y.; Jiang, L.; Zhu, D., Reversible Switching between Superhydrophilicity and Superhydrophobicity. *Angewandte Chemie International Edition* **2004,** *43* (3), 357-360.
105. Jonas, A. M.; Glinel, K.; Oren, R.; Nysten, B.; Huck, W. T. S., Thermo-Responsive Polymer Brushes with Tunable Collapse Temperatures in the Physiological Range. *Macromolecules* **2007,** *40* (13), 4403-4405.
106. Azzaroni, O.; Brown, A. A.; Huck, W. T., Tunable wettability by clicking counterions into polyelectrolyte brushes. *Adv Mater* **2007,** *19* (1), 151-154.
107. Higuchi, A.; Hamamura, A.; Shindo, Y.; Kitamura, H.; Yoon, B. O.; Mori, T.; Uyama, T.; Umezawa, A., Photon-Modulated Changes of Cell Attachments on Poly(spiropyran-co-methyl methacrylate) Membranes. *Biomacromolecules* **2004,** *5* (5), 1770-1774.
108. Kopyshev, A.; Galvin, C. J.; Patil, R. R.; Genzer, J.; Lomadze, N.; Feldmann, D.; Zakrevski, J.; Santer, S., Light-Induced Reversible Change of Roughness and Thickness of Photosensitive Polymer Brushes. *Acs Appl Mater Inter* **2016,** *8* (29), 19175-19184.
109. (a) Fries, K.; Samanta, S.; Orski, S.; Locklin, J., Reversible colorimetric ion sensors based on surface initiated polymerization of photochromic polymers. *Chem Commun* **2008,** (47), 6288-6290; (b) Samanta, S.; Locklin, J., Formation of Photochromic Spiropyran Polymer Brushes via Surface-Initiated, Ring-Opening Metathesis Polymerization: Reversible Photocontrol of Wetting Behavior and Solvent Dependent Morphology Changes. *Langmuir* **2008,** *24* (17), 9558-9565.
110. Guo, F.; Guo, Z., Inspired smart materials with external stimuli responsive wettability: a review. *Rsc Adv* **2016,** *6* (43), 36623-36641.
111. Callies, M.; Quéré, D., On water repellency. *Soft Matter* **2005,** *1* (1), 55-61.

112. Young, T., III. An essay on the cohesion of fluids. *Philosophical Transactions of the Royal Society of London* **1805,** *95*, 65-87.
113. Nguyen-Tri, P.; Tran, H. N.; Plamondon, C. O.; Tuduri, L.; Vo, D.-V. N.; Nanda, S.; Mishra, A.; Chao, H.-P.; Bajpai, A. K., Recent progress in the preparation, properties and applications of superhydrophobic nano-based coatings and surfaces: A review. *Progress in Organic Coatings* **2019,** *132*, 235-256.
114. Darband, G.; Aliofkhazraei, M.; Khorsand, S.; Sokhanvar, S.; Kaboli, A., Science and Engineering of Superhydrophobic Surfaces: Review of Corrosion Resistance, Chemical and Mechanical Stability. *Arab J Chem* **2018**.
115. Drelich, J.; Chibowski, E.; Meng, D. D.; Terpilowski, K., Hydrophilic and superhydrophilic surfaces and materials. *Soft Matter* **2011,** *7* (21), 9804-9828.
116. Vogler, E. A., Structure and reactivity of water at biomaterial surfaces. *Adv Colloid Interface Sci* **1998,** *74*, 69-117.
117. Asmatulu, R., Highly Hydrophilic Electrospun Polyacrylonitrile/ Polyvinypyrrolidone Nanofibers Incorporated with Gentamicin as Filter Medium for Dam Water and Wastewater Treatment. *Journal of Membrane and Separation Technology* **2016,** *5* (2), 38-56.
118. Cassie, A. B. D.; Baxter, S., Wettability of porous surfaces. *Transactions of the Faraday Society* **1944,** *40* (0), 546-551.
119. Liu, H.; Ding, Y.; Ao, Z.; Zhou, Y.; Wang, S.; Jiang, L., Fabricating Surfaces with Tunable Wettability and Adhesion by Ionic Liquids in a Wide Range. *Small* **2015,** *11* (15), 1782-1786.
120. Etzler, F. M., Determination of the Surface Free Energy of Solids. *Reviews of Adhesion and Adhesives* **2013,** *1* (1), 3-45.
121. Zisman, W. A., Relation of the Equilibrium Contact Angle to Liquid and Solid Constitution. In *Contact Angle, Wettability, and Adhesion*, AMERICAN CHEMICAL SOCIETY: 1964; Vol. 43, pp 1-51.
122. Fowkes, F. M., Attractive Forces at Interfaces. *Industrial & Engineering Chemistry* **1964,** *56* (12), 40-52.
123. Owens, D. K.; Wendt, R. C., Estimation of the surface free energy of polymers. *J Appl Polym Sci* **1969,** *13* (8), 1741-1747.
124. Van Oss, C. J.; Chaudhury, M. K.; Good, R. J., Interfacial Lifshitz-van der Waals and polar interactions in macroscopic systems. *Chemical Reviews* **1988,** *88* (6), 927-941.
125. Wang, X.; Ye, Q.; Liu, J.; Liu, X.; Zhou, F., Low surface energy surfaces from self-assembly of perfluoropolymer with sticky functional groups. *J Colloid Interf Sci* **2010,** *351* (1), 261-266.
126. (a) Jung, D.-H.; Park, I. J.; Choi, Y. K.; Lee, S.-B.; Park, H. S.; Rühe, J., Perfluorinated Polymer Monolayers on Porous Silica for Materials with Super Liquid Repellent Properties. *Langmuir* **2002,** *18* (16), 6133-6139; (b) Bhairamadgi, N. S.; Pujari, S. P.; Leermakers, F. A. M.; van Rijn, C. J. M.; Zuilhof, H., Adhesion and Friction Properties of Polymer Brushes: Fluoro versus Nonfluoro Polymer Brushes at Varying Thickness. *Langmuir* **2014,** *30* (8), 2068-2076; (c) Bhairamadgi, N. S.; Pujari, S. P.; van Rijn, C. J. M.; Zuilhof, H., Adhesion and Friction Properties of Fluoropolymer Brushes: On the Tribological Inertness of Fluorine. *Langmuir* **2014,** *30* (42), 12532-12540.
127. Sun, T.; Feng, L.; Gao, X.; Jiang, L., Bioinspired Surfaces with Special Wettability. *Accounts of Chemical Research* **2005,** *38* (8), 644-652.

128. Chen, T.; Ferris, R.; Zhang, J.; Ducker, R.; Zauscher, S., Stimulus-responsive polymer brushes on surfaces: Transduction mechanisms and applications. *Prog Polym Sci* **2010,** *35* (1), 94-112.
129. (a) Fu, Q.; Rama Rao, G. V.; Basame, S. B.; Keller, D. J.; Artyushkova, K.; Fulghum, J. E.; Lopez, G. P., Reversible control of free energy and topography of nanostructured surfaces. *J Am Chem Soc* **2004,** *126* (29), 8904-5; (b) Liu, H.; Zhang, X.; Wang, S.; Jiang, L., Underwater Thermoresponsive Surface with Switchable Oil-Wettability between Superoleophobicity and Superoleophilicity. *Small* **2015,** *11* (27), 3338-3342.
130. (a) Myshkin, N.; Kovalev, A., Adhesion and surface forces in polymer tribology—A review. *Friction* **2018,** *6* (2), 143-155; (b) Myshkin, N. K.; Petrokovets, M. I.; Kovalev, A. V., Tribology of polymers: Adhesion, friction, wear, and mass-transfer. *Tribology International* **2005,** *38* (11), 910-921.
131. Christenson, H. K., Adhesion and surface energy of mica in air and water. *The Journal of Physical Chemistry* **1993,** *97* (46), 12034-12041.
132. Scherge, M.; Kehrwald, B.; Gervé, A., Tribology and engine mechanics. *MTZ worldwide* **2002,** *63* (3), 19-24.
133. He, Y.; Zhu, B.; Inoue, Y., Hydrogen bonds in polymer blends. *Prog Polym Sci* **2004,** *29* (10), 1021-1051.
134. Christenson, H. K.; Horn, R. G., Direct measurement of the force between solid surfaces in a polar liquid. *Chemical Physics Letters* **1983,** *98* (1), 45-48.
135. Wang, H., Lateral Force Calibration in Atomic Force Microscopy: Minireview. *Sci Adv Mater* **2017,** *9* (1), 56-64.
136. Anderson, E. V.; Chakraborty, S.; Esformes, T.; Eggiman, D.; DeGraf, C.; Stevens, K. M.; Liu, D. L.; Burnham, N. A., Shape-Independent Lateral Force Calibration. *Acs Appl Mater Inter* **2011,** *3* (9), 3256-3260.
137. Bennewitz, R., Friction force microscopy. *Materials Today* **2005,** *8* (5), 42-48.
138. (a) Gong, J. P., Friction and lubrication of hydrogels—its richness and complexity. *Soft Matter* **2006,** *2* (7), 544-552; (b) Klein, J., Molecular mechanisms of synovial joint lubrication. *Proceedings of the Institution of Mechanical Engineers, Part J: Journal of Engineering Tribology* **2006,** *220* (8), 691-710.
139. Lee, S.; Müller, M.; Ratoi-Salagean, M.; Vörös, J.; Pasche, S.; De Paul, S. M.; Spikes, H. A.; Textor, M.; Spencer, N. D., Boundary Lubrication of Oxide Surfaces by Poly(L-lysine)-g-poly(ethylene glycol) (PLL-g-PEG) in Aqueous Media. *Tribology Letters* **2003,** *15* (3), 231-239.
140. (a) Klein, J., Repair or Replacement--A Joint Perspective. *Science* **2009,** *323* (5910), 47-48; (b) Klein, J.; Perahia, D.; Warburg, S., Forces between polymer-bearing surfaces undergoing shear. *Nature* **1991,** *352* (6331), 143-145.
141. An, R.; Dong, Y.; Zhu, J.; Rao, C., Adhesion and friction forces in biofouling attachments to nanotube- and PEG- patterned TiO2 surfaces. *Colloids and Surfaces B: Biointerfaces* **2017,** *159*, 108-117.
142. Zeng, H., *Polymer Adhesion, Friction, and Lubrication*. Wiley: 2013.
143. Nomura, A.; Okayasu, K.; Ohno, K.; Fukuda, T.; Tsujii, Y., Lubrication Mechanism of Concentrated Polymer Brushes in Solvents: Effect of Solvent Quality and Thereby Swelling State. *Macromolecules* **2011,** *44* (12), 5013-5019.
144. Ma, S.; Zhang, X.; Yu, B.; Zhou, F., Brushing up functional materials. *NPG Asia Materials* **2019,** *11* (1), 24.
145. (a) Zhang, R.; Ma, S.; Wei, Q.; Ye, Q.; Yu, B.; van der Gucht, J.; Zhou, F., The Weak Interaction of Surfactants with Polymer Brushes and Its Impact on Lubricating Behavior. *Macromolecules* **2015,** *48* (17), 6186-6196; (b) Mocny, P.; Klok, H.-A.,

Tribology of surface-grafted polymer brushes. *Molecular Systems Design & Engineering* **2016,** *1* (2), 141-154.
146. Kyomoto, M.; Moro, T.; Saiga, K.; Hashimoto, M.; Ito, H.; Kawaguchi, H.; Takatori, Y.; Ishihara, K., Biomimetic hydration lubrication with various polyelectrolyte layers on cross-linked polyethylene orthopedic bearing materials. *Biomaterials* **2012,** *33* (18), 4451-4459.
147. Chen, M.; Briscoe, W. H.; Armes, S. P.; Klein, J., Lubrication at Physiological Pressures by Polyzwitterionic Brushes. *Science* **2009,** *323* (5922), 1698-1701.
148. (a) Tairy, O.; Kampf, N.; Driver, M. J.; Armes, S. P.; Klein, J., Dense, Highly Hydrated Polymer Brushes via Modified Atom-Transfer-Radical-Polymerization: Structure, Surface Interactions, and Frictional Dissipation. *Macromolecules* **2015,** *48* (1), 140-151; (b) Kobayashi, M.; Terada, M.; Takahara, A., Polyelectrolyte brushes: a novel stable lubrication system in aqueous conditions. *Faraday Discussions* **2012,** *156* (0), 403-412.
149. Yang, J.; Chen, H.; Xiao, S.; Shen, M.; Chen, F.; Fan, P.; Zhong, M.; Zheng, J., Salt-Responsive Zwitterionic Polymer Brushes with Tunable Friction and Antifouling Properties. *Langmuir* **2015,** *31* (33), 9125-9133.
150. Raviv, U.; Giasson, S.; Kampf, N.; Gohy, J.-F.; Jérôme, R.; Klein, J., Lubrication by charged polymers. *Nature* **2003,** *425* (6954), 163-165.
151. Bielecki, R. M.; Benetti, E. M.; Kumar, D.; Spencer, N. D., Lubrication with Oil-Compatible Polymer Brushes. *Tribology Letters* **2012,** *45* (3), 477-487.
152. (a) Doms, M.; Feindt, H.; Kuipers, W. J.; Shewtanasoontorn, D.; Matar, A. S.; Brinkhues, S.; Welton, R. H.; Mueller, J., Hydrophobic coatings for MEMS applications. *J Micromech Microeng* **2008,** *18* (5); (b) Biswas, S. K.; Vijayan, K., Friction and Wear of Ptfe - a Review. *Wear* **1992,** *158* (1-2), 193-211.
153. (a) Sakata, H.; Kobayashi, M.; Otsuka, H.; Takahara, A., Tribological Properties of Poly(methyl methacrylate) Brushes Prepared by Surface-Initiated Atom Transfer Radical Polymerization. *Polymer Journal* **2005,** *37* (10), 767-775; (b) Landherr, L. J. T.; Cohen, C.; Agarwal, P.; Archer, L. A., Interfacial Friction and Adhesion of Polymer Brushes. *Langmuir* **2011,** *27* (15), 9387-9395.
154. (a) Wu, Y.; Cai, M.; Pei, X.; Liang, Y.; Zhou, F., Switching Friction with Thermal- Responsive Gels. *Macromol Rapid Comm* **2013,** *34* (22), 1785-1790; (b) Liu, D.; Broer, D. J., Self-assembled Dynamic 3D Fingerprints in Liquid-Crystal Coatings Towards Controllable Friction and Adhesion. *Angewandte Chemie* **2014,** *126* (18), 4630-4634; (c) Zeng, H.; Zhang, Y.; Mao, S.; Nakajima, H.; Uchiyama, K., A reversibly electro-controllable polymer brush for electro-switchable friction. *J Mater Chem C* **2017,** *5* (24), 5877-5881.
155. de Beer, S.; Kutnyanszky, E.; Schön, P. M.; Vancso, G. J.; Müser, M. H., Solvent-induced immiscibility of polymer brushes eliminates dissipation channels. *Nat Commun* **2014,** *5*, 3781.
156. Nordgren, N.; Rutland, M. W., Tunable Nanolubrication between Dual-Responsive Polyionic Grafts. *Nano Lett* **2009,** *9* (8), 2984-2990.
157. Zhang, Z.; Morse, A. J.; Armes, S. P.; Lewis, A. L.; Geoghegan, M.; Leggett, G. J., Effect of Brush Thickness and Solvent Composition on the Friction Force Response of Poly(2-(methacryloyloxy)ethylphosphorylcholine) Brushes. *Langmuir* **2011,** *27* (6), 2514-2521.
158. Wei, Q.; Cai, M.; Zhou, F.; Liu, W., Dramatically Tuning Friction Using Responsive Polyelectrolyte Brushes. *Macromolecules* **2013,** *46* (23), 9368-9379.

159. Ma, S.; Wang, D.; Liang, Y.; Sun, B.; Gorb, S. N.; Zhou, F., Gecko-Inspired but Chemically Switched Friction and Adhesion on Nanofibrillar Surfaces. *Small* **2015,** *11* (9-10), 1131-1137.
160. (a) Paripovic, D.; Klok, H.-A., Improving the Stability in Aqueous Media of Polymer Brushes Grafted from Silicon Oxide Substrates by Surface-Initiated Atom Transfer Radical Polymerization. *Macromol Chem Physic* **2011,** *212* (9), 950-958; (b) Quintana, R.; Gosa, M.; Jańczewski, D.; Kutnyanszky, E.; Vancso, G. J., Enhanced Stability of Low Fouling Zwitterionic Polymer Brushes in Seawater with Diblock Architecture. *Langmuir* **2013,** *29* (34), 10859-10867; (c) Li, Y.; Ko, Y.; Lin, Y.; Kiserow, D.; Genzer, J., Enhanced Stability of Surface-Tethered Diblock Copolymer Brushes with a Neutral Polymer Block and a Weak Polyelectrolyte Block: Effects of Molecular Weight and Hydrophobicity of the Neutral Block. *Macromolecules* **2017,** *50* (21), 8580-8587.
161. Wang, J.; Klok, H.-A., Swelling-Induced Chain Stretching Enhances Hydrolytic Degrafting of Hydrophobic Polymer Brushes in Organic Media. *Angewandte Chemie International Edition* **2019,** *0* (0).
162. Kraigsley, A. M.; Finkel, S. E., Adaptive evolution in single species bacterial biofilms. *FEMS Microbiol Lett* **2009,** *293* (1), 135-40.
163. Tiller, J. C., Coatings for Prevention or Deactivation of Biological Contamination. **2008**, 1013-1065.
164. Li, L.-L.; An, H.-W.; Peng, B.; Zheng, R.; Wang, H., Self-assembled nanomaterials: design principles, the nanostructural effect, and their functional mechanisms as antimicrobial or detection agents. *Materials Horizons* **2019**.
165. Walsh, C. T.; Wencewicz, T. A., Prospects for new antibiotics: a molecule-centered perspective. *The Journal Of Antibiotics* **2013,** *67*, 7.
166. Siedenbiedel, F.; Tiller, J. C., Antimicrobial Polymers in Solution and on Surfaces: Overview and Functional Principles. *Polymers-Basel* **2012,** *4* (1), 46-71.
167. Muñoz-Bonilla, A.; Fernández-García, M., Polymeric materials with antimicrobial activity. *Prog Polym Sci* **2012,** *37* (2), 281-339.
168. Jain, A.; Duvvuri, L. S.; Farah, S.; Beyth, N.; Domb, A. J.; Khan, W., Antimicrobial Polymers. *Adv Healthc Mater* **2014,** *3* (12), 1969-1985.
169. Lu, G. Q.; Wu, D. C.; Fu, R. W., Studies on the synthesis and antibacterial activities of polymeric quaternary ammonium salts from dimethylaminoethyl methacrylate. *React Funct Polym* **2007,** *67* (4), 355-366.
170. Pavithra, D.; Mukesh, D., Biofilm formation, bacterial adhesion and host response on polymeric implants—issues and prevention. *Biomedical Materials* **2008,** *3* (3), 034003.
171. (a) Percival, S. L.; Suleman, L.; Vuotto, C.; Donelli, G., Healthcare-associated infections, medical devices and biofilms: risk, tolerance and control. *Journal of Medical Microbiology* **2015,** *64* (4), 323-334; (b) Flemming, H.-C.; Wingender, J., The biofilm matrix. *Nature Reviews Microbiology* **2010,** *8* (9), 623.
172. (a) Hori, K.; Matsumoto, S., Bacterial adhesion: From mechanism to control. *Biochemical Engineering Journal* **2010,** *48* (3), 424-434; (b) Knetsch, M. L. W.; Koole, L. H., New Strategies in the Development of Antimicrobial Coatings: The Example of Increasing Usage of Silver and Silver Nanoparticles. *Polymers-Basel* **2011,** *3* (1), 340.
173. Willey, J. M.; Sherwood, L. M.; Woolverton, C. J., *Prescott's microbiology*. McGraw-Hill Education: New York, N.Y., 2017.
174. Singh, S.; Singh, S. K.; Chowdhury, I.; Singh, R., Understanding the Mechanism of Bacterial Biofilms Resistance to Antimicrobial Agents. *The Open Microbiology Journal* **2017,** *11* (1), 53-62.

175. Costerton, J. W.; Stewart, P. S.; Greenberg, E. P., Bacterial biofilms: a common cause of persistent infections. *Science* **1999,** *284* (5418), 1318-22.
176. Tuladhar, E.; Hazeleger, W. C.; Koopmans, M.; Zwietering, M. H.; Beumer, R. R.; Duizer, E., Residual viral and bacterial contamination of surfaces after cleaning and disinfection. *Appl Environ Microbiol* **2012,** *78* (21), 7769-75.
177. (a) Hasan, J.; Crawford, R. J.; Ivanova, E. P., Antibacterial surfaces: the quest for a new generation of biomaterials. *Trends Biotechnol* **2013,** *31* (5), 295-304; (b) Tiller, J. C.; Liao, C. J.; Lewis, K.; Klibanov, A. M., Designing surfaces that kill bacteria on contact. *P Natl Acad Sci USA* **2001,** *98* (11), 5981-5985.
178. Charnley, M.; Textor, M.; Acikgoz, C., *Designed polymer structures with antifouling-antimicrobial properties*. 2011; Vol. 71, p 329-334.
179. (a) Banerjee, I.; Pangule, R. C.; Kane, R. S., Antifouling Coatings: Recent Developments in the Design of Surfaces That Prevent Fouling by Proteins, Bacteria, and Marine Organisms. *Adv Mater* **2011,** *23* (6), 690-718; (b) Kirschner, C. M.; Brennan, A. B., Bio-Inspired Antifouling Strategies. *Annual Review of Materials Research* **2012,** *42* (1), 211-229.
180. (a) Lichter, J. A.; Thompson, M. T.; Delgadillo, M.; Nishikawa, T.; Rubner, M. F.; Van Vliet, K. J., Substrata mechanical stiffness can regulate adhesion of viable bacteria. *Biomacromolecules* **2008,** *9* (6), 1571-8; (b) Bratskaya, S.; Marinin, D.; Simon, F.; Synytska, A.; Zschoche, S.; Busscher, H. J.; Jager, D.; van der Mei, H. C., Adhesion and viability of two enterococcal strains on covalently grafted chitosan and chitosan/kappa-carrageenan multilayers. *Biomacromolecules* **2007,** *8* (9), 2960-8; (c) Whitehead, K. A.; Verran, J., The Effect of Surface Topography on the Retention of Microorganisms. *Food and Bioproducts Processing* **2006,** *84* (4), 253-259; (d) Zhang, X.; Wang, L.; Levanen, E., Superhydrophobic surfaces for the reduction of bacterial adhesion. *Rsc Adv* **2013,** *3* (30), 12003-12020.
181. Nurioglu, A. G.; Esteves, A. C. C.; de With, G., Non-toxic, non-biocide-release antifouling coatings based on molecular structure design for marine applications. *J Mater Chem B* **2015,** *3* (32), 6547-6570.
182. Chen, S.; Li, L.; Zhao, C.; Zheng, J., Surface hydration: Principles and applications toward low-fouling/nonfouling biomaterials. *Polymer* **2010,** *51* (23), 5283-5293.
183. Lowe, S.; O'Brien-Simpson, N. M.; Connal, L. A., Antibiofouling polymer interfaces: poly(ethylene glycol) and other promising candidates. *Polym Chem-Uk* **2015,** *6* (2), 198-212.
184. Branch, D. W.; Wheeler, B. C.; Brewer, G. J.; Leckband, D. E., Long-term stability of grafted polyethylene glycol surfaces for use with microstamped substrates in neuronal cell culture. *Biomaterials* **2001,** *22* (10), 1035-1047.
185. Yang, W. J.; Neoh, K.-G.; Kang, E.-T.; Lee, S. S. C.; Teo, S. L.-M.; Rittschof, D., Functional polymer brushes via surface-initiated atom transfer radical graft polymerization for combating marine biofouling. *Biofouling* **2012,** *28* (9), 895-912.
186. Krishnan, S.; Weinman, C. J.; Ober, C. K., Advances in polymers for anti-biofouling surfaces. *J Mater Chem* **2008,** *18* (29), 3405-3413.
187. Yandi, W.; Mieszkin, S.; Martin-Tanchereau, P.; Callow, M. E.; Callow, J. A.; Tyson, L.; Liedberg, B.; Ederth, T., Hydration and chain entanglement determines the optimum thickness of poly(HEMA-co-PEG(1)(0)MA) brushes for effective resistance to settlement and adhesion of marine fouling organisms. *ACS Appl Mater Interfaces* **2014,** *6* (14), 11448-58.
188. (a) Zhao, C.; Li, L.; Wang, Q.; Yu, Q.; Zheng, J., Effect of film thickness on the antifouling performance of poly(hydroxy-functional methacrylates) grafted surfaces.

*Langmuir* **2011,** *27* (8), 4906-13; (b) Ibanescu, S. A.; Nowakowska, J.; Khanna, N.; Landmann, R.; Klok, H. A., Effects of Grafting Density and Film Thickness on the Adhesion of Staphylococcus epidermidis to Poly(2-hydroxy ethyl methacrylate) and Poly(poly(ethylene glycol)methacrylate) Brushes. *Macromol Biosci* **2016,** *16* (5), 676-85.
189. Schlenoff, J. B., Zwitteration: Coating Surfaces with Zwitterionic Functionality to Reduce Nonspecific Adsorption. *Langmuir* **2014,** *30* (32), 9625-9636.
190. Zhang, Z.; Zhang, M.; Chen, S.; Horbett, T. A.; Ratner, B. D.; Jiang, S., Blood compatibility of surfaces with superlow protein adsorption. *Biomaterials* **2008,** *29* (32), 4285-4291.
191. Vladkova, T., *Surface Engineering for Non-toxic Biofouling Control*. 2007; Vol. 42, p 239-256.
192. Dafforn, K. A.; Lewis, J. A.; Johnston, E. L., Antifouling strategies: history and regulation, ecological impacts and mitigation. *Mar Pollut Bull* **2011,** *62* (3), 453-65.
193. Alvarez-Paino, M.; Munoz-Bonilla, A.; Fernandez-Garcia, M., Antimicrobial Polymers in the Nano-World. *Nanomaterials (Basel)* **2017,** *7* (2).
194. (a) Liu, F.; Grainger, D. W., 1.28 Fluorinated Biomaterials☆ A2 - Ducheyne, Paul. In *Comprehensive Biomaterials II*, Elsevier: Oxford, 2017; pp 648-663; (b) Colas, A.; Curtis, J., *Silicone biomaterials: History and chemistry*. 2004; p 80-86.
195. Magin, C. M.; Cooper, S. P.; Brennan, A. B., Non-toxic antifouling strategies. *Materials Today* **2010,** *13* (4), 36-44.
196. Moerman, F., Antimicrobial materials, coatings and biomimetic surfaces with modified microtography to control microbial fouling of product contact surfaces within food processing equipment: Legislation, requirements, effectiveness and challenges. *Journal of Hygienic Engineering and Design* **2014,** *7*, 8-29.
197. Zhu, P.; Meng, W.; Huang, Y., Synthesis and antibiofouling properties of crosslinkable copolymers grafted with fluorinated aromatic side chains. *Rsc Adv* **2017,** *7* (6), 3179-3189.
198. Francolini, I.; Vuotto, C.; Piozzi, A.; Donelli, G., Antifouling and antimicrobial biomaterials: an overview. *APMIS* **2017,** *125* (4), 392-417.
199. Bassegoda, A.; Ivanova, K.; Ramon, E.; Tzanov, T., Strategies to prevent the occurrence of resistance against antibiotics by using advanced materials. *Appl Microbiol Biot* **2018,** *102* (5), 2075-2089.
200. Neoh, K. G.; Li, M.; Kang, E.-T.; Chiong, E.; Tambyah, P. A., Surface modification strategies for combating catheter-related complications: recent advances and challenges. *J Mater Chem B* **2017,** *5* (11), 2045-2067.
201. Hadjesfandiari, N.; Yu, K.; Mei, Y.; Kizhakkedathu, J. N., Polymer brush-based approaches for the development of infection-resistant surfaces. *J Mater Chem B* **2014,** *2* (31), 4968-4978.
202. Rtimi, S.; Baghriche, O.; Pulgarin, C.; Lavanchy, J.-C.; Kiwi, J., Growth of TiO2/Cu films by HiPIMS for accelerated bacterial loss of viability. *Surface and Coatings Technology* **2013,** *232*, 804-813.
203. (a) Ramstedt, M.; Cheng, N.; Azzaroni, O.; Mossialos, D.; Mathieu, H. J.; Huck, W. T. S., Synthesis and Characterization of Poly(3-Sulfopropylmethacrylate) Brushes for Potential Antibacterial Applications. *Langmuir* **2007,** *23* (6), 3314-3321; (b) Asadinezhad, A.; Novák, I.; Lehocký, M.; Sedlařík, V.; Vesel, A.; Junkar, I.; Sáha, P.; Chodák, I., A Physicochemical Approach to Render Antibacterial Surfaces on Plasma-Treated Medical-Grade PVC: Irgasan Coating. *Plasma Processes and Polymers* **2010,** *7* (6), 504-514.

204. Hu, R.; Li, G.; Jiang, Y.; Zhang, Y.; Zou, J.-J.; Wang, L.; Zhang, X., Silver–Zwitterion Organic–Inorganic Nanocomposite with Antimicrobial and Antiadhesive Capabilities. *Langmuir* **2013,** *29* (11), 3773-3779.
205. Isquith, A. J.; Abbott, E. A.; Walters, P. A., Surface-bonded antimicrobial activity of an organosilicon quaternary ammonium chloride. *Appl Microbiol* **1972,** *24* (6), 859-63.
206. (a) Deka, S. R.; Sharma, A. K.; Kumar, P., Cationic polymers and their self-assembly for antibacterial applications. *Curr Top Med Chem* **2015,** *15* (13), 1179-95; (b) Tuladhar, E.; de Koning, M. C.; Fundeanu, I.; Beumer, R.; Duizer, E., Different virucidal activities of hyperbranched quaternary ammonium coatings on poliovirus and influenza virus. *Appl Environ Microbiol* **2012,** *78* (7), 2456-8.
207. Jiao, Y.; Niu, L.-n.; Ma, S.; Li, J.; Tay, F. R.; Chen, J.-h., Quaternary ammonium-based biomedical materials: State-of-the-art, toxicological aspects and antimicrobial resistance. *Prog Polym Sci* **2017,** *71*, 53-90.
208. Konai, M. M.; Bhattacharjee, B.; Ghosh, S.; Haldar, J., Recent Progress in Polymer Research to Tackle Infections and Antimicrobial Resistance. *Biomacromolecules* **2018,** *19* (6), 1888-1917.
209. (a) Aumsuwan, N.; Heinhorst, S.; Urban, M. W., The effectiveness of antibiotic activity of penicillin attached to expanded poly(tetrafluoroethylene) (ePTFE) surfaces: a quantitative assessment. *Biomacromolecules* **2007,** *8* (11), 3525-30; (b) Costa, F.; Carvalho, I. F.; Montelaro, R. C.; Gomes, P.; Martins, M. C., Covalent immobilization of antimicrobial peptides (AMPs) onto biomaterial surfaces. *Acta Biomater* **2011,** *7* (4), 1431-40.
210. Lewis, K.; Klibanov, A. M., Surpassing nature: rational design of sterile-surface materials. *Trends in Biotechnology* **2005,** *23* (7), 343-348.
211. Tiller, J. C.; Lee, S. B.; Lewis, K.; Klibanov, A. M., Polymer surfaces derivatized with poly(vinyl-N-hexylpyridinium) kill airborne and waterborne bacteria. *Biotechnology and Bioengineering* **2002,** *79* (4), 465-471.
212. (a) Lee, S. B.; Koepsel, R. R.; Morley, S. W.; Matyjaszewski, K.; Sun, Y.; Russell, A. J., Permanent, Nonleaching Antibacterial Surfaces. 1. Synthesis by Atom Transfer Radical Polymerization. *Biomacromolecules* **2004,** *5* (3), 877-882; (b) Huang, J.; Murata, H.; Koepsel, R. R.; Russell, A. J.; Matyjaszewski, K., Antibacterial Polypropylene via Surface-Initiated Atom Transfer Radical Polymerization. *Biomacromolecules* **2007,** *8* (5), 1396-1399.
213. Yang, W. J.; Cai, T.; Neoh, K.-G.; Kang, E.-T.; Dickinson, G. H.; Teo, S. L.-M.; Rittschof, D., Biomimetic Anchors for Antifouling and Antibacterial Polymer Brushes on Stainless Steel. *Langmuir* **2011,** *27* (11), 7065-7076.
214. (a) Charnley, M.; Textor, M.; Acikgoz, C., Designed polymer structures with antifouling-antimicrobial properties. *React Funct Polym* **2011,** *71*, 329-334; (b) Waschinski, C. J.; Zimmermann, J.; Salz, U.; Hutzler, R.; Sadowski, G.; Tiller, J. C., Design of Contact-Active Antimicrobial Acrylate-Based Materials Using Biocidal Macromers. *Adv Mater* **2008,** *20* (1), 104-108.
215. Gilbert, P.; Moore, L. E., Cationic antiseptics: diversity of action under a common epithet. *Journal of Applied Microbiology* **2005,** *99* (4), 703-715.
216. Wiegand, C.; Bauer, M.; Hipler, U.-C.; Fischer, D., Poly(ethyleneimines) in dermal applications: Biocompatibility and antimicrobial effects. *Int J Pharmaceut* **2013,** *456*.
217. Li, L.; Pu, T.; Zhanel, G.; Zhao, N.; Ens, W.; Liu, S., New Biocide with Both N-Chloramine and Quaternary Ammonium Moieties Exerts Enhanced Bactericidal Activity. *Adv Healthc Mater* **2012,** *1* (5), 609-620.

218. Li, F.; Weir, M. D.; Xu, H. H. K., Effects of Quaternary Ammonium Chain Length on Antibacterial Bonding Agents. *J Dent Res* **2013,** *92* (10), 932-938.
219. (a) Chen, C. Z.; Beck-Tan, N. C.; Dhurjati, P.; van Dyk, T. K.; LaRossa, R. A.; Cooper, S. L., Quaternary Ammonium Functionalized Poly(propylene imine) Dendrimers as Effective Antimicrobials: Structure−Activity Studies. *Biomacromolecules* **2000,** *1* (3), 473-480; (b) Panarin, E. F.; Solovskii, M. V.; Zaikina, N. A.; Afinogenov, G. E., Biological activity of cationic polyelectrolytes. *Die Makromolekulare Chemie* **1985,** *9* (S19851), 25-33.
220. (a) Kugler, R.; Bouloussa, O.; Rondelez, F., Evidence of a charge-density threshold for optimum efficiency of biocidal cationic surfaces. *Microbiol-Sgm* **2005,** *151*, 1341-1348; (b) Yang, Y. F.; Hu, H. Q.; Li, Y.; Wan, L. S.; Xu, Z. K., Membrane surface with antibacterial property by grafting polycation. *J Membrane Sci* **2011,** *376* (1-2), 132-141.
221. Asri, L. A. T. W.; Crismaru, M.; Roest, S.; Chen, Y.; Ivashenko, O.; Rudolf, P.; Tiller, J. C.; van der Mei, H. C.; Loontjens, T. J. A.; Busscher, H. J., A Shape- Adaptive, Antibacterial- Coating of Immobilized Quaternary- Ammonium Compounds Tethered on Hyperbranched Polyurea and its Mechanism of Action. *Adv Funct Mater* **2014,** *24* (3), 346-355.
222. Yatvin, J.; Gao, J.; Locklin, J., Durable defense: robust and varied attachment of non-leaching poly"-onium" bactericidal coatings to reactive and inert surfaces. *Chem. Commun.* **2014,** *50* (67), 9433-9442.
223. Tiller, J. C., Antimicrobial Surfaces. In *Bioactive Surfaces*, Börner, H. G.; Lutz, J.-F., Eds. Springer Berlin Heidelberg: Berlin, Heidelberg, 2011; pp 193-217.
224. Bieser, A. M.; Tiller, J. C., Mechanistic considerations on contact-active antimicrobial surfaces with controlled functional group densities. *Macromol Biosci* **2011,** *11* (4), 526-34.
225. Gao, J.; White, E. M.; Liu, Q. H.; Locklin, J., Evidence for the Phospholipid Sponge Effect as the Biocidal Mechanism in Surface-Bound Polyquaternary Ammonium Coatings with Variable Cross-Linking Density. *Acs Appl Mater Inter* **2017,** *9* (8), 7745-7751.
226. Wessels, S.; Ingmer, H., Modes of action of three disinfectant active substances: a review. *Regul Toxicol Pharmacol* **2013,** *67* (3), 456-67.
227. Zou, P.; Hartleb, W.; Lienkamp, K., It takes walls and knights to defend a castle – synthesis of surface coatings from antimicrobial and antibiofouling polymers. *J Mater Chem* **2012,** *22* (37), 19579-19589.
228. Cheng, L.; Liu, Q.; Lei, Y.; Lin, Y.; Zhang, A., The synthesis and characterization of carboxybetaine functionalized polysiloxanes for the preparation of anti-fouling surfaces. *Rsc Adv* **2014,** *4* (97), 54372-54381.
229. Yeh, S.-B.; Chen, C.-S.; Chen, W.-Y.; Huang, C.-J., Modification of Silicone Elastomer with Zwitterionic Silane for Durable Antifouling Properties. *Langmuir* **2014,** *30* (38), 11386-11393.
230. Li, Z.; Lee, D.; Sheng, X.; Cohen, R. E.; Rubner, M. F., Two-level antibacterial coating with both release-killing and contact-killing capabilities. *Langmuir* **2006,** *22* (24), 9820-3.
231. (a) Eby, D. M.; Luckarift, H. R.; Johnson, G. R., Hybrid Antimicrobial Enzyme and Silver Nanoparticle Coatings for Medical Instruments. *Acs Appl Mater Inter* **2009,** *1* (7), 1553-1560; (b) Worley, B. V.; Slomberg, D. L.; Schoenfisch, M. H., Nitric oxide-releasing quaternary ammonium-modified poly(amidoamine) dendrimers as dual action antibacterial agents. *Bioconjug Chem* **2014,** *25* (5), 918-27; (c) Ji, E.; Corbitt, T. S.;

Parthasarathy, A.; Schanzes, K. S.; Whitten, D. G., Light and Dark-Activated Biocidal Activity of Conjugated Polyelectrolytes. *Acs Appl Mater Inter* **2011,** *3* (8), 2820-2829.
232. Yin, J. J.; Wahid, F.; Zhang, Q.; Tao, Y. C.; Zhong, C.; Chu, L. Q., Facile Incorporation of Silver Nanoparticles into Ouaternized Poly(2-(Dimethylamino)Ethyl Methacrylate) Brushes as Bifunctional Antibacterial Coatings. *Macromol Mater Eng* **2017,** *302* (6).
233. Sambhy, V.; MacBride, M. M.; Peterson, B. R.; Sen, A., Silver Bromide Nanoparticle/Polymer Composites: Dual Action Tunable Antimicrobial Materials. *J Am Chem Soc* **2006,** *128* (30), 9798-9808.
234. Hon Ho, C.; Tobis, J.; Sprich, C.; Thomann, R.; Tiller, J., Nanoseparated Polymeric Networks with Multiple Antimicrobial Properties. *Adv Mater* **2004,** *16*, 957-961.
235. Yin, B.; Liu, T.; Yin, Y., Prolonging the Duration of Preventing Bacterial Adhesion of Nanosilver-Containing Polymer Films through Hydrophobicity. *Langmuir* **2012,** *28* (49), 17019-17025.
236. Yan, S.; Song, L.; Luan, S.; Xin, Z.; Du, S.; Shi, H.; Yuan, S.; Yang, Y.; Yin, J., A hierarchical polymer brush coating with dual-function antibacterial capability. *Colloids and Surfaces B: Biointerfaces* **2017,** *149*, 260-270.
237. Laloyaux, X.; Fautré, E.; Blin, T.; Purohit, V.; Leprince, J.; Jouenne, T.; Jonas, A. M.; Glinel, K., Temperature-Responsive Polymer Brushes Switching from Bactericidal to Cell-Repellent. *Adv Mater* **2010,** *22* (44), 5024-5028.
238. Mattheis, C.; Zhang, Y.; Agarwal, S., Thermo-Switchable Antibacterial Activity. *Macromol Biosci* **2012,** *12* (10), 1401-1412.
239. (a) Cao, Z.; Brault, N.; Xue, H.; Keefe, A.; Jiang, S., Manipulating sticky and non-sticky properties in a single material. *Angew Chem Int Ed Engl* **2011,** *50* (27), 6102-4; (b) Cao, Z.; Mi, L.; Mendiola, J.; Ella-Menye, J. R.; Zhang, L.; Xue, H.; Jiang, S., Reversibly switching the function of a surface between attacking and defending against bacteria. *Angew Chem Int Ed Engl* **2012,** *51* (11), 2602-5.
240. Yan, S. J.; Luan, S. F.; Shi, H. C.; Xu, X. D.; Zhang, J. D.; Yuan, S. S.; Yang, Y. M.; Yin, J. H., Hierarchical Polymer Brushes with Dominant Antibacterial Mechanisms Switching from Bactericidal to Bacteria Repellent. *Biomacromolecules* **2016,** *17* (5), 1696-1704.

# Chapter 2
# Experimental Section

## 2.1 Materials and Methods

Silicon wafers (100) were purchased from Sil'tronix with a 2-3 nm native $SiO_2$ top layer and were cut into square pieces of 1.5 $cm^2$. All solvents and reagents were purchased from Sigma-Aldrich or Alfa Aesar and were of analytical or HPLC grade. 2-(dimethylamino)ethyl methacrylate (DMAEMA, >98%), 2,2,2-(trifluoro)ethyl methacrylate (TFEMA, 99%), 2,2,3,3,4,4,5,5-(octafluoro)pentyl methacrylate (OFPMA, 98%) and 3,3,4,4,5,5,6,6,7,7,8,8,8-(tridecafluoro)octyl methacrylate (TDFOMA, 97%) were passed through an activated basic alumina column, to remove the inhibitors, were stirred overnight over calcium hydride and 2,2-diphenyl-1-picrylhydrazyl and was finally freshly distilled under vacuum before use. Copper(I) bromide (Cu(I)Br, 99.999%) was purified by washing sequentially with acetic acid and diethyl ether, filtered and left to dry in a vacuum oven before use. Tetrahydrofuran was refluxed three times over potassium metal and was freshly distilled prior to use. Ethyl 2-bromoisobutyrate (EBIB, 98%), 1,1,4,7,10,10-hexamethyltriethylenetetramine (HMTETA, 97%), 4,4'-dinonyl-2,2'-bipyridine (dNbpy, 97%), karstedt catalyst solution (platinum(0)-1-3-divinyl-1,1,3,3-tetramethyldisiloxane complex, 2% Pt), hydrogen peroxide ($H_2O_2$) solution (30 wt% in $H_2O$), sulfuric acid ($H_2SO_4$), dimethylethoxysilane (DMEOS, Gelest Inc.), triethoxysilane (TEOS, Sigma), iodomethane, 1-iodoethane, 1-iodopropane, 1-iodohexane, 1-iodododecane, 1-iodohexadecane, 1-iodooctadecane, n-butylamine and acid orange 7 (AO7) were used as received without further purification. 2-bromoisobutyryl bromide (BIBB), allyl alcohol (AA) and triethylamine (TEA), were freshly distilled before use. All other chemicals and solvents were used as received. Milli-Q water of specific resistivity of 18 MΩ.cm was used in all experiments.

## 2.2 Synthesis of homopolymer brushes

### 2.2.1 Synthesis of the (3-(2-bromoisobutyryl)propyl)dimethylethoxysilane (BIDS) surface-bound initiator

The surface-bound atom tranfer radical polymerization (ATRP) initiator (3-(2-bromoisobutyryl)propyl)dimethylethoxysilane (BIDS) was synthesized following the procedure developed by von Werne and co-workers.[1] Briefly, in the first step, freshly distilled 2-bromoisobutyryl bromide (BIBB) (8.85ml, 71.6 mmol) was added dropwise to a solution of allyl alcohol (AA) (4 ml, 58.8 mmol) and triethylamine (TEA) (15 ml,

107 mmol) in anhydrous tetrahydrofuran (THF, 40 ml) at 0 ºC. The mixture was stirred at room temperature for 20 h, filtered and the filtrate was evaporated to dryness under reduced pressure. The final product, allyl 2-bromoisobutyrate (ABIB) (3.9gr, 19.3 mmol) was collected by distillation as a colorless oil at 60 ºC and was stored under a nitrogen atmosphere. $^1$H NMR (300 MHz, $CDCl_3$): δ 5.93(m, 1H), 5.30(dd, 2H), 4.69(d, 2H), 1.98 (s, 6H).

In the second step, ABIB (3.9gr, 19.3 mmol) was placed in a flask followed by the dropwise addition of mono-functional dimethylethoxysilane (DMEOS) (5.3 ml, 38.6 mmol) and the Karstedt's catalyst solution (191 μl). The reaction was stirred at 70 ºC for 2 h. Next, the solvent and unreacted silane were removed under reduced pressure and the ATRP initiator BIDS (4 g, 12.8 mmol) was distilled at 120 ºC under vacuum as a slightly yellowish oil in quantitative yield and was stored at 0 ºC until use. $^1$H NMR (300 MHz, $CDCl_3$): δ 4.15 (2H, m), 3.69 (2H, q), 1.95 (6H, s), 1.73 (2H, m), 1.20 (3H, t), 0.60 (2H, m), 0.14 (6H, s).

### 2.2.2 Synthesis of the (3-(2-bromoisobutyryl)propyl)triethoxysilane (BIBPTES) ATRP initiator

The surface-bound ATRP initiator (3-(2-bromoisobutyryl)propyl)triethoxysilane (BIBPTES) was synthesized following the procedure of Wang and co-workers.[2] Briefly, in the first step, freshly distilled BIBB (8.85ml, 71.6 mmol) was added dropwise to a solution of AA (4 ml, 58.8 mmol) and TEA (15 ml, 107 mmol) in 40 ml anhydrous THF, at 0 ºC. The mixture was stirred at room temperature for 20 h, filtered and the filtrate was evaporated to dryness under reduced pressure. The final product, ABIB (3.9gr, 19.3 mmol) was collected by distillation as a colorless oil at 60 ºC and was stored under a nitrogen atmosphere. $^1$H NMR (300 MHz, $CDCl_3$): δ 5.93(m, 1H), 5.30(dd, 2H), 4.69(d, 2H), 1.98 (s, 6H).

In the second step, ABIB (3.9gr, 19.3 mmol) was placed in a flask containing anhydrous toluene (10 ml) followed by the dropwise addition of trifunctional triethoxysilane (TEOS) (7.1 ml, 38.7 mmol) and the Karstedt's catalyst solution (200 μl). The reaction was stirred at 60 ºC overnight. Next, the solvent and unreacted silane were removed under reduced pressure and the ATRP initiator BIBPTES (2.7 g, 7.2 mmol) was distilled at 140 ºC under vacuum as a slightly yellowish oil in quantitative yield and

was stored at 0 ºC, until use. $^1$H NMR (300 MHz, $CDCl_3$): δ 4.12 (2H, t), 3.81 (6H, q), 1.90 (6H, s), 1.76 (2H, m), 1.20 (9H, t), 0.66 (2H, t).

### 2.2.3 Immobilization of the ATRP initiators on silicon and glass substrates

For the formation of the self-assembled monolayer (SAM) of the initiator, planar glass slides and silicon wafers were sonicated in 2 -propanol for 10 min, dried with nitrogen and then cleaned with a freshly prepared "piranha" solution (1:1 v/v of a 30 vol% $H_2O_2$ aqueous solution and a 97 wt% $H_2SO_4$ solution) for 30 min to remove any organic residues and to increase the density of the reactive silanol groups on the substrates. Afterwards, the clean superhydrophilic surfaces were removed and rinsed extensively with nanopure water and 2-propanol. The substrates were dried under a nitrogen stream and were placed in a vacuum oven for at least 6 hours to dry. Subsequently, the substrates were placed into a 0.5, 1 or 2 v/v% solution of the BIDS initiator or BIBPTES initiator in anhydrous toluene at 25 ºC. After predetermined times of 3, 6, 12 and 24h the substrates were removed from the solution, washed with toluene and 2-propanol to remove the unattached BIDS, followed by drying with a nitrogen stream, baked at 120 ºC and were finally used or stored in ethanol at RT until use.

### 2.2.4 Surface-initiated atom transfer radical polymerization (SI-ATRP) of DMAEMA, TFEMA, OFPMA and TDFOMA

#### 2.2.4.1 Poly(2-(dimethylamino)ethyl methacrylate) (PDMAEMA) brushes

A typical SI-ATRP procedure in bulk was carried out as follows: BIDS-modified silicon wafers (0.5 v/v% solution in toluene, 24 h, at 25 ºC) were placed in a reaction flask, sealed with a PTFE/silicon septum cap and deoxygenated by five vacuum-purge nitrogen back-fill cycles. Ethyl 2-bromoisobutyrate (EBIB) (20 μl, 0.14 mmoles) was added as a free initiator to ensure the control of the polymerization. In a separate flask, 2-(dimethylamino)ethyl methacrylate (DMAEMA) (30 ml, 178 mmoles) and 1,1,4,7,10,10-hexamethyltriethylenetetramine (HMTETA) (76 μl, 0.28 mmoles) were purged with nitrogen for 10 min and next copper(I) bromide (Cu(I)Br) (20 mg, 0.14 mmoles) was added, followed by three freeze-pump-thaw cycles. The final green solution was transferred to the substrates via a syringe and the reaction was allowed to proceed at RT for certain periods of reaction time, before being quenched by exposure to air. Brushes of different thicknesses were obtained by varying the polymerization

time. After the polymerization, the surfaces were removed from the reaction mixture and were washed in THF for 24 h to eliminate the non-grafted polymer. Next, the samples were sonicated for 10 min in THF, rinsed thoroughly with 2-propanol and acetone and dried under a nitrogen stream. The reaction mixture was diluted with THF and was passed through a neutral alumina column to remove the ATRP catalyst. The PDMAEMA homopolymer was recovered from the THF solution by precipitation in cold n-hexane and was dried overnight under reduced pressure, before characterization by size exclusion chromatography (SEC). The above procedure was repeated for 1:1 and 4:1 volume ratios of DMAEMA and THF to prepare poly(2-(dimethylamino)ethyl methacrylate) (PDMAEMA) homopolymer films of different thicknesses. Table 2.1 summarizes the polymerization conditions used for the syntheses of the PDMAEMA films in bulk and in THF.

**Table 2.1.** Reaction conditions used for the synthesis of the PDMAEMA brushes.

| **Monomer** | **solvent** | **Polymerization conditions [M]:[Cu$^{I}$Br]:[EBIB]:[HMTETA]** | **Reaction time (h)** |
|---|---|---|---|
| DMAEMA | bulk | 500:1:1:2 | 3 |
| | | | 5 |
| | | | 9 |
| | | | 12 |
| | | | 15 |
| DMAEMA | THF 1:1 | 500:1:1:2 | 3 |
| | | | 6 |
| | | | 12 |
| | | | 18 |
| | | | 24 |
| DMAEMA | THF 4:1 | 500:1:1:2 | 3 |
| | | | 5 |
| | | | 7 |
| | | | 12 |
| | | | 15 |
| DMAEMA | THF 4:1 | 1300:1:1:2 | 3 |
| | | | 5 |
| | | | 7 |
| | | | 12 |
| | | | 38 |

### 2.2.4.2 Semi-fluorinated polymethacrylate brushes

2,2,2-(trifluoro)ethyl methacrylate (TFEMA, $C_F1$), 2,2,3,3,4,4,5,5-(octafluoro)pentyl methacrylate (OFPMA, $C_F4$) and 3,3,4,4,5,5,6,6,7,7,8,8,8-(tridecafluoro)octyl methacrylate (TDFOMA, $C_F6$) brushes were synthesized via SI-ATRP following a similar protocol. Table 2.2 summarizes the ATRP reaction conditions used for the synthesis of the semi-fluorinated polymer brushes. Briefly for the synthesis of poly(2,2,2-(trifluoro)ethyl methacrylate) (PTFEMA) brushes, initiator modified surfaces were placed in a reaction flask, sealed and deoxygenated by five vacuum purge-nitrogen back-fill cycles. In a separate flask, a 2:1 v/v mixture of α,α,α-trifluorotoluene (TFT) (3 ml), TFEMA (1.5 ml, 10.5 mmol) and 4,4'-dinonyl-2,2'-bipyridine (dNbpy) (0.14 mmol) was purged with nitrogen for 10 min and next Cu(I)Br (0.07 mmol) was added, followed by three freeze-pump-thaw cycles. The solution was heated for 10 min at 50 ºC until it became homogeneous and was transferred to the substrates via a syringe. EBIB (0.07 mmol) was added as a free initiator and the polymerization was allowed to proceed at 110 ºC for a predetermined period of time, before being quenched by exposure to air. After the polymerization, the PTFEMA surfaces were removed from the reaction mixture and were immersed in TFT for 24 h under vigorous stirring to remove the non-grafted polymer. Next, the samples were sonicated for 10 min in TFT, rinsed thoroughly with hexafluoroisopropanol (HFiP), isopropanol and acetone and were dried under a nitrogen stream. All samples were baked at 100 ºC for 30 min and were further dried under vacuum for 12 h at RT. The homopolymers were recovered from the TFT solutions by precipitation in cold n-hexane, were dried overnight under reduced pressure and were characterized by SEC. The poly(2,2,3,3,4,4,5,5-(octafluoro)pentyl methacrylate) (POFPMA) and poly(3,3,4,4,5,5,6,6,7,7,8,8,8-(tridecafluoro)octyl methacrylate) (PTDFOMA) brushes were prepared using OFPMA (2.2 ml, 10.5 mmol) and TDFOMA (3 ml, 10.5 mmol) as the monomer, respectively.

**Table 2.2.** Reaction conditions used for the synthesis of the PTFEMA, POFPMA and PTDFOMA polymer films.

| Monomer | solvent | Polymerization conditions [M]:[Cu$^{I}$Br]:[EBIB]:[dNbpy] | Reaction time (h) |
|---|---|---|---|
| TFEMA | TFT | 500:1:1:2 | 12 |
| | | | 24 |
| | | | 60 |
| OFPMA | | | 12 |
| | | | 24 |
| | | | 60 |
| TDFOMA | | | 12 |
| | | | 24 |
| | | | 60 |

### 2.2.4.3 Quaternization of the PDMAEMA brushes

The PDMAEMA brushes, obtained by SI-ATRP as described above, were reacted with different alkyl halides, iodomethane (C1), 1-iodoethane (C2) and 1-iodopropane (C3) in methanol, at 50 ºC, and 1-iodohexane (C6), 1-iodododecane (C12), 1-iodohexadecane (C16) and 1-iodooctadecane (C18) in chloroform, at 50 ºC, for approximately 48 h to yield the quaternized PDMAEMA (PQDMAEMA) brushes. For this, the PDMAEMA surfaces were placed in separate vials and an excess of a 30 mM solution of each alkyl halide was added, targeting to fully quaternize the PDMAEMA brushes. After the reaction, the quaternized films were washed repeatedly with deionized water, methanol and chloroform. Finally, the PQDMAEMA films were sonicated for 10 min in chloroform and were dried overnight under vacuum. Table 2.3 summarizes the PQDMAEMA films prepared after quaternization using as quaternization agents alkyl halides with different alkyl chain lengths (ACLs).

**Table 2.3.** Alkyl halides and solvents employed for the quaternization of the PDMAEMA brushes.

| Brush | Alkyl iodide | solvent |
|---|---|---|
| PQDMAEMA-C1 | C1 | MetOH |
| PQDMAEMA-C2 | C2 | MetOH |
| PQDMAEMA-C3 | C3 | MetOH |
| PQDMAEMA-C6 | C6 | $CHCl_3$ |
| PQDMAEMA-C12 | C12 | $CHCl_3$ |
| PQDMAEMA-C16 | C16 | $CHCl_3$ |
| PQDMAEMA-C18 | C18 | $CHCl_3$ |

## 2.3 Synthesis of diblock copolymer brushes

### 2.3.1 Synthesis and self-assembly of the ATRP initiator BIDS

The synthesis of the ATRP initiator BIDS and its immobilization onto silicon and glass substrates is described in paragraphs 2.2.1 and 2.2.2, respectively.

### 2.3.2 Synthesis of diblock copolymer brushes by surface-initiated atom transfer radical polymerization.

#### 2.3.2.1 Synthesis of PDMAEMA macroinitiator brushes via SI-ATRP

Scheme 2.1 illustrates the synthesis of the amphiphilic diblock copolymer brushes comprising a PDMAEMA block and a PTFEMA, POFPMA or PTDFOMA segment. For the synthesis of the block copolymers, first a surface-grafted PDMAEMA macroinitiator was synthesized following the procedure described in section 2.2.3.1 above. More specifically, in a flask sealed with a PTFE septum under dry conditions, THF (1.7 ml), DMAEMA (6.9 ml, 40.8 mmoles), Cu(I)Br (20 mg, 0.14 mmoles) and HMTETA (74.6 μl, 0.27 mmoles) were added. The reaction mixture was stirred for 15 min until it became homogeneous followed by three freeze-pump-thaw cycles. In a separate dry flask, the initiator immobilized surfaces and the free initiator EBIB (20 μl, 0.14 mmoles) were added and deoxygenated by five vacuum purge-nitrogen back-fill cycles. The green solution was transferred to the substrates via a syringe and the reaction was allowed to proceed at RT for 18 h, before being quenched by exposure to

air. The degree of polymerization of the brushes was varied by tuning the reaction time. After the polymerization, the surfaces were removed from the reaction mixture and were washed in THF for 24 hours to remove the non-grafted polymer. Next, the samples were sonicated for 10 min in THF, rinsed thoroughly with 2-propanol and acetone and were dried under a nitrogen stream.

The reaction mixture was diluted with THF and was passed through a neutral alumina column to remove the ATRP catalyst. The PDMAEMA homopolymer was recovered from the THF solution by precipitation in cold n-hexane, was dried overnight under reduced pressure and was characterized by GPC. Table 2.4 summarizes the polymerization conditions used for the synthesis of the PDMAEMA macroinitiator brushes in THF with targeted degrees of polymerization (DP = 150 and 300).

#### 2.3.2.2 Synthesis of amphiphilic diblock copolymer brushes

For the synthesis of the diblock copolymer brushes the procedure described in section 2.2.3.2 was repeated, using the PDMAEMA macroinitiator brushes and the PDMAEMA macroinitiator obtained above, as initiating sites. Table 2.4 summarizes the reaction conditions used for the SI-ATRP of the fluorinated monomers. In a reaction flask, TFEMA (3 ml) was dissolved in TFT (1.5 ml). Cu(I)Br and dNbpy were added and the solution was purged with nitrogen. In a separate flask, the PDMAEMA macroinitiator was dissolved in TFT and was added to the first reaction flask followed by three freeze-pump-thaw cycles. After deoxygenation, the reaction mixture was transferred to a third flask containing the PDMAEMA macroinitiator brushes. The polymerization was allowed to proceed for 48 h and 60 h, at 110 ºC, before being quenched by exposure to air. After the polymerization, the PDMAEMA-*b*-PTFEMA diblock copolymer films were removed from the reaction mixture and were immersed in TFT for 24 h under vigorous stirring to remove the non-grafted polymer. Next, the samples were sonicated for 10 min in TFT, rinsed thoroughly with HFiP, THF, isopropanol and acetone and were dried under a nitrogen stream. All samples were baked at 100 ºC for 30 min and were further dried under vacuum for 24 h. The PDMAEMA-*b*-PTFEMA diblock copolymer was recovered from the TFT solution by precipitation in cold n-hexane, was dried overnight under reduced pressure and was characterized by GPC. PDMAEMA-*b*-POFPMA and PDMAEMA-*b*-PTDFOMA

copolymer brushes were prepared following a similar procedure and using OFPMA (2.2 ml, 10.5 mmol) and TDFOMA (3 ml, 10.5 mmol) as the monomer, respectively.

**Table 2.4.** Reaction conditions used for the synthesis of the diblock copolymer brushes.

| Polymer brush | Reaction time Inner block (h) | Polymerization conditions [M]:[$Cu^{I}Br$]:[EBIB]:[HMTETA] | Reaction time Outer block (h) | Polymerization conditions [M]:[$Cu^{I}Br$]:[EBIB]:[dNbpy] |
|---|---|---|---|---|
| PDMAEMA-b-PTFEMA | 18 | 300:1:1:2 | 60 | 300:1:1:2 |
| PDMAEMA-b-PTFEMA | 9 | 150:1:1:2 | 48 | 150:1:1:2 |
| PDMAEMA-b-POFPMA | 18 | 300:1:1:2 | 60 | 300:1:1:2 |
| PDMAEMA-b-POFPMA | 9 | 150:1:1:2 | 48 | 150:1:1:2 |
| PDMAEMA-b-PTDFOMA | 18 | 300:1:1:2 | 60 | 300:1:1:2 |
| PDMAEMA-b-PTDFOMA | 9 | 150:1:1:2 | 48 | 150:1:1:2 |

### 2.3.3 Quaternization of the amphiphilic diblock copolymer brushes

The PDMAEMA-*b*-PTFEMA, PDMAEMA-*b*-POFPMA and PDMAEMA-*b*-PTDFOMA brushes, obtained by SI-ATRP as described above, were reacted with 1-iodopropane (C3) in methanol at 50 ºC for ~48 h to yield the PQDMAEMA-*b*-PTFEMA, PQDMAEMA-*b*-POFPMA and PQDMAEMA-*b*-PTDFOMA brushes. After the reaction, the quaternized films were washed repeatedly with deionized water, methanol and chloroform and were sonicated for 10 min in TFT before being dried overnight under vacuum.

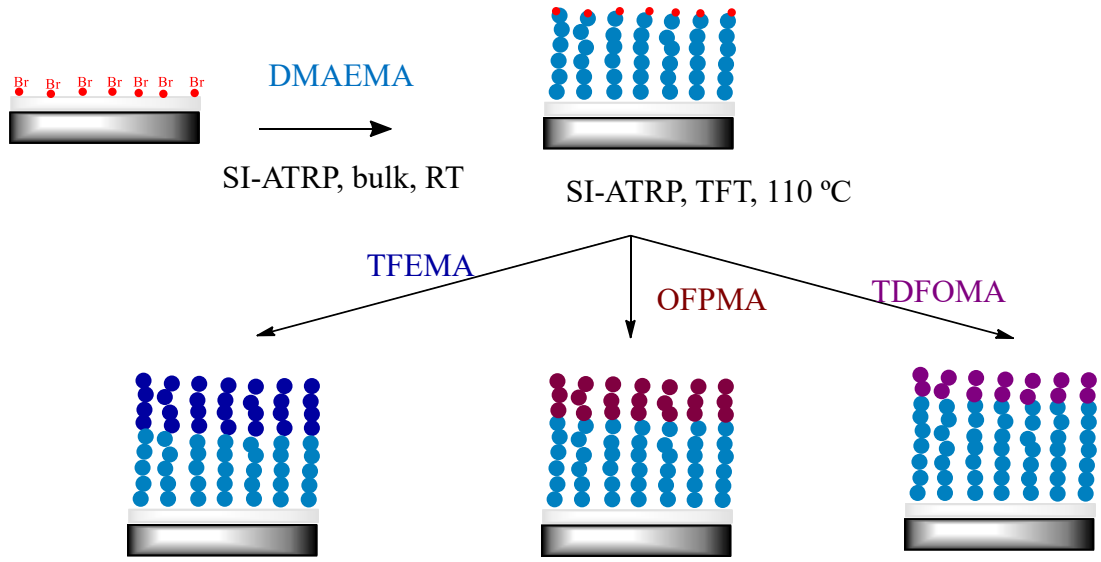


**Scheme 2.1.** Schematic illustration of the synthetic procedure followed for the synthesis of the diblock copolymer brushes.

## 2.4 Synthesis of mixed polymer brushes

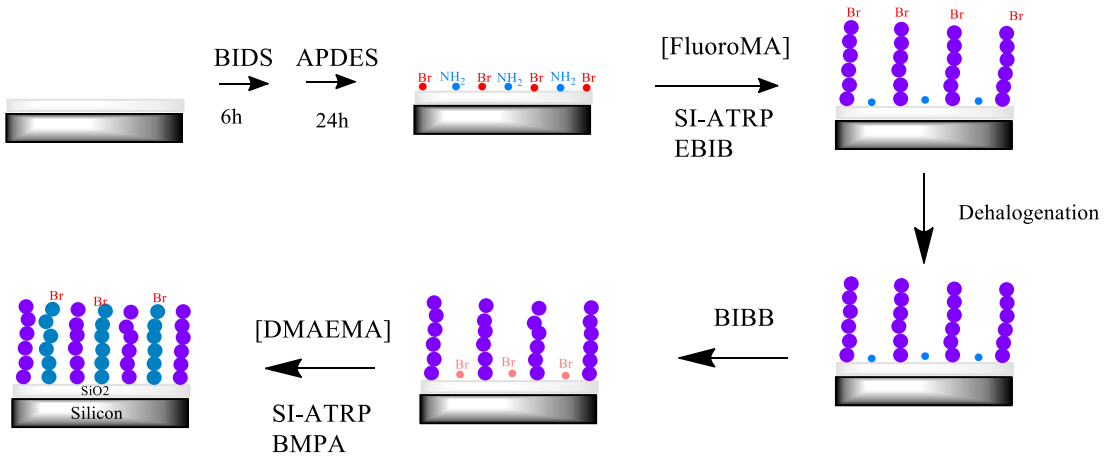


**Scheme 2.2.** Schematic illustration of the synthetic procedure followed for the synthesis of the mixed polymer brushes.

### 2.4.1 Synthesis of the ATRP initiators

#### 2.4.1.1 Synthesis of the 2-bromo-2-methyl-N-pentylpropanamide (BMPA) surface-bound initiator.

The model "sacrificial" initiator, 2-bromo-2-methyl-N-pentylpropanamide (BMPA), was prepared as follows. In a round bottom flask containing a stirrer bar, sealed with a rubber septum under nitrogen flow, were syringed in sequence 17 mL of freshly distilled THF, 4.9 mL amylamine (14 mmol) and 5 mL triethylamine (18 mmol). The mixture was cooled to 0 ºC in an ice bath followed by the slow addition of 2-bromoisobutyryl bromide 3 mL (12 mmol) under rigorous stir. The reaction mixture was stirred at 0 ºC for 1 h and then at room temperature for 6 h. The triethylammonium salt produced was removed using a glass filter. Next, the solvent, the triethylamine and any unreacted amylamine were removed under reduced pressure using a rotary evaporator, and the ATRP initiator BMPA (4 g, 12.8 mmol) was distilled at 70 ºC under vacuum as a yellowish oil in quantitative yield and was stored at RT under dark until use. $^{1}$H NMR (300 MHz, $CDCl_3$): δ 6.76 (1H, s), 3.25 (2H, t), 1.96 (6H, s), 1.55 (2H, m), 1.35 (4H, m), 0.92 (3H, m).

#### 2.4.1.2 Synthesis of the (3-(2-bromoisobutyryl)propyl)dimethylethoxysilane (BIDS) surface-bound initiator.

The surface-bound atom tranfer radical polymerization (ATRP) initiator BIDS was synthesized following the procedure developed by von Werne and co-workers.[1] Briefly, in the first step, freshly distilled BIBB (8.85ml, 71.6 mmol) was added dropwise to a solution of allyl alcohol (4 ml, 58.8 mmol) and TEA (15 ml, 107 mmol) in anhydrous THF at 0 ºC. The mixture was stirred at room temperature for 20 h, filtered and the filtrate was evaporated to dryness under reduced pressure. The final product, ABIB (3.9gr, 19.3 mmol) was collected by distillation as a colorless oil at 60 ºC and was stored under a nitrogen atmosphere. $^1$H NMR (300 MHz, $CDCl_3$): δ 5.93(m, 1H), 5.30(dd, 2H), 4.69(d, 2H), 1.98 (s, 6H). In the second step, ABIB (3.9gr, 19.3 mmol) was placed in a flask followed by the dropwise addition of mono-functional DMEOS (5.3 ml, 38.6 mmol) and the Karstedt's catalyst solution (191 μl). The reaction was stirred at 70 ºC for 2 h. Next, the solvent and the unreacted silane were removed under reduced pressure and the ATRP initiator BIDS (4 g, 12.8 mmol) was distilled at 120 ºC under vacuum as a slightly yellowish oil in quantitative yield and was stored at -20 ºC until use. $^1$H NMR (300 MHz, $CDCl_3$): δ 4.15 (2H, m), 3.69 (2H, q), 1.95 (6H, s), 1.73 (2H, m), 1.20 (3H, t), 0.60 (2H, m), 0.14 (6H, s).

### 2.4.2 Deposition of the mixed silanes on silicon wafers

*"Co-adsorption" method.* In a first approach, the "co-adsorption" method was utilized for the preparation of a mixed SAM of the two ATRP initiators, by immersing a clean silicon surface in a 0.5% v/v solution of a BIDS/APDES mixture at RT for 24 h. Mixtures of 100:0, 99:1, 90:0, 75:25, 50:50, 25:75 and 0:100 BIDS/APDES molar ratios in toluene were used for the formation of the mixed SAMs

*Stepwise method.* In another approach, the stepwise method was used for the preparation of a mixed SAM of the two ATRP initiators, by first immersing a clean substrate in a solution of BIDS for a predetermined length of time, followed by the immersion of the substrate in a solution of APDES.[3] The latter can be reacted in a subsequent step with BIBB to form an active amide initiator (see paragraph 2.4.5). Briefly, planar silicon wafers were rinsed with 2-propanol, dried under a nitrogen steam and then cleaned with a freshly prepared "piranha" solution (1:1 v/v of a 30 vol% $H_2O_2$

aqueous solution and a 97 wt% $H_2SO_4$ solution) for 30 min and were then removed and rinsed extensively with nanopure water and 2-propanol. The substrates were dried under a nitrogen stream and were placed in a vacuum oven for 10 min to dry. Subsequently, they were placed in a 0.5% v/v solution of BIDS initiator, in anhydrous toluene, at 25 ºC for 3, 6, 12 and 24 h. Next, the samples were washed with toluene and were immersed in a 0.5% v/v solution of APDES, in anhydrous toluene, at 25 ºC for 24 h.

In both cases, the wafers with the mixed BIDS/APDES monolayer were washed repetitively in toluene, chloroform, ethanol and dried under nitrogen steam.

The successful immobilization of the mixed silanes by both techniques utilized, was verified by the SI-ATRP of MMA, due to the high cost of the fluorinated monomers.

### 2.4.3 Surface-initiated atom transfer radical polymerization from the mixed-silane functionalized substrates.

PMMA brushes were synthesized by SI-ATRP as follows. A mixed silane-modified silicon wafer was placed in a reaction flask, sealed with a PTFE/silicon septum cap, and was deoxygenated by five vacuum purge-nitrogen back-fill cycles. EBIB (20 μl, 0.14 mmoles) was added as a free initiator to ensure the control of the polymerization. In a separate flask, MMA (14.5 ml, 136 mmoles) and dnbpy (222 mg, 0.55 mmoles) were purged with nitrogen for 10 min and next Cu(I)Br (39 mg, 0.27 mmoles) was added, followed by three freeze-pump-thaw cycles. The final solution was transferred to the substrates via a syringe and the reaction was allowed to proceed at 90 ºC, before being cooled down and quenched by exposure to air. After the polymerization, the polymer films were removed from the reaction mixture and were immersed in methanol for 24 hours under vigorous stirring to remove the non-grafted polymer. Next, the samples were sonicated for 10 min in methanol, rinsed thoroughly with 2-propanol and acetone and dried under a nitrogen stream. All samples were baked at 100 ºC for 30 min and were further dried under vacuum for 24 h.

The reaction mixture was diluted with THF and was passed through a neutral alumina column to remove the ATRP catalyst. The PMMA homopolymer was recovered from the THF solution by precipitation in cold n-hexane and was dried overnight under reduced pressure, before being characterized by size exclusion chromatography (SEC).

TFEMA, OFPMA and TDFOMA brushes were synthesized via SI-ATRP following a similar protocol. Briefly for the synthesis of the PTFEMA brushes, initiator modified surfaces were placed in a reaction flask, sealed and deoxygenated by five vacuum purge-nitrogen back-fill cycles. In a separate flask, a 2:1 v/v mixture of TFT (3 ml) and TFEMA (1.5 ml, 10.5 mmol) and dNbpy (56 mg ,0.14 mmol) were purged with nitrogen for 10 min and next Cu(I)Br (10 mg ,0.07 mmol) was added, followed by three freeze-pump-thaw cycles. Next, the solution was heated for 10 min at 50 ºC until it became homogeneous and was transferred to the substrates via a syringe. EBIB (10 μl, 0.07 mmol) was added as a free initiator and the polymerization was allowed to proceed at 110 ºC for a predetermined period of time, before being quenched by exposure to air. After the polymerization, the PTFEMA surfaces were removed from the reaction mixture and were immersed in TFT for 24 h under vigorous stirring to remove the non-grafted polymer. Next, the samples were sonicated for 10 min in TFT, were rinsed thoroughly with HFiP, isopropanol and acetone and were dried under a nitrogen stream. All samples were baked at 120 ºC for 30 min and were further dried under vacuum for 12 hours.

The homopolymers were recovered from the TFT solutions by precipitation in cold n-hexane, were dried overnight under reduced pressure and were characterized by GPC. The POFPMA and PTDFOMA brushes were prepared using OFPMA (2.2 ml, 10.5 mmol) and TDFOMA (3 ml, 10.5 mmol) as the monomer, respectively.

### 2.4.4 Dehalogenation of the brushes and synthesis of BIBAPDES.

*Dehalogenation.* The dehalogenation procedure has been widely used in several studies for the preparation of mixed polymer brushes.[4] Herein, the silicon wafers grafted with PMMA brushes were placed in a sealed vial with a rubber septum under a nitrogen flow. Anisole (5 ml), EBIB (0.2 mmol, 29 μL) and PMDETA (0.2 mmol, 41.6 μL) were added to a round bottom flask and were deoxygenated by three freeze-pump-thaw cycles. Afterwards the flask was backfilled with nitrogen and Cu(I)Br (0.2 mmol, 28.7 mg) was added to the frozen solution mixture. The mixture was deoxygenated again following three-freeze-pump-thaw cycles, was backfilled with nitrogen and was left to liquify at RT. The solution was transferred to the vial that contained the polymer brushes and the vial was placed to an oil bath at 50 ºC. Then, tri(n-butyl)tin hydride (0.6 mmol, 0.16 mL) was transferred to the vial and the reaction was allowed to proceed

for 2 h. After this period, the resulting dehalogenated PMMA brushes were excessively cleaned with dichloromethane and THF. The same procedure was employed for the dehalogenation of the PTFEMA, POFPMA and PTDFOMA mixed polymer brushes.

The efficiency of the dehalogenation process was assessed by the SI-ATRP of DMAEMA from the substrates bearing the halogen-free PMMA, PTFEMA, POFPMA or PTDFOMA brushes. No chain extension and increase in the film thickness should occur if the terminal Br atoms are not present. A typical protocol was followed as described in the section 2.3.2.1. The resulting polymer brushes were characterized by dry ellipsometry.

*Click synthesis of the surface-bound ATRP initiator BIBAPDES.* The surface-bound ATRP initiator (3-(2-bromoisobutyramido)propyl)dimethylethoxy silane (BIBAPDES) was synthesized following the procedure developed by Klok and co-workers.[5] Briefly, the silicon wafers grafted with PMMA, PTFEMA and POFPMA and PTDFOMA brushes were placed in a sealed vial with a rubber septum under a nitrogen atmosphere. Next, a solution of TEA (15 ml, 107 mmol) in anhydrous THF was injected, followed by the dropwise addition of freshly distilled BIBB (8.85ml, 71.6 mmol) at 0 ºC. The reaction was allowed to proceed for 24 h. After this period, the resulting PMMA/BIBAPDES, PTEMA/BIBAPDES, POFPMA/BIBAPDES and PTDFOMA/BIBAPDES brushes were excessively cleaned with THF and dried under a nitrogen flow.

### 2.4.5 Surface-initiated atom transfer radical polymerization of DMAEMA from the PMMA/BIBABDES, PTFEMA/BIBAPDES, POFPMA/BIBAPDES and PTDFOMA/BIBAPDES brushes.

Scheme 2.2 illustrates the steps followed for the synthesis of the mixed amphiphilic polymer brushes comprising PDMAEMA and PMMA, PTFEMA, POFPMA or PTDFOMA homopolymer chains grafted from silicon or glass substrates.
A typical SI-ATRP was carried out as follows. The PMMA/BIBAPDES, PTFEMA/BIBABDES, POFPMA/BIBAPDES or PTFEMA/BIBABDES-modified silicon wafers were placed in a reaction flask, sealed with a PTFE/silicon septum cap, and were deoxygenated by five vacuum purge-nitrogen back-fill cycles. EBIB (20 µl, 0.14 mmoles) was added as a free initiator to ensure the control of the polymerization.

In a separate flask, a 4:1 v/v mixture of DMAEMA (30 ml, 178 mmoles) and THF was added, followed by HMTETA (76 μl, 0.28 mmoles), and were purged with nitrogen for 10 min. Next Cu(I)Br (20 mg, 0.14 mmoles) was added, followed by three freeze-pump-thaw cycles. The final green solution was transferred to the substrates via a syringe and the reaction was allowed to proceed at RT for certain periods of reaction time, before being quenched by exposure to air. After the polymerization, the substrates were removed from the reaction mixture and were immersed in methanol or TFT for 24 h under vigorous stirring to remove the non-grafted polymer. Next, the samples were sonicated for 10 min in THF, rinsed thoroughly with 2-propanol and acetone and dried under a nitrogen stream. All samples were baked at 100 $^{o}$C for 30 min and were further dried under vacuum for 24 h.

The reaction mixture was diluted with THF and was passed through a neutral alumina column to remove the ATRP catalyst. The PDMAEMA homopolymer was recovered from the THF solution by precipitation in cold n-hexane and was dried overnight under reduced pressure, before being characterized by SEC. Table 2.5 summarizes the polymerization conditions used for the syntheses of the PMMA/PDMAEMA, PTFEMA/PDMAEMA, POFPMA/PDMAEMA and PTDFOMA/PDMAEMA mixed polymer films.

### 2.4.6 Synthesis of the PTFEMA/PQDMAEMA-C3, POFPMA/PQDMAEMA-C3 and PTDFOMA/PQDMAEMA-C3 brushes via quaternization.

The PTFEMA/PDMAEMA, POFPMA/PDMAEMA and PTDFOMA/PDMAEMA mixed polymer brushes were next reacted with 1-iodopropane (C3) in methanol at 50 $^{o}$C for approximately 48 h to yield the PTFEMA/PQDMAEMA-C3, POFPMA/PQDMAEMA-C3 and PTDFOMA/PQDMAEMA-C3 brushes. After the reaction, the quaternized films were washed repeatedly with deionized water, TFT, methanol and chloroform. All brushes were baked at 100 $^{o}$C for 30 min and were further dried under vacuum for 24 h.

**Table 2.5.** Reaction conditions employed for the synthesis of the mixed polymer brushes.

| Polymer brush | Reaction time $1^{ST}$ SI-ATRP (h) | $1^{ST}$ SI-ATRP [M]:[$Cu^{I}Br$]:[EBIB]:[dNbpy] Solvents: bulk, TFT | Reaction time $2^{ND}$ SI-ATRP (h) | $2^{ND}$ SI-ATRP [M]:[$Cu^{I}Br$]:[EBIB]:[ HMTETA] bulk |
|---|---|---|---|---|
| PMMA-PDMAEMA | 5 | 1000:2:1:4 | 24 | 600:1:1:2 |
| PTFEMA-PDMAEMA | 72 | 500:1:1:2 | | |
| POFPMA-PDMAEMA | 72 | 500:1:1:2 | 18 | 300:1:1:2 |
| PTDFOMA-PDMAEMA | 72 | 500:1:1:2 | | |

## 2.5 Responsive behavior of the amphiphilic diblock copolymer and mixed polymer brushes when varying the solvent quality

All diblock copolymer and mixed polymer brushes were treated with different selective solvents for the two polymers to test their responsive behavior as a function of the solvent quality. First, the films were immersed in THF, which is a good solvent for both polymers, and were next, thermally annealed at 100 ºC, which results in the extension of the tethered polymer chains with the fluorinated groups being at the outermost part of the surface, due to their affinity for the air interface. A good solvent for each polymer, HFiP for the fluoromethacrylates and water for PDMAEMA was used. The diblock copolymer and mixed polymer brushes were immersed in 10 ml of solvent for predetermined time (6 h in HFiP and 18 h in water) at RT. After immersion in the selective solvent, the samples were dried with a $N_2$ stream and were placed under vacuum oven for 1 h followed by characterizations with contact angle measurements and AFM.

## 2.6 Characterization techniques

### 2.6.1 Size exclusion chromatography (SEC)

The molecular weights and molecular weight distributions of the end grafted polymer chains prepared by SI-ATRP can be determined by size exclusion chromatography using two approaches. Either by the cleavage of the grafted polymer chains followed by SEC analysis or by the utilization of a free/"sacrificial" initiator in the reaction mixture, which produces free chains in solution assumed to have the same molecular weight as the polymer chains grown from the surfaces.

The number average molecular weights ($M_n$'s) and the molecular weight distributions ($M_w/M_n$'s) of the free PDMAEMA, PTFEMA and POFPMA chains and of the diblock copolymers PDMAEMA-*b*-PTFEMA, PDMAEMA-*b*-POFPMA and PDMAEMA-*b*-PTDFOMA formed in solution were determined by SEC The system comprised a Waters 515 HPLC pump, two PLgel mixed D and mixed E (Agilent Technologies) columns at 40 ºC, an UV Waters 2487 and a refractive index (RI) Waters 410 detector. THF with 2 v/v% triethylamine was used as the eluent at a flow rate of 1 ml $min^{-1}$. The calibration curve was based on five narrow PMMA standards with molecular weights ranging from 850 to 342,900 g $mol^{-1}$.

### 2.6.2 $^1$H NMR spectroscopy

$^1$H Nuclear Magnetic Resonance (NMR) spectra were recorded on a Bruker Advance DPX 300 NMR Spectrometer (300 MHz) using $CDCl_3$ as the solvent. The raw data were analyzed by the MestReC software. The composition of the diblock copolymers and the successful synthesis of the homopolymers was determined.

### 2.6.3 Spectroscopic ellipsometry measurements

The thickness of a polymer brush on a planar substrate is routinely measured by ellipsometry. This technique is non-distructive, facile and precise allowing to determine both the dry and the wet polymer film thickness. Ellipsometric measurements were performed on a variable angle spectroscopic ellipsometer (SE) (model VASE, J. A. Woolam Co., Inc.) to determine the dry thickness of the polymer films via the WVase32 software. The angles of incidence were set to 65º, 70º, 75º in the wavelength range 450-1200 nm. For thin layers below 10 nm, it is suggested to determine the film thickness by using a known refractive index. The thickness of the SAMs was determined using a two-layer model and a refractive index n = 1.46 and n = 1.51 for BIDS and the mixed BIDS/BIBAPDES ATRP initiators, respectively. A three-layer model was used for the homopolymer, diblock copolymer and mixed polymer brushes. The refractive indexes used are summarized in Table 2.6.

**Table 2.6.** Refractive indexes of the materials and polymers used in the ellipsometry measurements.

| Substrate | Refractive index | Extinction coefficient |
|---|---|---|
| Si | 3.89 | 0.02 |
| $SiO_2$ | 1.45 | 0 |
| Air | 1.00 | 0 |
| BIDS | 1.46 | 0 |
| BIDS-BIBAPDES | 1.51 | 0 |
| PDMAEMA | 1.47 | 0 |
| PTFEMA | 1.42 | 0 |
| POFPMA | 1.35 | 0 |
| PTDFOMA | 1.33 | 0 |
| THF | 1.40 | - |

### 2.6.4 Polymer densities

The polymer densities were measured using a Quantachrome Model NOVA 3200e sorption analyzer. Before measurement, the samples were heated and degassed overnight, under vacuum (<$10^{-4}$ mbar), in a custom-made tube to remove any moisture. A specific volume of 1 gr were estimated for the dried polymers using the general gas equation and was converted to the density of the polymer. Table 2.7 summarizes the characteristic properties of the polymers used in this study.

**Table 2.7.** Characteristic properties of the homopolymers

| Polymer | $M_n$ (g/mol) | Monomer density (g/ml) * | Bulk polymer density (g/cm$^3$) | $T_g$ (ºC)* |
|---|---|---|---|---|
| PDMAEMA | 43000 | 0.933 | 1.097 | ~26 |
| PTFEMA | 43000 | 1.181 | 1.451 | ~59 |
| POFPMA | 43000 | 1.432 | 1.610 | ~27 |
| PTDFOMA | NA | 1.496 | 1.763 | ~46 |

* literature values[6]

### 2.6.5 Polymer grafting density

The grafting density $\sigma$ (chains/nm$^2$) of the polymer chains on the surface was calculated as:

$$\sigma = \frac{d \times N_A \times h}{M_n} \quad (2.1)$$

Where, $h$ is the polymer film thickness (nm), $d$ is the bulk density of the grafted polymer, $M_n$ is the number-average molecular weight of the chains grafted on the surface assumed to be the same as that of the polymer chains in solution obtained by GPC and $N_A$ is the Avogadro's number ($6.023 \times 10^{23}$).

### 2.6.6 Degrees of quaternization

The mass balance of the polymer brushes before and after quaternization, was used to calculate the degrees of quaternization, from the change in the brush thickness upon modification, using the following equation:

$$DQ = 100 \times \frac{(h_{PQDMAEMA,exp} - h_{PDMAEMA,exp})}{(h_{PQDMAEMA,theo} - h_{PDMAEMA,exp})} \quad (2.2)$$

Where, $h_{PQDMAEMA,exp}$ and $h_{PDMAEMA,exp}$ are the dry polymer film thicknesses of the PQDMAEMA and PDMAEMA brushes, respectively, measured by ellipsometry, and $h_{PQDMAEMA,theo}$, is the calculated theoretical brush thickness for a 100% quaternized polymer brush (in nm).

$h_{PQDMAEMA,theo}$, can be calculated as:

$$h_{PQDMAEMA,theo} = \frac{\sigma \times M_{n,PQDMAEMA,theo}}{d \times N_A} \quad (2.3)$$

Where, $\sigma$ is the grafting density of the brush, $M_{n,PQDMAEMA,theo}$ is the calculated number-average molecular weight of the quaternized polymer grafted on the surface to include the mass of the alkyl iodide in every monomer repeat unit, and $N_A$ is the Avogadro number. An assumption of a constant grafting density, $\sigma$, and polymer bulk density, $d$, before and after quaternization of the PDMAEMA brushes with the various alkyl iodides, was made.[7]

Moreover, the thickness of the PDMAEMA brushes that was effectively quaternized by the alkyl halides was calculated using the following equation:

$$h_{Q,eff} = h_{PDMAEMA,exp} \times \frac{DQ}{100} \quad (2.4)$$

Where, $h_{PDMAEMA,exp}$ is the dry polymer film thicknesses of the PDMAEMA brushes measured by ellipsometry, and $DQ$, is the degrees of quaternization from the change in the brush thickness upon modification using equation (2.2).

### 2.6.7 FTIR spectroscopy

IR spectroscopy is a non-destructive method that provides chemical structure information of the polymer brushes. Two techniques have been used for the characterization of polymer brushes, namely transmission FTIR spectroscopy (Transmission FTIR) and attenuated total reflectance FTIR spectroscopy (ATR-FTIR).[8] In FTIR, the substrate of the polymer film should be (partially) transparent to infrared, so that the infrared light reaches through the sample the detector. Characterization by ATR-FTIR requires a direct contact of the polymer film with an ATR crystal, due to the fact that the extend of the evanescent infrared wave from the crystal is a few microns.

In the present thesis, both transmission FTIR and ATR-FTIR were used for the qualitative characterization of the polymer brushes on silicon surfaces. FTIR spectra were recorded on a Perkin Elmer Model Frontier FT-IR spectrometer. ATR-FTIR spectra were recorded on a Thermo Scientific Nicolet 6700 spectrometer. The spectra were measured in the 500-4000 $cm^{-1}$ range with a resolution of 2 $cm^{-1}$ and 128 scans were collected.

### 2.6.8 Contact angle measurements

The liquid contact angles are utilized to evaluate the wettability of the surfaces which can represent the polymer coverage and quality of a surface. Comparison of the angles before and after modification indicates if the surface has been modified.

Wettability was assessed by static contact angle (CA) measurements using a contact angle goniometer (OCA-40, Dataphysics) and the sessile drop method. A 5 μl droplet of nanopure water was used and the water contact angles (WCAs) were calculated from the digital images of the water droplets deposited on the surfaces, recorded by a camera, using the appropriate software.

Owens and Wendt approach (OWRK), was utilized to calculate the solid surface energy $\gamma_S$ of the polymer brush layers.[9] Diiodomethane was used as the non-polar liquid to estimate the dispersive component of the solid surface energy $\gamma_S^d$ and water as the polar liquid to estimate the polar component of the solid surface energy $\gamma_S^p$. The static contact angle measurements on all samples were used to estimate the total solid surface

energy. Liquid droplets of 5 μl were deposited onto the samples in each case. All data are expressed as the mean values from triplicate experiments taken after drop equilibration.

### 2.6.9 UV-Vis spectroscopy

In another approach, the degrees of quaternization and the surface charge densities of the PQDMAEMA brushes were determined by UV/Vis spectroscopy via a colorimetric method based on fluorescent complexation (Scheme 2.3).[10] All polymer brushes were placed in a reaction flask containing a 1 wt% aqueous solution of the anionic dye, (sodium 4-((2E)-2-(2-oxonaphthalen-1-ylidene)hydrazinyl) benzenesulfonate (AO7), for 1 h. The dye binds strongly to the cationic quaternary ammonium sites of the polymer and the unbound molecules can subsequently be removed by extensive washing with deionized water and immersion in a water bath. n-Butyltrimethylammonium iodide was synthesized and used as a detergent, to induce the desorption of the dye from the brushes (Scheme 2.3). For the synthesis of the detergent, first N,N-Dimethylbutylamine was placed in a flask with methanol and iodomethane at RT for 24 h. Following, the solvent was evaporated and the QAS molecule was washed excessively with THF, placed in a vacuum oven for 12 h and stored under a nitrogen atmosphere before use. The dyed polymer surfaces were immersed in a 0.5 wt% aqueous solution (3ml) of the monovalent salt for 1 h and were shaken for 30 min at 500 rpm. The absorbance of the supernatant solution was measured at 483 nm (Figure 2.1). The UV/Vis spectra were collected on a Perkin-Elmer LAMBDA 25 UV/Vis spectrophotometer in a wavelength range between 300 and 700 nm using plastic cuvettes with 1 cm optical path and distilled water as a reference. AO7 is an anionic molecule that adsorbs at 483 nm, showing a characteristic orange color. It was confirmed that the UV spectrum is not affected by exposure to sunlight since the intensity of the characteristic peak remains steady after ten days of exposure. The concentration $C_{AO7}$ of AO7 was calculated according to the Beer – Lambert law:

$$Abs_{483} = \varepsilon_{483} \times h \times C_{AO7} \tag{2.5}$$

using the absorbance of the unknown samples at 483 nm, plastic PS cuvettes with h = 1 cm optical path of the UV-light beam and an extinction coefficient for the dye calculated by the calibration curve (Figure 2.1) at a value of $\varepsilon_{483}$=17,3 $mM^{-1}$ $cm^{-1}$. An

assumption that every quaternary ammonium group of the polymer interacted with one dye molecule was made to convert the dye concentration determined by UV/vis spectroscopy to the degree of quaternization (DQ) and the charge density (CD) of the polymer brush. The cationic CD per $cm^2$ was calculated using the equation:

$$CD = V \times C \times N_A/A \tag{2.6}$$

Where, V is the volume of the extraction solution (3 ml), $N_A$ is the Avogadro number ($6.023 \times 10^{23}$) and A is the surface area of the polymer samples (1.5 $cm^2$).

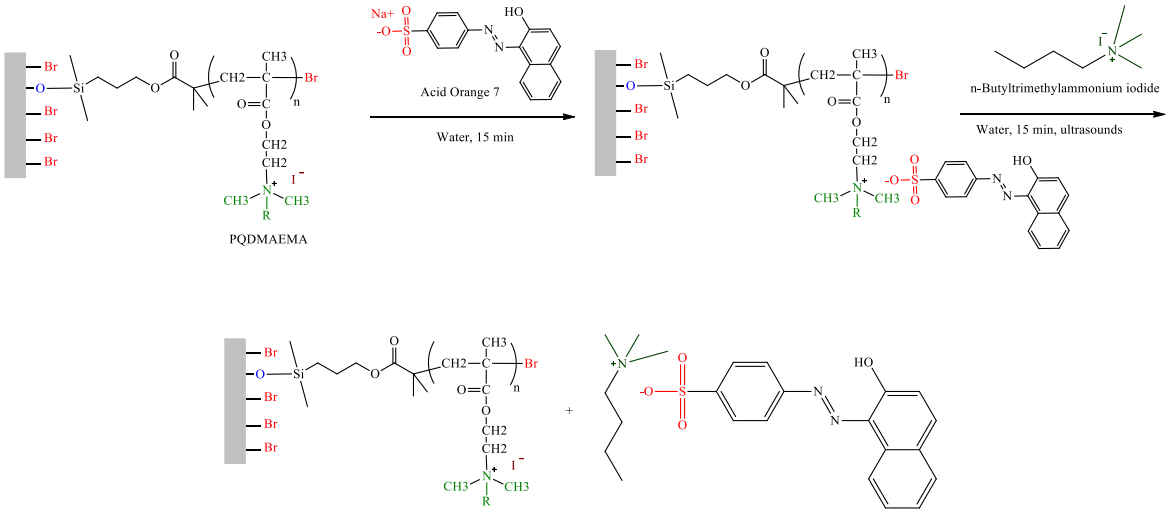


**Scheme 2.3.** Schematic representation of the procedure followed to determine the quaternary ammonium salt groups of the PQDMAEMA brushes.

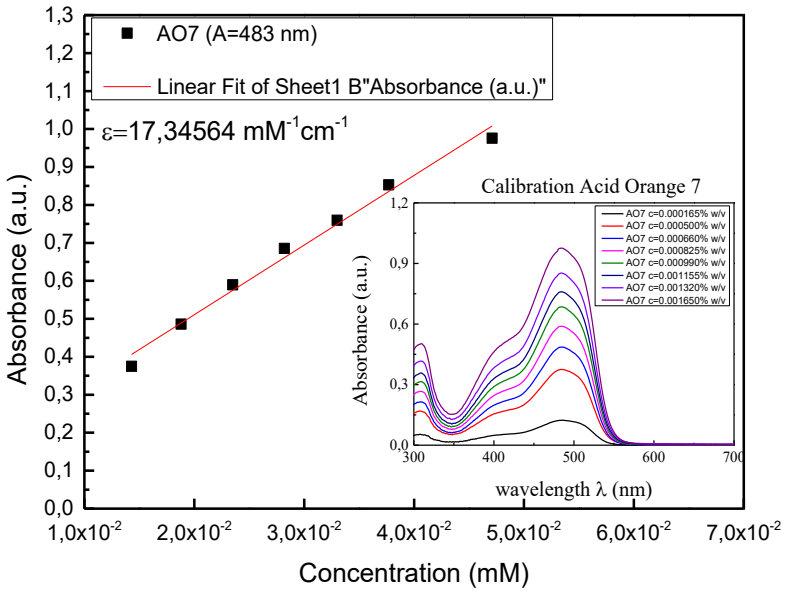

**Figure 2.1.** Absorbance as a function of concentration of the AO7 dye in water and the corresponding extinction coefficient. Inset: UV-Vis absorption spectra of the AO7 in water at different concentrations.

### 2.6.10 Atomic Force Microscopy (AFM)

The topography and the morphology of polymer brushes are mainly assessed by (atomic force microscopy) AFM measurements. AFM is an instrument that has been employed to image polymer brushes on surfaces, primarily providing details of their topography and morphological characteristics. AFM measurements, of the homopolymer and diblock copolymer brushes, were carried-out at ambient conditions with a relative humidity (RH) of ~40%, on a multimode scanning probe microscope (Nanoscope III instrument, Digital Instruments, Veeco) in tapping mode at 1.0 Hz scan rate. Cantilevers with silicon tips (RTESP-300, rectangular) from Bruker Corporation, having a normal spring constant of ~40 N/m and frequency of 300 kHz were used. The root-mean-square roughness was calculated utilizing the Nanoscope software.

The height and phase images of the mixed brushes were carried out at ambient conditions at a RH of 50%, using an MFP3D (Asylum Research, Oxford Instruments, CA) instrument in tapping mode at 0.5 Hz scan rate. These experiments were performed in the Leibniz Institute of Polymer Research Dresden (IPF) in Dresden, Germany. Cantilevers with a silicon tip (OTESPA, rectangular) from Bruker Corporation, having a normal spring constant of ~26 N/m and frequency of 300 kHz were used.

### 2.6.11 Lateral Force Microscopy (LFM)

An AFM-based technique, namely Lateral force microscopy (LFM) is used to make friction measurements in the micro and nanoscale. In traditional contact mode AFM, the topography is observed by the vertical deflection of the cantilever, whereas in the LFM, the twisting or lateral deflection of the cantilever is observed, that provides information about the friction between the tip and the surface. A drawback of contact mode AFM is the distortion of the features in the images, due to the high lateral forces

acting on the surface of the sample. Thus, probes or tips with low spring constants below 1 N/m are utilized that minimize the amount of applied force during scanning.

In this thesis, LFM was performed using an MFP3D (Asylum Research, Oxford Instruments, CA) to study nanoscale adhesion and friction generated between a silicon nitride tip and the polymer brushes. These experiments were performed in the Leibniz Institute of Polymer Research Dresden (IPF) in Dresden, Germany. Cantilevers (DNP, C triangular) from Bruker Corporation, having a normal spring constant of ~0.2 nN/nm were used for normal and lateral force measurements. The actual normal spring constant of the cantilevers were calibrated and measured by the thermal-noise method as described by Matei et. al using the resonance frequency of the cantilever from a thermal spectrum.[11] Silicon nitride tips were cleaned by UV/ozone treatment for 20 min, prior to each measurement.

Both adhesion and friction force measurements were performed in contact mode at room temperature with a relative humidity of around 50 %. After treatment with selective solvents, the polymer samples were dried under a nitrogen flow. For a given sample the force data measured were stable and reproducible.

The adhesion properties of the polymer brushes were measured from force *vs* distance curves over five different areas of the sample. The velocity of the approaching tip to the polymer brushes was kept constant for each sample, while the normal applied loads were varied between 10 and 125 nN. The adhesion forces $A_f$ (in nN) were calculated using the Hook's law, by multiplying the spring constant ($k$) of the cantilever with the average value of the cantilever deflection at the jump out point ($\overline{\Delta Y}$), from several spots (Equation 2.7).[12]

$$A_f = k \times \overline{\Delta Y} \tag{2.7}$$

The lateral force calibration method, which leads to a calibration/conversion factor (β) (nN/V) was performed as proposed by Anderson et al.[13] Briefly, this method requires the measurement of a normal spring constant, z-scanner displacement and average adhesion. The spring constant can be calculated by a thermal-noise method as described above, while the average adhesion between the tip and a sample with multiple range of sample angles (curved surface) can be found by acquiring multiple force curves along the apex of the micropipette, equally spaced along the length of the image. By assuming

Amontons' law for friction and resolving the forces acting on the cantilever, it is possible to calculate the lateral force applied at the tip from the normal load, adhesion, angle of response of the cantilever and the surface topography. The slope of a plot of a calculated lateral force against the measured lateral deflection gives the lateral conversion factor β in nanoNewtons per voltage.

Herein, a freshly cleaned glass pulled-micropipette (by heating) was glued on a glass coverslip and placed in the AFM with the long axis perpendicular to the fast scan direction, parallel to the long axis of the cantilever with a value of $k$, 0.17 nN/nm. The instrument was shut into a vibration and acoustic isolation hood to eliminate adjustments to the position of the laser spot on the cantilever. The average lateral sensitivity between the sample and the tip was found by acquiring force curves of 10 points from 2 different spots at the highest point of the capillary, with a deflection voltage setpoint of 0.2 V, a force distance of 1 μm and velocity of 5 μm/s. The sample was then moved to approach a flat clean area in the glass pipette and the cantilever was engaged for 10 further approach curves. The mean value of the Inverse Optical Lever Sensitivity (InvOLS) in nanometers of tip displacement per volt of detector signal was calculated from these lateral deflection-vs-Y piezo displacement curves.[14] Knowing the InvOLS and the spring constant of the cantilever, the deflection setpoint of voltage, $C$, that corresponds to the normal applied load, during the friction forces can be calculated by the equation:

$$C = \frac{N}{k \times InvOLS} \tag{2.8}$$

Where, $N$ is the normal applied load in nN, $k$ is the spring constant of the cantilever in nN/nm, and $InvOLS$ is the sensitivity of the cantilever in nm/V.

Next, a 20 × 20 μm$^2$ scan of 256 × 256 points (pixels) was taken at a line rate of 0.6 Hz and images of height (signal of the Z-piezo capacity), vertical deflection (feedback error signal) and lateral deflection were captured. A setpoint of 0.131 V that corresponds to 10 nN applied normal load was used. Following the image capturing, force approach curves were taken at 5 points along the pipette and the mean value of A was calculated. By employing a calibration program, that exploits the linearity between the lateral force and voltage, the calibration factor can be obtained. The program first averages the topography and LFM files. It then calculates the slope at each point using the averaged

topography data. The average lateral force is then plotted against the average lateral deflection signal and the slope of the fitted line gives the calibration factor β. The conversion factor of the cantilever, is utilized to convert the friction voltage signal (V) to force units (nN). The same steps were repeated for different normal applied load in a range of 10 to 125 nN. Figure 2.2 shows the conversion factor obtained from the different applied normal loads.

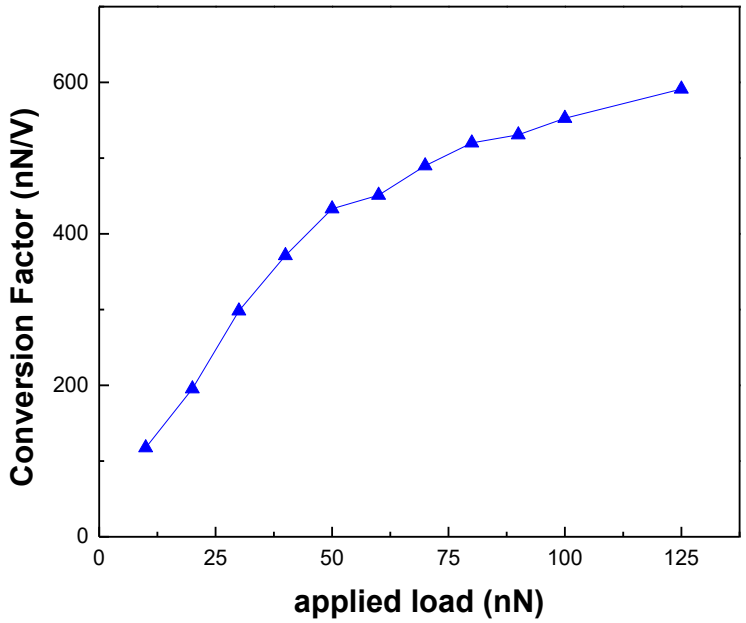


**Figure 2.2.** Conversion factor against the different normal applied loads

Next, friction loops were recorded by LFM for all polymer brushes by scanning laterally the silicon nitride cantilever over the brush surfaces. Friction force was measured for all samples at variable loads between 10 nN and 100 nN using a 90º scan angle, 5 μm scan size and scan rate of 0.2 Hz. In detail, friction loops comprising trace and retrace scans were attained for each polymer brush. Trace is the definition of lateral scan distance i.e. from left to right and retrace is the scanning distance backwards. The friction voltage signal was calculated by averaging the trace and retrace curves (half the difference between trace and retrace scans). The conversion of the average friction voltage signal, into friction force at the interface, was performed using different calibration factors from the above method. The slope of the plots of the friction force *vs* the normal applied load provides the coefficient of friction (COF) by assuming the Amontons' law.[15]

## 2.7 Antibacterial Assays

### 2.7.1 Bacterial strains and culturing

Two bacterial strains, *Bacillus cereus* (*B. cereus*) ATCC 14579 and *Escherichia coli* (*E. coli*), were chosen in the present study, as representative gram-positive and gram-negative bacteria, respectively. Both strains, were grown aerobically overnight at separate Luria-Bertani (LB) liquid medium from frozen stocks. Next, *B. cereus* and *E. coli* were cultivated each by streaking on LB agar plates and incubating at 37 ºC for 24 h. Then individual colonies were picked and incubated in 3 ml of LB liquid culture medium. The optical density of 1.0 was measured at 600 nm ($OD_{600}$). Both strains were shaken at 37 ºC for 24 h, and then diluted with LB to obtain a predetermined concentration of $1 \times 10^8$ CFU/ml. The concentration of bacteria was also verified by serial dilutions and spreading onto agar plates, followed by the enumeration of the colonies.

To prepare LB medium, 1.0 g tryptone, 1.0 g sodium chloride and 0. 5 g yeast extract and were dissolved in 100 ml distilled water and autoclaved. The LB medium, after cooling down, was stored at RT. To prepare LB agar plates, 5 g tryptone, 5 g sodium chloride, 2.5 g yeast extract and 7.5 g agar were dissolved in 500 ml distilled water and autoclaved. When the solution cooled down to 40-45 ºC, 20 ml of the solution was poured into the sterile plates of 10 cm diameter. The LB agar plates were conditioned at 4 ºC, not longer than 1 month. The LB medium was prepared using the same proportions of the reagents except from agar, and was autoclaved.

### 2.7.2 Bactericidal Assay

The bactericidal activity of the polymer surfaces was evaluated against *Bacillus cereus* (*B. cereus*) ATCC 14579 and *Escherichia coli* (*E. coli*). The antimicrobial activity was measured based on colony-forming units (CFU) by the plate counting method (PCM), as the log reduction of the living bacteria cells after 5 h contact with each polymer brush at 37 ºC, using the antibacterial drop test method, described previously.[16] Briefly, the samples were sterilized by immersion in methanol and were dried by heating at 100 ºC for 30 min. Then, the samples were transferred to a sterile 12-well plate using sterilized forceps under a Bunsen burner. Glass or Silicon substrates were used as control

surfaces. Cultures of *B. cereus* and *E. coli* ($10^8$ CFU/ml) were prepared by inoculating bacteria in 3 ml Luria-Bertani (LB) broth at 37 ºC for 24 h at a shaking speed of 200 rpm. The population was measured by optical density measurements at 600 nm ($OD_{600}$) following dilution in fresh medium to prepare a bacterial inoculum containing $10^7$ CFU/ml. A culture-based assay was conducted to evaluate the bactericidal activity of the polymer brushes as follows (Scheme 2.4). 100 µl of the initial bacteria culture in PBS were deposited onto each sample. The samples were sealed and placed in a cell culture thermostatic chamber at 37 ºC in humidified condition, were incubated for 5 h, and were diluted in PBS. Subsequently, both the suspensions and the polymer surfaces were placed in a falcon with glass sieves and were vortex stirred until their complete wreckage.[17] The suspension was diluted with PBS (Scheme 2.4, marks as T1 and so on) and 100 µl of each decimal dilution was spread in sterile LB agar culture plates. The LB plates with the bacterial suspensions were incubated at 37 ºC for 20 h to give visible colonies, which were enumerated to obtain the number of living bacteria. The results were expressed as colony forming units per ml (CFU/ml) and represent mean SD values of triplicates from three independent experiments. The bacteria reduction and the percentage of bactericidal action were then reported as:

$$\text{Logarithmic reduction} = \log(A/B) \tag{2.9}$$

and

$$\text{Bactericidal action (\%)} = (A - B)/A * 100 \tag{2.10}$$

where, A is the number of colony forming units per ml, counted for the control samples, and B is the number of bacteria retrieved from each polymer brush.[18]

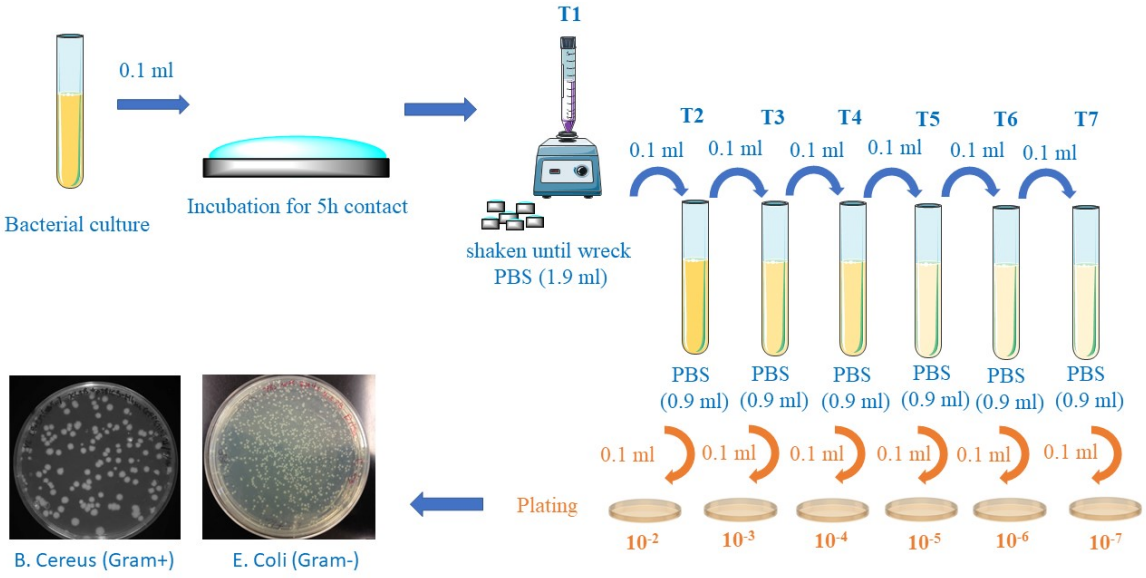


**Scheme 2.4.** The fundamental process for bactericidal assay of polymer brushes.

In a complementary study, the polymer brush surfaces were extensively washed with PBS, after the 5 h incubation of the bacteria on the surfaces, and were visualized by FESEM.

### 2.7.3 Antifouling Assay

The bacteria-releasing antifouling properties of the polymer brushes were investigated using *B. cereus* (ATCC 14579) and *E. coli* as the model organisms. *B. cereus* and *E. coli* were cultivated by streaking on Luria-Bertani (LB) agar plates and were incubated at 37 ºC for 24 h. Then individual colonies were picked and incubated in LB liquid culture medium. Both strains were shaken at 37 ºC for 24 h, and then diluted with LB to obtain a predetermined concentration of $1 \times 10^8$ CFU/ml. Duplicates of all the polymer brushes were rinsed with methanol and sterile water and sterilized at 100 ºC for 30 min, prior to the antifouling test procedure. Then, polymer films were placed in a 12-well plate in plastic holders to expose only the active layer to bacteria, and 1 ml of *B. cereus* or *E. coli* suspension was pipetted onto each well and put at 37 ºC for 2 h. After incubation, the films were washed gently with sterile PBS and then immersed in 1 ml of PBS at a shaking speed of 150 rpm for 1 h in order to study the bacterial-release capability of the brushes. Following, the substrates were fixed with 2.5%

glutaraldehyde (GDA) in PBS at pH 7.2 for at least 2 h, then rinsed with PBS to remove the unreacted GDA, and were prepared for analysis by FESEM.

In a complementary study, the extent of the bacterial-release was enumerated by a PCM method. After 24 h incubation of the bacteria on the surfaces, the polymer brush surfaces were immersed in 1 ml of PBS at a shaking speed of 150 rpm for 1 h and the polymer surfaces were placed in a falcon with glass sieves and were vortex stirred until their complete wreckage. The suspension was diluted with PBS and 100 µl of each decimal dilution was spread in sterile LB agar culture plates. The LB plates with the bacterial suspensions were incubated at 37 ºC for 20 h to give visible colonies, which were enumerated to obtain the number of detached bacteria from the surfaces. The results were expressed as colony forming units per ml (CFU/ml) and represent mean SD values of triplicates from three independent experiments.

### 2.7.4 FESEM of the polymer surfaces after incubation with the bacteria

Scanning electron microscopy images were captured using a JEOL JSM-7000F field emission scanning electron microscope (FESEM) at an accelerating voltage of 15 kV to visualize the morphology of the bacteria. The samples for FESEM were fixed with 2.5% GDA in PBS at pH 7.2 for at least 2 h, and were dehydrated by gradually increasing the ethanol concentration from 30 to 100% at RT for 10 minutes each. Then the samples were transferred to a critical point dryer (CPD 030 Bal-Tec) and were finally sputter-coated (SCD 050 Bal-Tec) with a 10 nm thick layer of Pd-Au to minimize charging before the measurement.

### 2.7.5 Kirby-Bauer zone of inhibition test

Finally, possible leaching of bactericidal compounds from the polymer brushes was examined via the zone of inhibition test or the disc diffusion method.[19] LB agar plates were produced as described above, followed by striking of 100 µl of *B. cereus* or *E. coli* suspension of a predetermined concentration of $1 \times 10^6$ CFU/ml. The samples were sterilized by immersion in methanol and were dried by heating at 100 ºC for 30 min. Then, they were transferred to the LB agar plates with the active layer of bacteria, using

sterilized forceps under a Bunsen burner. The LB plates with the bacterial suspensions and the polymer films were incubated at 37 ºC for 20 h to give colonies, with the presence of a zone of inhibition (ZOI) to declare leaching of bactericides towards the bacteria colonies, while the absence of a ZOI signifies a non-leaching contact-active surface.

## 2.8 References

1. von Werne, T.; Patten, T. E., Atom Transfer Radical Polymerization from Nanoparticles: A Tool for the Preparation of Well-Defined Hybrid Nanostructures and for Understanding the Chemistry of Controlled/"Living" Radical Polymerizations from Surfaces. *J Am Chem Soc* **2001,** *123* (31), 7497-7505.
2. Wang, H.; Xu, D.; Jiang, P.; Zhang, M.; Dong, X., Novel restricted access chiral stationary phase synthesized via atom transfer radical polymerization for the analysis of chiral drugs in biological matrices. *Analyst* **2010,** *135* (7), 1785-1792.
3. (a) Choi, I.; Kim, Y.; Kang, S. K.; Lee, J.; Yi, J., Phase Separation of a Mixed Self-Assembled Monolayer Prepared via a Stepwise Method. *Langmuir* **2006,** *22* (11), 4885-4889; (b) Feng, J.; Xu, G. H.; An, Y.; Zeng, X., Construction of the homogeneously mixed SAM composed of octyltriethoxysilane and octadecyltrichlorosilane by taking advantage of the molecular steric restriction. *Colloids and Surfaces A: Physicochemical and Engineering Aspects* **2008,** *316* (1), 194-201.
4. (a) Li, D. J.; Sheng, X.; Zhao, B., Environmentally responsive "Hairy" nanoparticles: Mixed homopolymer brushes on silica nanoparticles synthesized by living radical polymerization techniques. *J Am Chem Soc* **2005,** *127* (17), 6248-6256; (b) Ye, P. L.; Dong, H. C.; Zhong, M. J.; Matyjaszewski, K., Synthesis of Binary Polymer Brushes via Two-Step Reverse Atom Transfer Radical Polymerization. *Macromolecules* **2011,** *44* (7), 2253-2260.
5. Tugulu, S.; Arnold, A.; Sielaff, I.; Johnsson, K.; Klok, H.-A., Protein-Functionalized Polymer Brushes. *Biomacromolecules* **2005,** *6* (3), 1602-1607.
6. (a) Hansen, N. M. L.; Gerstenberg, M.; Haddleton, D. M.; Hvilsted, S., Synthesis, characterization, and bulk properties of amphiphilic copolymers containing fluorinated methacrylates from sequential copper-mediated radical polymerization. *Journal of Polymer Science Part A: Polymer Chemistry* **2008,** *46* (24), 8097-8111; (b) Villarroya, S.; Zhou, J.; Duxbury, C. J.; Heise, A.; Howdle, S. M., Synthesis of Semifluorinated Block Copolymers Containing Poly(ε-caprolactone) by the Combination of ATRP and Enzymatic ROP in scCO2. *Macromolecules* **2006,** *39* (2), 633-640.
7. (a) Galvin, C. J.; Dimitriou, M. D.; Satija, S. K.; Genzer, J., Swelling of Polyelectrolyte and Polyzwitterion Brushes by Humid Vapors. *J Am Chem Soc* **2014,** *136* (36), 12737-12745; (b) Arifuzzaman, S.; Ozcam, A. E.; Efimenko, K.; Fischer, D. A.; Genzer, J., Formation of surface-grafted polymeric amphiphilic coatings comprising ethylene glycol and fluorinated groups and their response to protein adsorption. *Biointerphases* **2009,** *4* (2), FA33-44.
8. (a) Edmondson, S.; Huck, W. T. S., Controlled growth and subsequent chemical modification of poly(glycidyl methacrylate) brushes on silicon wafers. *J Mater Chem*

**2004,** *14* (4), 730-734; (b) Mateescu, A.; Ye, J.; Narain, R.; Vamvakaki, M., Synthesis and characterization of novel glycosurfaces by ATRP. *Soft Matter* **2009,** *5* (8), 1621-1629; (c) Huang, J.; Murata, H.; Koepsel, R. R.; Russell, A. J.; Matyjaszewski, K., Antibacterial Polypropylene via Surface-Initiated Atom Transfer Radical Polymerization. *Biomacromolecules* **2007,** *8* (5), 1396-1399; (d) Li, J.; Chen, X.; Chang, Y.-C., Preparation of end-grafted polymer brushes by nitroxide-mediated free radical polymerization of vaporized vinyl monomers. *Langmuir : the ACS journal of surfaces and colloids* **2005,** *21* (21), 9562-9567.

9. K. J. Owens, D.; Wendt, R. C. J., *Owens, D. K. & Wendt, R. C. Estimation of the surface free energy of polymers. J. Appl. Polym. Sci. 13, 1741-1747*. 1969; Vol. 13, p 1741-1747.

10. Ziolkowska, D.; Szeflinska, I.; Shyichuk, A., Quantitation of poly(diallyldimethylammonium chloride) by complexation with Acid Orange 7 dye (Rapid Communication). *Polimery* **2014,** *59* (11/12), 859-861.

11. (a) Matei, G. A.; Thoreson, E. J.; Pratt, J. R.; Newell, D. B.; Burnham, N. A., Precision and accuracy of thermal calibration of atomic force microscopy cantilevers. *Review of Scientific Instruments* **2006,** *77* (8), 083703; (b) Butt, H. J.; Jaschke, M., Calculation of Thermal Noise in Atomic-Force Microscopy. *Nanotechnology* **1995,** *6* (1), 1-7.

12. Li, D. Y.; Li, W., Electron work function: A parameter sensitive to the adhesion behavior of crystallographic surfaces. *Applied Physics Letters* **2001,** *79* (26), 4337-4338.

13. Anderson, E. V.; Chakraborty, S.; Esformes, T.; Eggiman, D.; DeGraf, C.; Stevens, K. M.; Liu, D. L.; Burnham, N. A., Shape-Independent Lateral Force Calibration. *Acs Appl Mater Inter* **2011,** *3* (9), 3256-3260.

14. Mullin, N.; Hobbs, J. K., A non-contact, thermal noise based method for the calibration of lateral deflection sensitivity in atomic force microscopy. *Review of Scientific Instruments* **2014,** *85* (11), 113703.

15. Vyas, M. K.; Schneider, K.; Nandan, B.; Stamm, M., Switching of friction by binary polymer brushes. *Soft Matter* **2008,** *4* (5), 1024-1032.

16. (a) Druvari, D.; Koromilas, N. D.; Lainioti, G. C.; Bokias, G.; Vasilopoulos, G.; Vantarakis, A.; Baras, H.; Dourala, N.; Kallitsis, J. K., Polymeric Quaternary Ammonium-Containing Coatings with Potential Dual Contact-Based and Release-Based Antimicrobial Activity. *Acs Appl Mater Inter* **2016,** *8* (51), 35593-35605; (b) Zhao, J.; Millians, W.; Tang, S. D.; Wu, T. H.; Zhu, L.; Ming, W. H., Self-Stratified Antimicrobial Acrylic Coatings via One-Step UV Curing. *Acs Appl Mater Inter* **2015,** *7* (33), 18467-18472; (c) Karamdoust, S.; Yu, B. Y.; Bonduelle, C. V.; Liu, Y.; Davidson, G.; Stojcevic, G.; Yang, J.; Lau, W. M.; Gillies, E. R., Preparation of antibacterial surfaces by hyperthermal hydrogen induced cross-linking of polymer thin films. *J Mater Chem* **2012,** *22* (11), 4881-4889.

17. Kougia, E.; Tselepi, M.; Vasilopoulos, G.; Lainioti, G. C.; Koromilas, N. D.; Druvari, D.; Bokias, G.; Vantarakis, A.; Kallitsis, J. K., Evaluation of Antimicrobial Efficiency of New Polymers Comprised by Covalently Attached and/or Electrostatically Bound Bacteriostatic Species, Based on Quaternary Ammonium Compounds. *Molecules* **2015,** *20* (12), 21313-21327.

18. Li, L. D.; Zhou, H.; Gai, F. Y.; Chi, X. F.; Zhao, Y. B.; Zhang, F. X.; Zhao, Z. B., Synthesis of quaternary phosphonium N-chloramine biocides for antimicrobial applications. *Rsc Adv* **2017,** *7* (22), 13244-13249.

19. Zhao, J.; Ma, L.; Millians, W.; Wu, T. E. H.; Ming, W. H., Dual-Functional Antifogging/Antimicrobial Polymer Coating. *Acs Appl Mater Inter* **2016,** *8* (13), 8737-8742.

# Chapter 3

Surface properties of the homopolymer brushes

## 3.1 Introduction

This study aims in investigating the surface properties of homopolymer brushes with significantly different polymer characteristics. Tuning the surface properties of thin films is of significant interest, due to their potential applications in various fields i.e. microelectronics, biotechnology and other.[1] The term 'surface properties' includes several parameters such as wettability, surface energy, surface charge and chemical functionality. The physical or chemical properties of flat surfaces can be tuned to produce water repellent, antifouling or cell adhesive surfaces.[2] The development of self-assembled organic monolayers (SAM's) has been extensively investigated, however several limitations are encountered, regarding the layer thickness, the uniformity and stability of the monolayer and the range of the material surfaces that can be functionalized.[3] Contributions from SAM's and polymer coatings has led to the development of polymer brushes which are defined as dense layers of polymer chains tethered by one chain end to a surface. The distance between the chains is much less than the unperturbed dimensions of the tethered chains.[4] Polymer brushes with well-defined structure are useful for the determination of the surface properties of polymers at the nanoscale. "Smart" systems such as polymer brushes of different functional chemistries have been attained to produce surfaces with tunable properties.[5]

Several controlled/"living" radical polymerization (CRP) techniques have been employed to grow polymer brushes from solid surfaces via the "grafting from" technique, as they provide a precise control over the structure and composition of the polymer chains across a wide range of grafting densities.[6] Over the past years, atom transfer radical polymerization (ATRP) is the most widely employed technique to synthesize polymer brushes from flat and curved surfaces because, of the wide range of monomers that can be polymerized and its operation under mild conditions and temperatures. "Grafting from" or surface initiated ATRP (SI-ATRP) can provide polymer films with high density of anchored chains per surface area and good control over the surface characteristics such as the brush height, and the smoothness of the surface.[7]

The most common architecture constitutes the end-anchored homopolymer chains, comprising one type of monomer repeated unit. These systems can be further divided into neutral and charged polymer brushes. Neutral polymer brushes are based on

hydrophilic polymers such as poly(2-hydroxyethyl methacrylate) (PHEMA), poly(poly(ethylene glycol) methacrylate) (PPEGMA), poly(N-isopropylacrylamide) (PNIPAAm) and polyacrylamide (PAAm), nevertheless there are many examples of hydrophobic polymer brushes based on PMMA, PS, PGMA, that give their distinct properties to the surface of the material functionalized. Charged or polyelectrolyte (PEL) brushes have different properties compared to neutral brushes, and undergo changes in swelling and contraction in response to pH or ionic strength making them excellent candidates for "smart" surfaces. The charge density on a polymer chain in a polar solvent depends on the chain constitution and degree of dissociation of the ionizable groups. Based on the association of the charges and the polymer chains, PEL brushes are divided into (a) "strong" PEL brushes and (b) "weak" PEL brushes.[8] The weak PEL brushes do not have permanent charges and the pH or ionic strength changes of their surrounding can tune their charge ratio and control their properties. Weak polyanionic brushes accept protons at low pH and release them at neutral and high pH when they become negatively charged. Weak polycationic brushes are deprotonated at high pH and become positively charged at neutral and low pH. The structure and properties of such polymer layers are dominated by electrostatic interactions. Due to electrostatic interactions the polymer segments are strongly stretched and show physical properties which are very different compared to neutral polymer brushes.[8] Poly(methacrylic acid) (PMAA) and poly(2-(dimethylamino)ethyl methacrylate) (PDMAEMA) brushes are the most widely studied weak PEL brushes. On the other hand, in strong PEL brushes, permanent charges are associated with strong acid or base groups, the degree of dissociation is not affected by the environment and as a consequence these brushes are insensitive to the local pH. The most common strong polybasic brush is poly(2-(methacrylolyloxy)ethyltrimethylammonium chloride) (PMETAC) (which is the substituted form of PDMAEMA with methyl chloride), poly(methyl-4-vinylpyridinium) (PMePVP) and poly(vinylbenzyltrimethylammonium chloride) (PVBTMAC).

Strong PEL brushes with positively charged quaternary ammonium groups have been used thoroughly for switching the surface properties in several applications. A quaternization reaction, which involves the transformation of amino-based PEL brushes into the respective quaternary ammonium salt brushes has been employed to alter the wettability of the surfaces.[9] An important key factor determining the surface properties

proved to be the counterion type.[10] Moreover, Spruijt et al. examined the control over the surface wetting properties of poly(2-(methacryloyloxy)ethyltrimethylammonium chloride) brushes by changing the redox state of the counterions using electrode potentials.[11] On the other hand, Murata et al. investigated the antimicrobial activity and wettability of quaternized poly-(2-(dimethylamino)ethyl methacrylate) (PDMAEMA) brushes with small alkyl bromides of different alkyl chain lengths.[12] Lately, Armes et al introduced a pH-responsive wettability on quaternized PDMAEMA brushes in good and bad solvents using a long-alkyl chain iodide as the quaternization agent.[13] Nevertheless, the effect of the alkyl chain length of the quaternization agent on the properties of the polymer brushes has not been studied.

On the other hand, fluorinated polymer coatings have attracted great attention, due to their unique properties e.g. thermal and chemical stability, low dielectric constant, low friction, low surface energy, low refractive index and high hydrophobicity.[14] However, reports on the synthesis of fluorinated polymers grafted from solid surfaces are limited due to the difficulty to control the polymerization of fluorinated monomers. Takahara and co-workers have synthesized thick fluoropolymer brushes by ATRP using a PFA-C8 fluoroacrylate monomer and demonstrated the effect of the molecular weight dispersity of the fluorobrushes on the wetting behavior of the polymer surface.[15] In another study, Whittaker et al. evaluated the performance of fluorinated polyelectrolytes synthesized by transition metal mediated LRP as corona components in $^{19}$F-detectable nanoparticles.[16] Recently, Zuilhof and coworkers studied the tuning of the adhesion and friction properties of fluoropolymer brushes when increasing the fluorine content of the brush which can find applications in dry lubricants.[17]

In this chapter, we describe the synthesis of homopolymer brushes based on PDMAEMA or fluorinated methacrylates aiming to prepare polymer films that alter their surface properties at will. Silicon and glass were used as substrates. First the self-assembled monolayer technique was used to successfully graft the ATRP initiator on the substrate. Next, four types of polymer brush films e.g, PDMAEMA, PTFEMA, POFPMA and PTDFOMA were synthesized from BIDS-immobilized silicon and glass substrates via the "grafting from" technique using SI-ATRP. The effect of the fluorinated alkyl chain length (FCL) on the surface properties varying as 1, 4 and 6 fluorocarbon atoms ($C_F$), was explored, referring to PTFEMA, POFPMA and PTDFOMA brushes, respectively. In addition, PDMAEMA brushes are a convenient

model-system to investigate the surfaces properties upon a facile post-modification reaction introducing different alkyl chain lengths on the side groups of the end-grafted polymer chains. The alkylating agents react with the tertiary amine groups of the PDMAEMA grafted chains and form quaternized PDMAEMA (PQDMAEMA) brushes, which comprise a strong polyelectrolyte with permanent cationic charges along the polymer chains. The effect of the alkyl chain length (ACL) of the quaternization agent on the wettability of the polymer surfaces was examined. Although PQDMAEMA brushes have been examined thoroughly in the literature, to the best of our knowledge, a systematic study of the effect of the ACL (ranging from one to eighteen carbon atoms) of the quaternary ammonium salt moieties on the physicochemical properties of the PQDMAEMA brushes has not been reported so far.

Variations of the hydrophilicity/hydrophobicity and surface free energy of the brush as a function of the fluoroalkyl chain length and the alkyl chain length of the quaternization agent were determined by static contact angle (CA) measurements. Next, AFM silicon nitride tips were used to examine the adhesion and friction properties of the polymer brushes against sliding inorganic surfaces. Finally, the degrafting of the hydrophilic PDMAEMA and PQDMAEMA chains and the hydrophobic PTFEMA, POFPMA and PTDFOMA chains was examined.

## 3.2 Results and Discussion

### 3.2.1 Synthesis of the ATRP initiators

*Synthesis of the BIDS ATRP initiator.* The synthesis of the surface ATRP initiator (3-(2-bromoisobutyryl)propyl)dimethylethoxy silane (BIDS) was carried out via a two-step reaction. The first step involves the esterification of allyl alcohol (AA) with 2-bromoisobutyryl bromide to obtain allyl 2-bromoisobutyrate (ABIB). The synthetic approach is outlined in Scheme 3.1. The successful synthesis and the purity of the precursor molecule ABIB was verified by $^{1}$NMR spectroscopy in $CDCl_3$ (Figure 3.1). $^{1}$H NMR (300 MHz, $CDCl_3$): δ 5.93(m, 1H), 5.30(dd, 2H), 4.69(d, 2H), 1.98 (s, 6H). The appearance of a strong peak at 1.98 ppm is attributed to the methyl protons of the bromoisobutyrate moiety, which is required for the ATRP initiation. The two signals at 5.30 ppm and 5.53 ppm are attributed to the vinylic hydrogens. The successful synthesis of the ABIB precursor is confirmed by the peak of the methylene protons at 4.69 ppm, whereas its purity by the absence of any further peaks in the spectrum.

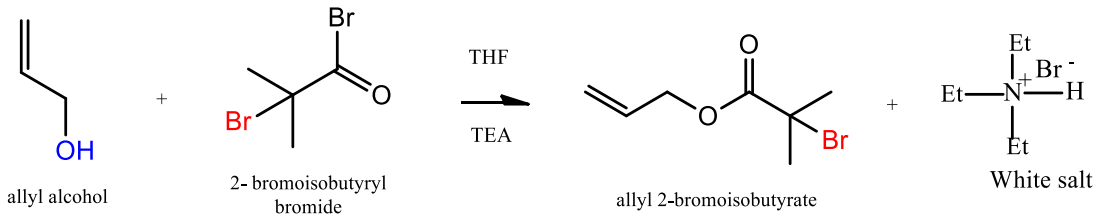


**Scheme 3.1.** Synthesis of the allyl 2-bromoisobutyrate precursor.

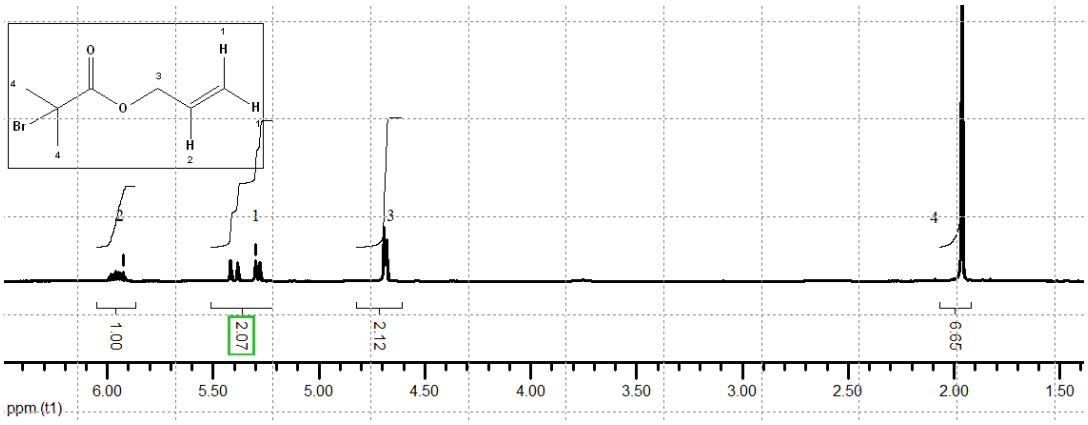


**Figure 3.1.** $^{1}$H NMR spectrum of allyl 2-bromoisobutyrate in $CDCl_3$.

The second step involves the hydrosilylation between ABIB and dimethylethoxysilane to synthesize a dual reactive molecule, namely BIDS, which comprises a mono-functional ethoxy silane group that can react with the surface silanol groups and form siloxane bonds, and the 2-bromoisobutyl group which is an active initiator for controlled ATRP. The synthetic approach of the mono-functional initiator molecule is outlined in Scheme 3.2. The successful synthesis and purity of the monoethoxy ATRP initiator BIDS was verified by $^{1}$NMR spectroscopy in $CDCl_3$ (Figure 3.2). $^{1}$H NMR (300 MHz, $CDCl_3$): δ 4.15 (2H, m), 3.69 (2H, q), 1.95 (6H, s), 1.73 (2H, m), 1.20 (3H, t), 0.60 (2H, m), 0.14 (6H, s). The presence of a new strong peak at 0.14 ppm is attributed to the methyl protons of the silane group, while the previously depicted peaks of the vinyl group at 5.30 ppm and 5.53 ppm are shifted to 1.73 ppm and 0.60 ppm, respectively, which evidence the successful transformation of ABIB to BIDS. Finally, the absence of any further peaks in the spectrum defines the purity of the initiator.

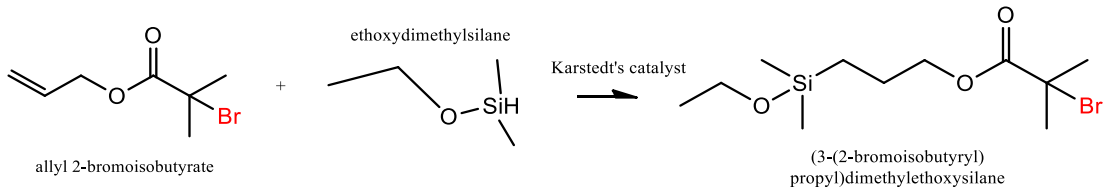


**Scheme 3.2.** Synthesis of the BIDS surface ATRP initiator.

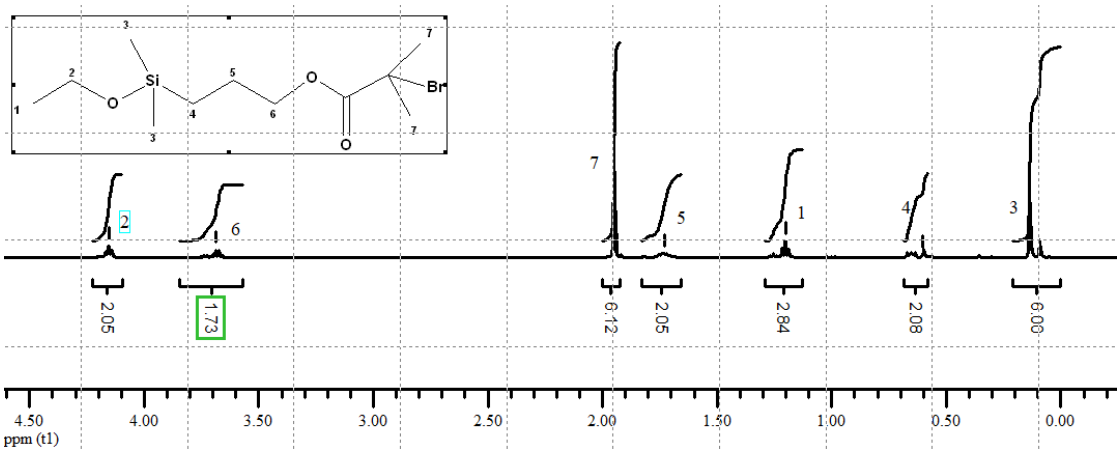


**Figure 3.2.** $^{1}$H NMR spectrum of BIDS in $CDCl_3$

*Synthesis of the BIBPTES ATRP initiator.* The synthesis of the surface ATRP initiator (3-(2-bromoisobutyryl)propyl)triethoxy silane (BIBPTES) was carried out via a two-step reaction. The first step involves the esterification of AA with BIBB to obtain the allyl 2-bromoisobutyrate (ABIB) precursor molecule as described previously in paragraph 1.2.1.

The second step involves the hydrosilylation between ABIB and triethoxy silane to synthesize a dual reactive molecule, namely BIBPTES, which comprises the 2-bromoisobutyl group, an active initiator for controlled ATRP and the tri-functional ethoxysilane group, that can form siloxane bonds with the surface silanol groups of the silicon or glass substrates and react with the neighboring silane molecules with lateral Si-O-Si bonds, to form a chemically bonded layer network. The synthetic approach of the tri-functional initiator is outlined in Scheme 3.3. The successful synthesis and purity of the monoethoxy ATRP initiator BIBPTES was verified by $^{1}$NMR spectroscopy in $CDCl_3$ (Figure 3.3). $^{1}$H NMR (300 MHz, $CDCl_3$): δ 4.12 (2H, t), 3.81 (6H, q), 1.90 (6H, s), 1.76 (2H, m), 1.20 (9H, t), 0.66 (2H, t).

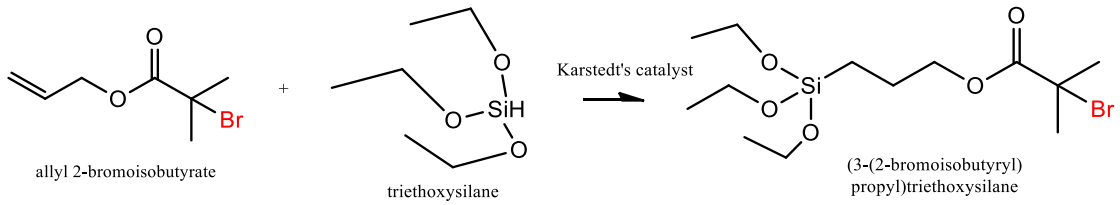


**Scheme 3.3.** Synthesis of the BIBPTES surface ATRP initiator.

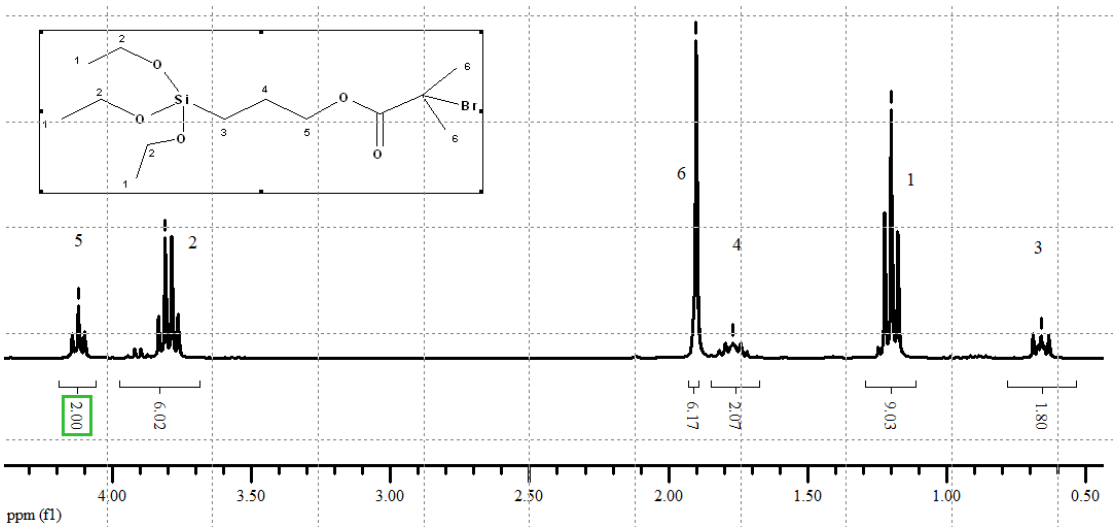


**Figure 3.3.** $^{1}$H NMR spectrum of BIBPTES in $CDCl_3$

### 3.2.2 Initiator self-assembled monolayer

In a first attempt to control the immobilization of the ATRP initiator on silicon substrates, we investigated the effect of immersion time and concentration of the two different types of ester initiators on the surface coverage and the morphology of the substrates. Samples were treated with a piranha solution, in order to increase the silanol binding sites of the surface and the successful treatment was verified via contact angle measurements and AFM (Table 3.1) which showed the formation of smooth superhydrophilic surfaces. Next, the samples were immersed in 0.5, 1 or 2 % v/v solutions of the mono- or tri-functional initiator in toluene for 3, 6, 12 and 24 h and were studied by ellipsometry, contact angle and AFM measurements. The modification of the silicon and glass substrates by the initiator via the SAM technique is illustrated in Scheme 3.4.

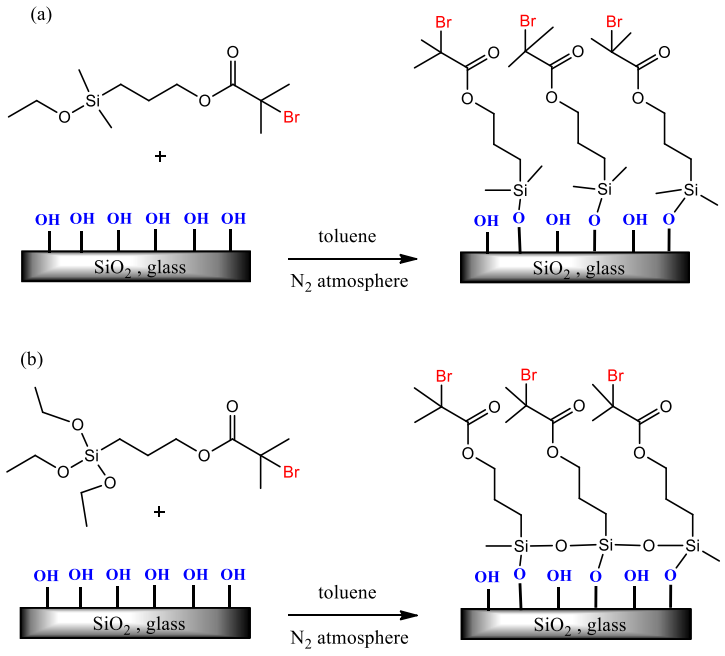


**Scheme 3.4.** Self-assembled monolayer (SAM) technique for the immobilization of the surface bound initiator BIDS (a) and BIBPTES (b) on planar substrates.

Figure 3.4 demonstrates the immersion time dependence of the dry layer for various concentrations of the BIBPTES (a) and BIDS (b) initiators in toluene for silanization times up to 3 h, the dry film thicknesses of the SAM's are quite low, less than 1 nm, for both BIBPTES and BIDS, which implies that the process of densely packed molecules is not completed, since the theoretical value of the stretched molecular lengths of the two molecules is 1.5-2 nm. After 6 h silanization time, the values of the dry layer thicknesses are between 0.8 and 1.7 nm for the BIDS layer and 2.2-2.3 nm for the 0.5 and 1 % v/v BIBPTES, while the layer thickness of the 2% v/v BIBPTES increased to 10 nm. This latter value indicates the aggregation of the initiator on the surface, probably due to hydrolysis and crosslinking of the triethoxysilane groups even in anhydrous toluene, and thus the formation of an intermolecular network of non-adsorbed molecules to the surface.[18] Nevertheless, ellipsometry measurements cannot provide information about the morphology and uniformity of the layers. Moreover, when the immersion time exceeds 6 h, we obtain different trends for the two initiators. For the BIBPTES film, the layer thickness is clearly affected by both the concentration of the initiator and the silanization time and only the film thickness for 0.5 % v/v BIBPTES is constant with time. On the other hand, the dry film thicknesses of the BIDS-modified surfaces, remain consistent at ~1.7 nm for up to 24 h, which means that

a monolayer of the mono-ethoxy initiator has been formed at 6 h for the 0.5, 1 and 2 % v/v BIDS. For the evaluation of the BIBPTES films, a further insight of the morphology of the surfaces is needed.

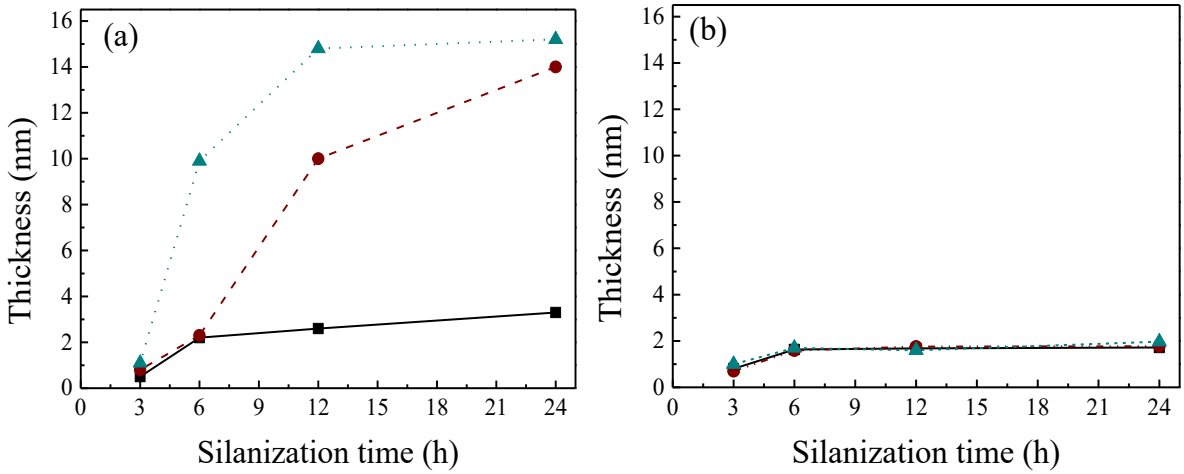


**Figure 3.4.** Dry thickness of the immobilized initiators BIBPTES (a) and BIDS (b) as a function of immersion time during the SAM process using 0.5% v/v (■, black), 1% v/v (●, wine) and 2% v/v (▲, dark cyan) initiator in toluene at RT.

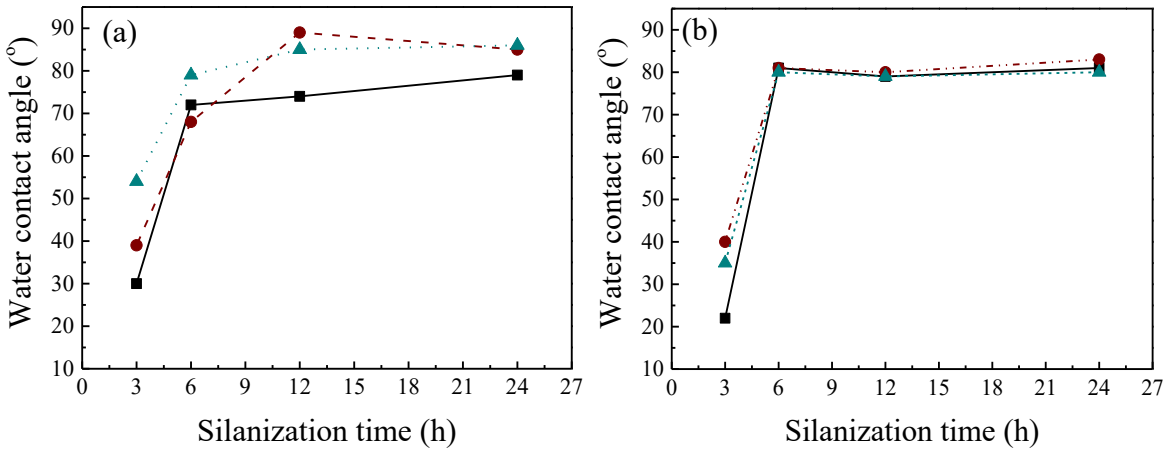


**Figure 3.5.** Static water contact angles (WCAs) for the immobilized initiators BIBPTES (a) and BIDS (b) as a function of immersion time during SAM process using 0.5% v/v (■, black), 1% v/v (●, wine) and 2% v/v (▲, dark cyan) in toluene at RT.

A qualitative chemical information of the silanization process can be extracted by the comparison of the wettability of the samples. In Figure 3.5, the silanization time dependence of the water contact angles of the surfaces for various concentrations of the BIBPTES (a) and BIDS (b) initiator in toluene is shown. Low contact angles for both

initiators are observed at low silanization times up to 3 h for all concentrations, which indicates a poor formation of the initiator layer since the immobilized films are expected to be moderately hydrophobic. For the 0.5 % v/v BIBPTES-modified surfaces, an abrupt transition to a slightly hydrophobic state of 72º at 6 h and 79º after 24 h, which is consistent with the CAs provided in the literature, implies the transformation of the substrates into hydrophobic surfaces and suggests full coverage by the hydrophobic molecules.[19] For the 1 and 2 % v/v BIBPTES solutions, higher contact angles between 85º and 89º are obtained, attributed to the larger dry layer film thickness discussed above. Finally, a profoundly consistent behavior of the wetting properties of the BIDS-modified substrates was observed for all concentrations above 6 h silanization time, with a WCA of ~81º.

**Table 3.1.** Ellipsometric film thickness, water contact angles and RMS data for silicon substrates modified with a mono-functional initiator BIDS and a tri-functional initiator BIBPTES at different silanization times.

| Sample | Immersion time (h) | Film thickness (nm)* | WCA (º)** | RMS (nm)*** |
|---|---|---|---|---|
| "piranha" treated silicon substrate | - | - | 12 ± 1 | 0.18 ± 0.02 |
| 0.5 % v/v BIBPTES | 3 | 0.8 ± 0.2 | 30 ± 2 | 0.78 ± 0.03 |
| | 6 | 2.2 ± 0.3 | 72 ± 2 | 0.56 ± 0.03 |
| | 24 | 3.3 ± 2.3 | 79 ± 2 | 2.4 ± 0.1 |
| 0.5 % v/v BIDS | 3 | 0.8 ± 0.3 | 22 ± 2 | 0.89 ± 0.03 |
| | 6 | 1.63 ± 0.3 | 80 ± 2 | 0.32 ± 0.02 |
| | **24** | **1.72 ± 0.4** | **81 ± 2** | **0.24 ± 0.03** |

*by ellipsometry, **by WCA measurements, ***by AFM

In order to assess the morphology of the films, AFM tapping mode was utilized. We studied samples modified with both the mono-functional BIDS and the tri-functional BIBPTES initiator, employing the same 0.5 % v/v solution in toluene, which was found to give consistent ellipsometry and water contact angle measurements. Figure 3.6 presents the AFM images for the BIBPTES modified silicon substrates (Figure 3.6a) and the BIDS modified surfaces (Figure 3.6b). The BIBPTES-modified samples present

a homogeneous morphology for silanization times up to 6 h, with average roughness values below 1 nm. Nevertheless, the homogeneity deteriorates at longer silanization times since the characteristic RMS values increased to 2.4 nm, which means that the initiator layer is less uniform, probably due to undesirable crosslinking of the triethoxysilane groups far from the surface. In contrast the BIDS modified substrates present excellent uniformity for all stages of the silanization process, with profoundly low RMS values, suggesting the preparation of uniform self-assembled monolayers. The time-dependent behavior of the two initiators during the silanization process is illustrated in Scheme 3.5. Table 3.1 summarizes the surface characteristics of the SAM's of the two initiators at the same concentration for three different immersion times.

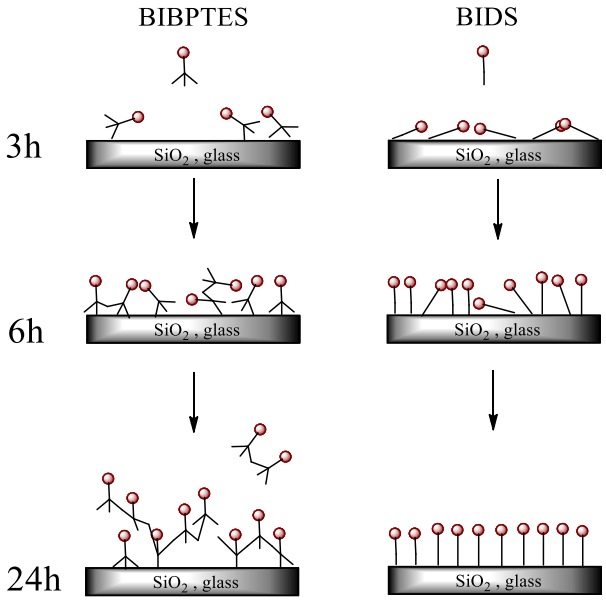


**Scheme 3.5.** Schematic representation of the formation of SAM of the tri-functional BIBPTES (left) and the mono-functional BIDS (right) initiator-modified surfaces, for immersion times 3, 6 and 24 h in a 0.5 % v/v initiator solution in toluene.

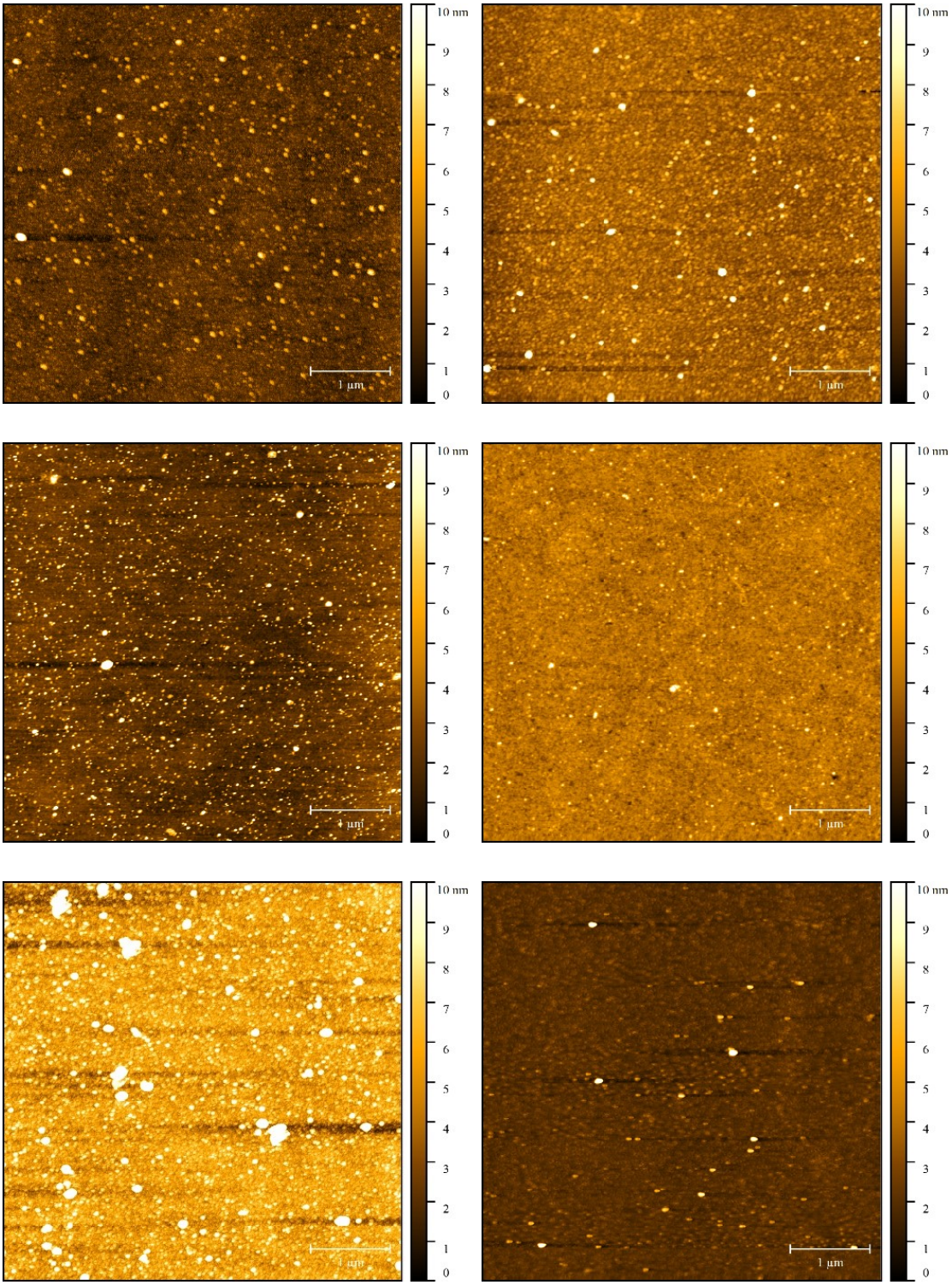


**Figure 3.6.** Tapping mode AFM images of tri-functional BIBPTES (left) and mono-functional initiator-modified surfaces (right), for immersion times 3, 6 and 24 h in 0.5 % v/v initiator solution in toluene. Each image resembles an area of 5 × 5 $\mu m^2$. Scale bar: 1 µm, Z-scale bar: 0-10 nm.

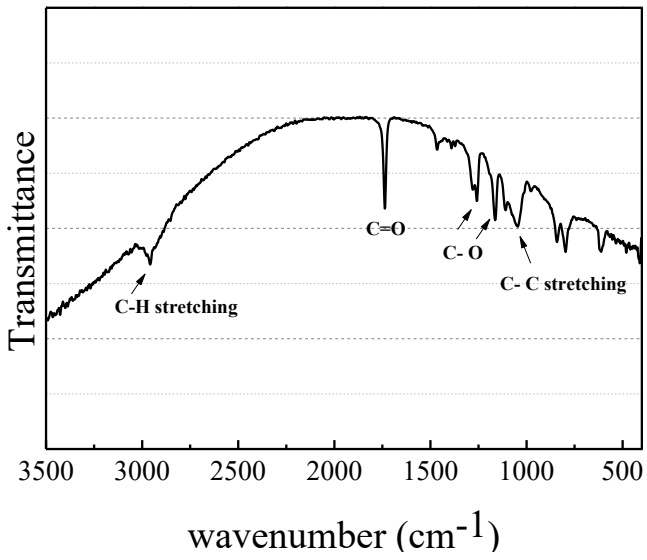


**Figure 3.7.** ATR-FTIR spectrum of the BIDS ATRP initiator immobilized on a silicon substrate.

For the synthesis of the homopolymer brushes, the mono-functional BIDS initiator was chosen to prepare the SAM of the initiator on silicon surfaces (0.5 v/v % initiator solution in toluene, 24 h, at 25 ºC). The successful immobilization of the initiator was verified by ATR-FTIR spectroscopy, contact angle measurements and ellipsometry. The transmittance FTIR spectrum is shown in Figure 3.7 indicating the appearance of a characteristic peak at 1737 $cm^{-1}$, which is attributed to the C=O stretching vibration of the carbonyl ester group, a peak at 2958 $cm^{-1}$ due to the C-H vibration modes of the methylene groups and finally, the peaks at 1257 $cm^{-1}$ and 1163 $cm^{-1}$, due to the C-O stretching and at 1045 $cm^{-1}$ due to the C-C vibrations. The characteristics of these surfaces are summarized in Table 3.1.

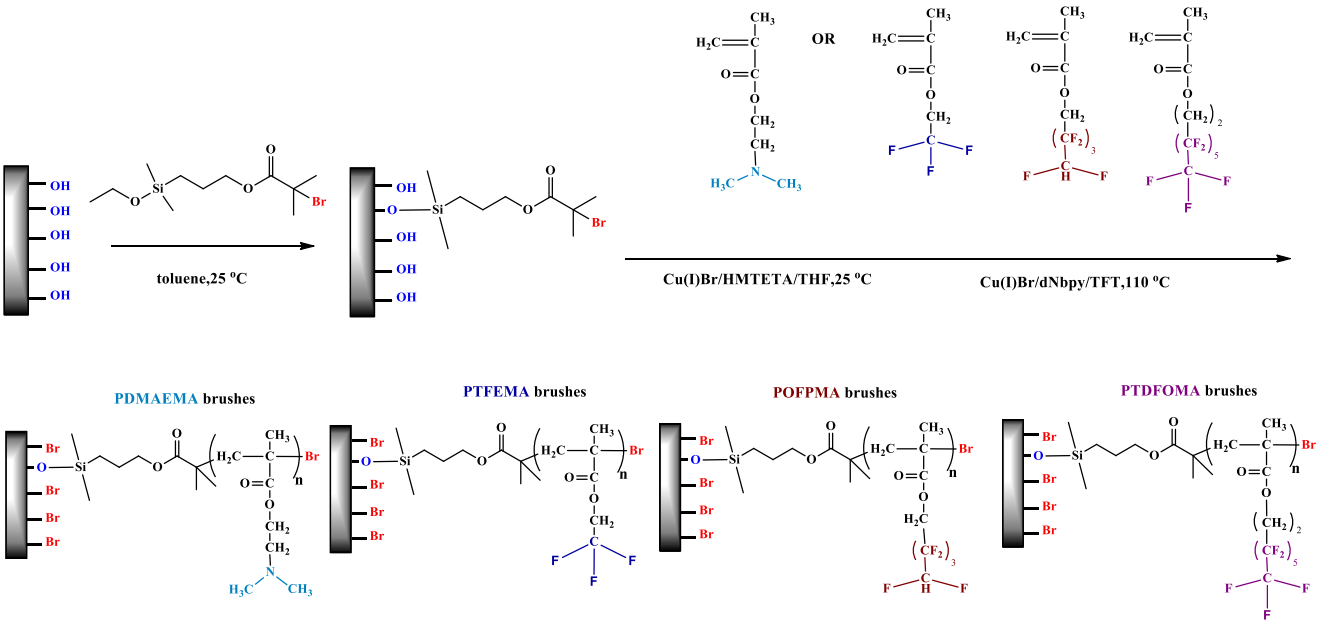


**Scheme 3.6.** Schematic representation of the synthetic procedure for the preparation of the SAM of the ATRP initiator and SI-ATRP of the functional methacrylates.

### 3.2.3 Synthesis of homopolymer brushes via SI-ATRP

A classical SI-ATRP of the functional DMAEMA and the semi-fluorinated TFEMA, OFPMA and TDFOMA methacrylate was carried out from the BIDS modified silicon substrates. The synthetic route for the preparation of all homopolymer brushes is shown in Scheme 3.6.

#### 3.2.3.1 Preparation of PDMAEMA brushes

The SI-ATRP of DMAEMA was carried out from the initiator functionalized silicon substrates using the grafting from technique (Scheme 3.6). Control over the reaction kinetics was established by using EBIB as a free initiator, with $Cu^{I}Br$/HMTETA acting as the catalyst system, at RT. The polymerizations were performed in the bulk, and in THF at constant molar ratios of [DMAEMA]/[$Cu^{I}Br$]/[HMTETA]/[EBIB] = 500/1/1/2. Figure 3.8a shows the evolution of dry film thicknesses, as a function of the polymerization time for the SI-ATRP of DMAEMA for three volume ratios of 1:0 (bulk), 1:1 and 4:1 v/v in THF, and a target degree of polymerization of 500. In these plots, higher initial growth rate of the polymer chains occurs in the absence of the moderately polar THF. A dry film thickness of 14 nm was obtained after 3 h, which indicates a rather fast growth rate of the polymer chains from the surfaces. The polymer

film thickness increases linearly up to 5 h after which it deviates and forms a plateau up to 15 h with a final dry film thickness of 38 nm. The loss of linearity in the longer reaction times is attributed to the reduced rate of monomer diffusion or to the partial loss of the active chain ends of the grafted polymer chains. This accelerated growth rate is thus not desirable. The presence of THF in a 1:1 v/v ratio affects clearly the polymerization rate and subsequently the thickness of the polymer brushes. An initial polymer film thickness of 7 nm at 3 h id obtained, followed by a linear increase for at least 18 h. Even though there is an excellent linear increase of the film thickness with time, the rate of polymerization and therefore the thickness of the final polymer film is profoundly decreased. The early termination in bulk polymerization and the moderate rate of polymerization in the 1:1 ratio of monomer to THF led to the study of a 4:1 volume ratio of DMAEMA to THF. The PDMAEMA brushes follow a constant polymerization rate up to high thicknesses (ca. 48 nm in 12 h), and thereafter the polymerization rate is slightly decreased.

The free polymers retrieved from the solution of the polymerization mixture were analyzed by SEC to obtain the molecular characteristics of the polymer brushes (see Table 3.2). Determining the molecular weight of the grafted polymer chains on a flat surface can be problematic, due to the tiny amount of polymer brush material in the typically explored areas of 1.0 - 1.5 $cm^2$. The addition of free sacrificial initiator to the reaction mixture is the most widely employed method for determining the polymer molecular weights and molecular weight distributions.[20] Figure 3.8b shows representative SEC traces of the free polymers obtained from the bulk and solution polymerizations at 12 h. Molecular weights varied between 28,000 and 77,000 for the synthesized polymers. Even though, the traces in all cases are monomodal, addition of THF in a 1:1 volume ratio led to a broader molecular weight distribution ($M_w/M_n$=1.38). On the other hand, the polydispersities of the polymers retrieved from the bulk and the 4:1 volume ratio, are narrow between 1.1 - 1.2, which define a controlled polymerization process.

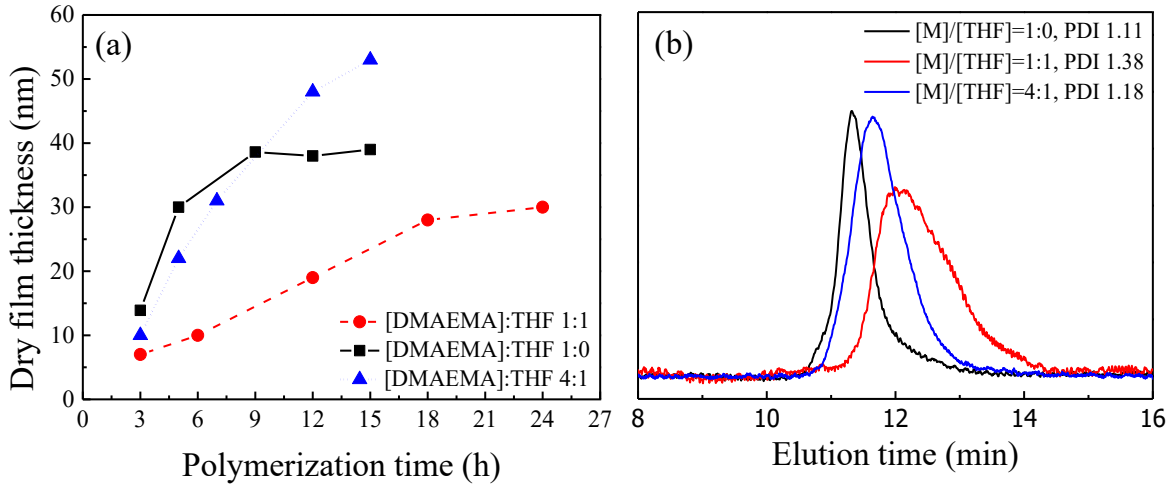


**Figure 3.8.** (a) Evolution of the dry film thickness vs polymerization time for the SI-ATRP of DMAEMA in the bulk (■, black) and in the presence of THF (●, red and ▲, blue). (b) SEC traces for the PDMAEMA homopolymers obtained after 12h in the bulk and in the presence of THF.

**Table 3.2.** Characterization data for the initiator SAM at 24 h silanization time and the synthesized PDMAEMA brushes after 12 h polymerization time.

| Monomer* | Solvent | Reaction time (h) | Ellipsometric thickness (nm) | $M_n$ (g/mol) | $M_w/M_n$ | Grafting density (chains/nm$^2$) | RMS (nm) |
|---|---|---|---|---|---|---|---|
| BIDS | toluene | 24 | 1.7 ± 0.3 | - | - | - | 0.24 |
| DMAEMA | THF 1:1 | 12 | 19 ± 1 | 28,000 | 1.38 | 0.41 | 1.7 |
| | bulk | | 38 ± 1 | 77,000 | 1.11 | 0.29 | 1.1 |
| | THF 4:1 | | 48 ± 1 | 61,000 | 1.18 | 0.47 | 0.8 |

* [M]:[I] = 500:1

Next, the grafting density σ, of the polymer chains on the surfaces was calculated using the equation (see Table 3.2):

$$\sigma = \frac{d \times N_A \times h}{M_n} \qquad (2.1)$$

where h is the dry polymer film thickness (nm), d is the bulk density of the polymer (1.097 g/cm$^3$ for PDMAEMA), $M_n$ is the number-average molecular weight of the

chains grafted on the surface assumed to be the same as that of the polymer chains in solution (determined by GPC) and $N_A$ is the Avogadro's number ($6.023\times10^{23}$). In the presence of a 1:1 volume ratio of DMAEMA to THF, the less concentrated polymerization mixture led to lower molecular weights on the surfaces thus resulting in low film thicknesses of the polymer brushes. At high polymerization times (12 h), the grafting density was calculated 0.41 chains/nm$^2$, suggesting densely grafted polymer brushes on the surfaces. On the other hand, the grafting density of the polymer chains prepared in the bulk polymerization is much lower ($\sigma$ = 0.29 chains/nm$^2$), which verifies that the change in the viscosity of the reaction mixture impacts the growth of the polymer chains on the substrate more than those in solution. Opposed to the viscous bulk polymerization, the presence of a low amount of a moderate polar solvent (4:1 v/v THF), resulted in the highest grafting density ($\sigma$ = 0.47 chains/nm$^2$) of the polymer chains.

Finally, the morphology of the PDMAEMA brushes was probed by AFM. Figure 3.9 shows the AFM images of the polymer films prepared in 1:0, 1:1 and 4:1 volume ratio of DMAEMA to THF via SI-ATRP for 12 h. For 1:0 and 4:1 ratio, the polymer films present a homogeneous morphology with average roughness values ~ 1 nm, suggesting the preparation of uniform polymer films. For 1:1 ratio the polymer film presents the highest value of RMS at 1.7 nm, which may be attributed to the higher distribution of the grafted polymer chains, observed by GPC (Table 3.2). One of the main objectives of this thesis is to obtain well-defined smooth polymer brushes of high grafting densities, and therefore the brushes prepared at [DMAEMA]/[THF] = 4:1 were chosen for further studies.

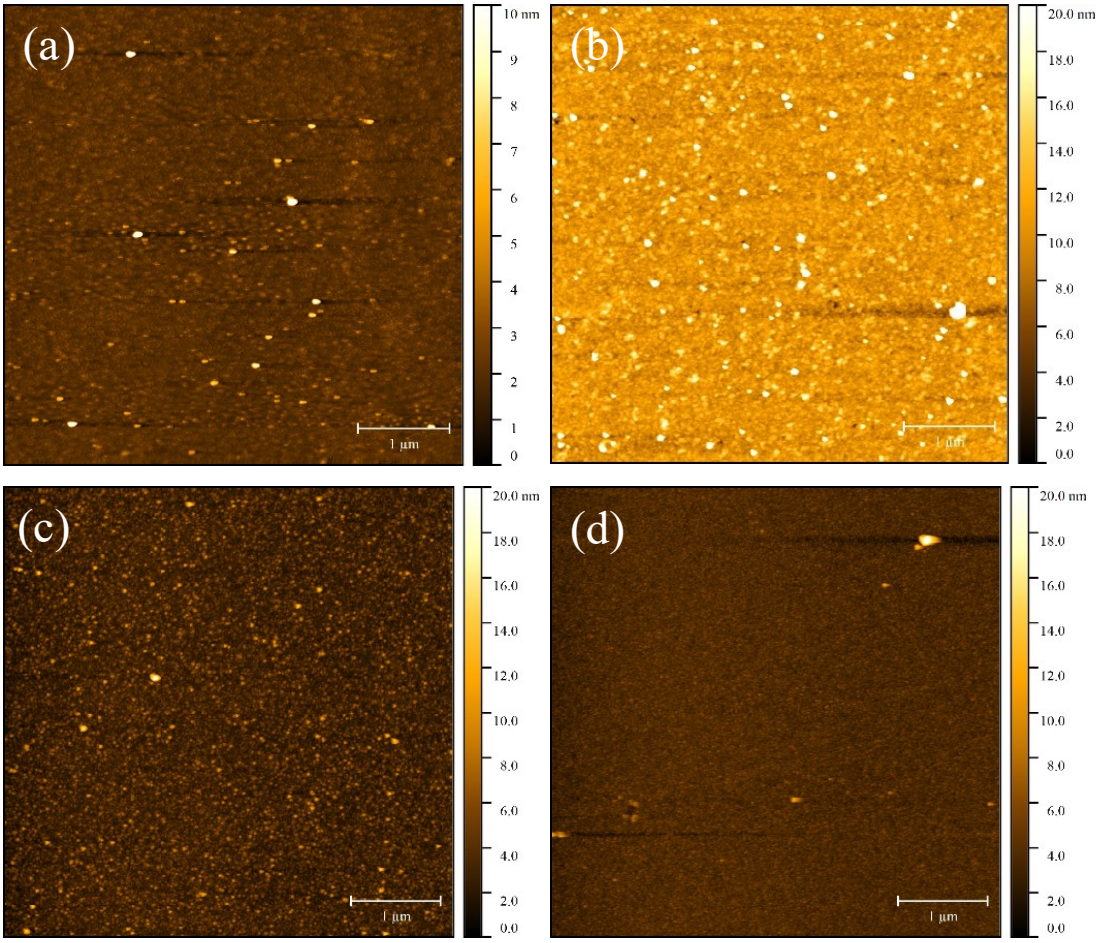


**Figure 3.9.** AFM height images of the BIDS initiator (Z:0-10 nm) (a) and the PDMAEMA brushes prepared at 1:1 v/v (b), 1:0 v/v (c) and 4:1 v/v (d) ratios of DMAEMA to THF. Each image resembles an area of 5 × 5 $\mu m^2$. Z-scale bar: 0-20 nm.

Well-defined PDMAEMA brushes were synthesized by SI-ATRP in a mixture monomer: THF mixture 4:1 v/v, with $M_n$'s between 11,000 gr $mol^{-1}$ and 170,000 gr $mol^{-1}$ and low molecular weight distributions ($M_w/M_n$=1.1 to 1.35) (by SEC). The corresponding dry thicknesses are 9 up to 130 nm, respectively (see Table 3.3). Figure 3.10a compares the dry film thicknesses of the attained PDMAEMA brushes and the molecular weights of the free polymers grown in solution, respectively, as a function of the polymerization time. A linear growth rate is vital for a good control of the polymerization and for high film thicknesses. Overall, a 9 nm film was obtained after 3 h of polymerization, which increased to 24, 58 and 131 nm by prolonging the reaction time to 5, 12 and 38 h, respectively. A linear increase of the film thickness with the

polymerization time was observed for PDMAEMA brushes up to 12 h, after which increase in the film thickness becomes slower. This can be attributed to either a loss of the living character of the polymerization due to undesirable termination reactions or to inaccessible active polymerization sites, due to the increase in the viscosity of the reaction mixture at higher polymerization times, when large polymer chains are present in the solution. In addition, Figure 3.10b shows the SEC traces of the free polymers obtained in solution during the SI-ATRP. In all cases, the traces are uniform and monomodal with narrow molecular weight distributions. The grafting density σ (chains $nm^{-2}$) of the PDMAEMA chains on the surface was calculated ~ 0.5 chains $nm^{-2}$ for film thicknesses above 9 nm, suggesting the synthesis of densely grafted polymer brushes. Table 3.3 summarizes the characteristics of the synthesized PDMAEMA brushes.

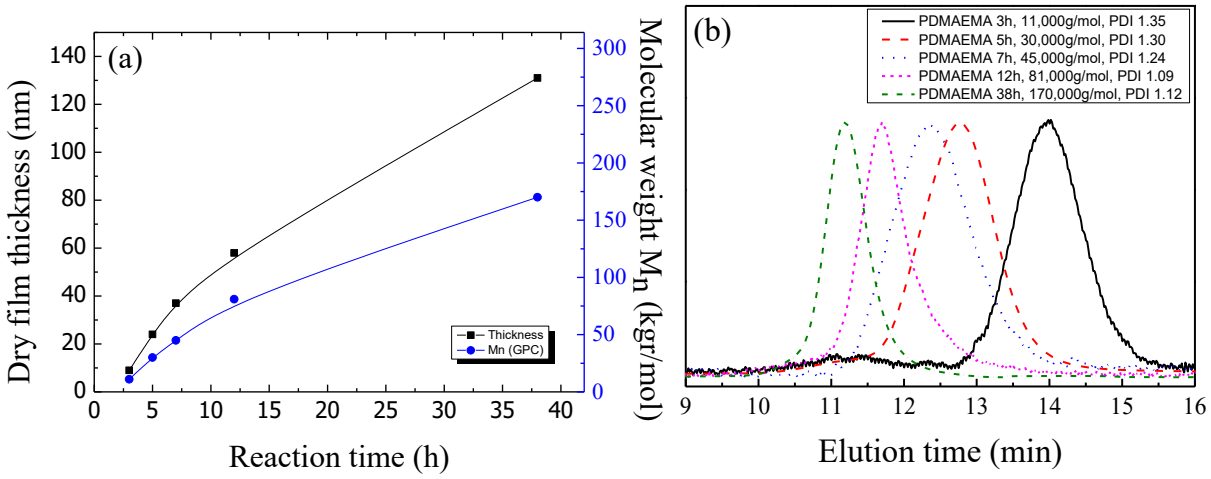


**Figure 3.10.** (a) Evolution of the dry film thickness (■, black) and the molecular weight of polymer chains in solution (●, blue) with the reaction time for the synthesis of the PDMAEMA brushes. (b) SEC traces for the free PDMAEMA obtained from the solution during the SI-ATRP of PDMAEMA brushes.

**Table 3.3.** Characterization data for the synthesized PDMAEMA brushes.

| Monomer | solvent | Reaction conditions [M]:[I] | Reaction time (h) | Ellipsometric thickness (nm) | $M_n$ (g/mol) | $M_w/M_n$ | Grafting density (chains/nm$^2$) |
|---|---|---|---|---|---|---|---|
| **BIDS** | toluene | - | 24 | 1.7 ± 0.3 | - | - | - |
| **DMAEMA$_a$** | THF 4:1 | 1300:1 | 3 | 9.0 ± 0.7 | 11,000 | 1.35 | 0.54 |
| | | | 5 (a=1) | 24 ± 1 | 30,000 | 1.30 | 0.53 |
| | | | 12 (a=2) | 58 ± 1 | 81,000 | 1.09 | 0.47 |
| | | | 38 (a=3) | 131 ± 3 | 170,000 | 1.12 | 0.51 |

In order to verify the presence of the homopolymer chains on the silicon substrates, we performed transmittance ATR-FTIR analysis of the polymer films. Figure 3.11 shows the FTIR spectra for the three thicker PDMAEMA films with dry thicknesses of (a) 24 nm, (b) 58 nm and (c) 130 nm, respectively (denoted as PDMAEMA$_a$, where a = 1, 2 or 3 (see Table 3.3)). The appearance of a characteristic peak at 1730 cm$^{-1}$ which corresponds to the C=O stretching vibration of the ester group and the peaks at 2822 and 2770 cm$^{-1}$ attributed to the $(CH_3)_2$-N symmetric and asymmetric stretching vibrations of the polymer were observed. In addition, the absence of a peak at ~1630 cm$^{-1}$, which is characteristic of the C=C bonds, indicates that there is no residual monomer within the grafted polymer films. Finally, the increase of the intensity of the carbonyl peak with the film thickness, implies that the amount of grafted polymer increases, which is consistent with the ellipsometric and SEC data, discussed above.

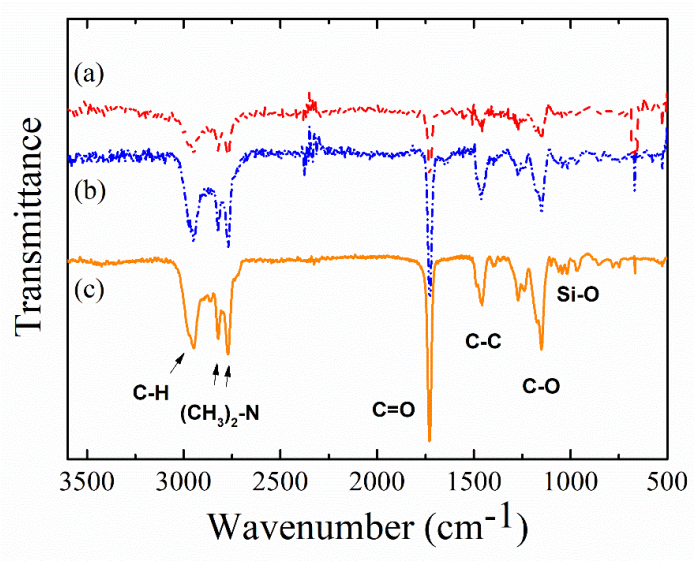


**Figure 3.11.** FTIR spectra of the (a) $PDMAEMA_1$, (b) $PDMAEMA_2$ and (c) $PDMAEMA_3$ brushes.

### 3.2.3.2 Preparation of semi-fluorinated polymer brushes

The SI-ATRP of TFEMA, OFPMA and TDFOMA was similarly carried out from the initiator functionalized substrates (Scheme 3.6). The low concentration of initiator on the surfaces cannot provide the sufficient amount of deactivator to control the ATRP reaction. Thus, sacrificial initiator, EBIB, was employed to synthesize well-defined brushes on the substrates. The polymerizations were performed in the presence of α,α,α-trifluorotoluene (TFT), as a solvent, at 100 °C and at constant molar ratios of [fluoroMA]/[$Cu^{I}Br$]/[dNbpy]/[EBIB]. TFT was used as a good solvent for the SI-ATRP of the fluorinated monomers.

The semi-fluorinated TFEMA, OFPMA and TDFOMA brushes differ in the amount of fluorine atoms present on the side groups of the grafted polymers, comprising three, eight and thirteen fluorine atoms bound to carbon atoms, respectively. The almost linear increase of the polymer film thickness with the polymerization time indicated a good control of the polymerization reaction (Figure 3.12a). A dry film thickness of 10 nm was obtained after 10 h polymerization of TFEMA, which indicates a rather moderate/slow growth rate of the polymer chains from the surfaces. The polymer film thickness increases almost linearly up to 48 h after which, it deviates for 60 h with a final dry film thickness of 26 nm. Deviations in the longer reaction times are attributed to the reduced rate of monomer diffusion or the partial loss of the active chain ends,

which slowed down the polymerization. Similarly, a 5 and 4 nm film was obtained after 10 h of polymerization of OFPMA and TDFOMA, respectively, which increased to 15 and 12 nm by prolonging the reaction time up to 60 h, respectively. The characterization data for the semi-fluorinated homopolymer brushes are summarized in Table 3.4 (denoted as $TFEMA_n$, $OFPMA_n$ and $TDFOMA_n$, where n = 1, 2 or 3 for 12, 24 and 60 h reaction time). The growth rate of the fluorinated brushes is slower compared to that of the PDMAEMA brushes using a 1:1 volume ratio of monomer to solvent, nonetheless direct comparison with the PDMAEMA brushes is not reliable since different catalyst systems and solvents were employed. The overall film thicknesses attained for the semi-fluorinated polymers decreased as the fluorinated alkyl groups became longer suggesting the slowdown of the polymerization reaction. Assuming that the reactivities of the semi-fluorinated methacrylate monomers are similar, the observed difference in the growth rate can be partly attributed to the larger size of the TDFOMA- and OFPMA-monomer in comparison to TFEMA (having 2.6 and 1.4 times higher molecular weight than TFEMA, respectively), so that propagation step adds more mass to the polymer layer in each case.

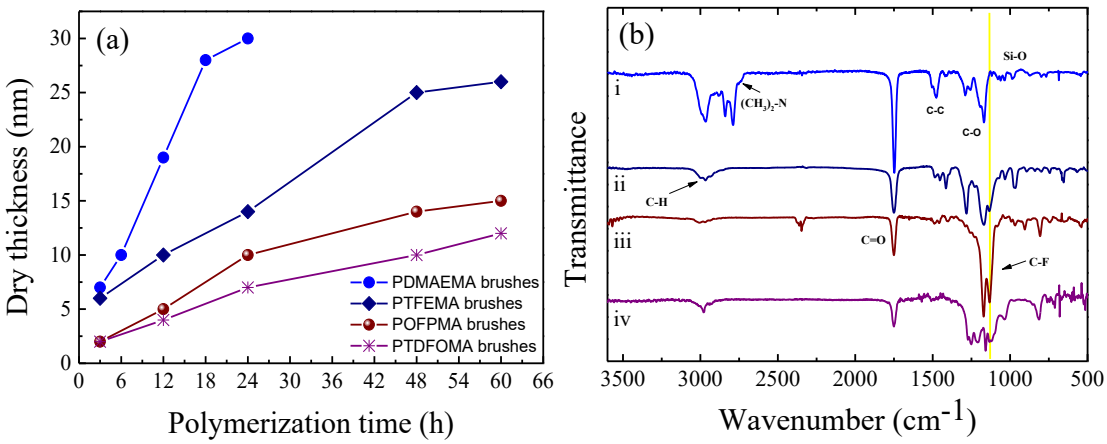


**Figure 3.12.** (a) Evolution of the dry film thickness with the polymerization time for the PDMAEMA (●, blue) PTFEMA (♦, dark blue) POFPMA (●, wine) and PTDFOMA (*, purple) homopolymer brushes (b) FTIR spectra of grafted (i) $PDMAEMA_1$, (ii) $PTFEMA_3$, (iii) $POFPMA_3$ and (iv) $PTDFOMA_3$ brushes. The vertical yellow line denotes the characteristic peak at 1131 $cm^{-1}$ attributed to the C-F stretching vibration.

The presence of the grafted semi-fluorinated $PTFEMA_3$, $POFPMA_3$ and $PTDFOMA_3$ chains on the substrates was confirmed by ATR-FTIR spectroscopy (Figure 3.12b). The appearance of a peak at 1730 $cm^{-1}$ which corresponds to the C=O stretching vibration

of the ester group and the characteristic peak at 1131 $cm^{-1}$ attributed to the C-F stretching vibration of the semi-fluorinated polymer units were observed.

**Table 3.4.** Characterization data for the synthesized fluorinated brushes.

| Monomer | Reaction time (h) | Ellipsometric thickness (nm) | $M_n$ (g/mol) | $M_w/M_n$ | Grafting density (chains/$nm^2$) |
|---|---|---|---|---|---|
| $TFEMA_n$ | 12 | 10 | 38,000 | 1.31 | 0.24 |
| | 24 | 14 | 47,000 | 1.22 | 0.26 |
| | 60 | 26 | 75,000 | 1.24 | 0.30 |
| $OFPMA_n$ | 12 | 5 | 24,000 | 1.23 | 0.20 |
| | 24 | 10 | 50,000 | 1.18 | 0.19 |
| | 60 | 15 | 70,000 | 1.16 | 0.20 |
| $TDFOMA_n$ | 12 | 4 | NA | NA | NA |
| | 24 | 7 | | | |
| | 60 | 12 | | | |

❖ TFT was used as a solvent for the polymerizations at 100 ºC.

The free polymers retrieved from the solution of the polymerization mixture were analyzed by SEC to obtain the molecular characteristics of the polymer brushes (see Table 3.2). The $M_n$'s were ranged between 38,000 gr $mol^{-1}$ and 75,000 gr $mol^{-1}$ for PTFEMA brushes and 24,000 gr $mol^{-1}$ and 70,000 gr $mol^{-1}$ for POFPMA brushes with low molecular weight distributions ($M_w/M_n$=1.16 to 1.31). The PTDFOMA polymer is insoluble in THF, thus its molecular weight and molecular weight distribution could not be analyzed by SEC. Figure 3.13 shows the SEC traces of the free polymers obtained in solution during the SI-ATRP of TFEMA and OFPMA. SEC is equipped with a refractive index detector (RI) and uses THF as the eluent. The SEC characterization of the POFPMA polymer gave a negative RI signal, which is characteristic for fluoropolymers with lower refractive index than that of the eluent solvent ($n_{popfma} < n_{thf}$). In all cases the traces are monomodal with narrow molecular

weight distributions (below 1.31) suggesting a good control of the polymerization reaction.

The grafting density σ (chains $nm^{-2}$) of the PTFEMA and POFPMA chains on the surface was calculated between 0.2 - 0.3 chains $nm^{-2}$, suggesting the synthesis of densely grafted polymer brushes (see Table 3.2).

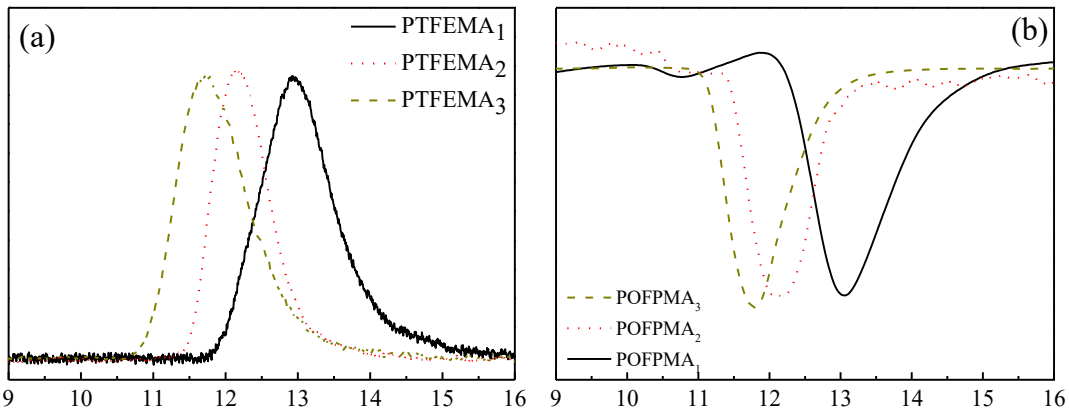


**Figure 3.13.** SEC traces of the free $PTFEMA_n$ (a) and $POFPMA_n$ (b) polymer obtained in solution during the SI-ATRP of the semi-fluorinated monomers after 12, 24 and 60 h polymerization time (n=1, 2 and 3, respectively)

### 3.2.4 Post-polymerization modification of the PDMAEMA brushes

Next, quaternization of the PDMAEMA brushes was carried out by a post-polymerization modification reaction to convert the tertiary amine groups of the DMAEMA units to their quaternary ammonium salt analogues. Alkyl halides with different alkyl chain lengths (ACLs) were employed (see Scheme 3.7) to investigate their effect on the polymer film properties and the antimicrobial activity of the resulting PQDMAEMA brushes (denoted as $PQDMAEMA_a$-CY, where a = 1, 2 or 3 and Y is the number of carbon atoms attached on the tertiary amine groups upon quaternization).

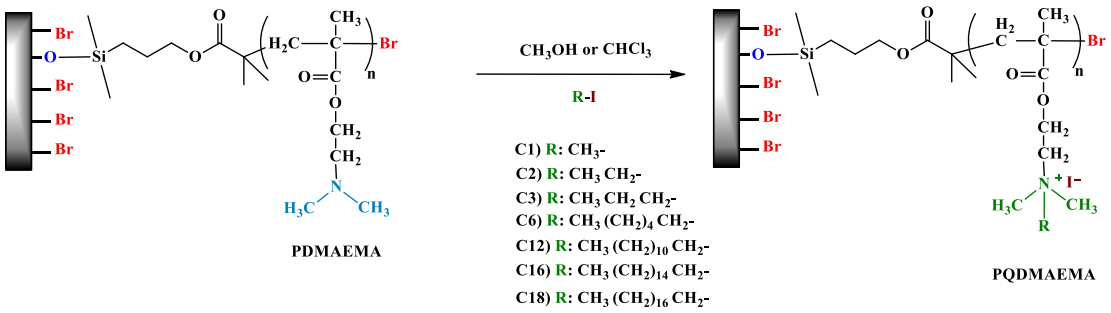


**Scheme 3.7.** Schematic illustration of the (i) initiator self-assembled monolayer formation, (ii) SI-ATRP of DMAEMA and (iii) quaternization of the PDMAEMA homopolymer brushes, using different alkyl halides, to obtain the PQDMAEMA brushes.

The PQDMAEMA brushes were characterized by FTIR spectroscopy and representative plots for non-quaternized and quaternized PDMAEMA brushes with short and long ACL are presented in Figure 3.14. A new peak appeared at 2854 $cm^{-1}$, which is attributed to the $(CH_3)_3$-$N^+$ vibration of the quaternary ammonium groups, verifying the successful quaternization reaction. The disappearance of the N-$(CH_3)_2$ stretching vibrations of the tertiary amine groups, at 2821 and 2771 $cm^{-1}$, for the PQDMAEMA-C1 brush, indicated the near quantitative quaternization of the amine groups. It is noted that the peaks, at 2821 and 2771 $cm^{-1}$, were still observed for the PQDMAEMA-C18 brush suggesting the presence of some remaining tertiary amine groups, which were not quaternized. Moreover, the peak in the 2887-3000 $cm^{-1}$ range, attributed to the C-H stretching vibration, became more intense after quaternization verifying the attachment of the alkyl chains on the polymer brushes.

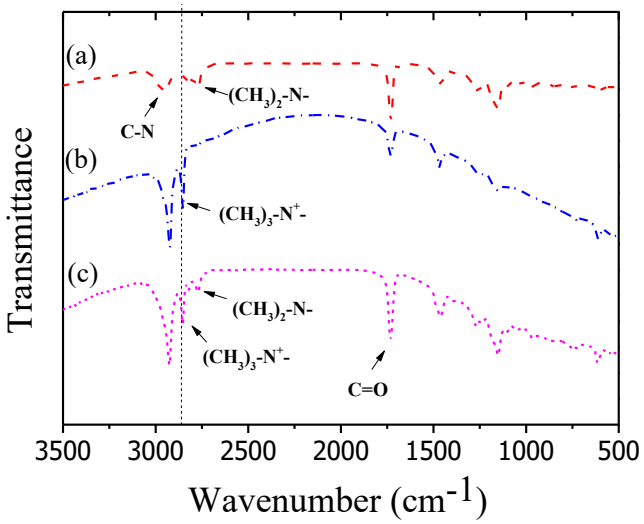


**Figure 3.14.** Transmittance FTIR spectra of the PDMAEMA brush of an initial dry thickness of 24 nm (a), the PQDMAEMA-C1 brush (b) and the PQDMAEMA-C18 brush (c). The vertical black dashed line denotes the characteristic peak at 2920-2857 $cm^{-1}$ attributed to the $N^{+}$-$(CH_3)_3$ vibration.

### 3.2.5 Surface properties of the homopolymer brushes

#### 3.2.5.1 Morphology of the homopolymer brushes

The surface properties of thin polymer films, such as the wettability, surface energy, friction, biological performance and others, are profoundly affected by the surface topography and the surface chemistry at the interface. The surface morphology of the homopolymer brush films was assessed via AFM measurements under ambient conditions. Figure 3.15a-d shows AFM height images of the $PQDMAEMA_1$ brushes and semi-fluorinated $PTFEMA_3$, $POFPMA_3$ and $PTDFOMA_3$ brushes. The average roughness of the polymer films was calculated from the AFM images and was found between 0.7 and 1.2 nm, indicating homogeneous and noticeable smooth surfaces. In addition, Figure 3.15e-f shows representative AFM height images for the $PQDMAEMA_1$-C3 and $PQDMAEMA_1$-C18 brushes. A small increase in the surface roughness was found after quaternization with an average RMS between 1.2 and 1.5 nm for the PQDMAEMA brushes in the dry state, indicating that the quaternization reaction affected only slightly the morphology of the surfaces. Table 3.5 summarizes the mean-root square roughness of each sample. Since the surface morphology of the polymer brushes was smooth, with negligible variations in the average roughness, it is

clear that the surface chemistry will determine the surface properties of the thin polymer films.

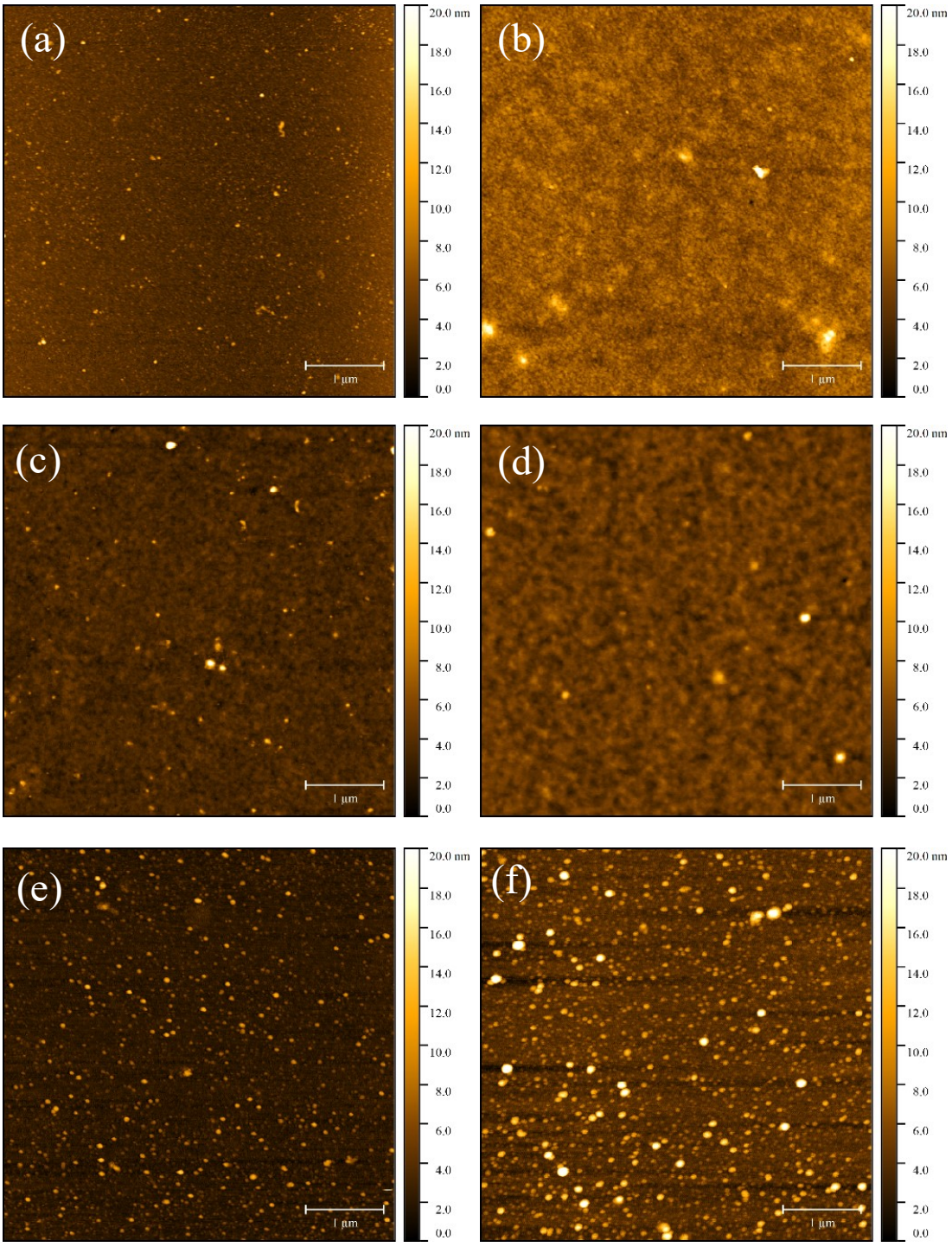


**Figure 3.15.** AFM images of the $PDMAEMA_1$ (a), $PTFEMA_3$ ($C_F1$) (b), $POFPMA_3$ ($C_F4$) (c) and $PDTDFOMA_3$ ($C_F6$) (d) homopolymer brushes and the PDMAEMA brushes after quaternization with iodopropane (e) and iodooctadecane (f). Each image resembles an area of 5 × 5 $\mu m^2$. Z-axis scale bar: 0-20 nm.

**Table 3.5.** Surface characteristics of the homopolymer brushes

| Monomer | Reaction time (h) | Ellipsometric thickness (nm) | RMS (nm) |
|---|---|---|---|
| **DMAEMA$_1$** | 5 | 24 | 0.7 |
| **TFEMA$_3$** | 60 | 26 | 0.9 |
| **OFPMA$_3$** | 60 | 15 | 1.1 |
| **TDFOMA$_3$** | 60 | 12 | 1.4 |
| **DMAEMA$_1$-C3** | - | 42 | 1.2 |
| **DMAEMA$_1$-C18** | - | 34 | 1.4 |

### 3.2.5.2 Wetting behavior of the homopolymer brushes

The surface wettability of the homopolymer brushes was investigated by static water contact angle (WCA) measurements, to study the effect of the ACL of the PQDMAEMA brushes and the number of fluorine atoms of the semi-fluorinated PTFEMA$_3$, POFPMA$_3$ and PTDFOMA$_3$ brushes (denoted as $C_FY$, where Y = 1, 4 or 6 is the number of fluorinated carbon atoms attached on the side groups of the TFEMA, OFPMA and TDFOMA monomers, respectively) on the polymer film properties. WCA measurements were performed after immersion of the polymer films in a good solvent, THF for the PDMAEMA brushes and HFiP for the fluorinated brushes. The insets in Figure 3.16 shows photographs of water droplets placed on the polymer brushes. Figure 3.16a represents the WCA values of the PDMAEMA and PQDMAEMA brushes for the three different film thicknesses. The WCA's on the PDMAEMA films were measured ~60$^o$ which is in good agreement with the values reported in the literature for PDMAEMA brushes. Even though, PDMAEMA is a polar polymer due to the amino group and is a water-soluble polymer, the corresponding PDMAEMA brushes have relatively high WCAs. Next, the WCAs of the semi-fluorinated brushes was studied (Figure 3.16b). The introduction of 3 fluorine atoms ($C_F1$) resulted in a hydrophobic

brush with contact angle 90°, whereas the contact angle increased to 108° and 118° for fluorinated alkyl chain lengths (FCL) of $C_F4$ and $C_F6$, corresponding to POFPMA and PTDFOMA brushes, respectively. This increase in WCA can be attributed to the presence of the fluorinated alkyl side chains at the outermost surface of the brush. The surfaces of the films are enriched with fluorinated domains, due to the phenomenon of vertical alignment of neighboring perfluoroalkyl units,[21] attributed to the tendency of the fluorinated films to lower their overall free energy through migration of the low-energy fluorine groups to the outer surface resulting in higher hydrophobicity.

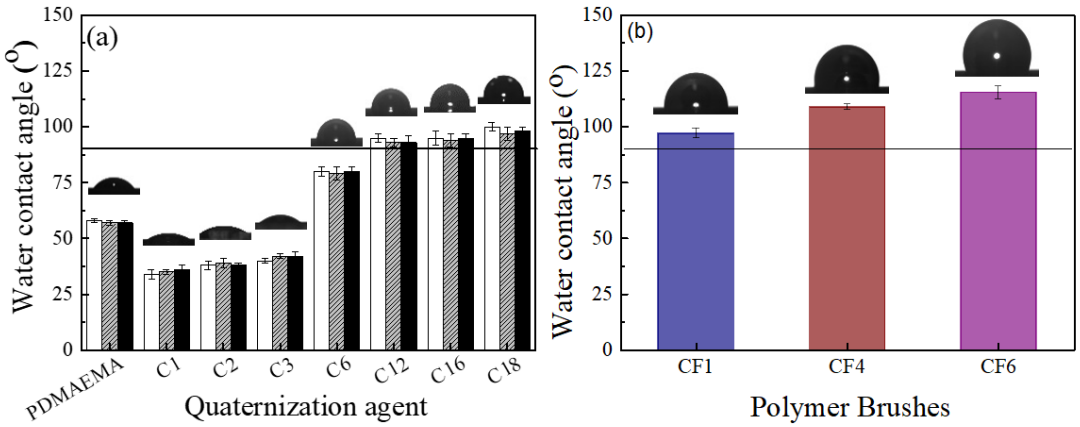


**Figure 3.16.** Static water contact angles (WCAs) for the homopolymer brushes (a) $PDMAEMA_a$ and $PQDMAEMA_a$-CY brushes quaternized with different alkyl halides and (b) $PTFEMA_3$, $POFPMA_3$ and $PTDFOMA_3$ with $C_F1$, $C_F4$ and $C_F6$ FCL, respectively. The black line denotes the value of 90°, which separates hydrophilic and hydrophobic surfaces. Insets: WCA images of the homopolymer brushes.

The surface wettability of the PQDMAEMA brushes was examined as a function of the ACL of the alkylating agent bearing the same halide (iodide). Figure 3.16 depicts the WCA values as a function of the ACL (C1-C18) of the quaternization agent for the PQDMAEMA brushes. For small ACLs (C1-C3) of the quaternization agents, the WCAs were found lower than the value measured for the precursor PDMAEMA brush (57 ° ± 2 °), indicating that the permanent positive charge on the polymer side groups increases the hydrophilicity of the surface. Moreover, the WCA increased monotonically from 36 ° for C1, 39 ° for C2 and 42 ° for C3, signifying the influence of each additional methylene unit of the alkyl chain on the surface wettability. However,

the wettability of the surface changed dramatically for longer ACLs (C≥6), and a hydrophilic-to-hydrophobic transition was observed for C12 to C18 with WCAs in the range of 90 º-100 º. This suggests that despite the charged quaternary ammonium salt moieties, the surface wettability is dominated by the long hydrophobic alkyl chains attached onto the polymer side-groups, and renders the quaternization reaction a novel and facile approach to tune the hydrophilicity/hydrophobicity of a polyamine surface at will. It is noted that, the WCAs were not affected by the polymer molecular weight and therefore the thickness of the polymer films, when quaternized with the same alkyl halide, verifying that the wettability is a surface property influenced only by the outermost layer of the film.

#### 3.2.5.3 Surface free energy of the homopolymer brushes

The surface free energy (SFE) values of the $PQDMAEMA_1$ brushes were calculated from the static CA measurements of Milli-Q water and diiodomethane, using the equation of Owens and Wendt.[22] Figure 3.17a shows the surface energy values of the homopolymer brushes. The surface energy of the neat silicon substrate after piranha solution was measured at 70 mN/m, which is similar to that of water at 72 mN/m. Moreover, the surface energy values decreased to 53º for the $PDMAEMA_1$ brush ($C_F0$), signifying the influence of the polar tertiary amine groups on the surface energy. However, the surface energy changed dramatically for the semi-fluorinated polymers ($C_F1$, $C_F4$, and $C_F6$), and obtained values of 10, 15 and 23 mN/m. This suggests that, the surface wettability is dominated by the long-fluorinated alkyl chains and decreases monotonically with the increase of the FCL. This is again attributed to the tendency of the fluorinated units to migrate to the surface and thus lowering the surface energy.

Figure 3.17b depicts the surface energy values as a function of the ACL (C1-C18) of the quaternization agent for the $PQDMAEMA_1$ brushes. The $PQDMAEMA_1$ brushes with small ACLs (C1-C3) exhibited higher surface energies compared to the value calculated for the $PDMAEMA_1$ brush (53 mN/m), indicating the formation of a polar strong polyelectrolyte brush. Moreover, the surface energy values decrease slightly, from 62 to 60 mN/m, with the increase of the ACL (C1 to C3) of the quaternization agent. A more abrupt decrease of the surface energy, down to 33, 32, 29 and 27 mN/m, was found for the longer ACLs, C6, C12, C16 and C18, respectively, and verifies the presence of the long hydrophobic alkyl chains at the air-polymer interface, which

diminish the surface free energy of the films. Table 3.6 summarizes the surface energy values of the homopolymer brushes.

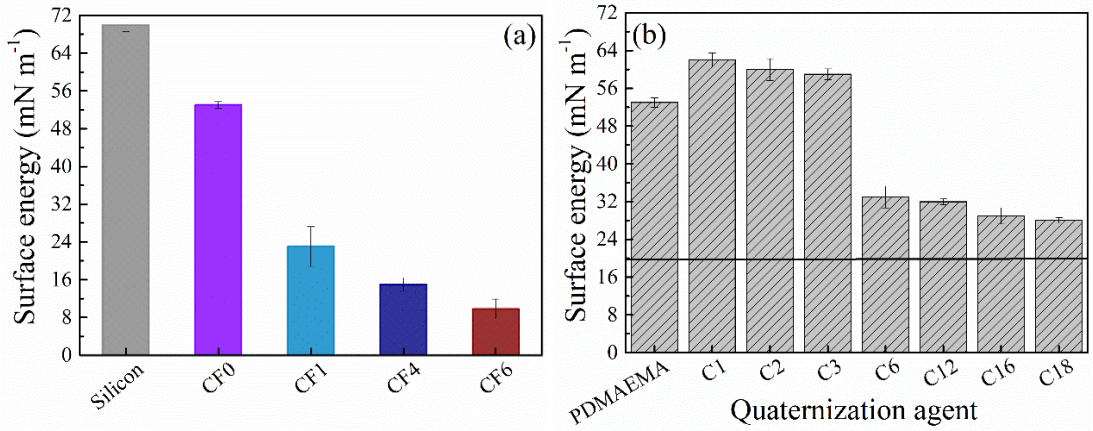


**Figure 3.17.** Surface energy values for the (a) homopolymer brushes and (b) PQDMAEMA$_1$ brushes quaternized with different alkyl halides. The horizontal black line denotes the equilibrium value (~20 mN/m), which describes the transition between low and high surface energy films.

**Table 3.6.** Contact angle and surface energy values of the homopolymer brushes and the PQDMAEMA$_1$ brushes quaternized with C3 and C18.

| Monomer | Water CA (º) | Diiodomethane CA (º) | SFE $\gamma_{SV}$ (mN/m) |
|---|---|---|---|
| **DMAEMA ($C_F$0)** | 58 | 38 | 53 |
| **TFEMA ($C_F$1)** | 97 | 78 | 23 |
| **OFPMA ($C_F$4)** | 108 | 87 | 15 |
| **TDFOMA ($C_F$6)** | 118 | 100 | 10 |
| **QDMAEMA-C3** | 40 | 31 | 60 |
| **QDMAEMA-C18** | 96 | 60 | 27 |

### 3.2.5.4 Film thickness and degree of quaternization of the PQDMAEMA brushes

The dry film thicknesses of the PDMAEMA and PQDMAEMA brushes were measured by spectroscopic ellipsometry (Figure 3.18). For all samples, irrespective of the dry thickness of the precursor PDMAEMA brush, an increase in the film thickness was measured after quaternization, which was dependent on the ACL of the quaternization agent. A two-fold increase in the dry film thickness was found for the polymer brushes quaternized with iodomethane and was attributed to the increase of the molecular weight of the monomer repeat units, as well as to any remaining chemically-bound water molecules within the charged polymer brush. On the other hand, the increase in film thickness was lower as the ACL of the quaternization agent increased, suggesting that the mass balance alone, which increases with the ACL of the alkyl halide, cannot justify the measured film thicknesses for the PQDMAEMA brushes, assuming 100% quaternization of the tertiary amine groups.

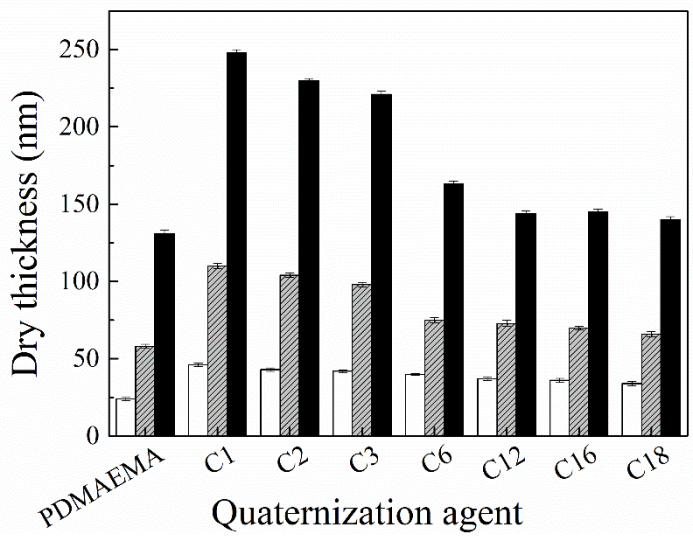


**Figure 3.18.** Dry film thicknesses for the $PQDMAEMA_1$ (white), $PQDMAEMA_2$ (grey) and $PQDMAEMA_3$ (black) brushes quaternized with different alkyl halides.

In order to elucidate further the effect of the ACL of the quaternization agent on the dry polymer film thickness, the chain swelling, defined as the difference of the dry brush thickness after quaternization, to the thickness of the precursor PDMAEMA brush, was calculated. The chain swelling was determined at 40% relative humidity and room temperature, at which conditions the PDMAEMA brush has been shown in the literature to exhibit negligible water uptake.[23] Figure 3.19a depicts the chain swelling values for

the PQDMAEMA$_1$, PQDMAEMA$_2$ and PQDMAEMA$_3$ brushes as a function of the ACL of the quaternization agent. For the PQDMAEMA brushes quaternized with small ACLs (C1-C3) high chain swelling values were obtained, which decreased gradually with the increase of the ACL (C1 to C3) of the quaternization agent, whereas, an abrupt decrease of the chain swelling was observed for longer ACLs (C≥6) and attained an almost constant value of ~13 nm for all PQDMAEMA$_1$, PQDMAEMA$_2$ and PQDMAEMA$_3$ brushes, quaternized with C12, C16 and C18. These results are consistent with the discussion above that the mass balance of the PQDMAEMA brushes cannot justify the increase in the dry polymer film thickness and the chain swelling, assuming a 100% yield of the quaternization reaction.

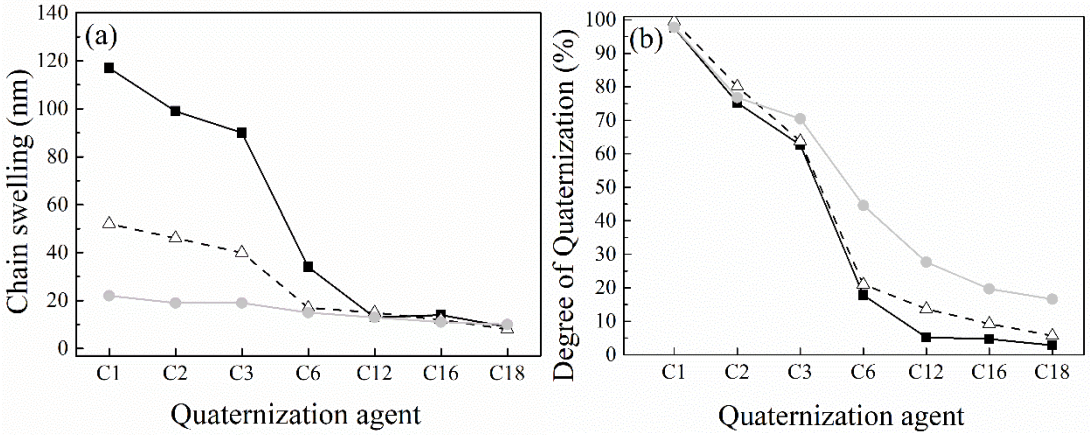


**Figure 3.19.** (a) Chain swelling values and (b) degrees of quaternization for the PQDMAEMA$_1$ (●, grey), PQDMAEMA$_2$ (△, blank) and PQDMAEMA$_3$ (■, black) brushes using different alkyl halides.

Next, the dry thicknesses of the brushes after quaternization were used to calculate the effective degrees of quaternization, by a mass balance using a modified value for the molecular weight of the monomer repeat unit to include the mass of the quaternization agent (equations 2 and 3).[24] The degrees of quaternization, shown in Figure 3.19b, and listed in Table 3.7 for PQDMAEMA$_1$, decreased from ~92% to ~70% for the quaternization agents with short ACLs, C1, C2 and C3, irrespective of the initial brush thickness. Upon further increasing the ACL (C≥6) the degrees of quaternization decreased further, but deviated for the three PDMAEMA brushes of different film thickness, and became very low (<20%) for the thicker brushes and for C≥12.

**Table 3.7.** Characteristics of the $PDMAEMA_1$ and $PQDMAEMA_1$ brushes.

| Brush | Thickness (nm) | DQ (%) (by ellipsometry) | DQ (mol %) (by UV/vis) |
|---|---|---|---|
| **$PDMAEMA_1$** | 24 ± 1 | - | - |
| **$PQDMAEMA_1$-C1** | 46 ± 1 | 92 | 94 |
| **$PQDMAEMA_1$-C2** | 43 ± 1 | 81 | 78 |
| **$PQDMAEMA_1$-C3** | 43 ± 1 | 69 | 65 |
| **$PQDMAEMA_1$-C6** | 40 ± 1 | 50 | 48 |
| **$PQDMAEMA_1$-C12** | 37 ± 1 | 38 | 30 |
| **$PQDMAEMA_1$-C16** | 36 ± 1 | 26 | 29 |
| **$PQDMAEMA_1$-C18** | 34 ± 1 | 18 | 24 |

The degrees of quaternization of the $PQDMAEMA_1$ brushes were also determined by UV/Vis spectroscopy, using a colorimetric method based on fluorescent complexation (Chapter 2). The successful synthesis of the n-butyltrimethylammonium iodide detergent (Scheme 3.8) is confirmed by the peak of the methylene protons at 2.90 ppm, whereas its purity due to the absence of any further peaks in the $^1H$ NMR spectrum (Figure 3.20). Figure 3.21 shows the UV/Vis spectra of the solutions of the adsorbed fluorescent dye for each $PQDMAEMA_1$ brush. The characteristic absorbance peak of AO7 at 483 nm is observed. The peak intensity decreased with the increase of the ACL of the quaternization agent, suggesting a lower concentration of adsorbed dye, and hence, a decrease in the degree of quaternization of the polymer brush. The degrees of quaternization of the $PDMAEMA_1$ brush ranged from 94.4% to 23.9% (Table 3.7), assuming a 1:1 interaction of the dye molecules with the quaternary ammonium groups of the polymer brush, as the ACL of the quaternization agent increased from C1 to C18, in good agreement with the values discussed above for the ellipsometric data, and the FTIR spectra. These results imply that small alkyl halides (C1-C3) can effectively diffuse within the dense hydrophilic polymer brush, and react quantitatively with the tertiary amine groups of DMAEMA, whereas, the diffusion of the alkyl halides with

longer ACLs (C≥6) in the brush is restricted and quaternize only partially the PDMAEMA brush.

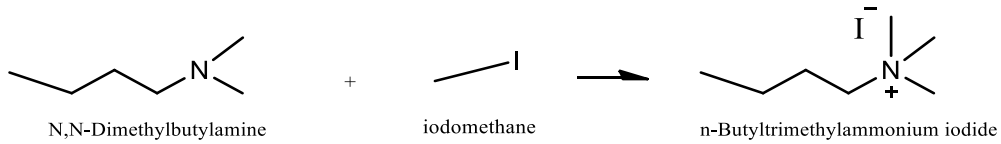


**Scheme 3.8.** Synthesis of the detergent molecule n-butyltrimethylammonium iodide.

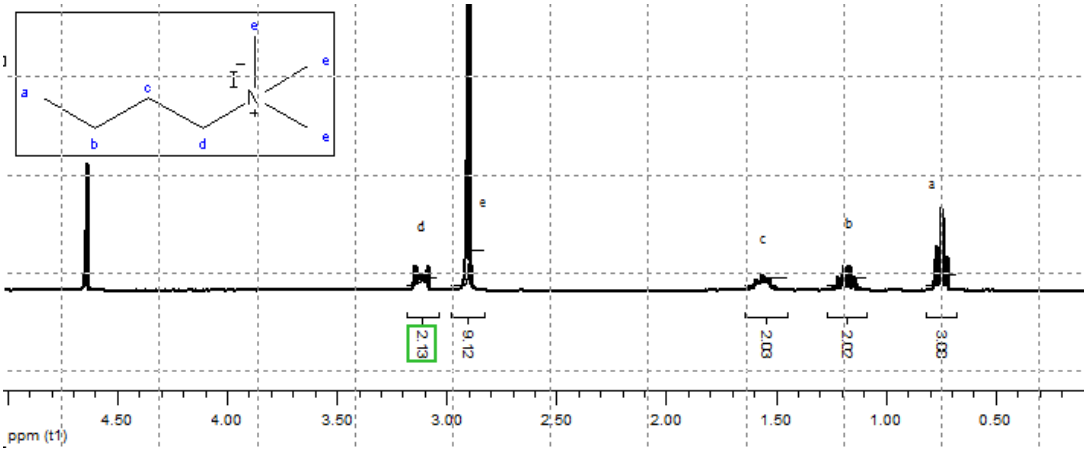


**Figure 3.20.** $^1$H NMR *spectrum* (in $CDCl_3$) of the n-butyltrimethylammonium iodide. $^1$H NMR (300 MHz, $CDCl_3$): δ 3.11 (2H, t), 2.90 (9H, s), 1.56 (2H, m), 1.16 (2H, q), 0.74 (3H, t)

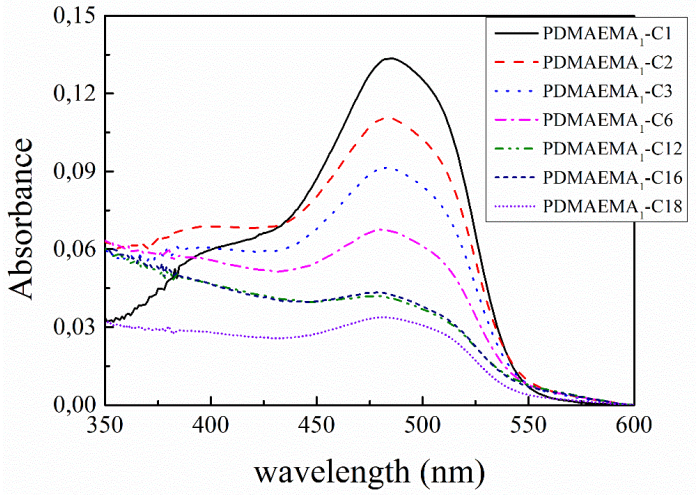


**Figure 3.21.** UV/vis absorption *spectra* of the supernatant solutions following desorption of the adsorbed dye, AO7, from the $PQDMAEMA_1$ brushes.

The thickness of the PDMAEMA films which was effectively quaternized by the alkyl halides was calculated using equation 2.2 (Figure 3.22). The quaternized thickness followed a similar trend to the chain swelling values discussed above, and was found to decrease gradually with the increase of the ACL (C1 to C3) of the quaternization reaction agent attaining a constant value of ~4-6 nm for the $PQDMAEMA_1$, $PQDMAEMA_2$ and $PQDMAEMA_3$ brushes, quaternized with C12, C16 and C18, irrespective of the initial brush thickness. These results suggest that a constant outermost layer of the film becomes quaternized with the long ACLs, which prevents further diffusion of the alkyl halide molecules deeper into the brush (Scheme 3.9a).[13, 25]

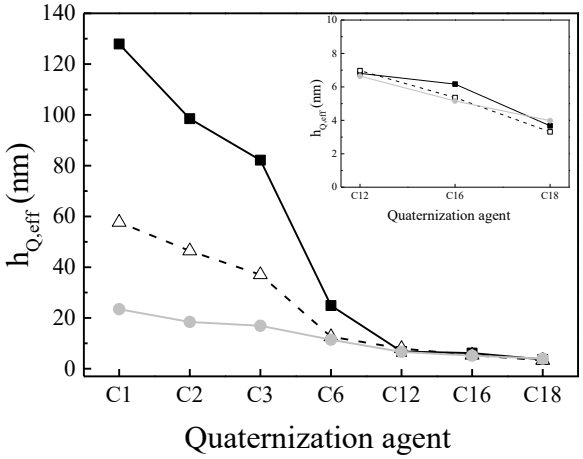


**Figure 3.22.** Effective quaternized thickness of the $PQDMAEMA_1$ (grey circles), $PQDMAEMA_2$ (white squares) and $PQDMAEMA_3$ (black squares) brushes using different alkyl halides. Inset: Magnification of the plot for $PQDMAEMA_1$ (grey circles), $PQDMAEMA_2$ (white squares) and $PQDMAEMA_3$ (black squares) brushes for long ACLs.

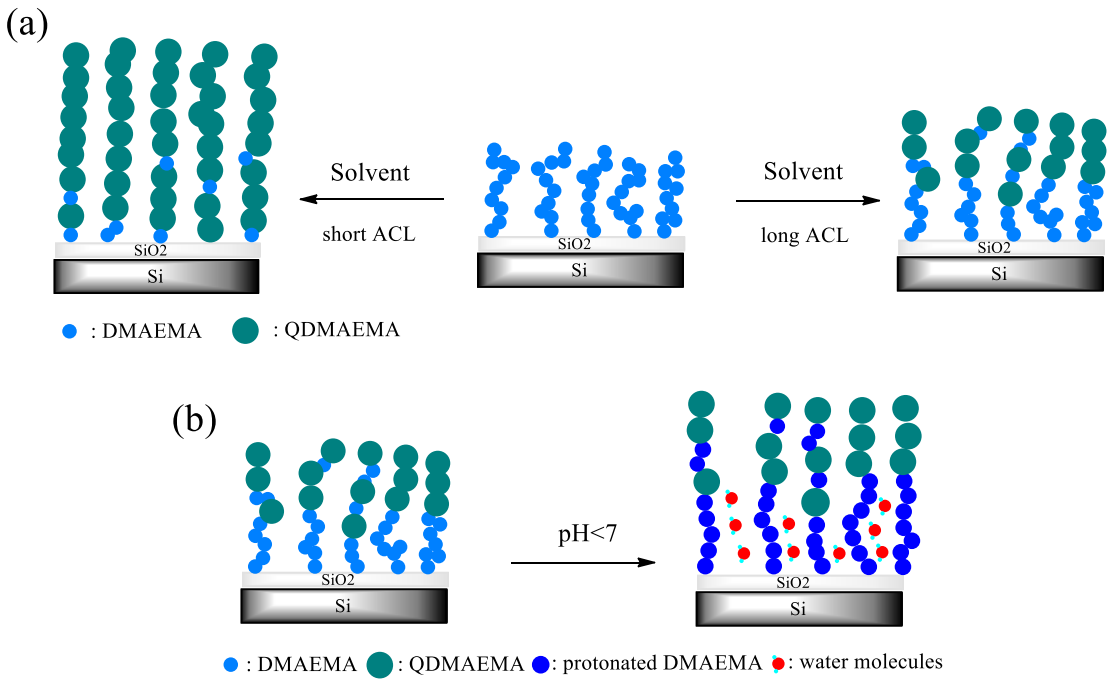


**Scheme 3.9.** Schematic representation of the (a) effective quaternization of the PDMAEMA brushes with alkyl halides of different ACLs and (b) protonation of the PQDMAEMA brushes bearing long ACLs at the quaternary ammonium salt groups.

### 3.2.5.5 pH-responsive behavior of the PQDMAEMA brushes

PDMAEMA brushes have been widely explored for their pH-responsive behavior in aqueous solutions.[9, 13, 26] The effective p$K_\alpha$ of PDMAEMA homopolymer, which is a weak polybase, has been reported around 7-7.5.[27] Therefore, the addition of a strong acid (HCl) in water-immersed PDMAEMA brushes, results in the protonation of the tertiary amine groups, and the polymer chains become stretched away from the surface to minimize the electrostatic interactions. Nevertheless, quaternization of the tertiary amine groups of PDMAEMA leads to the formation of a strong polyelectrolyte and eliminates the pH-responsive character of the polymer brushes. Between these two extreme cases, partially quaternized PDMAEMA brushes are expected to possess accessible tertiary amine groups, which can become protonated by acid, thus retaining the pH-responsive behavior of the brush. The pH-response of the PQDMAEMA brushes prepared in this work was studied by immersing the samples in water at pH values, 3, 7 and 11, under vigorous stirring. The effect of the solution pH was monitored by measuring the variation of the ellipsometric dry film thickness of the samples at the three pH values (Figure 3.23). For short ACL (C1-C3) the brushes presented only a

small decrease in the film thickness upon increasing the solution pH suggesting that only very few accessible amine groups are present in the brush, and verifying the near quantitative quaternization of the polymer. In contrast, the $PQDMAEMA_1$ brushes bearing long ACLs (C≥6) exhibit a maximum in size at acidic conditions, and a significant decrease in thickness at high pH values, indicating the deprotonation of the non-quaternized amine groups of the brush. These results are consistent with the discussion above suggesting the quaternization of an outermost layer of the polymer brush when using alkyl halides with long ACLs and yield pH-responsive PQDMAEMA brushes. It is noted that, small HCl molecules can diffuse effectively through the dense polymer chains and protonate the free tertiary amine at low pH values (Scheme 3.9b).

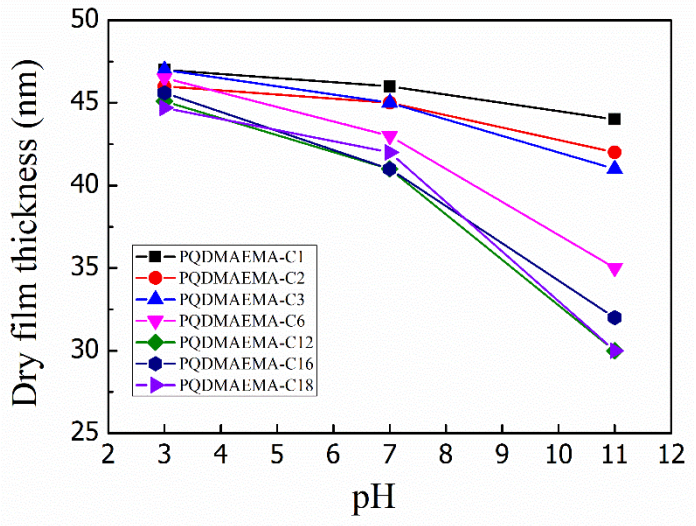


**Figure 3.23.** Dry film thickness vs. the pH, at values of 3, 7 and 11, for the $PQDMAEMA_1$ brushes Surface characteristics of PDMAEMA and PQDMAEMA brushes. The lines are guides to the eye.

### 3.2.6 Tribological behavior of the homopolymer brushes

Surface forces control the adhesion and friction and play a significant role in the assembly, manipulation and operation of nanoscale devices or biological implants. AFM in the LFM mode enables the quantitative probing of the adhesion and friction forces at the nanoscale by measuring force-distance curves or lateral friction forces at given normal applied loads. The measurements were performed after treating the homopolymer brushes with a selective solvent.

### 3.2.6.1 Adhesion

Adhesion measurements were performed under ambient conditions (RH ~50%) to obtain the tribological properties of the homopolymer brushes. Atomic force microscopy was employed for the determination of the adhesion properties under various applied loads using a silicon nitride ($Si_3N_4$) tip. Figure 3.24 shows the characteristic adhesion force *vs* distance curves for (a) a silicon wafer, (b) the PDMAEMA, (c) PTFEMA, (d) POFPMA and PTDFOMA brushes at 20 nN normal applied load. The silicon tip approaches the polymer brush until a maximum normal load of 20 nN is reached with a velocity of 0.25 μm/s and a distance of 2 μm. Upon retraction of the tip, an adhesive interaction is observed for all systems, which decreases as the number of the fluorine atoms in the side-group of the polymer increases. The high adhesion force and the adhesion hysteresis between the $Si_3N_4$ tip and the UVO-cleaned silicon surface is related to the strong capillary forces, due to the adsorption of water molecules on the superhydrophilic surfaces. For the PDMAEMA brushes we also observe an adhesion hysteresis for over 0.5 μm, while for the PTFEMA, POFPMA and PTDFOMA brushes it is kept at ~0.2 μm. This suggests that the collapsed hydrophilic PDMAEMA chains in the dry state interact more strongly with the silicon nitride probe upon retraction compared to the semi-fluorinated films and is ascribed to interactions between the AFM tip and the polymer chains (i.e. hydrogen bonding, meniscus effect, electrostatic interactions).

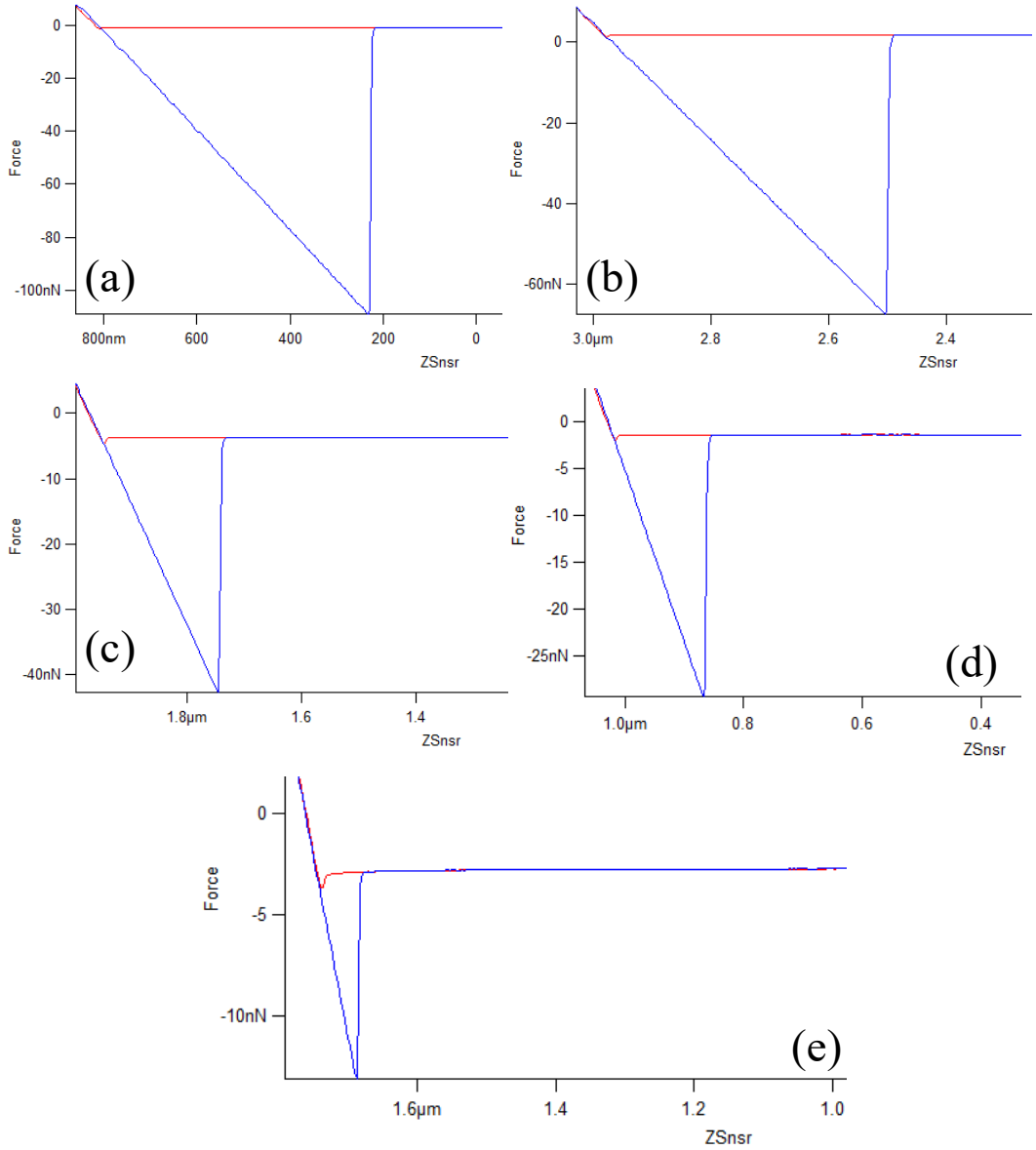


**Figure 3.24.** Typical force *vs* distance curves of the (a) silicon wafer, (b) PDMAEMA, (c) PTFEMA, (d) POFPMA and PTDFOMA brushes at 20 nN normal applied load.

Figure 3.25 shows the adhesion force values on the silicon substrate and the PDMAEMA, PTFEMA, POFPMA and PTDFOMA homopolymer brushes when increasing the normal applied loads from 10 to 100 nN, under ambient conditions. A meniscus effect, formed between the sharp silicon nitride tip and the surface under ambient conditions, is responsible for the relatively high values of adhesion obtained for the freshly cleaned silicon substrates. Lower adhesion force values are obtained for the PDMAEMA brush, which reduce even further for the semi-fluorinated brush. The increase of the FCL results in lower adhesion force values between the polymer films

and the AFM probe attributed to the so-called tribological inertness of the fluorine atoms.[17a] The interfacial adhesion force on the silicon surface was measured at 110 nN, the PDMAEMA brushes at 60 nN and the fluorinated brushes, <30 nN, under a constant normal applied force of 20 nN, implying that the silicon tip is highly attracted by the hydrophilic surfaces and not the hydrophobic. The lowest adhesion force value of 25 nN was measured for the PTDFOMA brushes. This behavior is in agreement with the experimental work by Bhairamadgi et al., using colloidal probe microscopy on semi-fluorinated homopolymer brushes, bearing 0, 3, 7 and 17 fluorine atoms.[17a] The higher values of adhesion force measured in our study are related to the difference in the radius curvature of the silicon nitride tip (20 nm) compared to the silica sphere colloidal probe (2 μm) used by others, and reflects to a possible deeper penetration of the silicon nitride sharp tip upon contact with the polymer brush surface. The differences between the AFM tips on the adhesion force measurements have been also explained in the study of Stamm et. al on the dry lubrication properties of polymer brushes.[28] The low adhesion forces and the low surface energy values measured for these systems, confirm the low polarizability of the terminal $CF_2$ and $CF_3$ groups.

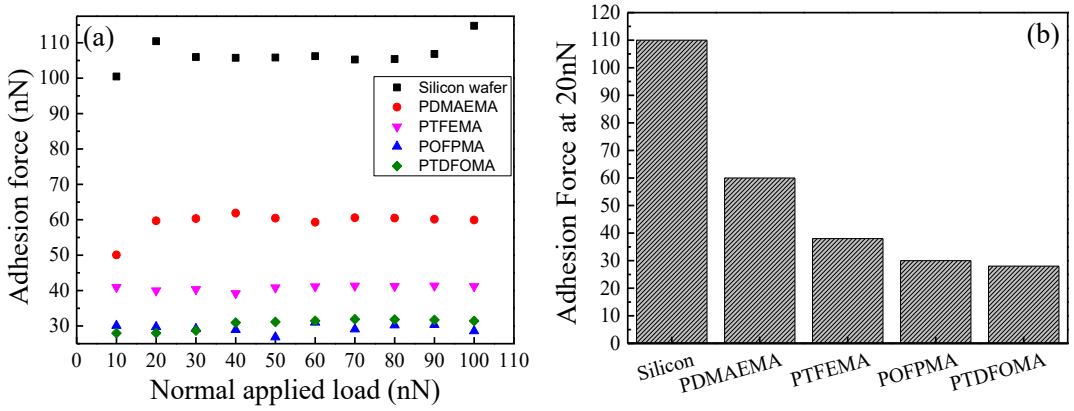


**Figure 3.25.** (a) Adhesion forces at various normal applied loads (from 10 to 100 nN) for the homopolymer brushes and (b) the adhesion forces measured at 20 nN normal applied load.

### 3.2.6.2 Friction

To estimate the friction between the silicon wafers modified with the homopolymer brushes and an inorganic surface (silicon nitride tip), LFM measurements using an MFP-3D atomic force microscope (Asylum) were performed for all homopolymer brushes, under ambient conditions at RT. Figure 3.26a shows the friction forces on the

PDMAEMA, PTFEMA, POFPMA and PTDFOMA homopolymer brushes when increasing the applied load from 10 to 100 nN, under ambient conditions. The recorded friction force increases linearly with the normal applied load for all systems. Friction measurements with sharp tips have shown that the friction response depends on the extension and rigidity of the brush layer. Linear friction and low friction coefficients (COF's) are observed in non-adhesive systems, while non-linear friction is observed for collapsed brushes, when the probe adheres to the surface.[29]

The friction coefficient values were extracted from the slopes of the friction force curves under different normal applied loads (Figure 3.26b). A relatively high COF value of 0.57 and 0.27 was found for the silicon surface and the PDMAEMA brush at pH 4, respectively, due to strong adhesive interactions between the silicon or PEL brush and the surface of the tip. Without suitable surface modification, silicon surfaces show high friction and adhesion.[30] As explained above, the silicon surfaces showed an extensive adhesion due to the meniscus effect associated with the humidity (60%) and the formation of stable capillary bridges. In addition, an oxygen plasma treated tip was utilized, which has a negative charge due to the silanol groups at the outer surface, and thus interfacial interactions can occur with the positively charged PDMAEMA at pH 4. The $pK_a$ of PDMAEMA is around 7, which means that at this pH value the PDMAEMA brushes are typically carrying a positive charge. This is also consistent with the lower COF value of 0.20 measured for PDMAEMA at pH 9, when the polymer is uncharged, and thus electrostatic interactions are eliminated. In contrast, the PTFEMA brush showed a much lower COF value, under humid air (60%), of 0.074, which is one order of magnitude lower than that found for the silicon surface. Meanwhile, the increase of the FCL from $C_F1$ to $C_F4$ and $C_F6$, results in a further decrease the COF values for these brushes. Low-surface energy coatings based on fluorocarbons (i.e. PTFE) are generally used in micro/nano-electromechanical systems (MEMS/NEMS) to prevent unwanted stiction associated with high adhesion and friction forces in the solid state. It has been shown, that the factors that influence friction in organic coatings are: (a) the chemical structure, (b) the surface coverage, (c) mechanical properties, such as the elastic constant and rigidity, (d) terminal polar or non-polar groups and (e) surface dipole orientations.[31] In our case, the unique properties of the apolar C-F bonds compared to C-H bonds provide high hydrophobicity and low polarizability to the outer surface of the fluorinated polymer brushes, which are crucial to obtain low-friction coatings. The

lower polarizability of fluorine compared to that of hydrogen leads to very weak van der Waals interactions among the $CF_3$ groups and polar water molecules, thus limiting the increase of adhesion and friction forces, due to capillary condensation. In addition, the high grafting density of the semi-fluorinated polymer chains results in a more stretched conformation of the polymer chains, that leads to a reduced compressibility and interactions with the opposing surface, and thus lower adhesion and friction.[17b]

The COF values obtained in this study are typically not as low as those measured for fluorinated homopolymer brushes in the dry state, in the literature. This is attributed to the effective penetration of the sharp tip within the polymer layers, compared to the largest silica colloidal probes used in other studies.[17a] Nevertheless, it is sparkly clear, that the fluorinated brush layers can serve as dry lubricants, thereby reducing the interactions between the surface and the tip.

The low adhesion and friction properties of the semi-fluorinated PTFEMA, POFPMA and PTDFOMA brushes prepared herein renders them effective solid lubricating polymeric films under dry conditions, which can be significant for applications in microfluidics and MEMS/NEMS.[17b]

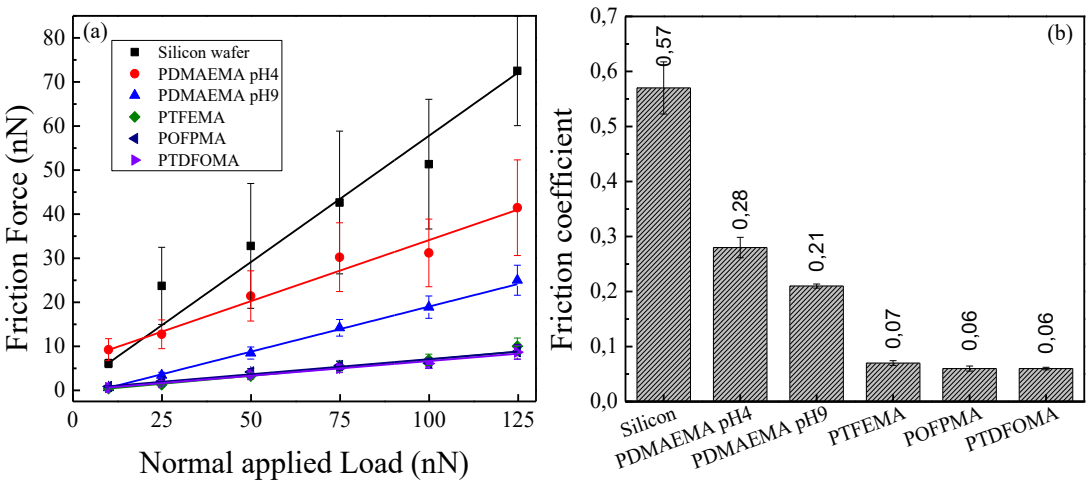


**Figure 3.26.** (a) Friction forces at various normal applied loads (10 to 125 nN) under ambient conditions and (b) COF values for the homopolymer brushes obtained from the slopes of the friction force *vs* applied load curves.

### 3.2.7 Stability of the homopolymer brushes

The stability of the homopolymer brushes in good solvents for the polymer in which the brush will undergo strong swelling, was studied. Ellipsometry was employed to characterize the degrafting process by determining the dry film thickness of the homopolymer brushes at regular time intervals, following their immersion in the solvent medium.

First, the $PDMAEMA_1$ brush, with initial dry brush thickness of 24 nm, and their hydrophilic quaternized analogues, $PQDMAEMA_1$-C1 and $PQDMAEMA_1$-C3, with initial dry brush thicknesses of 46 and 43 nm, respectively, were incubated in two solvents, dry methanol and water and the dry film thicknesses of the brushes were monitored for prolonged time periods, of up to 3 months. As illustrated in Figure 3.27a, prolonged exposure of the $PDMAEMA_1$, $PQDMAEMA_1$-C1 and $PQDMAEMA_1$-C3 brushes to dry methanol did not reveal any alterations of their dry film thickness, suggesting that the brushes are stable. Nevertheless, incubation in water resulted in quite fast degrafting of the hydrophilic polymer chains. As shown in Figure 3.27b, degrafting occurs for the weak $PDMAEMA_1$ brush in water after 30 days, whereas the degrafting is faster for the PQDMAEMA brushes at 7 and 14 days for the PQDMAEMA-C1 and PQDMAEMA-C3 brush, respectively. It is also noted that a minimum film thickness is obtained in each case, below which degrafting of the polymer layer does not occur further. The above results suggest that the degrafting of the polymer brushes in water is due to the tension applied as a result of the swelling of the dense end-grafted polymer chains, which may facilitated the hydrolytic cleavage of the siloxane or ester bonds at the polymer brush-substrate interface. As the incubation time progresses, the degrafting is slowed down and reaches a minimum value below which it does not occur anymore since the polymer grafting density and thus the tension at the polymer-substrate interface has decreased. At this point, further hydrolytic cleavage of the bonds does not take place and the dry polymer film thickness remains constant. The fact that, the degrafting process does not take place in methanol, which is a good solvent for the PDMAEMA and PQDMAEMA chains, suggests that the presence of water is necessary for the cleavage of the bonds at the brush-substrate interface.

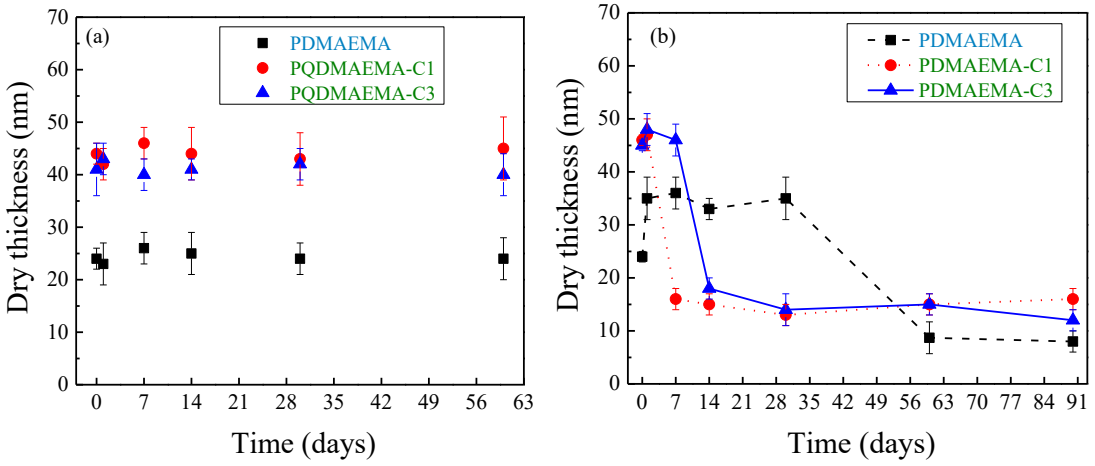


**Figure 3.27.** Ellipsometric dry film thickness for the $PDMAEMA_1$ (■, black), $PQDMAEMA_1$-C1 (●, red) and $PQDMAEMA_1$-C3 (▲, blue) brushes as a function of incubation time in (a) methanol and (b) water. The lines are guides to the eye.

Next the PTFEMA, POFPMA and PTDFOMA brushes were incubated in HFiP (good solvent) and water (non-solvent), respectively followed by the monitoring of the dry film thickness for prolonged time periods of up to 3 months. As illustrated in Figure 3.28a, long time exposure of the PTFEMA, POFPMA and PTDFOMA brushes to HFiP did not reveal any changes in the dry film thickness attributed to the lack of water, which induces the hydrolysis process. Similarly, no changes were observed in the dry film thickness of the fluorinated brushes after incubation in water (Figure 3.28b). This is explained because water is a bad solvent for the fluorinated polymer chains, which limit the access of the solvent to the polymer brush-silicon interface, thus increasing the stability of the polymer layer.

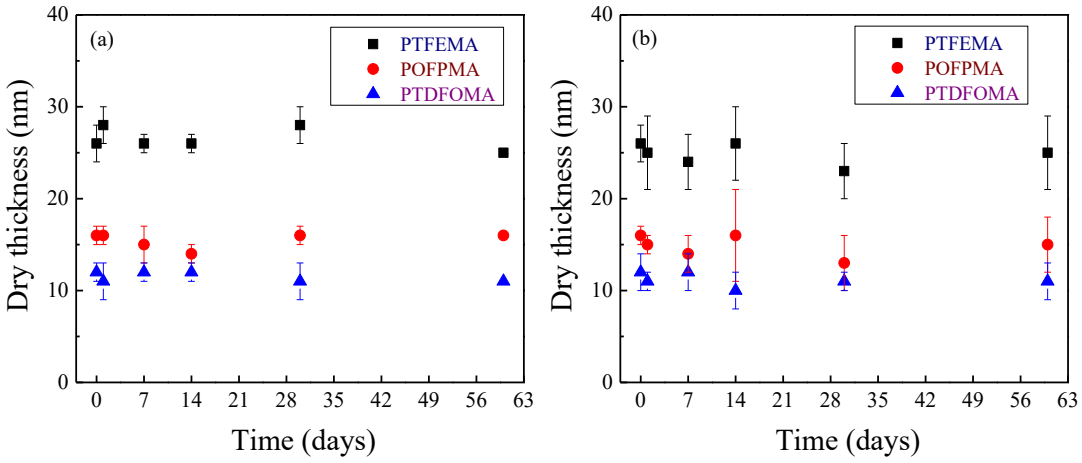

**Figure 3.28.** Ellipsometric dry film thickness of the PTFEMA (■, black), POFPMA (●, red) and PTDFOMA (▲, blue) brushes as a function of incubation time in (a) hexafluoroisopropanol and (b) water.

Chain stretching in densely grafted polymer brushes can result in a tension that reflects on the bonds that are present in the vicinity of the polymer-substrate interface. The presence of a good solvent, which induces the swelling of the polymer brushes enhances this tension, nevertheless this is not sufficient for the degrafting of the swollen polymer chains. Degrafting can only occur when water is present, which induces the hydrolysis of the bonds in good agreement with reports in the literature.[32] Moreover the introduction of permanent charges in strong PEL brushes, also promotes the tension on the anchoring points leading to faster cleavage of the brushes.[33] Fluoropolymer chains can act as barriers for the water molecules to access the brush-substrate interface and therefore, prevent the hydrolytic cleavage of the labile ester or siloxane bonds of the ATRP initiator, leading to the stabilization of the polymer-brush layer. Finally, degrafting occurs until a limited threshold value, below which the tension is decreased by the lower grafting density, and the degrafting process ceases.

## 3.3 Conclusions

Non-fluorinated and semi-fluorinated polymer brushes bearing different fluorinated side chain groups were successfully synthesized by SI-ATRP from silicon surfaces. The effect of the FCL on the surface properties was examined for end-grafted semi-fluorinated methacrylate chains bearing 3, 8 and 13 fluorine atoms. The fluorinated polymers resulted in moderate hydrophobic surfaces, with the hydrophobicity increasing with the FCL. In addition, the surface free energies of the polymer brushes decreased significantly with the increase of the FCL. Adhesion and friction studies between the semi-fluorinated brushes and inorganic silicon nitride surfaces (AFM tip) revealed that the introduction of the fluorinated moieties results in dry lubricant polymer layers that reduce their interaction with the tip.

Moreover, PQDMAEMA brushes bearing different ACLs were prepared, by a facile post polymerization quaternization reaction of the tertiary amine groups of PDMAEMA using suitable alkyl halides. The effect of the ACL of the quaternary ammonium salt groups of the polymer on the surface properties of the quaternized PDMAEMA brushes was investigated. PQDMAEMA brushes were hydrophilic upon quaternization with

short ACLs (C1-C3), due to the permanent positive charges on the polymer side groups, whereas long ACLs (C≥6) yielded hydrophobic surfaces verifying that the alkyl chains dominate the surface wettability of the films. The degrees of quaternization and the chain swelling of the polymer films suggested that small alkyl halides (C1-C3) can diffuse more effectively within the dense polymer brush and react quantitatively with the tertiary amine groups of PDMAEMA, whereas the diffusion of alkyl halides with long ACLs (C ≥ 6) in the brush is hindered and thus only a top layer of the polymer film becomes quaternized. As a result, PDMAEMA brushes quaternized with short ACLs lose their pH-responsive behavior, whereas, partially quaternized brushes with long ACLs retain their pH-responsive character, after quaternization.

Finally, it was found that upon immersion of the PQDMAEMA brushes in water, a significant amount of the chains is degrafted after only a few weeks. This process is attributed to the hydrolysis of either the silane or the ester bonds of the initiator at the brush-substrate interface, and is enhanced by the tension of the chains after immersion in a good solvent. The presence of charges on the polymer leads to stretching of the chains and therefore produces extensive tension at the interface. In the present study, the PDMAEMA brushes have both a high grafting density and are charged at pH below 7 which favor the hydrolysis process in water. The PQDMAEMA brushes promote even higher tension to the anchoring points leading to faster cleavage upon incubation of the brushes in water, in the timeframe of a few days. This process is detrimental, because the morphology and the composition of the polymer films change and therefore their application underwater for prolonged periods of time is impossible. To address this problem, the grafting of fluorinated polymer brushes on the substrate which act as a "polymer carpet" underwater to repel the water molecules from the polymer-substrate interface prevents the hydrolysis process and stabilizes the grafted polymer layer.

## 3.4 References

1. (a) Alonzi, M.; Lanari, D.; Marrocchi, A.; Petrucci, C.; Vaccaro, L., Synthesis of polymeric semiconductors by a surface-initiated approach. *RSC Advances* **2013,** *3* (46), 23909-23923; (b) Mendes, P. M., Stimuli-responsive surfaces for bio-applications. *Chemical Society Reviews* **2008,** *37* (11), 2512-2529; (c) Stuart, M. A. C.; Huck, W. T. S.; Genzer, J.; Muller, M.; Ober, C.; Stamm, M.; Sukhorukov, G. B.; Szleifer, I.; Tsukruk, V. V.; Urban, M.; Winnik, F.; Zauscher, S.; Luzinov, I.; Minko, S., Emerging applications of stimuli-responsive polymer materials. *Nat Mater* **2010,** *9* (2), 101-113.

2. (a) Stratakis, E.; Mateescu, A.; Barberoglou, M.; Vamvakaki, M.; Fotakis, C.; Anastasiadis, S. H., From superhydrophobicity and water repellency to superhydrophilicity: smart polymer-functionalized surfaces. *Chem Commun* **2010,** *46* (23), 4136-4138; (b) Rana, D.; Matsuura, T., Surface Modifications for Antifouling Membranes. *Chemical Reviews* **2010,** *110* (4), 2448-2471; (c) Wei, Q.; Becherer, T.; Angioletti-Uberti, S.; Dzubiella, J.; Wischke, C.; Neffe, A. T.; Lendlein, A.; Ballauff, M.; Haag, R., Protein Interactions with Polymer Coatings and Biomaterials. *Angewandte Chemie International Edition* **2014,** *53* (31), 8004-8031.
3. Aswal, D. K.; Lenfant, S.; Guerin, D.; Yakhmi, J. V.; Vuillaume, D., Self assembled monolayers on silicon for molecular electronics. *Analytica chimica acta* **2006,** *568* (1–2), 84-108.
4. Milner, S., Polymer brushes. *Science* **1991,** *251* (4996), 905-914.
5. Galvin, C. J.; Genzer, J., Applications of surface-grafted macromolecules derived from post-polymerization modification reactions. *Prog Polym Sci* **2012,** *37* (7), 871-906.
6. (a) Barbey, R.; Lavanant, L.; Paripovic, D.; Schüwer, N.; Sugnaux, C.; Tugulu, S.; Klok, H.-A., Polymer Brushes via Surface-Initiated Controlled Radical Polymerization: Synthesis, Characterization, Properties, and Applications. *Chemical Reviews* **2009,** *109* (11), 5437-5527; (b) Zhao, B.; Brittain, W. J., Polymer brushes: surface-immobilized macromolecules. *Prog Polym Sci* **2000,** *25* (5), 677-710.
7. (a) Khabibullin, A.; Mastan, E.; Matyjaszewski, K.; Zhu, S., Surface-Initiated Atom Transfer Radical Polymerization. In *Adv Polym Sci*, Vana, P., Ed. Springer International Publishing: 2016; Vol. 270, pp 29-76; (b) Joanna, P.; Lindsay, B.; Brian, C.; Jinyu, H.; Jeffrey, P.; Tomasz, K.; Krzysztof, M., Controlling Polymer Chain Topology and Architecture by ATRP from Flat Surfaces. In *Stimuli-Responsive Polymeric Films and Coatings*, American Chemical Society: 2005; Vol. 912, pp 28-42; (c) Edmondson, S.; Osborne, V. L.; Huck, W. T. S., Polymer brushes via surface-initiated polymerizations. *Chemical Society Reviews* **2004,** *33* (1), 14-22.
8. Rühe, J.; Ballauff, M.; Biesalski, M.; Dziezok, P.; Gröhn, F.; Johannsmann, D.; Houbenov, N.; Hugenberg, N.; Konradi, R.; Minko, S.; Motornov, M.; Netz, R. R.; Schmidt, M.; Seidel, C.; Stamm, M.; Stephan, T.; Usov, D.; Zhang, H., Polyelectrolyte Brushes. In *Polyelectrolytes with Defined Molecular Architecture I*, Schmidt, M., Ed. Springer Berlin Heidelberg: Berlin, Heidelberg, 2004; pp 79-150.
9. Sanjuan, S.; Perrin, P.; Pantoustier, N.; Tran, Y., Synthesis and Swelling Behavior of pH-Responsive Polybase Brushes. *Langmuir* **2007,** *23* (10), 5769-5778.
10. Azzaroni, O.; Brown, A. A.; Huck, W. T., Tunable wettability by clicking counterions into polyelectrolyte brushes. *Adv Mater* **2007,** *19* (1), 151-154.
11. Spruijt, E.; Choi, E.-Y.; Huck, W. T. S., Reversible Electrochemical Switching of Polyelectrolyte Brush Surface Energy Using Electroactive Counterions. *Langmuir* **2008,** *24* (19), 11253-11260.
12. Murata, H.; Koepsel, R. R.; Matyjaszewski, K.; Russell, A. J., Permanent, non-leaching antibacterial surfaces—2: How high density cationic surfaces kill bacterial cells. *Biomaterials* **2007,** *28* (32), 4870-4879.
13. Cheng, N.; Bao, P.; Evans, S. D.; Leggett, G. J.; Armes, S. P., Facile Formation of Highly Mobile Supported Lipid Bilayers on Surface-Quaternized pH-Responsive Polymer Brushes. *Macromolecules* **2015,** *48* (9), 3095-3103.
14. Rastogi, A.; Paik, M. Y.; Ober, C. K., Development of a Directly Patterned Low-Surface-Energy Polymer Brush in Supercritical Carbon Dioxide. *Acs Appl Mater Inter* **2009,** *1* (9), 2013-2020.

15. Yamaguchi, H.; Kikuchi, M.; Kobayashi, M.; Ogawa, H.; Masunaga, H.; Sakata, O.; Takahara, A., Influence of Molecular Weight Dispersity of Poly{2-(perfluorooctyl)ethyl acrylate} Brushes on Their Molecular Aggregation States and Wetting Behavior. *Macromolecules* **2012,** *45* (3), 1509-1516.
16. Nurmi, L.; Peng, H.; Seppala, J.; Haddleton, D. M.; Blakey, I.; Whittaker, A. K., Synthesis and evaluation of partly fluorinated polyelectrolytes as components in 19F MRI-detectable nanoparticles. *Polymer Chemistry* **2010,** *1* (7), 1039-1047.
17. (a) Bhairamadgi, N. S.; Pujari, S. P.; van Rijn, C. J. M.; Zuilhof, H., Adhesion and Friction Properties of Fluoropolymer Brushes: On the Tribological Inertness of Fluorine. *Langmuir* **2014,** *30* (42), 12532-12540; (b) Bhairamadgi, N. S.; Pujari, S. P.; Leermakers, F. A. M.; van Rijn, C. J. M.; Zuilhof, H., Adhesion and Friction Properties of Polymer Brushes: Fluoro versus Nonfluoro Polymer Brushes at Varying Thickness. *Langmuir* **2014,** *30* (8), 2068-2076.
18. Yang, Y. A.; Bittner, A. M.; Baldelli, S.; Kern, K., Study of self-assembled triethoxysilane thin films made by casting neat reagents in ambient atmosphere. *Thin Solid Films* **2008,** *516* (12), 3948-3956.
19. Hadjicharalambous, C.; Flouraki, C.; Narain, R.; Chatzinikolaidou, M.; Vamvakaki, M., *Controlling pre-osteoblastic cell adhesion and spreading on glycopolymer brushes of variable film thickness*. 2018; Vol. 29.
20. (a) Ejaz, M.; Yamamoto, S.; Ohno, K.; Tsujii, Y.; Fukuda, T., Controlled graft polymerization of methyl methacrylate on silicon substrate by the combined use of the Langmuir-Blodgett and atom transfer radical polymerization techniques. *Macromolecules* **1998,** *31* (17), 5934-5936; (b) Husseman, M.; Malmström, E. E.; McNamara, M.; Mate, M.; Mecerreyes, D.; Benoit, D. G.; Hedrick, J. L.; Mansky, P.; Huang, E.; Russell, T. P.; Hawker, C. J., Controlled Synthesis of Polymer Brushes by "Living" Free Radical Polymerization Techniques. *Macromolecules* **1999,** *32* (5), 1424-1431.
21. Kim, J.; Efimenko, K.; Genzer, J.; Carbonell, R. G., Surface properties of poly[2-(perfluorooctyl)ethyl acrylate] deposited from liquid CO2 high-pressure free meniscus coating. *Macromolecules* **2007,** *40* (3), 588-597.
22. K. J. Owens, D.; Wendt, R. C. J., *Owens, D. K. & Wendt, R. C. Estimation of the surface free energy of polymers. J. Appl. Polym. Sci. 13, 1741-1747*. 1969; Vol. 13, p 1741-1747.
23. Galvin, C. J.; Genzer, J., Swelling of Hydrophilic Polymer Brushes by Water and Alcohol Vapors. *Macromolecules* **2016,** *49* (11), 4316-4329.
24. (a) Galvin, C. J.; Dimitriou, M. D.; Satija, S. K.; Genzer, J., Swelling of Polyelectrolyte and Polyzwitterion Brushes by Humid Vapors. *J Am Chem Soc* **2014,** *136* (36), 12737-12745; (b) Santos, D. E. S.; Li, D.; Ramstedt, M.; Gautrot, J. E.; Soares, T. A., Conformational Dynamics and Responsiveness of Weak and Strong Polyelectrolyte Brushes: Atomistic Simulations of Poly(dimethyl aminoethyl methacrylate) and Poly(2-(methacryloyloxy)ethyl trimethylammonium chloride). *Langmuir* **2019,** *35* (14), 5037-5049.
25. (a) Schüwer, N.; Geue, T.; Hinestrosa, J. P.; Klok, H.-A., Neutron Reflectivity Study on the Postpolymerization Modification of Poly(2-hydroxyethyl methacrylate) Brushes. *Macromolecules* **2011,** *44* (17), 6868-6874; (b) Tan, K. Y.; Ramstedt, M.; Colak, B.; Huck, W. T. S.; Gautrot, J. E., Study of thiol–ene chemistry on polymer brushes and application to surface patterning and protein adsorption. *Polym Chem-Uk* **2016,** *7* (4), 979-990.
26. Moglianetti, M.; Webster, J. R. P.; Edmondson, S.; Armes, S. P.; Titmuss, S., Neutron Reflectivity Study of the Structure of pH-Responsive Polymer Brushes Grown

from a Macroinitiator at the Sapphire−Water Interface. *Langmuir* **2010,** *26* (15), 12684-12689.
27. Manouras, T.; Koufakis, E.; Anastasiadis, S. H.; Vamvakaki, M., A facile route towards PDMAEMA homopolymer amphiphiles. *Soft Matter* **2017**.
28. Vyas, M. K.; Schneider, K.; Nandan, B.; Stamm, M., Switching of friction by binary polymer brushes. *Soft Matter* **2008,** *4* (5), 1024-1032.
29. Yu, Y.; Cirelli, M.; Kieviet, B. D.; Kooij, E. S.; Vancso, G. J.; de Beer, S., Tunable friction by employment of co-non-solvency of PNIPAM brushes. *Polymer* **2016,** *102*, 372-378.
30. Pujari, S.; Spruijt, E.; Stuart, M.; Rijn, C. J. M.; Paulusse, J.; Zuilhof, H., Ultralow Adhesion and Friction of Fluoro-Hydro Alkyne-Derived Self-Assembled Monolayers on H-Terminated Si(111). *Langmuir : the ACS journal of surfaces and colloids* **2012,** *28*.
31. Kim, H. I.; Koini, T.; Lee, T. R.; Perry, S. S., Systematic Studies of the Frictional Properties of Fluorinated Monolayers with Atomic Force Microscopy: Comparison of CF3- and CH3-Terminated Films. *Langmuir* **1997,** *13* (26), 7192-7196.
32. (a) Tugulu, S.; Klok, H.-A., Stability and Nonfouling Properties of Poly(poly(ethylene glycol) methacrylate) Brushes under Cell Culture Conditions. *Biomacromolecules* **2008,** *9* (3), 906-912; (b) Bain, E. D.; Dawes, K.; Özçam, A. E.; Hu, X.; Gorman, C. B.; Šrogl, J.; Genzer, J., Surface-Initiated Polymerization by Means of Novel, Stable, Non-Ester-Based Radical Initiator. *Macromolecules* **2012,** *45* (9), 3802-3815; (c) Galvin, C. J.; Bain, E. D.; Henke, A.; Genzer, J., Instability of Surface-Grafted Weak Polyacid Brushes on Flat Substrates. *Macromolecules* **2015,** *48* (16), 5677-5687.
33. Wang, J.; Klok, H.-A., Swelling-Induced Chain Stretching Enhances Hydrolytic Degrafting of Hydrophobic Polymer Brushes in Organic Media. *Angewandte Chemie International Edition* **2019,** *0* (0).

# Chapter 4

Responsive amphiphilic diblock copolymer brushes

## 4.1 Introduction

The development of functional surfaces is challenging and important for a plethora of fundamental and industrial applications. Polymer surfaces have received great interest in the past decades, due to their ability to control the surface properties such as wettability, adhesion, friction and others, in many applications.[1] A versatile method to control the surface properties of a polymer layer is by the utilization of covalently grafted polymer chains with high grafting densities on the surface which force the chains to stretch away from the surface forming the so called polymer brush.[2] Polymer brushes of different chemistries have been attained to produce surfaces with tunable properties.[3] Responsive polymer brushes are particularly attractive because they can switch their surface properties under the influence of external chemical or physical stimuli. Such "smart" surfaces, which can reversibly switch their properties as a function of the solvent type, pH, temperature, biochemical triggers or light irradiation have been proposed for use in different applications.[4]

Atom transfer radical polymerization (ATRP) is the most widely used technique to synthesize polymer brushes from flat and curved surfaces because, of the wide range of monomers that can be polymerized and its operation under mild conditions and temperatures. "Grafting-from" or surface-initiated ATRP (SI-ATRP) can provide polymer films with high grafting densities of the anchored chains and good control over the film characteristics such as the brush height and the smoothness of the surface.[5] Due to the "living" character of ATRP, interesting architectures, such as block copolymer brushes comprising two or more different homopolymer segments connected via a chemical bond, have been prepared.[6] The advantage of these systems is the ability to control their surface properties via the rearrangement of the blocks of the tethered polymer chains.

Responsive diblock copolymer brushes have been employed to switch the surface properties, such as the wettability of the surface, by exposing the films to different solvents. In an interesting work, Zhao and coworkers, have demonstrated the rearrangement of PS-*b*-PMMA block copolymer brushes upon treatment with selective solvents.[7] Husseman et al. employed NMP polymerization to prepare diblock copolymer brushes on silicon substrates comprising a PS inner block and a random copolymer PS-*co*-PMMA outer block. SI-ATRP was utilized by Matyjaszewski's

group to synthesize amphiphilic PS-*b*-PAA brushes, after hydrolysis of the precursor PS-*b*-PtBA diblock copolymers.[8]

Fluoropolymers are materials exhibiting excellent water repellent properties and low surface energies.[9] However, reports on the synthesis of diblock copolymer brushes consisting of fluorinated methacrylates grafted from solid surfaces are limited due to the difficulty to control the polymerization of the fluorinated monomers. Granville et al. studied the behavior of semi-fluorinated diblock copolymer brushes comprising poly(methyl acrylate) and poly(n-fluoro acrylate) blocks (n = 3, 5, 17), in a good and a poor solvent for the fluorinated segments.[10] It was found that solvent-responsive rearrangements of the two blocks resulted the tunability of the wetting properties of the diblock copolymer brushes, with the fluorine atoms playing a distinct role in the nearly full rearrangement of the polymer chains. AFM images of the diblock copolymer brushes upon selective solvent treatment suggested that the chains did not undergo the traditional phase separation reported for PS-*b*-PMMA brushes to form a regular nanopattern of pinned micelles, on the surface. An increase in the surface roughness, combined with the alteration in contact angle measurements upon treatment with selective solvents, and the natural affinity of the fluorinated segments to migrate to the air-polymer interface, led to the indication of some type of rearrangement being localized on the outermost surface, with no discernible regular nanomorphology.

In this chapter, we present the synthesis, characterization and responsive behavior of amphiphilic diblock copolymer brushes, comprising a hydrophilic PDMAEMA block and a hydrophobic low-surface energy fluorocarbon block, grafted from silicon substrates via SI-ATRP. Semi-fluorinated methacrylates with 3, 8 and 13 fluorine atoms namely TFEMA, OFPMA and PTDFOMA were used as the monomers to prepare PDMAEMA-*b*-PTFEMA, PDMAEMA-*b*-POFPMA and PDMAEMA-*b*-PTDFOMA diblock copolymer brushes. Two families of brushes were prepared, the first comprising a lower content of the fluorocarbon block compared to the hydrophilic segment ($PDMAEMA_{267}$-*b*-$PTFEMA_{220}$, $PDMAEMA_{267}$-*b*-$POFPMA_{103}$ and $PDMAEMA_{267}$-*b*-$PTDFOMA_{34}$ brushes) and the second comprising a symmetric amphiphilic diblock copolymer ($PDMAEMA_{100}$-*b*-$PTFEMA_{108}$ and $PDMAEMA_{100}$-*b*-$POFPMA_{72}$ brushes). The switching of the wettability of the amphiphilic semi-fluorinated diblock copolymer brushes, upon immersion in different selective solvents for the two blocks, was investigated exhibiting large changes from 60° to 110° for water droplets. Nevertheless,

evidence of unwanted degrafting was found, attributed to the hydrolysis of the ester or siloxane bonds of the surface-bound initiator, after exposure in aqueous media for prolonged time periods.

## 4.2 Results and Discussion

### 4.2.1 Synthesis and self-assembly of the ATRP initiator

In the first step a mono-functional ATRP initiator, namely BIDS, was synthesized and used to form the initiator self-assembled monolayers as described in Chapter 3. The deposition of BIDS on silicon and glass substrates was carried out in anhydrous toluene and the successful grafting of the initiator monolayer was verified by ellipsometry, ATR-FTIR and water contact angle measurements (see section 3.2.2).

### 4.2.2 SI-ATRP for the synthesis of the diblock copolymer brushes

As described in the experimental section (Chapter 2), the synthesis of a series of amphiphilic diblock copolymer brushes was carried out via sequential SI-ATRP from the initiator functionalized silicon substrates. The synthetic procedure followed for the synthesis of the diblock copolymer brushes is shown in Scheme 4.1.

First, well-defined PDMAEMA homopolymer macroinitiator brushes, were successfully prepared from the BIDS-modified silicon substrates, with $M_n$'s 16,200 gr mol$^{-1}$ and 41,900 gr mol$^{-1}$ and corresponding dry thicknesses of 12 nm (9 h) and 32 nm (18 h), respectively. Figure 4.1a and b show the SEC traces of the free polymers obtained in solution during the SI-ATRP. The molecular weight distributions ($M_w/M_n$) remained low (below 1.3), which is typical for a control/living polymerization process. The grafting density σ (chains nm$^{-2}$) of the PDMAEMA chains on the surface was calculated at 0.49 for film thickness of 12 nm and 0.51 chains nm$^{-2}$ for film thickness of 32 nm (denoted as PDMAEMA$_x$-Br, where x = 103 or 267, is the degree of polymerization obtained by GPC (see Table 4.1)), suggesting the synthesis of densely grafted homopolymer brushes.

Following the first SI-ATRP step, two families of amphiphilic diblock copolymer brushes, comprising a lower content of the fluorinated block compared to the

hydrophilic segments and an almost equal content of the two comonomers respectively, were synthesized on the silicon substrates.

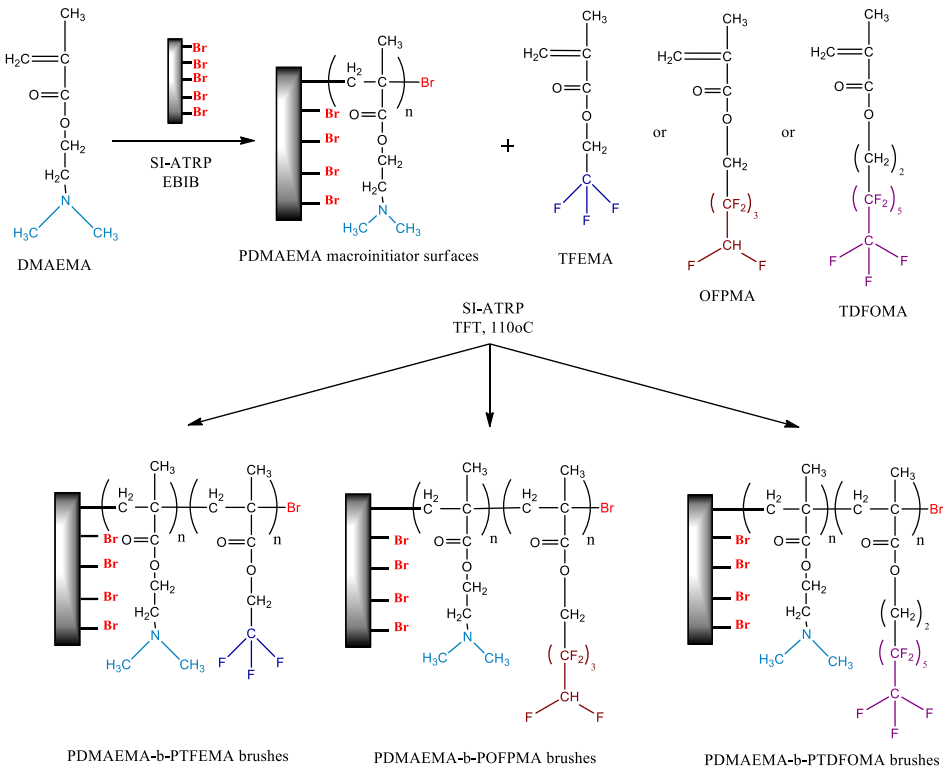


**Scheme 4.1.** Schematic representation of the synthesis of the diblock copolymer brushes

### 4.2.2.1 Characterization of the free diblock copolymers synthesized in solution

Representative GPC traces of the PDMAEMA-Br, PDMAEMA-*b*-PTFEMA, PDMAEMA-*b*-POFPMA and PDMAEMA-*b*-PTDFOMA polymers obtained in solution using the free initiator during the SI-ATRP are shown in Figure 4.1a and b. In all cases the traces are monomodal with a narrow molecular weight distribution. The shift of the signal towards lower elution times upon chain extension, without any trace of the PDMAEMA-Br homopolymer, verifies the successful synthesis of the amphiphilic diblock copolymers. The $M_n$*'s* of the diblock copolymer chains are depicted in Figure 4.1c and d and Table 4.1. For the copolymers with a lower content of the fluorinated block compared to the hydrophilic segments, the $M_n$'s of

$PDMAEMA_{267}$ homopolymer increased from 41,900 gr $mol^{-1}$ to 78,900 gr $mol^{-1}$, 73,200 gr $mol^{-1}$ and 57,400 gr $mol^{-1}$, respectively, suggesting the successful synthesis of the diblock copolymer chains (denoted as $PDMAEMA_{267}$-*b*-$PTFEMA_y$, $PDMAEMA_{267}$-*b*-$POFPMA_y$ and $PDMAEMA_{267}$-*b*-$PTDFOMA_y$, where y = 220, 104 or 35 is the degree of polymerization calculated by the $M_n$*'s* measured by GPC (Figure 4.1c)). Similarly, for the copolymers with an almost equal content of the two comonomers the $M_n$'s of $PDMAEMA_{103}$ homopolymers increased from 16,200 gr $mol^{-1}$ to 34,300 gr $mol^{-1}$ and 37,700 gr $mol^{-1}$, respectively (denoted as $PDMAEMA_{103}$-*b*-$PTFEMA_{108}$, and $PDMAEMA_{103}$-*b*-$POFPMA_{72}$, where z = 108 or 72, the degree of polymerization by GPC (Figure 4.1d)). Sample $PDMAEMA_{103}$-*b*-$PTDFOMA_{??}$ could not be analysed by GPC because the final block copolymer is insoluble to THF, which is used as the eluent in GPC. This was attributed to the long fluorocarbon side chains which render the polymer insoluble in polar media such as THF. The $M_w/M_n$ remained low (below 1.3), which is consistent with a controlled polymer chain growth. It is noted that for $PDMAEMA_{103}$-*b*-$POFPMA_{72}$ SEC characterization showed a complete inversion of the RI signal. The negative dRI signal is attributed to the lower refractive index of the fluoropolymer segments compared to the eluent ($n_{polymer}<n_{THF}$), which dominates the dn/dc of the diblock copolymer for the fluoropolymer with the higher number of fluorine atoms and the higher content of the fluorinated block.[11] All $M_n$ and $M_w/M_n$ values of the diblock copolymer chains are summarized in Table 4.1.

**Table 4.1.** Characteristics of the diblock copolymer brushes

| Polymer brush | Thickness Inner block (nm) | Thickness Outer block (nm) | Total thickness (nm) | $M_n$* Inner block | $M_n$* Outer block | $M_n$* Diblock | $M_w/M_n$* | σ (chains nm$^{-2}$) | Composition fluorinated segment** |
|---|---|---|---|---|---|---|---|---|---|
| PDMAEMA$_{267}$-Br | 32 | - | - | 41,900 | - | - | 1.27 | 0.51 | 0 |
| PDMAEMA$_{103}$-Br | 12 | - | - | 16,200 | - | - | 1.10 | 0.49 | 0 |
| PDMAEMA$_{267}$-*b*-PTFEMA$_{220}$ | 32 | 15 | 47 | 41,900 | 37,000 | 78,900 | 1.23 | 0.44 | 39 |
| PDMAEMA$_{103}$-*b*-PTFEMA$_{108}$ | 12 | 7 | 19 | 16,200 | 18,100 | 34,300 | 1.18 | 0.42 | 45 |
| PDMAEMA$_{267}$-*b*-POFPMA$_{104}$ | 32 | 12 | 44 | 41,900 | 31,400 | 73,200 | 1.22 | 0.46 | 34 |
| PDMAEMA$_{103}$-*b*-POFPMA$_{72}$ | 12 | 7 | 19 | 16,200 | 21,500 | 37,700 | 1.24 | 0.41 | 42 |
| PDMAEMA$_{267}$-*b*-PTDFOMA$_{35}$ | 32 | 6 | 38 | 41,900 | 15,600 | 57,400 | 1.19 | 0.48 | 30 |
| PDMAEMA$_{103}$-*b*-PTDFOMA$_{??}$ | 12 | 4 | 16 | 16,200 | NA | NA | NA | - | NA |

* Determined by GPC
** by $^1$H NMR spectroscopy

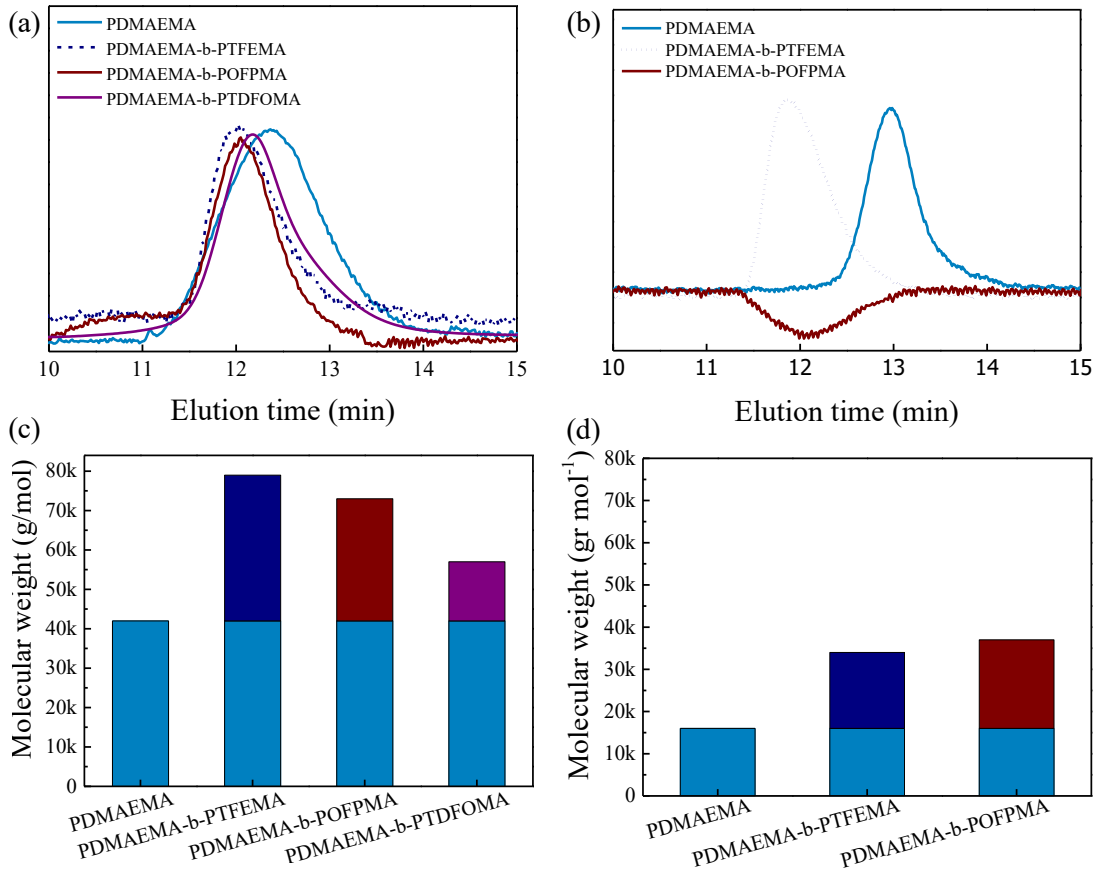


**Figure 4.1.** SEC traces for the free (a) $PDMAEMA_{267}$, $PDMAEMA_{267}$-*b*-$PTFEMA_{220}$, $PDMAEMA_{267}$-*b*-$POFPMA_{104}$ and $PDMAEMA_{267}$-*b*-$PTDFOMA_{35}$ and (b) $PDMAEMA_{103}$, $PDMAEMA_{103}$-*b*-$PTFEMA_{108}$ and $PDMAEMA_{103}$-*b*-$POFPMA_{72}$ (co)polymers obtained in solution during the SI-ATRP. Molecular weight values of the (c) $PDMAEMA_{267}$, $PDMAEMA_{267}$-*b*-$PTFEMA_{220}$, $PDMAEMA_{267}$-*b*-$POFPMA_{104}$ and $PDMAEMA_{267}$-*b*-$PTDFOMA_{35}$ and (d) $PDMAEMA_{103}$, $PDMAEMA_{103}$-*b*-$PTFEMA_{108}$ and $PDMAEMA_{103}$-*b*-$POFPMA_{72}$ (co)polymers. PDMAEMA is denoted in light blue, PTFEMA in navy, POFPMA in wine and PTDFOMA in purple.

The composition of the copolymers was determined by $^1$H NMR analysis. Table 4.2 summarizes the compositions of the synthesized PDMAEMA-*b*-PTFEMA, PDMAEMA-*b*-POFPMA and PDMAEMA-*b*-PTDFOMA copolymers.

Typical $^1$H NMR spectra for the $PDMAEMA_{267}$-*b*-$PTFEMA_{220}$, $PDMAEMA_{267}$-*b*-$POFPMA_{104}$ and $PDMAEMA_{267}$-*b*-$PTDFOMA_{35}$, diblock copolymers are shown in Figure 4.2. The compositions of the diblock copolymer chains were determined by comparing the integrals of the peak at 4.01-4.05 ppm (peak d), assigned to the protons of the methylene groups of PDMAEMA, to the peaks at 4.30 ppm (peak e), 5.97 ppm

(peak g) and 4.24 ppm (peak f), assigned to the protons of the methylene groups of PTFEMA, the difluoromethyl groups of POFPMA and the methylene groups of PTDFOMA, respectively. Similarly, the compositions of the $PDMAEMA_{103}$-*b*-$PTFEMA_{108}$ and $PDMAEMA_{103}$-*b*-$POFPMA_{72}$ copolymers were calculated by $^1H$ NMR, nevertheless the $PDMAEMA_{103}$-*b*-$PTDFOMA_{??}$ chains could not be analyzed, due to their insolubility in $CDCl_3$.

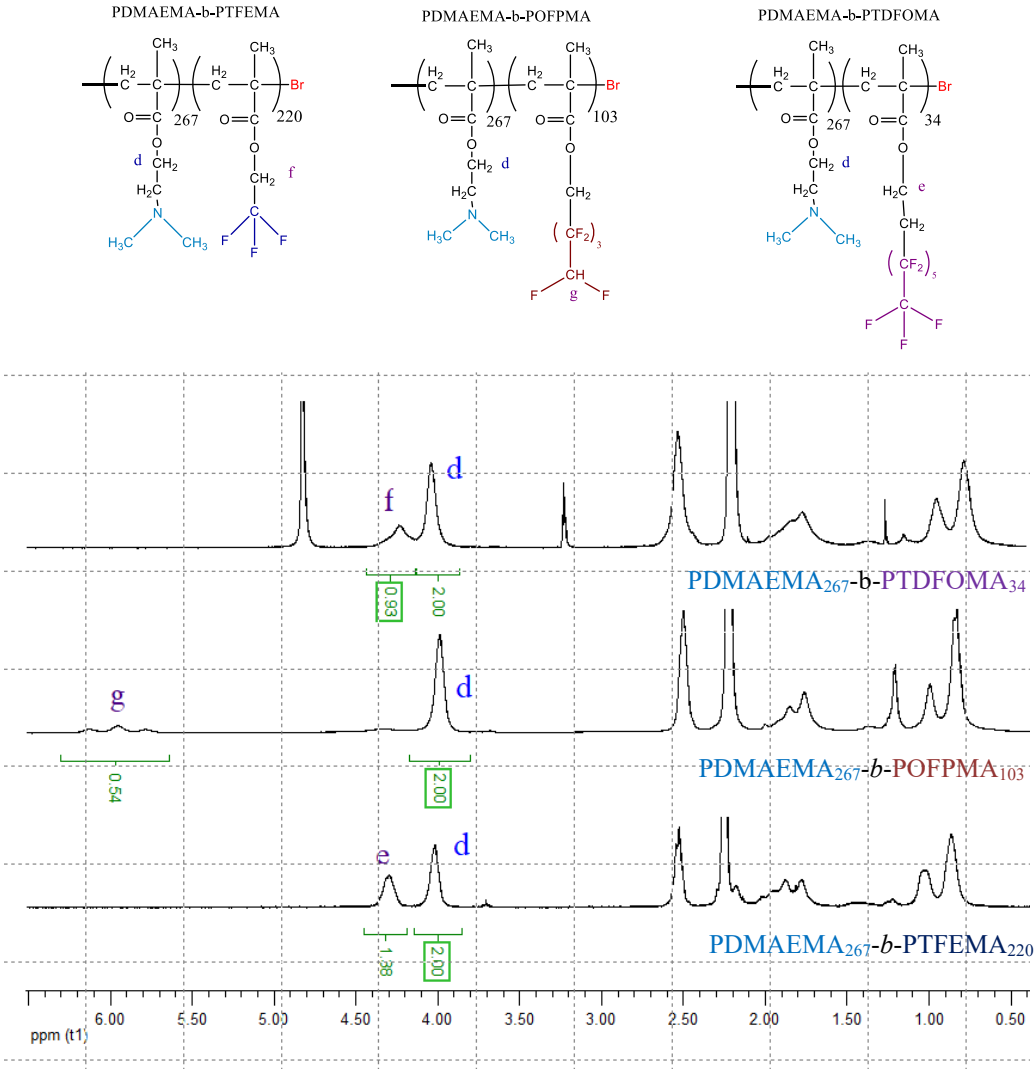


**Figure 4.2.** Chemical structures (upper) and $^1H$ NMR spectra in $CDCl_3$ (lower) of the $PDMAEMA_{267}$-*b*-$PTFEMA_{220}$, $PDMAEMA_{267}$-*b*-$POFPMA_{104}$, and $PDMAEMA_{267}$-*b*-$PTDFOMA_{35}$ copolymers.

The volume fractions of the amphiphilic diblock copolymer brushes were calculated from the molar and mass fractions of the PDMAEMA and PTFEMA, POFPMA and PTDFOMA blocks and their respective bulk densities (1.097 g/cm$^3$ for PDMAEMA, 1.451 g/cm$^3$ for PTFEMA, 1.610 g/cm$^3$ for POFPMA and 1.763 g/cm$^3$ for PTDFOMA)

(see Table 4.2). As shown in Figure 4.3, two series of amphiphilic diblock copolymer brushes, with 0.40 and 0.46 PTFEMA volume fraction, 0.34 and 0.48 POFPMA volume fraction, and 0.18 PTDFOMA volume fraction, were prepared. The $PDMAEMA_{100}$-*b*-$PTDFOMA_{??}$ chains were insoluble in $CDCl_3$, and other deuterated solvents, and therefore, its composition could not be determined by $^1H$ NMR spectroscopy.

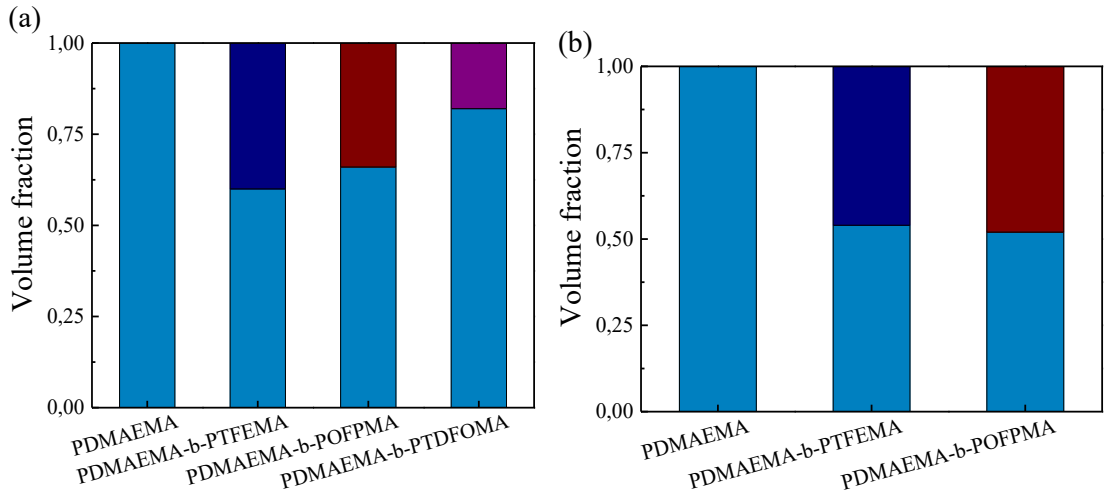


**Figure 4.3.** Volume fractions of the (a) $PDMAEMA_{267}$, $PDMAEMA_{267}$-*b*-$PTFEMA_{220}$, $PDMAEMA_{267}$-*b*-$POFPMA_{104}$ and $PDMAEMA_{267}$-*b*-$PTDFOMA_{35}$ and (b) $PDMAEMA_{103}$, $PDMAEMA_{103}$-*b*-$PTFEMA_{108}$ and $PDMAEMA_{103}$-*b*-$POFPMA_{72}$ (co)polymers. DMAEMA is denoted in light blue, PTFEMA in navy, POFPMA in wine and PTDFOMA in purple.

**Table 4.2.** Composition of the diblock copolymers.

| Polymer brush | Molar fraction a* | Molar fraction b | Weight fraction a | Volume fraction a** |
|---|---|---|---|---|
| $PDMAEMA_{267}$-*b*-$PTFEMA_{220}$ | 0.55 | 0.45 | 0.53 | 0.60 |
| $PDMAEMA_{103}$-*b*-$PTFEMA_{109}$ | 0.47 | 0.53 | 0.46 | 0.54 |
| $PDMAEMA_{267}$-*b*-$POFPMA_{104}$ | 0.72 | 0.28 | 0.57 | 0.66 |
| $PDMAEMA_{103}$-*b*-$POFPMA_{72}$ | 0.58 | 0.42 | 0.43 | 0.52 |
| $PDMAEMA_{267}$-*b*-$PTDFOMA_{35}$ | 0.88 | 0.12 | 0.74 | 0.82 |

* a corresponds to the PDMAEMA block

** The bulk densities measured for each homopolymer (1.097 g/cm$^3$ for PDMAEMA, 1.451 g/cm$^3$ for PTFEMA, 1.610 g/cm$^3$ for POFPMA and 1.763 g/cm$^3$ for PTDFOMA) were used.

#### 4.2.2.2 Film thickness and grafting density of the brushes

The film thicknesses of the homopolymer and diblock copolymer brushes were measured by ellipsometry. Figure 4.4 and Table 4.1 shows the dry film thicknesses for the PDMAEMA and the diblock copolymer brushes. Polymerization of TFEMA, OFPMA and TDFOMA for 60 h from the $PDMAEMA_{267}$-Br macroinitiator brush increased the film thicknesses from 32 nm to 47, 44 and 38 nm, respectively, due to the formation of a 15, 12 and 6 nm PTFEMA, POFPMA and PTDFOMA layer, respectively (Figure 4.4a). A similar procedure was followed for the synthesis of the amphiphilic diblock copolymer brushes using the $PDMAEMA_{103}$-Br macroinitiator brush. The 12 nm PDMAEMA films obtained after 9 h reaction, increased to a total thickness of 19, 19 and 16 nm after 48 h polymerization of the TFEMA, OFPMA and TDFOMA monomers, respectively, (Figure 4.4b).

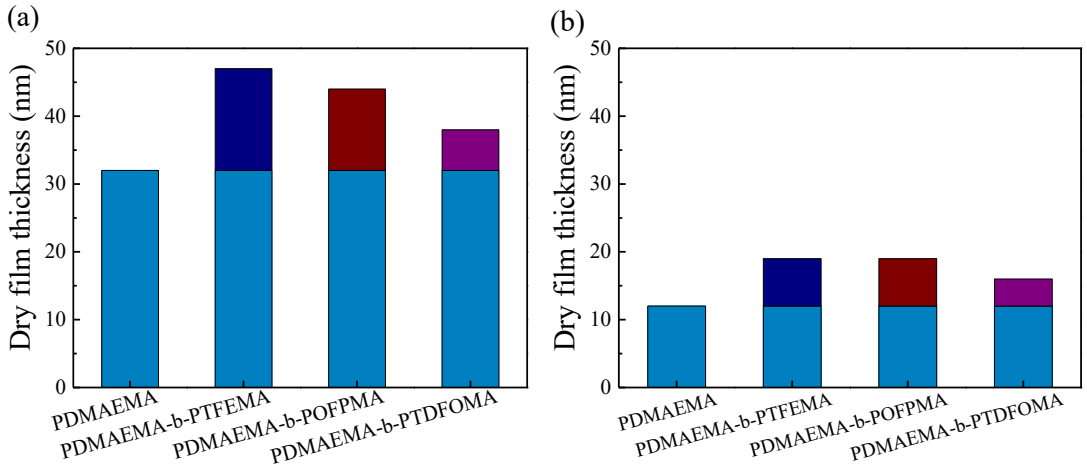


**Figure 4.4.** Dry film thicknesses for the (a) $PDMAEMA_{267}$, $PDMAEMA_{267}$-*b*-$PTFEMA_{220}$, $PDMAEMA_{267}$-*b*-$POFPMA_{104}$ and $PDMAEMA_{267}$-*b*-$PTDFOMA_{35}$ and (b) $PDMAEMA_{103}$, $PDMAEMA_{103}$-*b*-$PTFEMA_{108}$, $PDMAEMA_{103}$-*b*-$POFPMA_{72}$ and $PDMAEMA_{103}$-*b*-$PTDFOMA_{??}$ (co)polymers. PDMAEMA is denoted in light blue, PTFEMA in navy, POFPMA in wine and PTDFOMA in purple.

The grafting density (chains $nm^{-2}$) of each block was calculated using the equation (assuming that the initiation efficiency for the second block is very high):

$$\sigma = \frac{d \times N_A \times h}{M_n} \qquad (2.1)$$

where h: is the dry polymer film thickness (nm),

d: is the bulk density of the polymer (1.097 g/cm$^3$ for PDMAEMA, 1.451 g/cm$^3$ for PTFEMA, 1.610 g/cm$^3$ for POFPMA and 1.763 g/cm$^3$ for PTDFOMA)

$M_n$: is the number-average molecular weight of the chains grafted on the surface assumed to be the same as that of the polymer chains in solution (determined by GPC).

$N_A$: is the Avogadro's number ($6.023\times10^{23}$).

**Table 4.3.** Grafting densities of the diblock copolymer brushes.

| Polymer brush | σ (chains/nm$^2$) inner block | σ (chains/nm$^2$) outer block | σ (chains/nm$^2$) diblock |
|---|---|---|---|
| PDMAEMA$_{267}$-Br | 0.51 | - | - |
| PDMAEMA$_{103}$-Br | 0.49 | - | - |
| PDMAEMA$_{267}$-*b*-PTFEMA$_{220}$ | 0.51 | 0.35 | 0.44 |
| PDMAEMA$_{103}$-*b*-PTFEMA$_{108}$ | 0.49 | 0.34 | 0.42 |
| PDMAEMA$_{267}$-*b*-POFPMA$_{104}$ | 0.51 | 0.37 | 0.46 |
| PDMAEMA$_{103}$-*b*-POFPMA$_{72}$ | 0.49 | 0.32 | 0.41 |
| PDMAEMA$_{267}$-*b*-PTDFOMA$_{35}$ | 0.51 | 0.41 | 0.48 |
| PDMAEMA$_{103}$-*b*-PTDFOMA$_{??}$ | 0.49 | - | - |

The grafting density values are listed in Table 4.3. The grafting density of the PDMAEMA$_{267}$-Br and PDMAEMA$_{103}$-Br brushes was calculated 0.51 and 0.49 chains nm$^{-2}$, respectively, suggesting the synthesis of densely grafted homopolymer brushes.

Two approaches have been used to calculate the grafting densities of the diblock copolymer brushes. In the first case, the grafting density of each block is calculated from equation 2.1, and the values ranged from 0.35 to 0.34 chains nm$^{-2}$ for the PTFEMA blocks, 0.37 to 0.32 chains nm$^{-2}$ for the POFPMA blocks and 0.41 chains nm$^{-2}$ for the PTDFOMA block. The decrease in the grafting density for the second block is mainly attributed to the partial loss of the PDMAEMA macroinitiator active sites upon chain extension.

The grafting densities of the diblock copolymers can be also obtained from the total film thickness, the system density and the molecular weight of the diblock copolymer. Grafting densities from 0.44 to 0.42 chains nm$^{-2}$ for the PDMAEMA-*b*-PTFEMA brushes, 0.46 to 0.41 chains nm$^{-2}$ for the PDMAEMA-*b*-POFPMA brushes and 0.48 chains nm$^{-2}$ for the PDMAEMA-*b*-PTDFOMA were calculated.

In both cases the grafting density values obtained suggest the synthesis of densely grafted diblock copolymer chains.

### 4.2.3 Surface properties of the diblock copolymer brushes

Contact angle (CA) measurements were performed in order to verify the successful synthesis of the diblock copolymer brushes (Table 4.4). The static water CAs increased after polymerization from ~60 º for the $PDMAEMA_{267}$ brush to 94 º, 103 º and 110 º for $PTFEMA_{220}$, $POFPMA_{104}$ and $PTDFOMA_{35}$, respectively which confirmed the successful growth of the hydrophobic fluorinated blocks. Similar contact angles were obtained for the PTFEMA, POFPMA and PTDFOMA brushes grown from the $PDMAEMA_{103}$-Br brushes (90 º, 105 º and 108 º, respectively). It is also noted that the measured CAs are in good agreement with the values measured for the PTFEMA, POFPMA and PTDFOMA homopolymer brushes (see Chapter 3).

**Table 4.4.** Thickness and surface characteristics of the diblock copolymer brushes

| Polymer brush | Ellipsometric Thickness (nm) | RMS (nm) | WCA (º) inner block | WCA (º) diblock |
|---|---|---|---|---|
| $PDMAEMA_{267}$-Br | 32 | 0.8 | - | 61 |
| $PDMAEMA_{103}$-Br | 12 | 0.8 | - | 59 |
| $PDMAEMA_{267}$-*b*-$PTFEMA_{220}$ | 47 | 1.6 | 61 | 94 |
| $PDMAEMA_{103}$-*b*-$PTFEMA_{108}$ | 19 | 1.3 | 59 | 90 |
| $PDMAEMA_{267}$-*b*-$POFPMA_{104}$ | 44 | 1.5 | 60 | 103 |
| $PDMAEMA_{103}$-*b*-$POFPMA_{72}$ | 19 | 1.1 | 59 | 105 |
| $PDMAEMA_{267}$-*b*-$PTDFOMA_{35}$ | 38 | 1.8 | 60 | 110 |
| $PDMAEMA_{103}$-*b*-$PTDFOMA_{??}$ | 16 | 1.6 | 62 | 108 |

### 4.2.4 Morphology of the diblock copolymer brushes

The morphology of the polymer films was assessed by AFM height images using the tapping mode. Typical images of the inner block layers and the diblock copolymer films

at ambient conditions are shown in Figure 4.5. In all cases, the surface topography of the PDMAEMA homopolymer films revealed a smooth and uniform layer with a roughness ($R_q$) below 1 nm (Table 4.4). Moreover, the growth of the second block from the PDMAEMA brushes had a slight impact on the roughness of the films which increased for the PDMAEMA$_{267}$-*b*-PTFEMA$_{220}$, PDMAEMA$_{267}$-*b*-POFPMA$_{104}$ and PDMAEMA$_{267}$-*b*-PTDFOMA$_{35}$ brushes, between 1.5 and 1.9 nm under ambient conditions. Roughness is defined as the root-mean-square (RMS) of the height deviations taken from the mean data plane. The growth of the fluorinated blocks was featureless to the smooth morphology of the polymer brushes via sequential SI-ATRP, which is consistent with the literature on morphological studies of amphiphilic diblock copolymer brushes.[12]

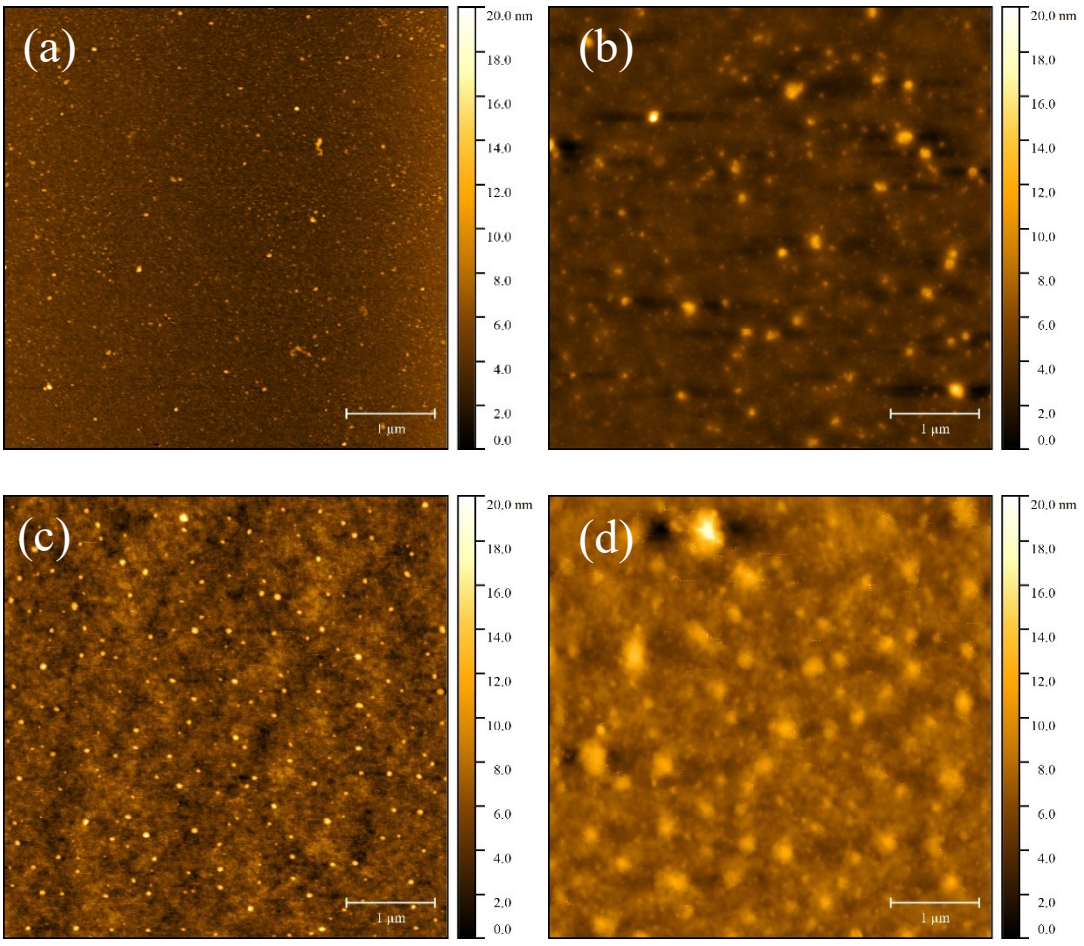


**Figure 4.5.** Tapping mode AFM images of the (a) PDMAEMA$_{267}$-Br (b)PDMAEMA$_{267}$-*b*-PTFEMA$_{220}$ (c) PDMAEMA$_{267}$-*b*-POFPMA$_{104}$ and (d) PDMAEMA$_{267}$-*b*-PTDFOMA$_{35}$ diblock copolymer brushes after sequential SI-ATRP. Each image resembles an area of 5 × 5 µm$^2$. Scale bar: 1 µm, Z-scale bar: 0-20 nm.

#### 4.2.4.1 Reversible wetting behavior and morphology of the diblock copolymer brushes

The wetting properties of amphiphilic diblock copolymer brushes are widely known to be influenced by solvents of different polarity. The reversible wettability upon treatment with a selective solvent for each block was studied for the amphiphilic PDMAEMA-*b*-PTFEMA, PDMAEMA-*b*-POFPMA and PDMAEMA-*b*-PTDFOMA brushes of different compositions. HFiP was used as a good solvent for the fluorinated blocks and nanopure water as a good solvent for the PDMAEMA block.

First, all samples with a lower content of the fluorinated blocks, namely 40, 34 and 18 vol% of PTFEMA, POFPMA and PTDFOMA, respectively, were immersed in HFiP, which is a selective solvent for the perfluorocarbon blocks and a bad solvent for the PDMAEMA blocks, at RT for 6 h and were dried under a nitrogen steam. The polymer brushes were subjected to thermal annealing at 100 °C for 1 h, and were subsequently studied by static water contact angle (WCA) measurements. WCA values of 94 °, 103 ° and 110 °, were measured for the PDMAEMA$_{267}$-*b*-PTFEMA$_{220}$, PDMAEMA$_{267}$-*b*-POFPMA$_{104}$ and PDMAEMA$_{267}$-*b*-PTDFOMA$_{35}$, diblock copolymer brushes, respectively. These values are only slightly lower compared to the WCA values measured for the PTFEMA, POFPMA and PTDFOMA homopolymer brushes (97 °, 109 ° and 115 °, respectively). The high WCA values obtained suggested that the fluorinated hydrophobic chains are exposed at the free surface and dominate the wettability of the surfaces. Next, the switching of the diblock copolymer brushes from hydrophobic to hydrophilic polymer surfaces was conceived by soaking the polymer films in nanopure water at RT for 12 h. The WCA values were measured below 65° for all three brushes, which suggests that the polar function groups of the hydrophilic PDMAEMA chains are oriented towards the free surface (Figure 4.6).

Seemingly, the higher number of fluorine atoms in the side groups of the hydrophobic blocks resulted in larger transitions from hydrophobicity to hydrophilicity. The contact angle variations were found to be around 33°, 43° and 50° for the PDMAEMA$_{267}$-*b*-PTFEMA$_{220}$, PDMAEMA$_{267}$-*b*-POFPMA$_{104}$ and PDMAEMA$_{267}$-*b*-PTDFOMA$_{35}$ brushes, which constitute the largest switching in the wettability for flat surfaces reported in the literature so far. These results indicate that the polymer chains rearrange within the brush to alter the surface composition leading to an enrichment of the surface

with C-F groups or water-soluble -$N(CH_3)_2$ moieties following immersion in a selective solvent.

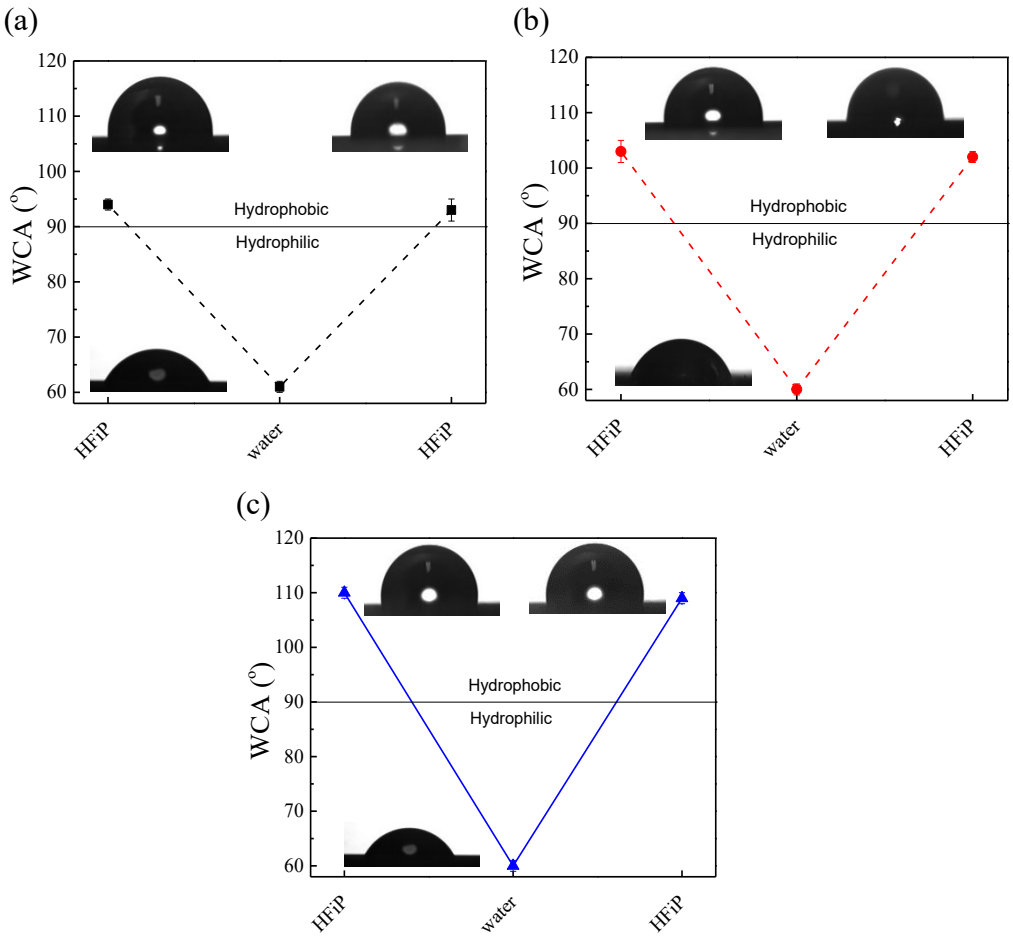


**Figure 4.6.** WCA values for the (a) PDMAEMA$_{267}$-*b*-PTFEMA$_{220}$ (■, black) (b) PDMAEMA$_{267}$-*b*-POFPMA$_{104}$ (●, red) and (c) PDMAEMA$_{267}$-*b*-PTDFOMA$_{35}$ (▲, blue) brushes, following immersion in HFiP, water and HFiP again. The insets show the water droplets on the brush surface.

The reversibility of the re-organization of the brushes was examined by the sequential immersion of the samples in the two selective solvents for several cycles. The average contact angles of water droplets residing on the block copolymer brushes for five solvent cycles are presented in Figure 4.7. An excellent responsive behavior was observed with a transition from the hydrophilic to the hydrophobic state with no deviations in the WCA values for at least 5 solvent cycles. This behavior implied that the polymer brushes are capable of internal rearrangements exhibiting a smart memory behavior of their surface wettability for repetitive solvent cycles.

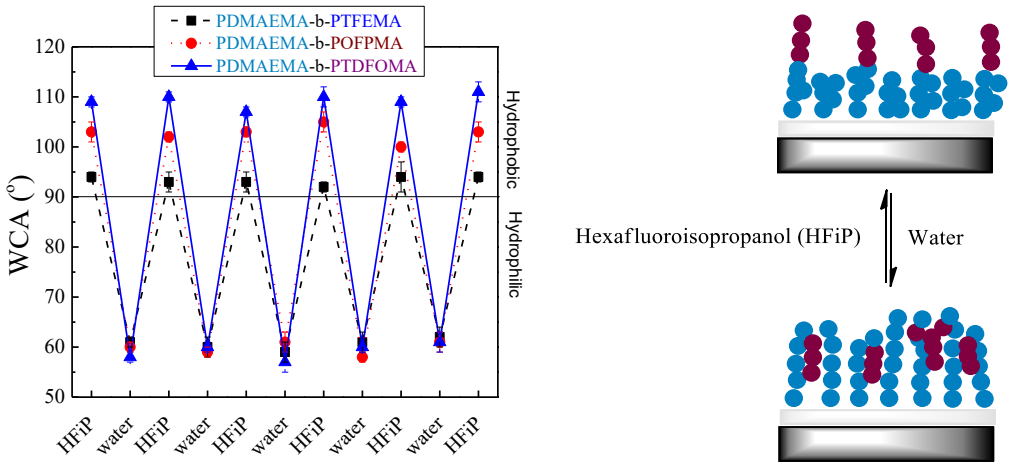


**Figure 4.7.** Average WCA values for the PDMAEMA$_{267}$-*b*-PTFEMA$_{220}$ (■, black), PDMAEMA$_{267}$-*b*-POFPMA$_{104}$ (●, red) and PDMAEMA$_{267}$-*b*-PTDFOMA$_{35}$ (▲, blue) brushes following successive immersion in HFiP and water. The schematic illustration in the right represents the structure of the brush in each selective solvent (●:DMAEMA and ●:fluoromonomer).

However, a remarkably different behavior was found for the symmetric diblock copolymer brushes. Figure 4.8 shows the WCA of the brushes treated consecutively with HFiP, water and HFiP again (one cycle). The contact angles in one solvent cycle varied from 91° to 89° to 92° for PDMAEMA$_{103}$-*b*-PTFEMA$_{108}$, 100° to 96° to 97° for PDMAEMA$_{103}$-*b*-POFPMA$_{72}$ and 106° to 101° to 103° for the PDMAEMA$_{103}$-*b*-PTDFOMA$_{??}$ copolymer brush. These results suggest that the brushes with the higher fluoropolymer content cannot rearrange to switch the wettability of the surface, and it is the outer hydrophobic block that remains constantly exposed at the free surface governing the polymer-air interface, despite the shorter length of these blocks compared to those of the lower fluoropolymer content brushes.[13]

From the above we can conclude that the diblock copolymer brushes can attain two different morphologies, following immersion in water which is a good solvent for the surface anchored PDMAEMA inner block, which depend on the copolymer composition. For higher PDMAEMA content, the brush adopts the so-called "collapsed" morphology with the fluorinated blocks collapsing on the surface and the PDMAEMA blocks migrating at the outer free surface of the brush to shield the interactions between the fluorinated blocks and water.[13] At lower PDMAEMA content, the "exposed" morphology prevails and the fluorinated blocks remain exposed to the bad solvent despite the stretching of the PDMAEMA block. At the high grafting

densities studied in this work, it seems that the increase in the fluorinated segment content prevents the organization of the brush and diminishes the responsive behavior of the grafted diblock polymer chains.

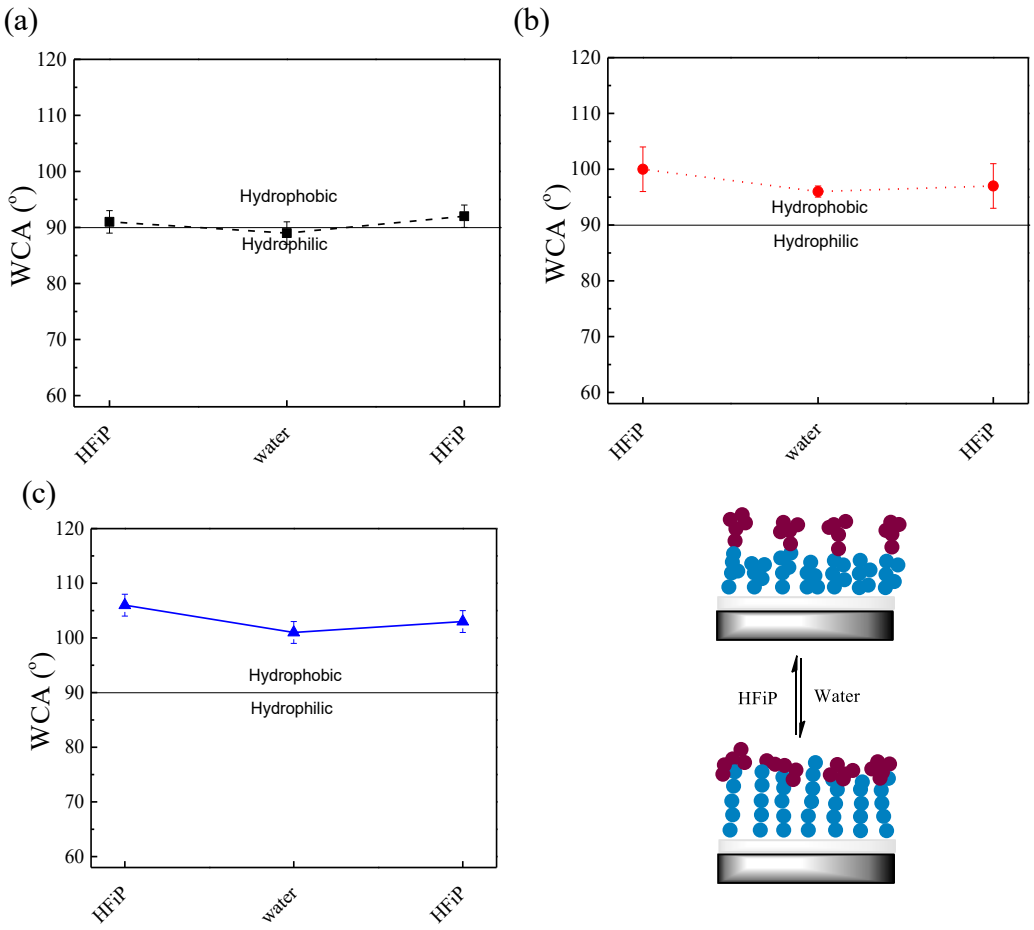


**Figure 4.8.** Average WCA values for the (a) DMAEMA$_{103}$-*b*-PTFEMA$_{108}$ (■, black), (b) PDMAEMA$_{103}$-*b*-POFPMA$_{72}$ (●, red) and (c) PDMAEMA$_{103}$-*b*-PTDFOMA$_{??}$ (▲, blue) brushes, following immersion in HFiP, water and HFiP again. The schematic illustration in the right represents the structure of the brush in each selective solvent (●:DMAEMA and ●:fluoromonomer).

AFM studies were contacted to further investigate the solvent-responsive behavior of the diblock copolymer brushes and determine the surface morphology following immersion in the selective solvents. Figure 4.9 shows typical AFM height images for the PDMAEMA$_{267}$-*b*-PTFEMA$_{220}$, PDMAEMA$_{267}$-*b*-POFPMA$_{104}$ and PDMAEMA$_{267}$-

*b*-PTDFOMA$_{35}$ brushes, after treatment with HFiP (Figure 4.9a, b, c) and water (Figure 4.9d, e, f). The average roughness values calculated from the height deviations of these images are listed in Table 4.4. The surface morphology of the brushes varied depending on the solvent immersed. Immersion in HFiP resulted in a relatively smooth surface with a surface roughness of 1.1 - 1.3 nm, even lower than the RMS found after treatment with TFT (1.5 - 1.8 nm). This suggests that the outer fluorinated blocks are localized at the polymer-air interface and the PDMAEMA block is segregated on the grafted surface, to give relatively smooth and uniform surfaces. However, when the diblock copolymer brushes were treated with water, which is a selective solvent for the inner block, the surface roughness increased to 2.0 - 3.1 nm suggesting the re-organization of the brush to adopt a non-linear conformation with the outer fluorinated blocks bending towards the inner part of the brush and contributing to the increased roughness. These results are consistent with the WCA values discussed above for the two solvents. It is noted however, that no discernible regular nanomorphology, which would suggest the microphase separation of the fluorinated blocks, was observed upon immersion of the brush in water. The proposed conformation rearrangement considers that the short fluorinated outer blocks loop back from the polymer-water interface and become miscible with the inner PDMAEMA blocks, which become stretched to reach the polymer-water interface (See illustration in Figure 4.7). A more detailed study of the phase behavior and conformational re-arrangements of the diblock copolymer brushes is essential to further elucidate the brush structure following immersion in the two selective solvents.

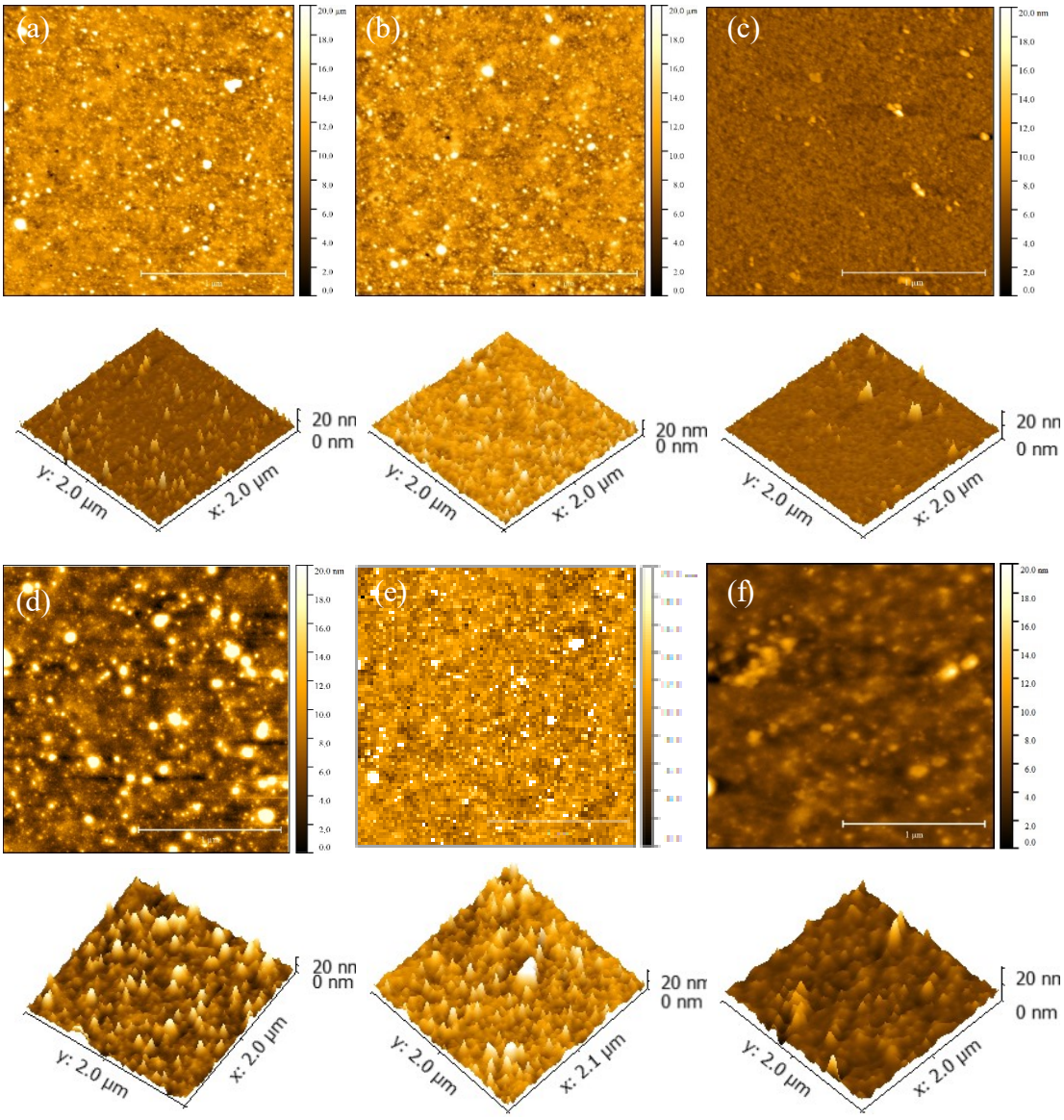


**Figure 4.9.** AFM topography images in 2D and 3D (2 x 2 µm$^2$, Z: 20nm) for the (a and d) PDMAEMA$_{267}$-*b*-PTFEMA$_{220}$, (b and d) PDMAEMA$_{267}$-*b*-POFPMA$_{104}$ and (c and e) PDMAEMA$_{267}$-*b*-PTDFOMA$_{35}$ block copolymer brushes following immersion in HFiP (a - c) and water (d - f). Scale bar: 1 µm.

**Table 4.5.** Surface roughness values of the diblock copolymer brushes following immersion in TFT, HFiP and water.

| Polymer brush | RMS TFT (nm)* | RMS HFiP (nm)* | RMS $H_2O$ (nm)* |
|---|---|---|---|
| $PDMAEMA_{267}$-Br | 0.8 | 0.7 | 0.7 |
| $PDMAEMA_{267}$-*b*-$PTFEMA_{220}$ | 1.6 | 1.1 | 2.7 |
| $PDMAEMA_{267}$-*b*-$POFPMA_{104}$ | 1.5 | 1.3 | 3.1 |
| $PDMAEMA_{267}$-*b*-$PTDFOMA_{35}$ | 1.8 | 1.1 | 2.0 |

* measured by AFM

#### 4.2.4.2 Effect of quaternization on the switching behavior of the diblock copolymer brushes

Quaternization of the PDMAEMA segments of the $PDMAEMA_{267}$-*b*-$PTFEMA_{220}$, $PDMAEMA_{267}$-*b*-$POFPMA_{104}$, and $PDMAEMA_{267}$-*b*-$PTDFOMA_{35}$ brushes was carried out by a post-polymerization reaction to convert the tertiary amine groups of the DMAEMA units to their quaternary ammonium salt analogues. 1-Iodopropane was used as the quaternization agent, in methanol at 50 ºC for 48 h.

Table 4.6 summarizes the characteristics of the quaternized diblock copolymer brushes. For all copolymer brushes, a ~1.5-fold increase of the dry film thickness was measured after quaternization reaction, which is ascribed to the increase of the molecular weight of the DMAEMA monomer repeat units, as well as to any remaining chemically-bound water molecules within the charged polymer layer, as described in detail in Chapter 3 for the PDMAEMA homopolymer brushes.

**Table 4.6.** Characterization data of the quaternized semi-fluorinated diblock copolymer brushes.

| Polymer brush | Thickness Inner block (nm) | Thickness Outer block (nm) | Total thickness (nm) |
|---|---|---|---|
| PDMAEMA$_{267}$-Br | 32 | - | - |
| PQDMAEMA$_{267}$-*b*-PTFEMA$_{220}$ | 48 | 15 | 63 |
| PQDMAEMA$_{267}$-*b*-POFPMA$_{104}$ | 50 | 12 | 62 |
| PQDMAEMA$_{267}$-*b*-PTDFOMA$_{35}$ | 45 | 6 | 51 |

After quaternization, the diblock copolymer brushes were characterized by contact angle measurements following immersion in the two selective solvents, HFiP and water. As shown in Figure 4.10, the contact angles varied between 81$^{o}$ and 90$^{o}$ for PQDMAEMA$_{267}$-*b*-PTFEMA$_{220}$, 80$^{o}$ and 93$^{o}$ for PQDMAEMA$_{267}$-*b*-POFPMA$_{104}$ and 85$^{o}$ and 94$^{o}$ for the PQDMAEMA$_{267}$-*b*-PTDFOMA$_{35}$ copolymer brushes. These values are between the WCAs measured for the PQDMAEMA brush (42 $^{o}$, see Chapter 3) and the PTFEMA, POFPMA or PTDFOMA homopolymer brushes (97 $^{o}$, 109 $^{o}$ and 115 $^{o}$, respectively), in each case, suggesting that partial rearrangement of the two blocks and the switching behavior of the diblock copolymer brushes occurred, but to a much less extent compared to the precursor diblock copolymer brushes before quaternization.

It was expected, that the tethered semi-fluorinated diblocks consisting of a PQDMAEMA inner block would exhibit a greater contact angle change upon solvent rearrangement compared to the corresponding PDMAEMA-based semi-fluorinated diblock copolymer brushes. The rearrangement of the diblock copolymer brushes has been reported to depend on several factors such as the length of the blocks, the copolymer composition and the Flory-Higgins interaction parameter ($\chi$) of the two polymers. It is speculated that in our case the increase in the solubility parameter, the $\chi$ value, between the two blocks after quaternization prevents the complete rearrangement of the block copolymer brushes.[14]

In addition, the fluoropolymer chains with long fluorinated alkyl chains (17 fluorine atoms) have been shown to present crystallinity of the polymer side groups in dense polymer brushes, which contributes to a diminished flexibility of the polymer chains.[15] In this thesis, PTFEMA, POFPMA and PTDFOMA were shown to possess a decent in flexibility upon their introduction in diblock copolymer brushes. Therefore, the deterioration of the responsiveness of these brushes upon quaternization can be attributed to the loss of the flexibility of the polymer chains. Apparently, the quaternization reaction results in a further constrain of the two immiscible PQDMAEMA and PTFEMA or POFPMA or PTDFOMA chains, which is supported by the semi-crystallinity of the mixed brushes at RT.

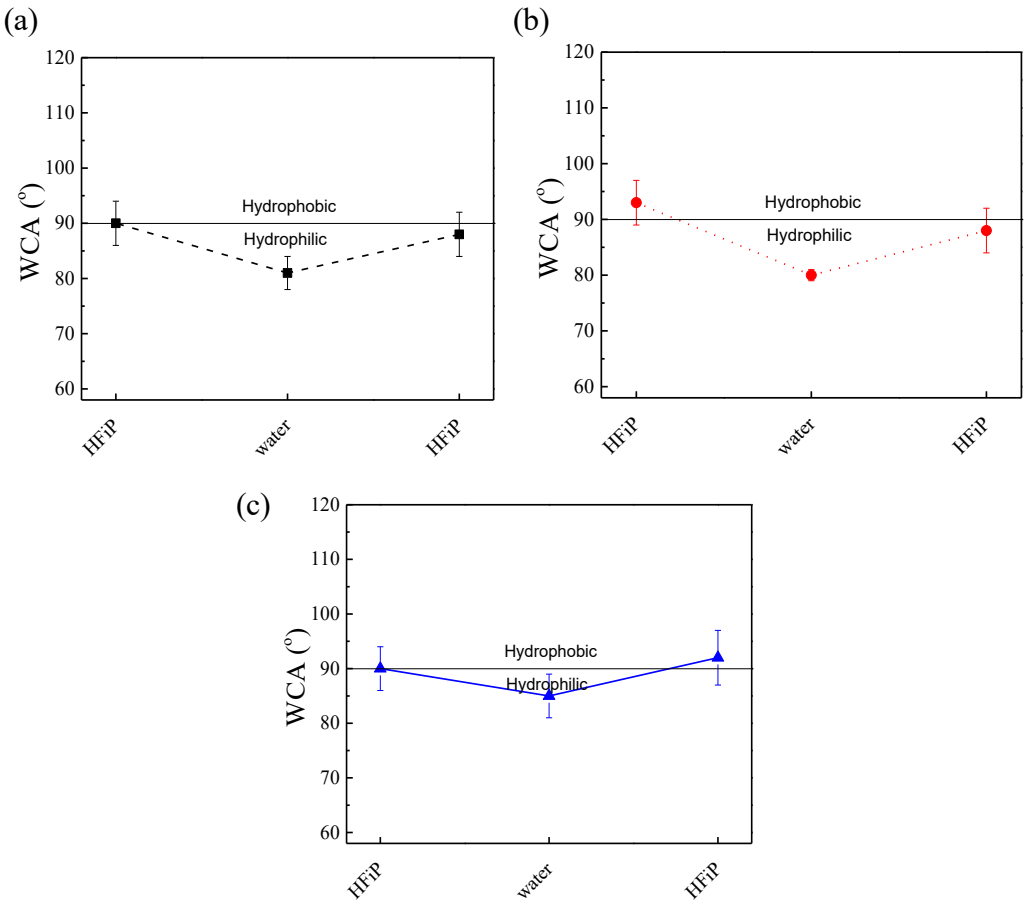


**Figure 4.10.** Average WCA values for the (a) PQDMAEMA$_{267}$-*b*-PTFEMA$_{220}$ (■, black), (b) PQDMAEMA$_{267}$-*b*-POFPMA$_{104}$ (●, red) and (c) PQDMAEMA$_{267}$-*b*-PTDFOMA$_{35}$ (▲, blue) brushes following immersion in HFiP, water and HFiP again.

Next, the morphologies of the brushes were studied by tapping mode AFM. Topography and phase images were captured to assess changes on the morphological characteristics of the brushes upon solvent treatment. The height images provide the topography and the characteristic roughness of the surface, while the phase images show the distribution of the two polymers in the film. AFM height images of the PQDMAEMA$_{267}$-*b*-PTFEMA$_{220}$, PQDMAEMA$_{267}$-*b*-POFPMA$_{104}$ and PQDMAEMA$_{267}$-*b*-PTDFOMA$_{35}$, diblock copolymer brushes showed the loss of surface homogeneity of the brush and the possible formation nanostructures, signifying the phase separation of the two blocks which are both present at the polymer-air interphase (see Figure 4.11). This was verified by phase image AFM, which clearly shows the phase contrast in the polymer films verifying the microphase separation of the two blocks when immersed in water (Figure 4.12), whereas similar morphologies were obtained in HFiP. The phase separation of the diblock copolymer brushes depends on the copolymer composition, the polymer grafting density and the Flory-Higgins interaction parameter ($\chi$).[16] For high $\chi$ values of the two blocks, phase separation occurs due to the immiscibility of the polymer segments. Herein, the $\chi$ value between the two block increases after quaternization due to the presence of very dissimilar polymers, charged PQDMAEMA and semi-fluorinated PTFEMA, POFPMA or PTDFOMA chains. Thus, it is believed that after quaternization the two different blocks cannot fully rearrange upon exposure to a selective solvent for the inner block, and both blocks co-exist in the outer surface, thus each affecting partially the surface properties of the film. This behavior is in agreement with similar studies on diblock copolymer brushes.[10, 12b, 13]

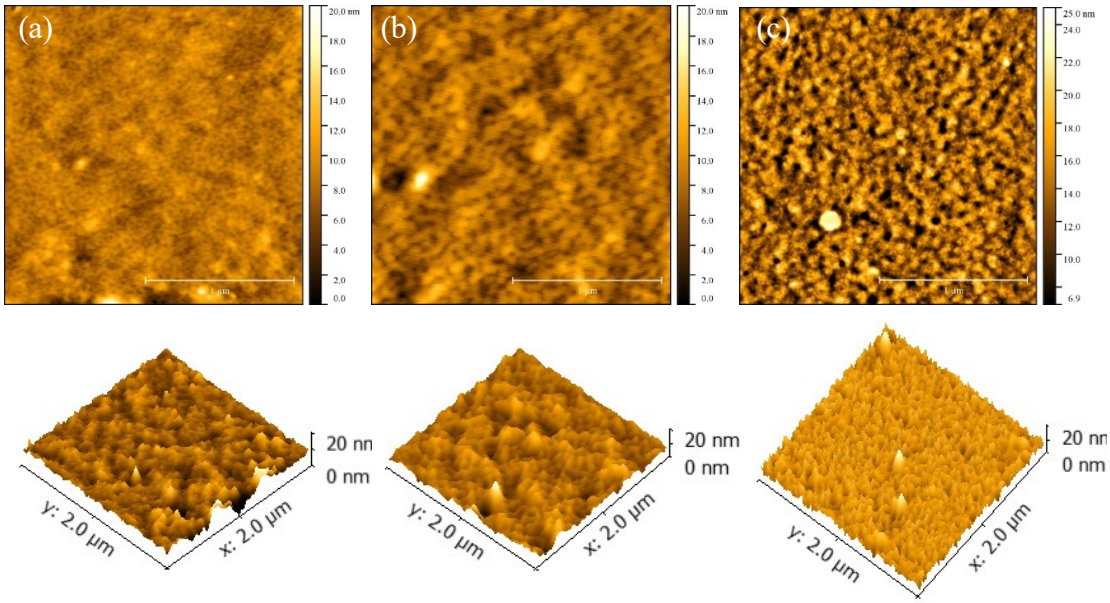


**Figure 4.11.** AFM topography images in 2D and 3D (2 x 2 µm$^2$, Z: 20nm) for the (a) PQDMAEMA$_{267}$-*b*-PTFEMA$_{220}$, (b) PQDMAEMA$_{267}$-*b*-POFPMA$_{104}$ and (c) PQDMAEMA$_{267}$-*b*-PTDFOMA$_{35}$ diblock copolymer brushes after immersion in nanopure water.

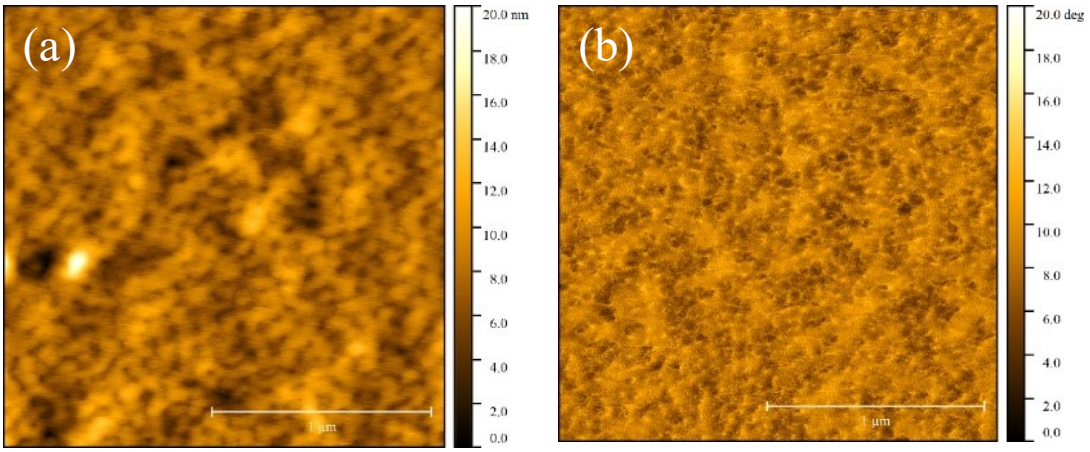


**Figure 4.12.** AFM height (a, 2 x 2 µm$^2$, Z: 20nm) and phase image (b, 2 x 2 µm$^2$, Z: 20 deg) for the PQDMAEMA$_{267}$-*b*-POFPMA$_{104}$ block copolymer brush after immersion in water.

### 4.2.5 Stability tests of the amphiphilic diblock copolymer brushes

The degrafting of the diblock copolymer brushes, upon prolonged immersion in fluorinated organic solvent and in water, was studied. Ellipsometry was employed to

characterize the degrafting process before and after quaternization, by determining the dry film thickness of the PDMAEMA$_{267}$-*b*-PTFEMA$_{220}$, PDMAEMA$_{267}$-*b*-POFPMA$_{104}$ and PDMAEMA$_{267}$-*b*-PTDFOMA$_{35}$ brushes and their respective quaternized analogues at regular time intervals.

Figure 4.13a shows the dry brush thickness as a function of immersion time in nanopure water. Incubation in water resulted in the degrafting of the end-grafted diblock polymer chains after 14 days, with the dry film thickness decreasing from 41, 37 and 40 nm in day 1, to 20, 13 and 14 nm in day 30, for the PDMAEMA$_{267}$-*b*-PTFEMA$_{220}$, PDMAEMA$_{267}$-*b*-POFPMA$_{104}$ and PDMAEMA$_{267}$-*b*-PTDFOMA$_{35}$ brushes, respectively, whereas thereafter it decreased slightly or remained almost constant until day 60. On the other hand, the rate of degrafting increased significantly for the strong polyelectrolyte PQDMAEMA brushes (Figure 4.13b) and degrafting occurred immediately with the thickness decreasing from 57, 54 and 49 nm in day 1 to 26, 20 and 18 nm after 7 days in water for the PQDMAEMA$_{267}$-*b*-PTFEMA$_{220}$, PQDMAEMA$_{267}$-*b*-POFPMA$_{104}$, PQDMAEMA$_{267}$-*b*-PTDFOMA$_{35}$ brushes, respectively irrespectively of the length of the fluorocarbon side group. Again, after this time, the film thickness decreased slightly or remained almost constant until day 30. Similar to the discussion in Chapter 3, the degrafting of polymer brushes in water is attributed to the swelling of the end-grafted chains which is believed to facilitate the hydrolytic cleavage of the siloxane or ester bonds at the polymer brush-substrate interface. After a certain degrafting of the chains, the grafting density and thus the tension at the interface decreases, which slows down significantly the degrafting process, leading to an almost constant polymer film thickness (Scheme 4.2).

For the diblock copolymer brushes, the grafting density was high (~0.5 chains/nm$^2$ for the inner PDMAEMA block), and therefore the de-grafting process was fast, whereas an accelerated degrafting was observed after quaternization. In the latter case, the DMAEMA moieties carry a permanent charge and the PQDMAEMA blocks are highly stretched in water, to limit the electrostatic repulsions between the polymer chains. Therefore, the hydrolysis of the bonds at the brush-substrate interface is mechanically activated by the increased tension exerted on the chain, that results to the degrafting process. It is however interesting that, the degrafting process is faster for the diblock copolymer brushes (14 days for the PDMAEMA$_{267}$-*b*-PTFEMA$_{220}$, PDMAEMA$_{267}$-*b*-POFPMA$_{104}$, PDMAEMA$_{267}$-*b*-PTDFOMA$_{35}$ brushes and 7 days for the

PQDMAEMA$_{267}$-*b*-PTFEMA$_{220}$, PQDMAEMA$_{267}$-*b*-POFPMA$_{104}$, PQDMAEMA$_{267}$-*b*-PTDFOMA$_{35}$ brushes), compared to the respective PDMAEMA and PQDMAEMA homopolymer brushes discussed in Chapter 3 (degrafting after 30 days for PDMAEMA and 14 days for PQDMAEMA-C3). It is suggested that the tension on the chain and the cleavage of the initiator bonds cannot be explained only by the introduction of the charged moieties, since the presence of the fluorinated segments at the outer surface seems to contribute to the process, when the brushes are immersed in water. A possible contribution could be a further increase in mechanical tension, caused by the partial rearrangement and the switching behavior of the diblock copolymer brushes, compared to the PQDMAEMA homopolymer brushes.

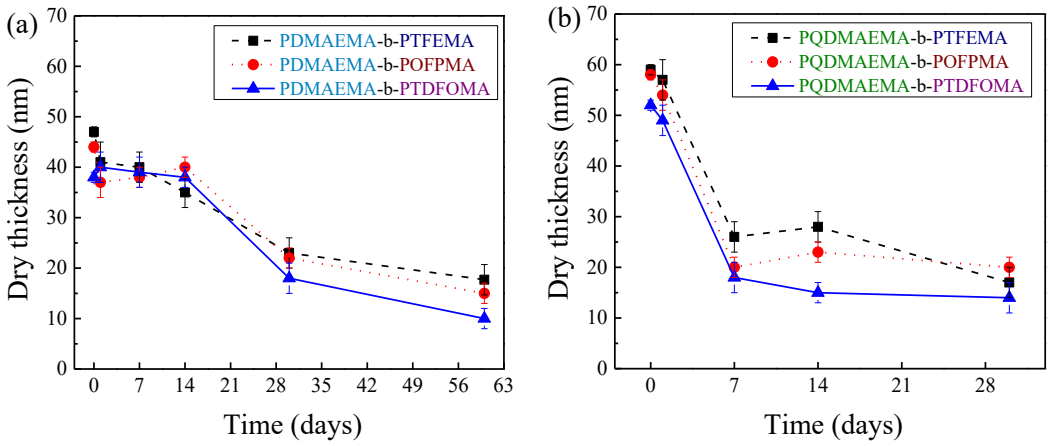


**Figure 4.13.** Ellipsometric dry thickness of (a) the PDMAEMA$_{267}$-*b*-PTFEMA$_{220}$ (■, black), PDMAEMA$_{267}$-*b*-POFPMA$_{104}$ (●, red) and PDMAEMA$_{267}$-*b*-PTDFOMA$_{35}$ (▲, blue) brushes and (b) the PQDMAEMA$_{267}$-*b*-PTFEMA$_{220}$ (■, black), PQDMAEMA$_{267}$-*b*-POFPMA$_{104}$ (●, red) and PQDMAEMA$_{267}$-*b*-PTDFOMA$_{35}$ (▲, blue) brushes, as a function of their incubation time in water.

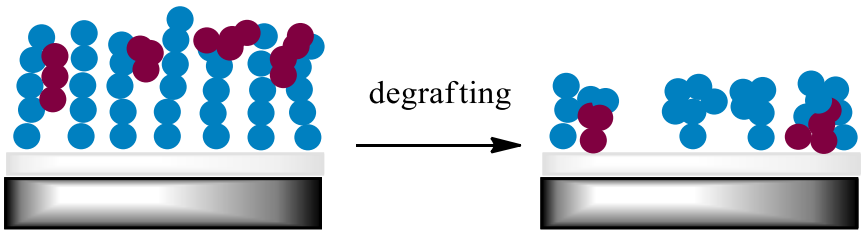


**Scheme 4.2.** Schematic representation of the degrafting process to reach a minimum in the grafting density and the dry film thickness.

## 4.3 Conclusions

In summary, amphiphilic diblock copolymer brushes (PDMAEMA-*b*-PTFEMA, PDMAEMA-*b*-POFPMA, PDMAEMA-*b*-PTDFOMA) were successfully synthesized from silicon substrates via SI-ATRP. The diblock copolymer brushes exhibited a profound responsive behavior and their surface wettability was altered upon immersion in different solvents such as TFT, HFiP and water. The symmetric diblock copolymers could not undergo a rearrangement of their chains to expose the solvent soluble block at the free surface of the film, whereas the re-arrangement took place at higher contents of the inner PDMAEMA block. In addition, it was shown that quaternization of the amine groups of the responsive diblock copolymer brushes, deteriorated their responsiveness. This was attributed to the larger $\chi$ value between the two blocks after quaternization, due to the presence of two very dissimilar polymers, charged PQDMAEMA and fluorinated PTFEMA, POFPMA or PTDFOMA chains which leads to phase separation with both polymers being present at the polymer-air interface. Finally, the stability of the amphiphilic diblock copolymer brushes depends on the charge density along the polymer chains with the PQDMAEMA brushes undergoing significant degrafting in the first 7 days in water, whereas the non-quaternized analogues were stable for the first 14 days and exhibited significant degrafting between day 15 and 30 in the aqueous medium.

## 4.4 References

1. (a) Stuart, M. A. C.; Huck, W. T. S.; Genzer, J.; Muller, M.; Ober, C.; Stamm, M.; Sukhorukov, G. B.; Szleifer, I.; Tsukruk, V. V.; Urban, M.; Winnik, F.; Zauscher, S.; Luzinov, I.; Minko, S., Emerging applications of stimuli-responsive polymer materials. *Nat Mater* **2010,** *9* (2), 101-113; (b) Mendes, P. M., Stimuli-responsive surfaces for bio-applications. *Chemical Society Reviews* **2008,** *37* (11), 2512-2529.
2. Milner, S., Polymer brushes. *Science* **1991,** *251* (4996), 905-914.
3. Galvin, C. J.; Genzer, J., Applications of surface-grafted macromolecules derived from post-polymerization modification reactions. *Prog Polym Sci* **2012,** *37* (7), 871-906.
4. (a) Mizutani, A.; Kikuchi, A.; Yamato, M.; Kanazawa, H.; Okano, T., Preparation of thermoresponsive polymer brush surfaces and their interaction with cells. *Biomaterials* **2008,** *29* (13), 2073-2081; (b) Xu, F. J.; Zhong, S. P.; Yung, L. Y. L.; Kang, E. T.; Neoh, K. G., Surface-Active and Stimuli-Responsive Polymer−Si(100)

Hybrids from Surface-Initiated Atom Transfer Radical Polymerization for Control of Cell Adhesion. *Biomacromolecules* **2004,** *5* (6), 2392-2403.
5. (a) Khabibullin, A.; Mastan, E.; Matyjaszewski, K.; Zhu, S., Surface-Initiated Atom Transfer Radical Polymerization. In *Adv Polym Sci*, Vana, P., Ed. Springer International Publishing: 2016; Vol. 270, pp 29-76; (b) Edmondson, S.; Osborne, V. L.; Huck, W. T. S., Polymer brushes via surface-initiated polymerizations. *Chemical Society Reviews* **2004,** *33* (1), 14-22.
6. (a) Zhao, B.; Brittain, W. J., Synthesis, Characterization, and Properties of Tethered Polystyrene-b-polyacrylate Brushes on Flat Silicate Substrates. *Macromolecules* **2000,** *33* (23), 8813-8820; (b) Tomlinson, M. R.; Genzer, J., Formation and properties of multivariant assemblies of surface-tethered diblock and triblock copolymers. *Polymer* **2008,** *49* (22), 4837-4845.
7. Zhao, B.; Brittain, W. J.; Zhou, W. S.; Cheng, S. Z. D., Nanopattern formation from tethered PS-b-PMMA brushes upon treatment with selective solvents. *Journal of the American Chemical Society* **2000,** *122* (10), 2407-2408.
8. Matyjaszewski, K.; Miller, P. J.; Shukla, N.; Immaraporn, B.; Gelman, A.; Luokala, B. B.; Siclovan, T. M.; Kickelbick, G.; Vallant, T.; Hoffmann, H.; Pakula, T., Polymers at interfaces: Using atom transfer radical polymerization in the controlled growth of homopolymers and block copolymers from silicon surfaces in the absence of untethered sacrificial initiator. *Macromolecules* **1999,** *32* (26), 8716-8724.
9. (a) Hansen, N. M. L.; Jankova, K.; Hvilsted, S., Fluoropolymer materials and architectures prepared by controlled radical polymerizations. *European Polymer Journal* **2007,** *43* (2), 255-293; (b) Yao, W.; Li, Y.; Huang, X., Fluorinated poly(meth)acrylate: Synthesis and properties. *Polymer* **2014,** *55* (24), 6197-6211; (c) Chen, Y.; Chen, D.; Ma, Y.; Yang, W., Multiple levels hydrophobic modification of polymeric substrates by UV-grafting polymerization with TFEMA as monomer. *Journal of Polymer Science Part A: Polymer Chemistry* **2014,** *52* (8), 1059-1067.
10. Granville, A. M.; Boyes, S. G.; Akgun, B.; Foster, M. D.; Brittain, W. J., Synthesis and Characterization of Stimuli-Responsive Semifluorinated Polymer Brushes Prepared by Atom Transfer Radical Polymerization. *Macromolecules* **2004,** *37* (8), 2790-2796.
11. Discekici, E. H.; Anastasaki, A.; Kaminker, R.; Willenbacher, J.; Truong, N. P.; Fleischmann, C.; Oschmann, B.; Lunn, D. J.; Read de Alaniz, J.; Davis, T. P.; Bates, C. M.; Hawker, C. J., Light-Mediated Atom Transfer Radical Polymerization of Semi-Fluorinated (Meth)acrylates: Facile Access to Functional Materials. *J Am Chem Soc* **2017,** *139* (16), 5939-5945.
12. (a) Wu, H.-X.; Tan, L.; Yang, M.-Y.; Liu, C.-J.; Zhuo, R.-X., Protein-resistance performance of amphiphilic copolymer brushes consisting of fluorinated polymers and polyacrylamide grafted from silicon surfaces. *Rsc Adv* **2015,** *5* (16), 12329-12337; (b) Wu, H.-X.; Zhang, X.-H.; Huang, L.; Ma, L.-F.; Liu, C.-J., Diblock Polymer Brush (PHEAA-b-PFMA): Microphase Separation Behavior and Anti-Protein Adsorption Performance. *Langmuir* **2018,** *34* (37), 11101-11109; (c) Brittain, W. J.; Boyes, S. G.; Granville, A. M.; Baum, M.; Mirous, B. K.; Akgun, B.; Zhao, B.; Blickle, C.; Foster, M. D., Surface Rearrangement of Diblock Copolymer Brushes—Stimuli ResponsiveFilms. In *Surface-Initiated Polymerization II*, Jordan, R., Ed. Springer Berlin Heidelberg: Berlin, Heidelberg, 2006; pp 125-147.
13. Xu, C.; Wu, T.; Drain, C. M.; Batteas, J. D.; Fasolka, M. J.; Beers, K. L., Effect of Block Length on Solvent Response of Block Copolymer Brushes: Combinatorial Study with Block Copolymer Brush Gradients. *Macromolecules* **2006,** *39* (9), 3359-3364.

14. (a) Zhulina, E. B.; Singh, C.; Balazs, A. C., Self-Assembly of Tethered Diblocks in Selective Solvents. *Macromolecules* **1996,** *29* (25), 8254-8259; (b) Zhulina, E. B.; Singh, C.; Balazs, A. C., Forming Patterned Films with Tethered Diblock Copolymers. *Macromolecules* **1996,** *29* (19), 6338-6348.
15. Bhairamadgi, N. S.; Pujari, S. P.; van Rijn, C. J. M.; Zuilhof, H., Adhesion and Friction Properties of Fluoropolymer Brushes: On the Tribological Inertness of Fluorine. *Langmuir* **2014,** *30* (42), 12532-12540.
16. Zhao, B.; Brittain, W. J.; Zhou, W.; Cheng, S. Z. D., AFM Study of Tethered Polystyrene-b-poly(methyl methacrylate) and Polystyrene-b-poly(methyl acrylate) Brushes on Flat Silicate Substrates. *Macromolecules* **2000,** *33* (23), 8821-8827.

# Chapter 5

Binary mixed polymer brushes with tunable surface and friction properties

## 5.1 Introduction

Functional or "smart" materials have been attracting increased attention during the past decade.[1] The development of novel intelligent systems that can switch their surface properties, upon exposure to different stimuli, constitutes a prime demand. Stimuli-responsive surfaces with switchable properties including wettability, cell adhesion, and so on, have been developed, operating under the application of the solution temperature and pH, light irradiation, solvent treatment, electric and magnetic fields.[2] Among these stimuli, the solvent quality is the most frequently utilized, to switch the surface properties of polymer brush surfaces. Diblock copolymer and mixed polymer brushes have been prepared for the development of stimuli-responsive surfaces with potential use in several applications including switchable stabilization/destabilization of colloidal dispersions, gating of mass transport, sensors, biointerfaces, designing of superhydrophobic surfaces and coatings, surfaces with tuned adhesion and electrochemical devices.[3]

Tuning reversibly the friction of a surface by light, temperature, solvent, counter ions and electric field has been shown in the literature. Friction is a force that opposes the relative lateral motion of two solid surfaces in contact and constitutes a prime concern for energy loses and the mechanical deformation of materials. One way to reduce these side effects is the application of viscous liquid lubricants that combine properties such as low volatility, high chemical and thermal stability, anti-flammability, biocompatibility, etc. Polymer brush surfaces, as lubricating or hydrating layers have been introduced for industrial, technological and biological applications. Lubrication is related to the solvency of the polymer brushes, nevertheless, the presence of solvents as lubricants prohibtis the use of polymer brushes in systems or devices where liquids are excluded e.g. micro/nano electromechanical systems (MEMS/NEMS).[4] So far, physisorbed PTFE thin coatings are employed to reduce the adhesion and friction forces on these devices, nevertheless these coatings possess long term mechanical instability and low wear resistance.[5] Toward this direction, Bhairamadgi et al. introduced high dry lubrication layers with low adhesion and friction forces, by synthesizing homopolymer brushes that contain $CF_2$ and $CF_3$ fluoroalkyl groups on the side groups of each monomer unit.[6] Moreover, simulation studies indicated that indeed the presence of fluorine atoms on the polymer brushes induced a marked reduction in the frictional forces that occur in the dry state.[7] Binary mixed polymer brushes have been shown to

function as polymer surfaces with controllable and tunable dry friction and adhesion properties upon immersion in different good solvents.[8] Amphiphilic mixed brushes comprising PDMAEMA chains and perfluorinated alkane units would not only form surfaces with reduced friction forces in the dry state, but may also provide surfaces with tunable dry friction properties.

In this chapter, we report the synthesis of amphiphilic binary mixed polymer brushes comprising functional PDMAEMA chains and low-surface energy PTFEMA, POFPMA or PTDFOMA chains. The co-adsorption and step-wise methods were tested for the successful preparation of mixed SAMs from two ATRP initiator sites. First, the semi-fluorinated homopolymer chains were grafted from a pre-modified SAM on silicon substrates, via SI-ATRP. Next, the PDMAEMA chains were introduced via a second SI-ATRP process, to form the binary mixed brushes. We investigated the solvent-switchable surface properties of the brushes, such as wettability and friction, which are manipulated by the selective solvency of the binary amphiphilic mixed polymer brushes. Finally, the amphiphilic mixed polymer brushes show a remarkable stability in an aqueous environment. To the best of our knowledge, the mixed brush systems developed herein, comprise the first example reported in the literature, that reveal switchable friction properties with a shape memory functionality in the dry state.

## 5.2 Results and Discussion

### 5.2.1 Synthesis and self-assembly of the ATRP initiators and model mixed brush synthesis

#### 5.2.1.1 Synthesis of the "sacrificial" ATRP initiator

The model sacrificial initiator, 2-bromo-2-methyl-N-pentylpropanamide (BMPA), was prepared, since it possesses similar chemistry to the surface-bound and the free initiator, which has been shown to be significant for the correlation of the polymer grown from the surfaces to those formed in solution.[9] The synthetic approach followed for the preparation of the free amide initiator is outlined in Scheme 5.1. The successful synthesis and the purity of the molecule was verified by $^1$NMR spectroscopy in $CDCl_3$ (Figure 5.1). $^1$H NMR (300 MHz, $CDCl_3$): δ 6.76 (1H, s), 3.25 (2H, t), 1.96 (6H, s), 1.55 (2H, m), 1.35 (4H, m), 0.92 (3H, m). The presence of a peak at 0.14 ppm, attributed

to the proton of the amide group, evidences the successful reaction of amylamine with BIBB to form BMPA. Finally, the absence of any further peaks, attributed to the precursor molecules or possible side-products in the spectrum, defines the purity of the initiator.

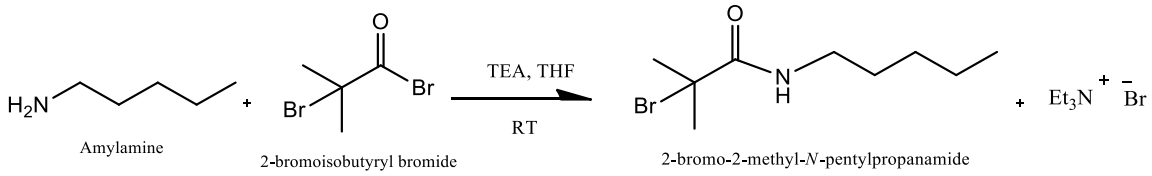


**Scheme 5.1.** Synthesis of the sacrificial initiator, 2-bromo-2-methyl-N-pentylpropanamide (BMPA), via an amidation reaction between amylamine and 2-bromoisobutyryl bromide.

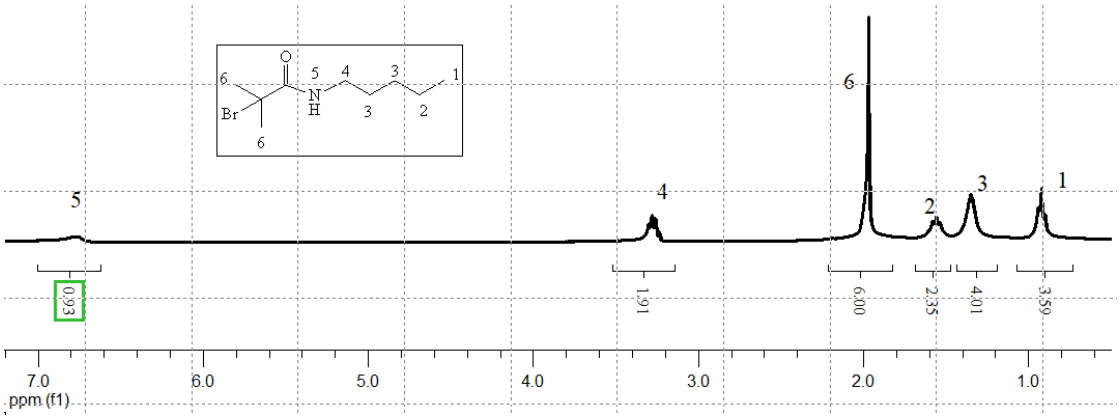


**Figure 5.1.** $^{1}$H NMR spectrum of BMPA in $CDCl_3$.

### 5.2.1.2 Mixed initiator SAMs and PMMA/PDMAEMA mixed polymer brush synthesis

For the synthesis of the binary mixed brushes via a two-step "grafting from" technique, monolayers comprising the ATRP initiator BIDS and the APDES precursor molecule were generated via the "co-adsorption" method, targeting the covalent binding of mixed silanes on the silicon surfaces, by condensation between their silanol groups (Scheme 5.2). According to the literature, the ratio of the grafted molecules is hypothesized to be similar to that in the solution mixture, when the two organosilanes have comparable size and are well mixed.[10] Mixtures of 100:0, 99:1, 90:0, 75:25, 50:50, 25:75 and 0:100

BIDS/APDES molar ratios in toluene at RT were used for the preparation of the mixed SAMs.

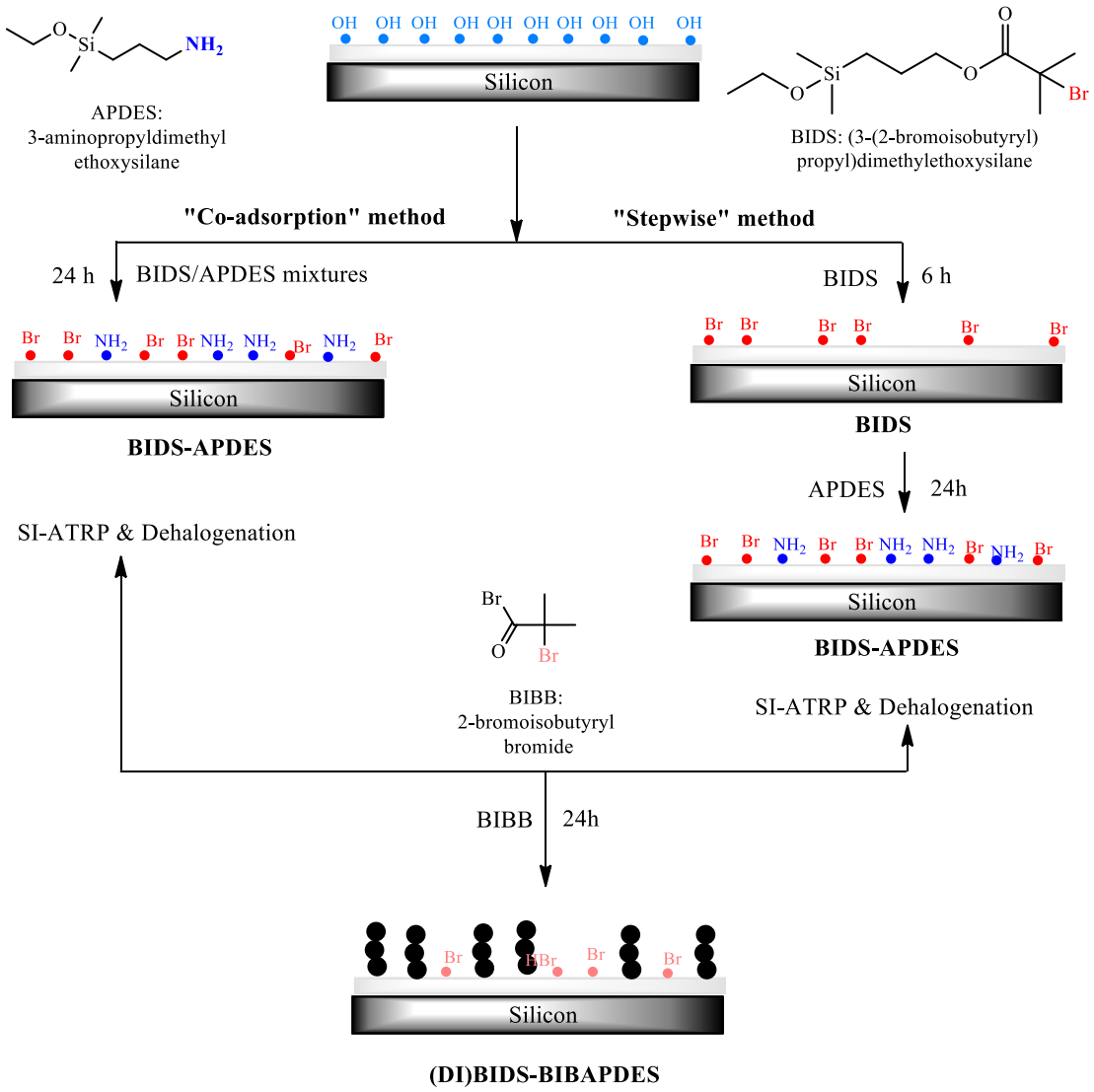


**Scheme 5.2.** Schematic representation of the synthetic approach followed for the preparation of the mixed ATRP initiator SAMs via the co-adsorption and the stepwise method.

When the mixed SAM was anchored on the silicon substrates, the binary mixed polymer brushes were synthesized via sequential SI-ATRP, as summarized in Scheme 5.3. MMA and DMAEMA were used for the synthesis of the mixed polymer brushes, in order to evaluate the different BIDS/APDES molar ratios used for the SAM

formation. The first polymer was grafted using SI-ATRP. Next, the terminal bromine atoms were removed by dehalogenation in order to avoid synthesizing diblock copolymer brushes and an ATRP initiator was again immobilized on the surface. Finally, the second polymer was grafted again by SI-ATRP.

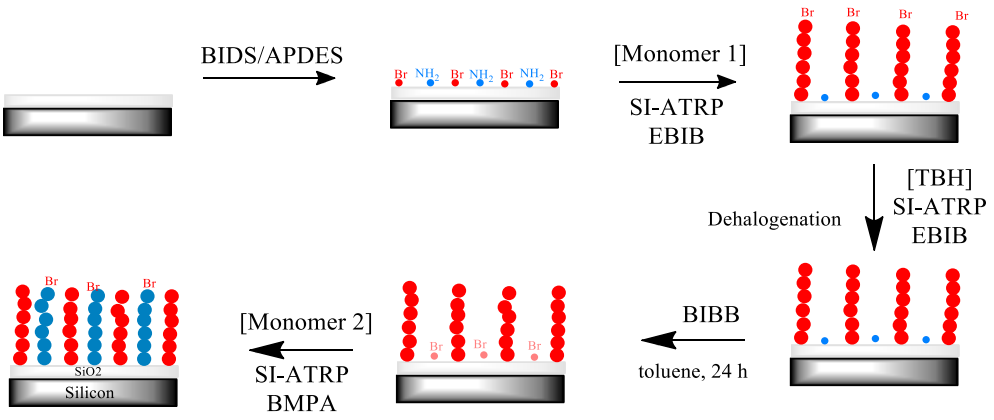


**Scheme 5.3.** Schematic illustration of the synthetic procedure followed for the preparation of the mixed polymer brushes by SI-ATRP from mixed silane modified silicon substrates.

The first grafted polymer was PMMA. The polymerization time was adjusted to prepare free PMMA chains with $M_n$ = 80,000 gr/mol in solution. This resulted in the preparation of a 57 nm thick polymer film for the substrates grafted with a 100:0 BIDS/APDES molar ratio. The grafting density of the polymer was calculated at 0.43 chains/nm$^2$. Mixed SAMs prepared using different molar ratios of BIDS/APDES were placed in the same reaction to grow the PMMA brushes. Table 5.1 summarizes the polymer brush thicknesses obtained in each case and the grafting density values calculated using the $M_n$ of the free polymer chains in solution. As seen, in the Table the immobilization of APDES decreased the PMMA film thickness from 24 to 9 nm with the decrease of the BIDS/APDES molar ratio from 99:1 to 25:75. This is obviously due to the decrease of the amount of active ATRP initiator on the surface for the SI-ATRP of MMA. Interestingly, the grafting density of the PMMA chains also decreased from 0.43 chains/nm$^2$ for the PMMA chains grafted from the 100:0 BIDS/APDES mole ratio to ~0.2 chains/nm$^2$ for 99:1 BIDS/APDES and then remained constant at ~0.10 chains/nm$^2$ for all other BIDS/APDES mole ratios. This clearly indicates that the anchoring of the BIDS and APDES molecules, does not depend solely on the feed ratio of the two compounds in the solution mixture, but a preferential anchoring of the

APDES molecules takes place possibly due to their smaller size compared to BIDS or their higher polarity, which renders their chemisorption on the silicon surface energetically favored.[11] This is expected to have a direct impact on the composition of the mixed PMMA/PDMAEMA brushes, after the second polymerization step, and therefore, the approach is not preferred for the synthesis of the mixed polymer brushes.

**Table 5.1.** Characteristics of the mixed PMMA/PDMAEMA brushes prepared by the co-adsorption and the stepwise method.

| moles BIDS | moles BIBAPDES | PMMA vol % | Thickness[a] (nm) | σ (chains/nm$^2$) | PDMA vol % | Thickness[b] (nm) | σ (chains/nm$^2$) | Thickness$_{mixed}$ (nm) | σ$_{mixed}$ (chains/nm$^2$) |
|---|---|---|---|---|---|---|---|---|---|
| 100 | 0 | 100 | 57 | 0.43 | 0 | 0 | - | 57 | 0.43 |
| 99 | 1 | 33 | 24 | 0.19 | 67 | 36 | 0.30 | 60 | 0.49 |
| 90 | 10 | 18 | 12 | 0.09 | 82 | 55 | 0.46 | 67 | 0.55 |
| 75 | 25 | 18 | 11 | 0.08 | 82 | 45 | 0.37 | 63 | 0.45 |
| 50 | 50 | 21 | 13 | 0.10 | 79 | 48 | 0.44 | 61 | 0.54 |
| 25 | 75 | 14 | 9 | 0.07 | 86 | 54 | 0.45 | 63 | 0.52 |
| 0 | 100 | 0 | - | - | 100 | 76 | 0.63 | 76 | 0.63 |
| **BIDS time (h)** | **BIBAPDES time (h)** | **PMMA vol %** | **Thickness[c] (nm)** | **σ (chains/nm$^2$)** | **PDMA vol %** | **Thickness[d] (nm)** | **σ (chains/nm$^2$)** | **Thickness$_{mixed}$ (nm)** | **σ$_{mixed}$ (chains/nm$^2$)** |
| 24 | 0 | 100 | 84 | 0.60 | 0 | - | - | 84 | 0.60 |
| 24 | 24 | 79 | 83 | 0.61 | 21 | 22 | 0.17 | 105 | 0.78 |
| 12 | 24 | 81 | 85 | 0.60 | 19 | 19 | 0.15 | 104 | 0.75 |
| **6** | **24** | **53** | **60** | **0.43** | **47** | **53** | **0.41** | **113** | **0.84** |
| 3 | 24 | 39 | 42 | 0.31 | 61 | 66 | 0.51 | 108 | 0.82 |
| 0 | 24 | 0 | - | - | 100 | 84 | 0.61 | 84 | 0.61 |

a: $M_n$ of free PMMA chains in solution 81,400 g/mol
b: $M_n$ of free PDMAEMA chains in solution 79,800 g/mol
c: $M_n$ of free PMMA chains in solution 86,200 g/mol
d: $M_n$ of free PDMAEMA chains in solution 83,700 g/mol

Despite the above observations, the terminal bromine atoms of the PMMA chains grafted from the surface, were removed using a dehalogenation reaction in order to prevent the formation of diblock copolymer brushes. The dehalogenation procedure was adopted by Ionov and Minko using tri(n-butyl)tin hydride (TBH) and a temperature of 130 ºC.[3b] TBH is known to deactivate the living PMMA chains, during the formation of radicals by the copper catalyst in SI-ATRP.

Next, the BIBAPDES ATRP initiator was synthesised on the surfaces, by the reaction of the free amino groups of APDES with BIBB. Along with the homopolymer brushes prepared in the first SI-ATRP, a silicon substrate modified with a 0:100 BIDS/APDES mole ratio was employed to form a BIBAPDES SAM. Next, the second SI-ATRP process commenced to grow the PDMAEMA chains from the surfaces. The reaction was adjusted again to prepare PDMAEMA chains with $M_n$ = 80,000 gr/mol in solution. Table 5.1 summarizes the thicknesses of the mixed polymer brushes and the PDMAEMA brushes (as the difference of the total thickness minus the thickness of the PMMA layer), the corresponding values of the grafting densities and the volume fractions of the PMMA and PDMAEMA chains, calculated using the dry polymer film thicknesses.

The successful synthesis of the binary mixed PMMA/PDMAEMA brushes was verified by the increase in the film thickness after the second SI-ATRP step from 36 nm up to 54 nm. The PMMA homopolymer brushes, grafted from the 100:0 BIDS/APDES SAM verified that the dehalogenation reaction was successful, since the dry film thickness of this brush did not change after the second polymerization step. The preparation of a 76 nm thick polymer film was obtained for the substrate grafted with the 0:100 BIDS/BIBAPDES molar ratio, from which the grafting density was calculated at 0.63 chains/nm$^2$ which is higher compared to the grafting density of the BIDS-anchored substrates (0.43 chains/nm$^2$). Moreover, the grafting densities for all mixed brushes after the second polymerization varied was calculated between 0.45 and 0.55 chains/nm$^2$, which are significantly higher than the values calculated for the respective homopolymer brushes after the first polymerization step, suggesting the synthesis of the mixed polymer chains on the surface.

The volume fractions of the PMMA chains were calculated by the ratio of the dry thickness of PMMA brushes, after the first SI-ATRP of MMA from the mixed initiator

modified surfaces, to the thickness of the final mixed brush, measured after the second SI-ATRP of DMAEMA. Nevertheless, in all cases the fraction of the PDMAEMA chains was higher compared to the PMMA chains, which indicates that indeed BIBAPDES is preferentially anchored on the substrates compared to BIDS initiator. These results suggest that the preparation of 50:50 mixed PMMA/PDMAEMA brushes, employing the co-adsorption of BIDS and APDES molecules is complicated, due to the faster absorption kinetics of the APDES moieties.

To evade the above problem, the "stepwise" method, for the immobilization of the ATRP initiating sites on the surface, was used (Scheme 5.3).[12] In this approach, freshly cleaned substrates, using a piranha solution, were immersed in a 2% v/v solution of the BIDS initiator for a predetermined period of time, followed by a second immersion in a 2% v/v solution of the APDES molecules, aiming to fill the gaps of the first monolayer deposition. A qualitative analysis of the silanization process can be made by comparing the thickness and the wettability of the samples after each immersion step in the saline solution. Following the first SAM formation, WCA values of 80º were measured and a thin layer of 1.5 nm was formed, which denotes that the hydrophobic initiator was successfully grafted onto the silicon substrates. Next, upon the deposition of the second silane (APDES), a decrease of the WCA to 71º was found, suggesting the adsorption of the polar APDES moieties on the substrate. It is noted that the WCA of 71º is intermediate between the value for the pure APDES and BIDS SAMs (64º and 80º, respectively), verifying the mixed SAM formation. Moreover, a small increase in the film thickness to 1.6 nm was measured after the second immersion step, however, the difference is within the error bar of the measurements, and therefore, cannot justify the mixed SAM formation.

Next, a similar sequential SI-ATRP process of MMA and DMAEMA commenced with an intermediate dehalogenation step, as described above. The data for the mixed polymer brushes prepared are summarized in Table 5.1.

Again, the first grafted polymer was PMMA. Well-defined PMMA homopolymer brushes, were successfully prepared from the BIDS-APDES modified silicon substrates, with $M_n$=86,200 gr mol$^{-1}$ in solution and corresponding dry thickness of 84 nm for the substrates immersed for 24 h in BIDS. The grafting density of the polymer was calculated at 0.60 chains/nm$^2$. Mixed SAMs prepared using different immersion

times first in BIDS and then in APDES were placed in the same reaction to grow the PMMA brushes. Table 5.1 summarizes the polymer brush thicknesses obtained in each case and the grafting density values calculated using the $M_n$ of the free polymer chains in solution.

The thicknesses obtained for SAM's formed by immersion at 3, 6, 12 and 24 h in BIDS, followed by immersion in APDES for 24 h, were 42, 60, 85 and 83 nm, respectively. It is obvious that the PMMA film thickness remained constant at ~84 nm with the substrates immersed in BIDS above 12 h. Decreasing the immersion time to 3 and 6 h in BIDS, the PMMA film thickness decreased up to 42 nm. This clearly indicates that the anchoring of BIDS was less, implying the anchoring of both BIDS and APDES molecules following immersion of the BIDS functionalized substrates in APDES for 24 h. Similarly, the grafting density of the PMMA chains remained constant for immersion times 12:24 h BIDS/APDES and 24:24 h BIDS/APDES, followed by a decrease from ~0.6 chains/nm$^2$ to ~0.3 chains/nm$^2$ for 3:24 h BIDS/APDES.

Again, the terminal bromine atoms of the PMMA chains grafted from the surface, were removed using a dehalogenation reaction in order to prevent the formation of diblock copolymer brushes. The BIBAPDES ATRP initiator was synthesized on the surfaces, by the reaction of the free amino groups of APDES with BIBB. Along with the homopolymer brushes prepared in the first SI-ATRP, a silicon substrate modified with a 0:24 h BIDS/APDES was employed to form a BIBAPDES SAM.

Next, the second SI-ATRP process commenced to grow the PDMAEMA chains from the surfaces. The successful synthesis of the binary mixed PMMA/PDMAEMA brushes was studied by ellipsometry. An increase of the film thickness between 19 and 66 nm, after the second SI-ATRP process, was measured. An almost 50:50 PMMA/PDMAEMA brush was prepared from the substrate immersed in BIDS initiator for 6 h, followed by its immersion in APDES for 24h. Above 6 h for the first deposition of BIDS, polymer brushes of higher PMMA volume fractions were obtained, whereas for times lower than this threshold value produced brushes with higher PDMAEMA volume fractions.

Another interesting aspect emanates from the higher grafting densities of the mixed polymer brushes, ~0.8 chains/nm$^2$, compared to the grafting densities of the two homopolymer brushes synthesized from the single initiator SAM (~0.6 chains/nm$^2$).

This can be attributed to the different grafting coverage of BIDS or BIBAPDES, the conversion of APDES to BIBAPDES and the size exclusion volume of PMMA and PDMAEMA. It seems that for a fully covered BIDS SAM, after 24 h, the addition of APDES molecules results in an increase of the grafting density suggesting that the APDES molecules are more pervasive. However, for a fully covered APDES SAM, either the larger size of PDMAEMA or the lower conversion of APDES to BIBAPDES results in a lower grafting density.

### 5.2.2 Synthesis of binary semi-fluorinated mixed brushes

Scheme 5.3 shows the general procedure for the synthesis of the binary mixed PTFEMA/PDMAEMA, POFPMA/PDMAEMA and PTDFOMA/PDMAEMA brushes, carried out using sequential SI-ATRP. The "stepwise" method was utilized for the preparation of the mixed SAMs. After the deposition of BIDS for 6 h, followed by the immobilization of APDES for 24 h, the modified surfaces were studied by ellipsometry. The thickness of the SAM layer was found 1.5 nm.

Next, the binary semi-fluorinated mixed brushes were prepared by first polymerizing the fluorinated monomer (TFEMA, OFPMA or TDFOMA) by SI-ATRP followed by a second SI-ATRP process to grow the PDMAEMA chains, as described above for the PMMA/PDMAEMA brushes. Table 5.2 summarizes the characteristics of the prepared mixed polymer brushes. In all cases, homopolymer chains with molecular weights of 42,700 g/mol for PDMAEMA, 43,100 g/mol for PTFEMA and 43,900 g/mol for POFPMA, were synthesized, as assessed by SEC analysis of the free polymer chains in solution (Figure 5.2a). The molecular weight distributions were also low, below 1.3, suggesting good control of the polymerization reaction. PTDFOMA is insoluble in THF, and therefore, its molecular weight and molecular weight distribution could not be determined by GPC. Figure 5.2b shows the film thicknesses of the mixed PTFEMA/PDMAEMA, POFPMA/PDMAEMA and PTDFOMA/PDMAEMA brushes measured by ellipsometry after each polymerization step. After the first SI-ATRP process, thin film with thicknesses of about 10 nm were measured for the fluorinated homopolymer brushes. The grafting densities of the brushes were calculated ~0.20 chains/nm$^2$ for all systems. Following the second SI-ATRP of DMAEMA, the polymer

film thicknesses increased to 30, 28 and 26 nm for the mixed PTFEMA/PDMAEMA, POFPMA/PDMAEMA and PTDFOMA/PDMAEMA brushes, respectively (Figure 5.2b), indicating the successful formation of the mixed polymer brushes. The grafting densities increased from ~0.2 to 0.5 chains/nm$^2$, which also evidences the formation of mixed homopolymer brushes. The volume fraction of the fluorinated chains in the mixed brush was estimated around 30% (Figure 5.2c). This might be due to the different size or side group flexibility of the fluoro-methacrylates compared to MMA used in the control experiments (see previous section). Nevertheless, in Chapter 4 we showed that the optimum performance in terms of reversible wettability was found for the PDMAEMA-b-PTFEMA, PDMAEMA-b-POFPMA and PDMAEMA-b-PTDFOMA brushes with the lower content of fluoropolymer segments, since they are highly hydrophobic. Therefore, we decided to proceed with the investigation of the surface properties of these asymmetric binary mixed polymer brushes, whereas XPS measurements in the future would be highly advantageous to precisely determine the composition of the brushes.

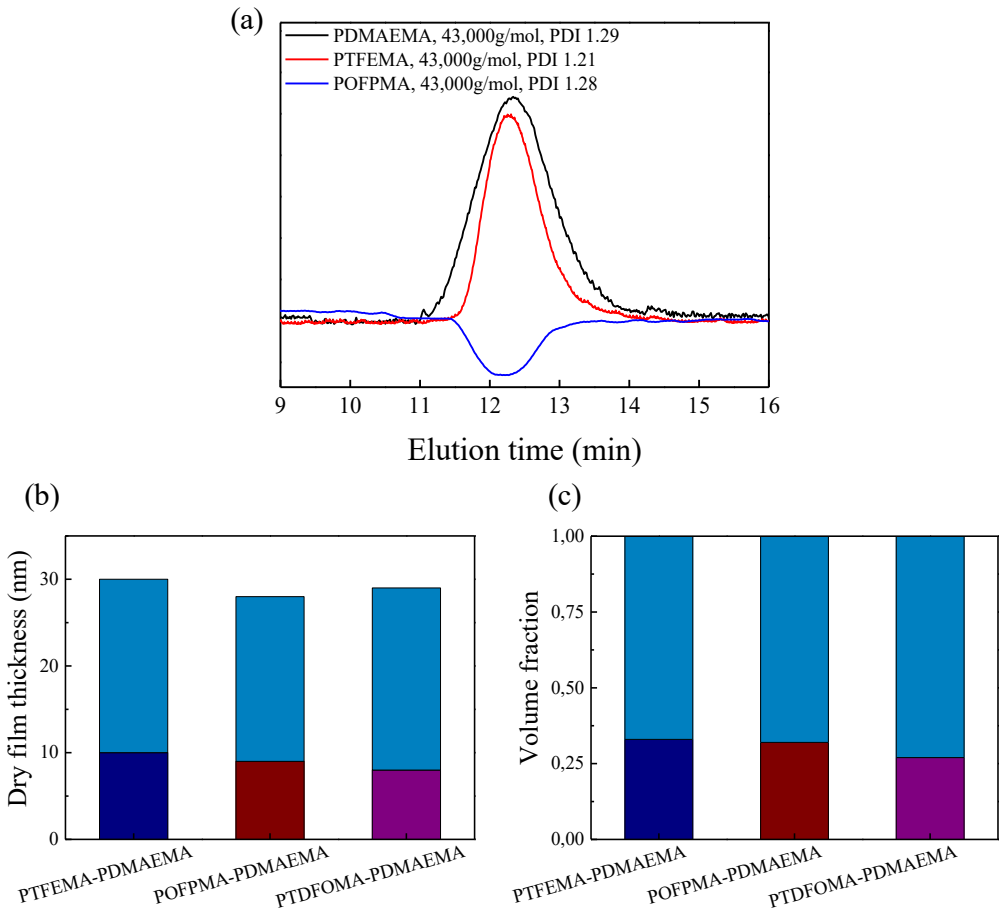


**Figure 5.2.** (a) SEC traces of the free PDMAEMA, PTFEMA and POFPMA chains obtained from the solution during the SI-ATRP process for the synthesis of the amphiphilic binary mixed brushes. (b) Film thicknesses and (c) volume fractions of the PTFEMA/PDMAEMA, POFPMA/PDMAEMA and PTDFOMA/PDMAEMA mixed brushes.

**Table 5.2.** Characterization data of the semi-fluorinated mixed polymer brushes.

| Sample | PFMA vol % | Thickness PFMA (nm) | σ (chains/nm$^2$) | Thickness PDMA (nm) | σ (chains/nm$^2$) | Thickness$_{mixed}$ (nm) | σ$_{mixed}$ (chains/nm$^2$) |
|---|---|---|---|---|---|---|---|
| PTFEMA-PDMAEMA | 33 | 10 | 0.20 | 20 | 0.31 | 30 | 0.51 |
| POFPMA-PDMAEMA | 32 | 9 | 0.20 | 19 | 0.29 | 28 | 0.49 |
| PTDFOMA-PDMAEMA | 27 | 7 | NA | 19 | 0.29 | 26 | 0.46 |

a: $M_n$ of free PDMAEMA chains in solution 42,700 g/mol
b: $M_n$ of free PTFEMA chains in solution 43,100 g/mol
c: $M_n$ of free POFPMA chains in solution 43,900 g/mol

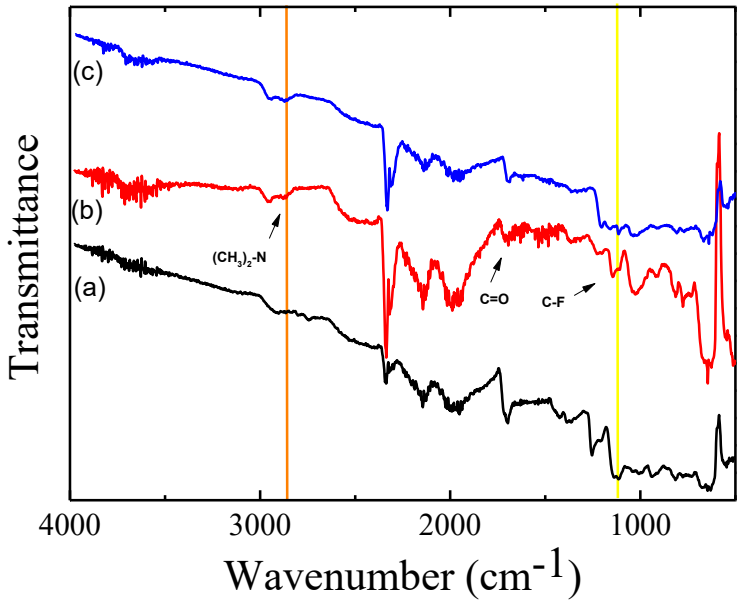


**Figure 5.3.** ATR-FTIR spectra of the (a) PTFEMA/PDMAEMA, (b) POFPMA/PDMAEMA and (c) PTDFOMA/PDMAEMA brushes. The vertical yellow line denotes the characteristic peak at 1131 $cm^{-1}$ attributed to the C-F stretching vibration, while the orange line depicts the peaks at 2852 $cm^{-1}$ attributed to the $(CH_3)_2$-N stretching vibration of PDMAEMA.

Qualitative confirmation of the presence of the end-grafted mixed brushes on the substrates was obtained by ATR-FTIR analysis. Representative spectra, presented in Figure 5.3, show the appearance of a characteristic peak at 1710 $cm^{-1}$, which corresponds to the C=O stretching vibration of the ester group, and the peaks at 2852, attributed to the $(CH_3)_2$-N symmetric and asymmetric stretching vibrations, proving the successful grafting of the PDMAEMA chains. The presence of a new characteristic peak at 1131 $cm^{-1}$, attributed to the bending frequency of the C-F bonds, verifies the successful synthesis of the PTFEMA/PDMAEMA, POFPMA/PDMAEMA and PTDFOMA/PDMAEMA mixed polymer brushes.

#### 5.2.2.1 Quaternization of the binary mixed polymer brushes

Quaternization of the PDMAEMA moieties of the PTFEMA/PDMAEMA, POFPMA/PDMAEMA and PTDFOMA/PDMAEMA mixed brushes was carried out by a post-polymerization reaction to convert the tertiary amine groups to their quaternary ammonium salt analogues. 1-Iodopropane was used as the quaternization agent in methanol at 50 ºC for 48 h.

**Table 5.3.** Characterization data of the quaternized semi-fluorinated mixed polymer brushes.

| Sample | PFMA vol % | Thickness PFMA (nm) | PQDMA vol % | Thickness PQDMA (nm) | $Thickness_{mixed}$ (nm) |
|---|---|---|---|---|---|
| PTFEMA-PQDMAEMA | 22 | 10 | 78 | 36 | 46 |
| POFPMA-PQDMAEMA | 21 | 9 | 79 | 33 | 42 |
| PTDFOMA-PQDMAEMA | 19 | 7 | 81 | 30 | 37 |

Table 5.3 summarizes the characteristics of the quaternized mixed polymer brushes. For all mixed brushes, an ~1.8-fold increase of the film thickness was measured after the quaternization reaction, which is attributed to the increase of the molecular weight of the DMAEMA monomer repeat units, as described in Chapter 3 for the PDMAEMA homopolymer brushes. The volume fraction of the fluorinated polymer chains therefore decreased to 22, 21 and 19%, for the PTFEMA/PDMAEMA, POFPMA/PDMAEMA and PTDFOMA/PDMAEMA brushes, respectively. The successful quaternization of the mixed brushes was also verified by CA measurements discussed below in Section 5.2.3.2.

### 5.2.3 Surface properties of the binary mixed polymer brushes

#### 5.2.3.1 Morphology of the mixed polymer brushes

Samples were conditioned in TFT (non-selective solvent) and were then exposed to a selective solvent, either HFiP (for the PTFEMA, POFPMA and PTDFOMA chains) or water (for the PDMAEMA chains), then dried under a nitrogen steam to freeze the conformation and were characterized by AFM and CA measurements. In the dry state, both the PTFEMA and PDMAEMA chains are collapsed and the morphology of the surface depends on the solvent treatment prior to the AFM measurement. The morphologies of the brushes were studied in tapping mode AFM. Topography and phase images were captured to assess changes on the morphological characteristics of the brushes upon solvent treatment. Studies on mixed polymer brushes have shown that the surface properties can be vastly changed upon treatment with selective solvents.[8, 13]

Figure 5.4 shows the characteristic AFM height images for the fluorinated mixed brushes after applying a single flattening procedure. After treatment with HFiP, which is a good solvent for PTFEMA and bad solvent for PDMAEMA, the PTFEMA/PDMAEMA brushes showed an increased RMS roughness (1.9 nm) (Figure 5.4a') but no discernible domain formation. No comparable domain formation was found also for the PTFEMA/PDMAEMA mixed brush after immersion in water, however lower RMS roughness was obtained (1.3 nm) (Figure 5.4a), possibly due to localization of the PDMAEMA chains at the outermost layer of the brush. Similar results were obtained for POFPMA/PDMAEMA and PTDFOMA/PDMAEMA mixed brushes with the roughness increasing up to 2.5 nm which however, still renders the surface as smooth.

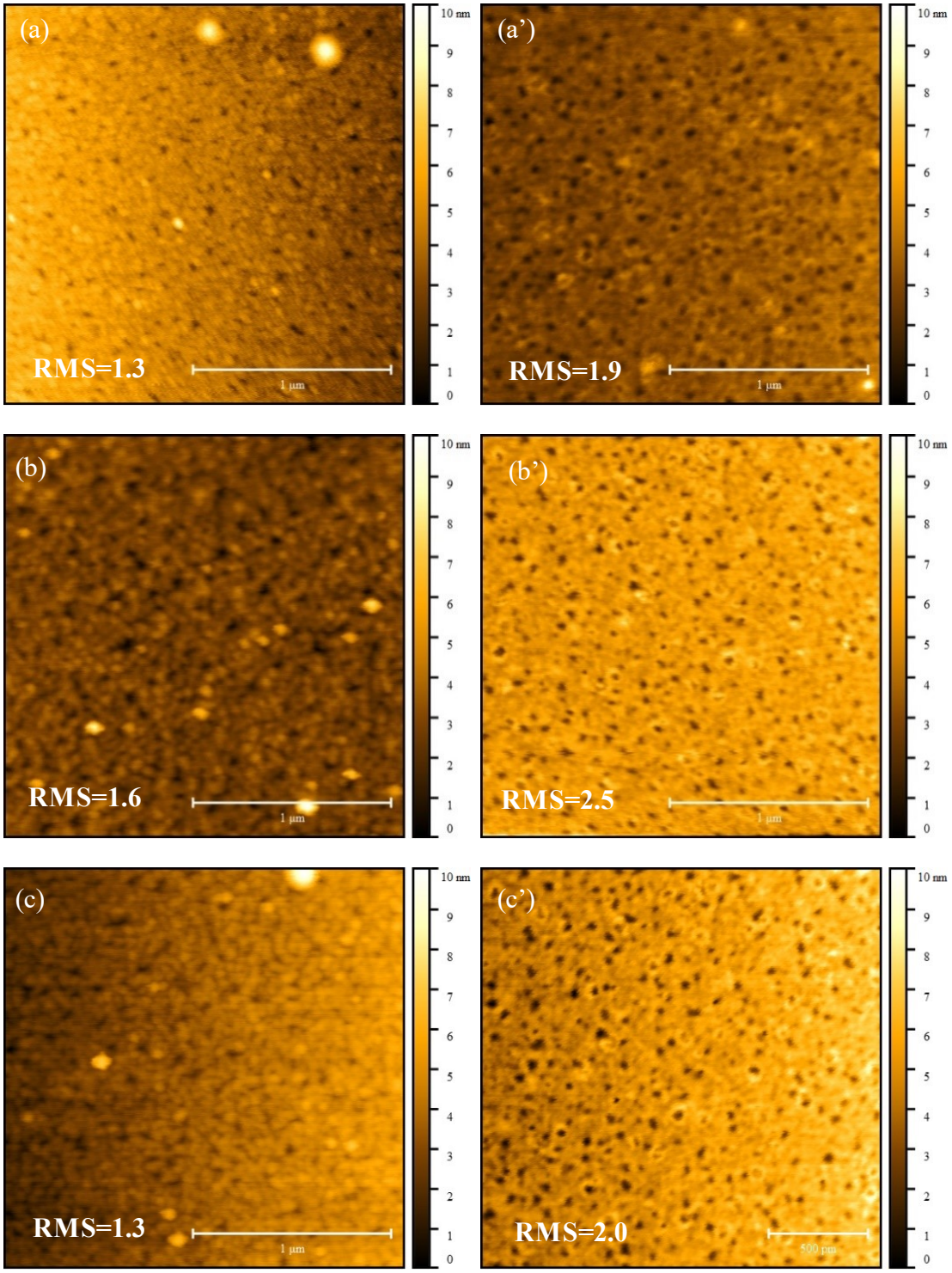


**Figure 5.4.** AFM height images of the PTFEMA/PDMAEMA, POFPMA/PDMAEMA and PTDFOMA/PDMAEMA mixed brushes after immersion in water (a,b,c) and HFiP (a',b',c'). Each image resembles an area of 2 × 2 $\mu m^2$. Scale bar: 1 µm, Z-scale bar: 0-10 nm.

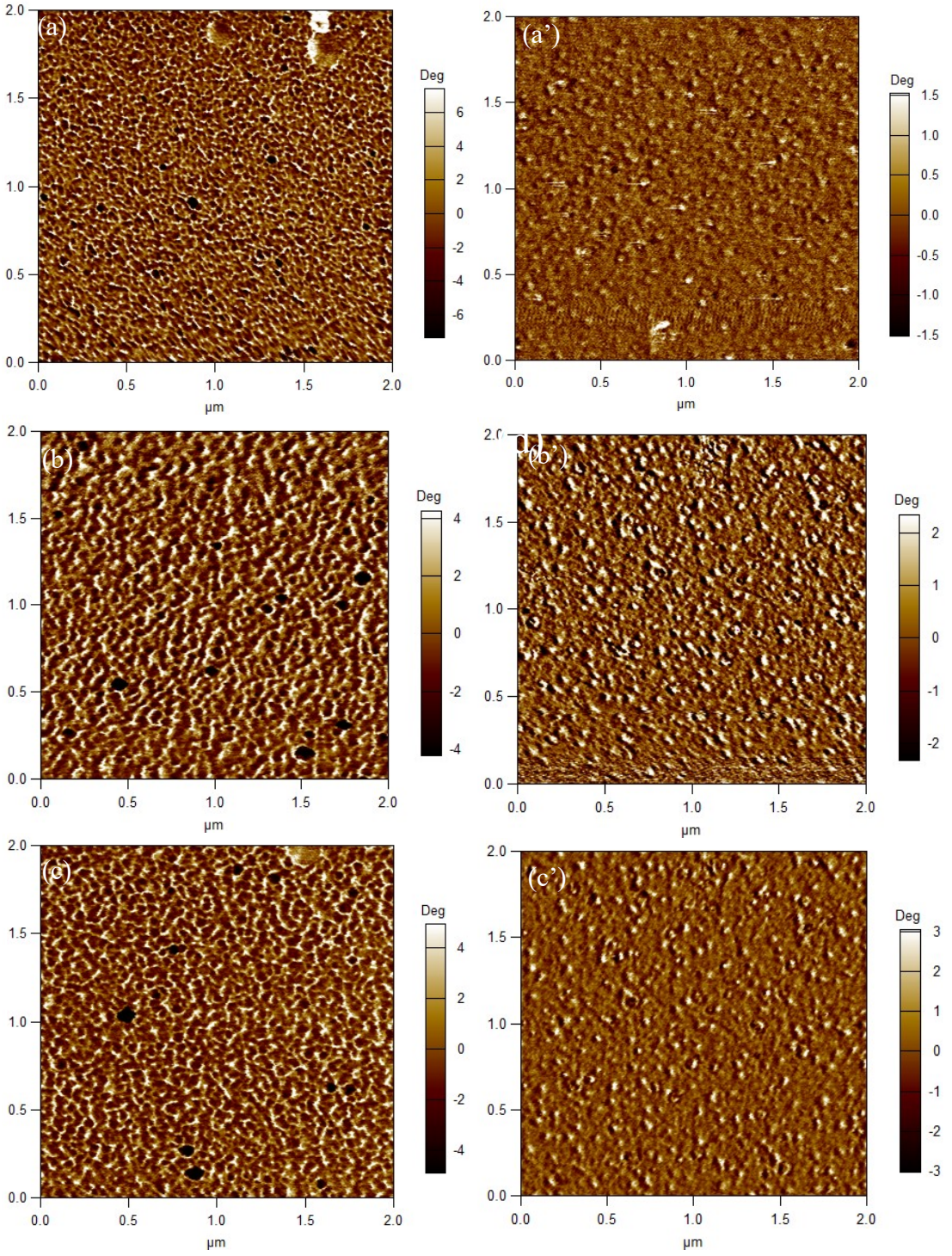


**Figure 5.5.** AFM phase images of the PTFEMA/PDMAEMA, POFPMA/PDMAEMA and PTDFOMA/PDMAEMA mixed brushes after immersion in water (a,b,c) and HFiP (a',b',c'). Each image resembles an area of 2 × 2 µm$^2$.

The lateral phase segregation upon treatment with a selective solvent is clearly visible in the AFM phase images of the brushes. Figure 5.5 shows the characteristic phase images of the PTFEMA/PDMAEMA, POFPMA/PDMAEMA and PTDFOMA/PDMAEMA mixed brushes. After HFiP treatment, a "dimple" brush morphology was obtained with bright and dark domains for all brushes, whereas treatment with water results in a stronger lateral segregation exhibiting a "ripple" brush elongated morphology. These changes in the domain size and the different microphase separation of the systems into two states, clearly support their switchable properties upon HFiP and water treatment. The switching between the morphologies can be reasoned to the stretching or shrinkage of the semi-fluorinated and PDMAEMA chains, that occurs to minimize the interfacial energy under the applied solvent exposure. In HFiP, the PTFEMA, POFPMA or PTDFOMA chains are swollen whereas the PDMAEMA chains are collapsed towards the silicon surface. Since the fluorinated polymer chains have higher affinity for HFiP, the as-depicted bright domains in the phase images are attributed to the hydrophobic polymer and the dark domains to the hydrophilic PDMAEMA which is insoluble in the fluorinated solvent. When the mixed brushes are immersed in water, the non-polar fluorinated chains will migrate towards the inner layer of the brush to avoid contact with water, and simultaneously the PDMAEMA chains will extent to cover the outer surface. Since the volume fraction of the PDMAEMA chains is higher in the brush, the PDMAEMA chains cover a broader area compared to the fluorinated polymer chains, and smoother surfaces with lower RMS roughness (from ~2 nm down to ~1.3 nm) are obtained in water. Moreover, a slightly increase in the domain size is observed for the POFPMA/PDMAEMA and PTDFOMA/PDMAEMA brushes after immersion in HFiP, compared to the PTFEMA/PDMAEMA mixed brushes. This may be attributed to the longer fluorocarbon side groups of POFPMA and PTDFOMA which exhibit a stronger segregation towards the outer brush surface upon immersion in the fluorinated solvent. The rippled and dimpled switching morphologies (Scheme 5.4) have been observed previously in other experimental and theoretical studies on stimuli-responsive mixed polymer brushes.[14] The dominant role of the interactions between the polymer chains and the solvent appears when the grafting density is moderate (< 1.0 chains/nm$^2$).[15]

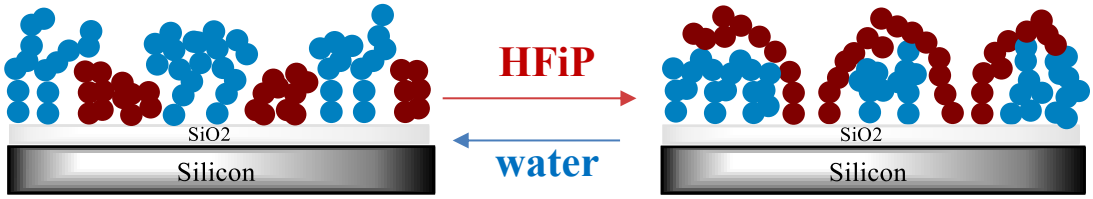


**Scheme 5.4.** Schematic representation of the observed changes in the surface morphology of the binary mixed brushes upon immersion in the two selective solvents, water and HFiP.

### 5.2.3.2 Wettability of the mixed brushes

The surface properties, such as the wettability, morphology and the surface charge are known to significantly affect the performance of substrates. To assess the surface wettability of the mixed polymer brushes the WCAs (Figure 5.6a,b,c) and the surface energies (Figure 5.6a',b',c') were measured.

The static WCAs were determined after each synthetic step taking place in a common solvent. The WCA increased significantly from 67º to 91º, after the SI-ATRP of TFEMA which is slightly lower than the WCA of the PTFEMA homopolymer brush (Figure 5.6a). Subsequent polymerization of DMAEMA decreased the WCA to 84º due to the hydrophilicity of PDMAEMA, but still the CA remained quite high. Quaternization of the PDMAEMA chains with propyl iodide induced a larger reduction in the WCA to 58º, which corresponds to a moderately hydrophilic surface. This indicates the surface hydration of the amphiphilic binary PTFEMA/PQDMAEMA brush, nevertheless, the WCA is much higher than that found for the corresponding PQDMAEMA homopolymer brush (42 º, see Chapter 3), which indicates the presence of hydrophobic moieties on the outer surface of the brush.

Similarly, the WCA increases to 107º after the synthesis of the POFPMA brush, and decreases slightly to ~93º after the formation of the mixed POFPMA/PDMAEMA brush (Figure 5.6b). Upon quaternization of the PDMAEMA chains, a relatively hydrophobic surface with WCA ~ 87º is obtained, which is ascribed to the presence of both the POFPMA and PQDMAEMA chains in the outermost surface of the brush. It is noted though that the WCA value is much higher than that corresponding to the PQDMAEMA homopolymer brush (42 º), indicating that the POFPMA chains play a

dominant role on the surface wettability of the mixed POFPMA/PQDMAEMA brushes covering mostly the outer surface. Finally, the WCA values of the mixed PTDFOMA/PQDMAEMA brush exhibit a similar behavior suggesting again that the PTDFOMA chains dominate the surface wettability (Figure 5.6c).

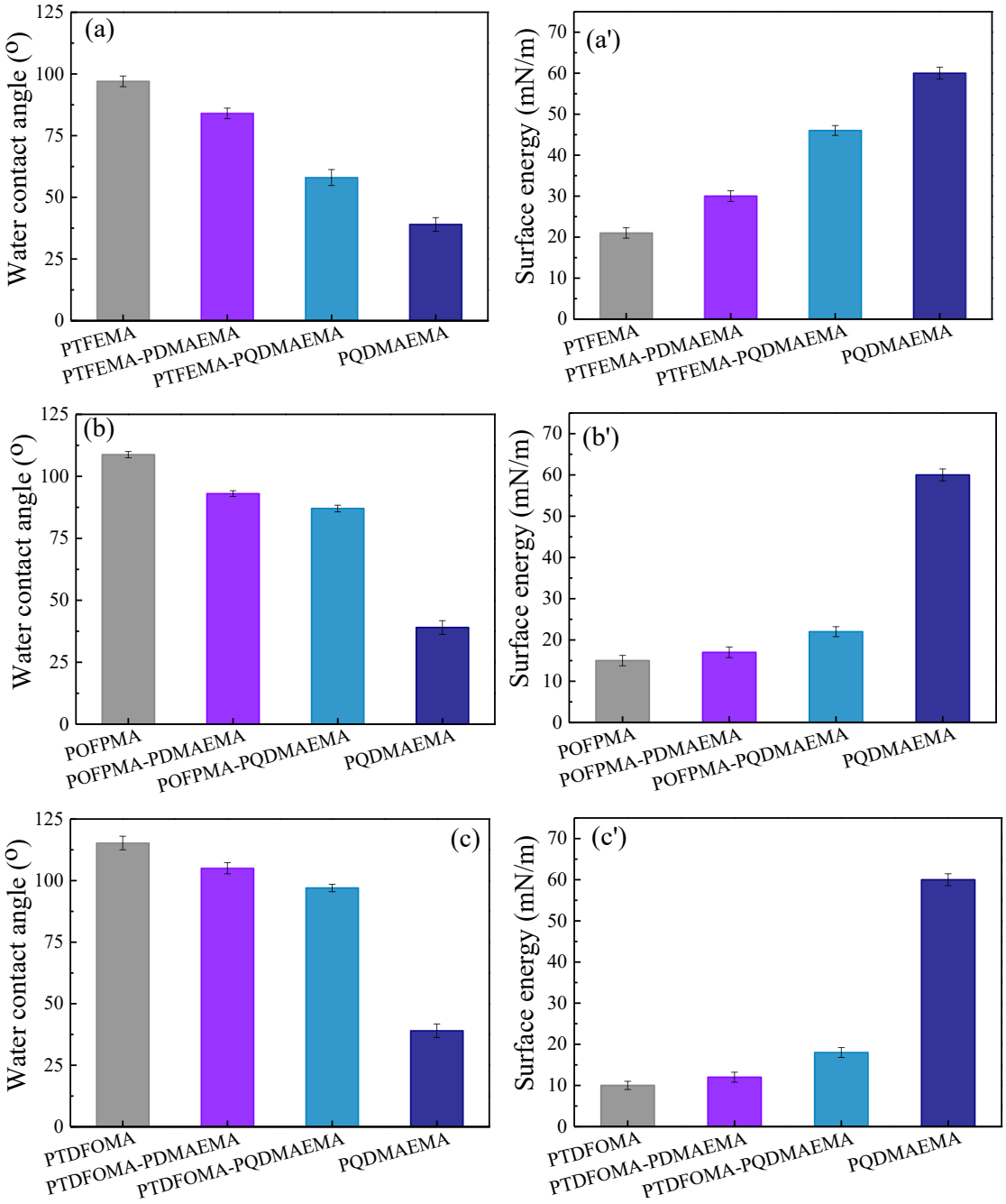


**Figure 5.6.** WCA (a,b,c) and surface energy (a',b',c') values of the (a) PTFEMA, PTFEMA/PDMAEMA, PTFEMA/PQDMAEMA and PQDMAEMA brushes, (b) POFPMA, POFPMA/PDMAEMA, POFPMA/PQDMAEMA and PQDMAEMA brushes, and (c) PTDFOMA, PTDFOMA/PDMAEMA, PTDFOMA/PQDMAEMA and PQDMAEMA brushes.

When the surface energy of the solid is comparable to that of the liquid, a transition from partial to complete wetting is observed thus surfaces with very low surface energies are difficult to wet. The surface energy values of the PTFEMA/PDMAEMA, POFPMA/PDMAEMA, and PTDFOMA/PDMAEMA brushes were calculated from the static CA measurements of two liquids, water and diiodomethane, using the OWRK method.[16] Figure 5.6a',b',c' depicts the surface energy values for all the mixed brushes synthesized in this work and the values of the respective homopolymer brushes (the surface energy of the silicon substrate after piranha solution was measured at 70 mN/m, which is similar to that of water at 72 mN/m). The PTFEMA, POFPMA and PTDFOMA homopolymer brushes prepared in the first SI-ATRP process, gave low surface energy values of 21, 15 and 10 mN/m, respectively, which are comparable to those of similar homopolymer brushes discussed in Chapter 3, indicating the formation of a non-polar brush layer. The surface energy value of the binary mixed PTFEMA/PDMAEMA brush increased to 30 mN/m, verifying the presence of the higher surface energy polymer. After quaternization the surface energy increased further to 46 mN/m for the PTFEMA/PQDMAEMA brush, which renders the polymer film a high surface energy material. On the other hand, the surface energy values of the mixed POFPMA/PQDMAEMA and PTDFOMA/PQDMAEMA brushes, remained low, between 19 – 25 mN/m, which verifies the presence of the long fluorinated alkyl chains at the air-polymer interface.

#### 5.2.3.3 Solvent-responsive wettability of the mixed polymer brushes

In order to examine the responsive wettability of the mixed polymer brushes, all samples were first immersed in TFT, which is a non-selective solvent for both the fluorinated and non-fluorinated polymer chains. Next, the polymer brushes were dried under a nitrogen atmosphere, were placed in a vacuum oven for 6 h and were subsequently characterized by static WCA measurements. WCAs of 84º, 93º and 105º were measured for the PTFEMA/PDMAEMA, POFPMA/PDMAEMA and PTDFOMA/PDMAEMA mixed brushes, respectively. These values are lower than the WCA values of the PTFEMA, POFPMA and PTDFOMA homopolymer brushes (97º,

109º and 115º), respectively and higher than the WCA of the PDMAEMA brush (~60º), suggesting that both the fluorinated polymer chains and the hydrophilic PDMAEMA are exposed on the surface of the film. Immersion of the PTFEMA/PDMAEMA, POFPMA/PDMAEMA and PTDFOMA/PDMAEMA brushes, for 6 h in HFiP (a good solvent for the fluorinated polymer chains and a bad solvent for the PDMAEMA chains), followed by drying under a nitrogen flow and thermal annealing at 80 °C for 1 h, resulted in a further increase of the WCA values at 95º, 108º and 111º, respectively, suggesting that the hydrophobic fluorinated chains have segregated at the free surface of the film. Next, the polymer films were soaked in nanopure water at RT for 18 h which induced the switching of the mixed brushes from hydrophobic into hydrophilic and a WCA lower than 60º was measured for all three brushes, suggesting that the hydrophilic PDMAEMA chains have migrated to the free surface. These results indicate that the polymer chains rearrange within the brush layer to expose the solvent-soluble block at the outer surface of the film, which is in good agreement with the morphological rearrangements discussed above by AFM. Moreover, the PTFEMA/PDMAEMA, POFPMA/PDMAEMA and PTDFOMA/PDMAEMA brushes were stable with controllable and reproducible wettability switching for at least 5 cycles (Figure 5.7a).

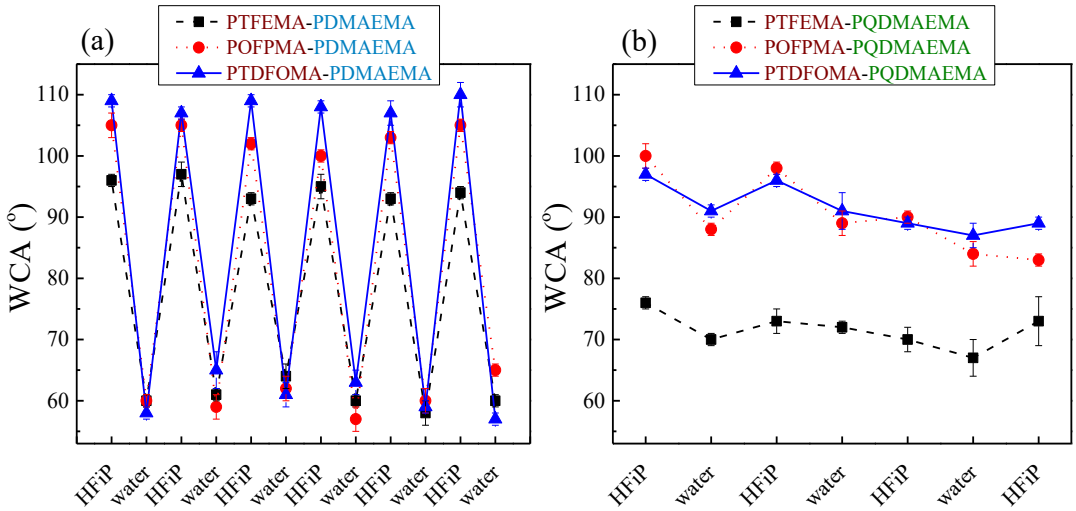


**Figure 5.7.** Static WCA values of the (a) PTFEMA/PDMAEMA (■, black), POFPMA/PDMAEMA (●, red) and PTDFOMA/PDMAEMA mixed brushes (▲, blue) and the (b) PTFEMA/PQDMAEMA (■, black), POFPMA/PQDMAEMA (●, red) and PTDFOMA/PQDMAEMA mixed brushes (▲, blue) quaternized with propyl iodide, upon successive immersion in HFiP and water.

Figure 5.7b shows the switching of the wettability of the quaternized mixed brush analogues. Surprisingly, the WCA values of the quaternized mixed brushes varied only by ~6-10º, for the first cycle, after which the switching property deteriorated.

Similar to the diblock copolymer brushes, discussed above, the increase in the χ value of the two polymers after quaternization is responsible for the incomplete polymer rearrangement.[17] In addition, the deterioration of the responsiveness of these brushes upon quaternization can be attributed to the loss of the flexibility of the polymer chains. Apparently, the quaternization reaction results in a further constrain of the two immiscible PQDMAEMA and PTFEMA or POFPMA or PTDFOMA chains, which is supported by the semi-crystallinity of the mixed brushes at RT.

### 5.2.4 Friction properties of the mixed polymer brushes

Surface forces that control friction play a significant role in the assembly, manipulation and operation of nanoscale devices or biological implants. AFM enables the quantitative probing of friction forces at the nanoscale, by measuring lateral friction forces at given normal applied loads. To evaluate the solvent-switchable friction of the mixed polymer brushes, we investigated the kinetic friction between an inorganic surface (silicon nitride AFM tip) and the mixed PTFEMA/PDMAEMA, POFPMA/PDMAEMA and PTDFOMA/PDMAEMA brushes sliding in contact mode. The friction-*vs*-normal applied load profiles recorded by LFM showed that after the first immersion in HFiP, a linear friction force was obtained for the PTFEMA/PDMAEMA, POFPMA/PDMAEMA and PTDFOMA/PDMAEMA brushes (Figure 5.8a). The COF values extracted from these plots were low, μ = 0.07, 0.06 and 0.05, respectively, but comparable to those of the homopolymer brushes (Figure 5.8b).

After immersion in water, the friction forces increased again linearly with the normal applied load, and the profiles demonstrated an increase in the friction between the mixed brushes and the silicon tip to μ=0.19, 0.19 and 0.23, respectively. This verifies the responsive reorientation of the polymer chains upon exposure to the two different selective solvent, and results in the switching of the frictional properties of the smart

mixed brushes. The reversible transition from a high to a low friction coefficient was proven upon immersion in HFiP again (Figure 5.8b). The nanotribological properties of the binary mixed brushes appear to be uniquely ruled by their exposure in different selective solvents, either HFiP for the fluorinated polymer chains or water for the PDMAEMA chains, which makes them excellent smart systems.

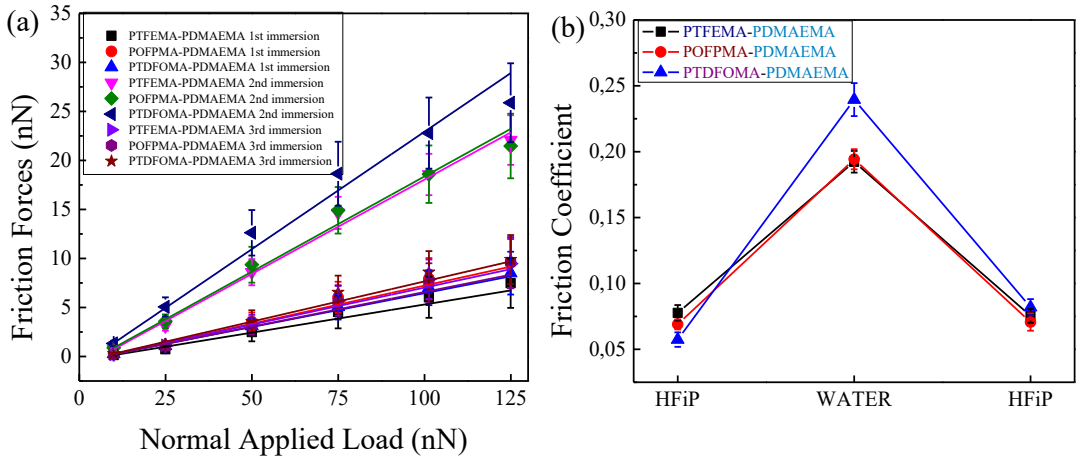


**Figure 5.8.** (a) Friction-versus-applied load profiles recorded by LFM on the PTFEMA/PDMAEMA, POFPMA/PDMAEMA and PTDFOMA/PDMAEMA brushes. The plots were recorded while applying a normal load between 10 and 125 nN using a silicon tip with a spring constant of 0.25 N/m. (b) Friction coefficients of the PTFEMA/PDMAEMA (■, black), POFPMA/PDMAEMA (●, red) and PTDFOMA/PDMAEMA (▲, blue) brushes upon immersion in HFiP, water and HFiP again.

### 5.2.5 Stability of the semi-fluorinated mixed polymer brushes

Poor stability of polyelectrolyte brush layers has been reported in water. In the presence of ppm of water highly solvated polymer brushes are subjected to osmotic forces that can catalyze the degrafting of the polymer chains due to hydrolysis or other chemical degradation of the surface anchoring groups. This drawback limits the potential applications of polymer brushes in engineering fields. To address this problem, a novel synthetic strategy proposes the formation of a barrier for the water molecules to access the substrate-polymer interface, thus improving the structural stability of the brush-coatings.[18]

The stability of the amphiphilic mixed polymer brushes in an aqueous environment was examined via ellipsometry. Figure 5.9a shows the dry thicknesses of the mixed PTFEMA/PDMAEMA, POFPMA/PDMAEMA and PTDFOMA/PDMAEMA brushes as a function of immersion time in water. It is evident that no degrafting occured for at least 6 months, since the dry film thickness remained constant. The amphiphilic mixed brushes comprising PDMAEMA chains and perfluorinated alkane units provide fluorous confined spaces in water that prevent polymer degrafting. In addition, quaternization of the PDMAEMA chains to form the hydrophilic PQDMAEMA analogues, did not affect the stability of the brush in the aqueous medium, which clearly proves that the fluorinated polymer chains act as hydrophobic barriers under water, capable of protecting the labile initiator bonds (Scheme 5.5), in contrast to the fluorinated diblock copolymer brushes discussed in Chapter 4. The confined multi-chain aggregation of the perfluorinated polymers has been shown in water.[19] This behavior is very important for the use of the brushes in underwater applications.

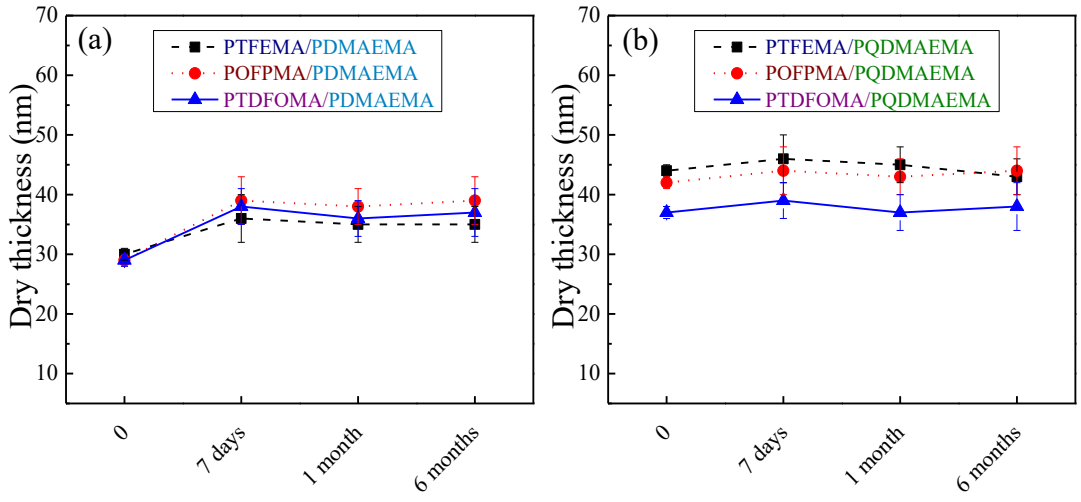


**Figure 5.9.** Ellipsometric dry thickness of the (a) PTFEMA/PDMAEMA (■, black), POFPMA/PDMAEMA (●, red) and PTDFOMA/PDMAEMA (▲, blue) and the (b) PTFEMA/PQDMAEMA (■, black), POFPMA/PQDMAEMA (●, red) and PTDFOMA/PQDMAEMA (▲, blue) brushes, quaternized with propyl iodide, as a function of the incubation time in water.

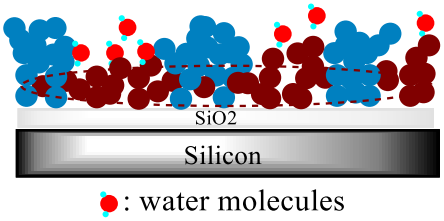


**Scheme 5.5.** Schematic representation of the brush structure under water.

## 5.3 Conclusions

Semi-fluorinated amphiphilic binary mixed brushes were synthesized by two sequential SI-ATRP steps from mixed-silane modified surfaces using TFEMA, OFPMA and TDFOMA as the fluorinated monomers and DMAEMA as a functional hydrophilic monomer. ATR-FTIR measurements confirmed the grafting of the polymer chains on the silicon and glass substrates, whereas water contact angle measurements were employed to assess the wettability of the polymer films, which was found to decrease as the fluorinated alkyl chain length of the monomer repeat units increased. Solvent-switchable surface properties (wettability, surface energy and friction) were shown for the amphiphilic mixed polymer brushes. An excellent reversible transition from a hydrophilic to a hydrophobic surface was found for all polymer brushes, following successive immersion in water and hexafluoroisopropanol (HFiP) (selective solvents for PDMAEMA and the fluorinated polymers, respectively) for at least 6 cycles. Rearrangement of the end-grafted homopolymer chains in the selective solvent medium induced the exposure of the solvent soluble moieties at the free film surface, and thus the change in the surface wettability and the surface energy, respectively exhibiting a responsive and shape-memory behavior. Moreover, the presence of the fluorocarbon side groups in the mixed polymer brushes introduced remarkable dry lubrication properties to the films. A reversible transition from low to high adhesion and friction forces, was observed, upon immersion of the films in HFiP and water, respectively. Quaternization of the DMAEMA units resulted in the loss of the responsiveness of the systems, however their surface energy values imply a compositional heterogeneity of their surface which may favor their use in non-fouling applications. Finally, the stability of the polymer films immersed in water over long time periods, was monitored by ellipsometry. A novel synthetic strategy is proposed to increase the stability of the

polyelectrolyte chains upon long-term exposure in water, by forming a fluorinated barrier for the water molecules to access the polymer-substrate interface. These surfaces with tunable wettability, friction and surface energy, in response to certain external stimuli, are significant for use in bio-nano-electronic devices, etc.

## 5.4 References

1. Mendes, P. M., Stimuli-responsive surfaces for bio-applications. *Chemical Society Reviews* **2008,** *37* (11), 2512-2529.
2. (a) Zeng, H.; Zhang, Y.; Mao, S.; Nakajima, H.; Uchiyama, K., A reversibly electro-controllable polymer brush for electro-switchable friction. *J Mater Chem C* **2017,** *5* (24), 5877-5881; (b) Zoppe, J. O.; Ataman, N. C.; Mocny, P.; Wang, J.; Moraes, J.; Klok, H.-A., Surface-Initiated Controlled Radical Polymerization: State-of-the-Art, Opportunities, and Challenges in Surface and Interface Engineering with Polymer Brushes. *Chemical Reviews* **2017,** *117* (3), 1105-1318.
3. (a) Barbey, R.; Lavanant, L.; Paripovic, D.; Schüwer, N.; Sugnaux, C.; Tugulu, S.; Klok, H.-A., Polymer Brushes via Surface-Initiated Controlled Radical Polymerization: Synthesis, Characterization, Properties, and Applications. *Chemical Reviews* **2009,** *109* (11), 5437-5527; (b) Ionov, L.; Minko, S., Mixed Polymer Brushes with Locking Switching. *Acs Appl Mater Inter* **2012,** *4* (1), 483-489.
4. Palacio, M.; Bhushan, B., Ultrathin wear-resistant ionic liquid films for novel MEMS/NEMS applications. *Adv Mater* **2008,** *20* (6), 1194-+.
5. (a) Doms, M.; Feindt, H.; Kuipers, W. J.; Shewtanasoontorn, D.; Matar, A. S.; Brinkhues, S.; Welton, R. H.; Mueller, J., Hydrophobic coatings for MEMS applications. *J Micromech Microeng* **2008,** *18* (5); (b) Biswas, S. K.; Vijayan, K., Friction and Wear of Ptfe - a Review. *Wear* **1992,** *158* (1-2), 193-211.
6. (a) Bhairamadgi, N. S.; Pujari, S. P.; Leermakers, F. A. M.; van Rijn, C. J. M.; Zuilhof, H., Adhesion and Friction Properties of Polymer Brushes: Fluoro versus Nonfluoro Polymer Brushes at Varying Thickness. *Langmuir* **2014,** *30* (8), 2068-2076; (b) Bhairamadgi, N. S.; Pujari, S. P.; van Rijn, C. J. M.; Zuilhof, H., Adhesion and Friction Properties of Fluoropolymer Brushes: On the Tribological Inertness of Fluorine. *Langmuir* **2014,** *30* (42), 12532-12540.
7. Uehara, S.; Liu, Z. M.; Xu, J. X.; Ootani, Y.; Ozawa, N.; Kubo, M., Effect of Fluorination on Friction Forces between Concentrated Polymer Brushes in the Dry State: All-atom Molecular Dynamics Simulation Study. *Chem Lett* **2018,** *47* (6), 784-786.
8. Vyas, M. K.; Schneider, K.; Nandan, B.; Stamm, M., Switching of friction by binary polymer brushes. *Soft Matter* **2008,** *4* (5), 1024-1032.
9. (a) Nomura, A.; Okayasu, K.; Ohno, K.; Fukuda, T.; Tsujii, Y., Lubrication Mechanism of Concentrated Polymer Brushes in Solvents: Effect of Solvent Quality and Thereby Swelling State. *Macromolecules* **2011,** *44* (12), 5013-5019; (b) Watson, S.; Nie, M.; Wang, L.; Stokes, K., Challenges and developments of self-assembled monolayers and polymer brushes as a green lubrication solution for tribological applications. *Rsc Adv* **2015,** *5* (109), 89698-89730; (c) Yamamoto, S.; Ejaz, M.; Tsujii, Y.; Fukuda, T., Surface Interaction Forces of Well-Defined, High-Density Polymer

Brushes Studied by Atomic Force Microscopy. 2. Effect of Graft Density. *Macromolecules* **2000,** *33* (15), 5608-5612.
10. Fu, Y.; Yang, Y.; Xiao, S.; Zhang, L.; Huang, L.; Chen, F.; Fan, P.; Zhong, M.; Tan, J.; Yang, J., Mixed polymer brushes with integrated antibacterial and antifouling properties. *Progress in Organic Coatings* **2019,** *130*, 75-82.
11. Sui, X.; Zapotoczny, S.; Benetti, E. M.; Memesa, M.; Hempenius, M. A.; Vancso, G. J., Grafting mixed responsive brushes of poly(N-isopropylacrylamide) and poly(methacrylic acid) from gold by selective initiation. *Polym Chem-Uk* **2011,** *2* (4), 879.
12. (a) Choi, I.; Kim, Y.; Kang, S. K.; Lee, J.; Yi, J., Phase Separation of a Mixed Self-Assembled Monolayer Prepared via a Stepwise Method. *Langmuir* **2006,** *22* (11), 4885-4889; (b) Feng, J.; Xu, G. H.; An, Y.; Zeng, X., Construction of the homogeneously mixed SAM composed of octyltriethoxysilane and octadecyltrichlorosilane by taking advantage of the molecular steric restriction. *Colloids and Surfaces A: Physicochemical and Engineering Aspects* **2008,** *316* (1), 194-201.
13. (a) Vyas, M. K.; Nandan, B.; Schneider, K.; Stamm, M., Nanowear studies in reversibly switchable polystyrene-poly(acrylic acid) mixed brushes. *J Colloid Interf Sci* **2008,** *328* (1), 58-66; (b) Lemieux, M.; Usov, D.; Minko, S.; Stamm, M.; Shulha, H.; Tsukruk, V. V., Reorganization of Binary Polymer Brushes: Reversible Switching of Surface Microstructures and Nanomechanical Properties. *Macromolecules* **2003,** *36* (19), 7244-7255.
14. (a) Price, A. D.; Hur, S.-M.; Fredrickson, G. H.; Frischknecht, A. L.; Huber, D. L., Exploring Lateral Microphase Separation in Mixed Polymer Brushes by Experiment and Self-Consistent Field Theory Simulations. *Macromolecules* **2011,** *45* (1), 510-524; (b) Messerschmidt, M.; Janke, A.; Simon, F.; Hanzelmann, C.; Riske, T.; Stamm, M.; Raether, B.; da Costa e Silva, O.; Uhlmann, P., Fluorocarbon-Free Dual-Action Textile Finishes Based on Covalently Attached Thermoresponsive Block Copolymer Brush Coatings. *Acs Appl Mater Inter* **2018,** *10* (46), 40088-40099.
15. Wang, L.; Zhong, T.; Quan, X.; Zhou, J., Solvent-responsiveness of PS–PEO binary mixed polymer brushes: a coarse-grained molecular dynamics study. *Molecular Simulation* **2017,** *43* (13-16), 1322-1330.
16. Owens, D. K.; Wendt, R. C., Estimation of the surface free energy of polymers. *J Appl Polym Sci* **1969,** *13* (8), 1741-1747.
17. (a) Zhulina, E. B.; Singh, C.; Balazs, A. C., Self-Assembly of Tethered Diblocks in Selective Solvents. *Macromolecules* **1996,** *29* (25), 8254-8259; (b) Zhulina, E. B.; Singh, C.; Balazs, A. C., Forming Patterned Films with Tethered Diblock Copolymers. *Macromolecules* **1996,** *29* (19), 6338-6348.
18. Wang, J.; Klok, H.-A., Swelling-Induced Chain Stretching Enhances Hydrolytic Degrafting of Hydrophobic Polymer Brushes in Organic Media. *Angewandte Chemie International Edition* **2019,** *0* (0).
19. Koda, Y.; Terashima, T.; Sawamoto, M.; Maynard, H. D., Amphiphilic/fluorous random copolymers as a new class of non-cytotoxic polymeric materials for protein conjugation. *Polym Chem-Uk* **2015,** *6* (2), 240-247.

# Chapter 6

# Dual-functional antimicrobial surfaces: bacterial-contact killing and bacterial-releasing properties

## 6.1 Introduction

Life-threatening infectious diseases, due to the microbial contamination of surfaces, constitute a prime concern of the global public health, with major risks in food packaging and storage, water filtration-purification processes, household sanitation, agriculture and the biomedical field.[1] The widespread and injudicious use of antibiotics, to control the growth of bacteria, has resulted in antibiotic-resistant microorganisms that intensify the problem. Material scientists have focused on alternative methods to prevent the microbial contamination of surfaces, including the development of novel, contact-active, antimicrobial surfaces, which exert the killing of antibiotic-resistant bacteria by severe cell-wall distortion. The goal of these antimicrobial surfaces is to retard biofilm formation, and therefore inhibit the spread of microbial infections.

Among the various biocidal materials developed so far, cationic polymers, bearing quaternary ammonium salt moieties along the polymer chains, have been shown to exhibit high efficacy in preventing the growth of drug-resistant microbes. Such polymers act primarily as non-leaching biocides and constitute an ideal platform for the development of long lasting, contact-active bactericidal surfaces.[2] Electrostatic interactions between the anionic cell-wall of the bacteria and the quaternary ammonium groups of the polymers have been shown to induce severe cell membrane disruption, leading to the lysis of the cell.[3] A hypothesis that the quaternary ammonium salt groups possess a different mechanism of biocidal action when confined on surfaces, compared to that in solution, has been reported.[4] Major key factors, affecting the antimicrobial efficiency of these surface immobilized polymers, have been claimed to be either the polymer charge density or the alkyl chain length (ACL) of the cationic moieties or both.[5] The effect of the ACL of the cationic moieties on their antimicrobial properties in solution has been studied extensively, demonstrating that quaternary ammonium groups which bear alkyl chains with ten or more carbon atoms possess optimal bactericidal activity.[6] Nevertheless, studies considering the effect of the ACL of the quaternary ammonium groups on the contact-killing action of surface-grafted polymers are inconclusive so far.

In 2001, Tiller and coworkers, reported that poly(4-vinyl-N-alkylpyridinium bromide) brushes alkylated with 3, 4 and 6 carbon atoms exhibited higher bactericidal activity against both gram-positive and gram-negative bacteria strains compared to those functionalized with 8, 10, 12, and 16 carbon atoms.[7] Similarly, other studies have

employed shorter ACL to produce polymer surfaces with enhanced antimicrobial properties.[4b, 5a, 8] However, in 2013 Gozzellino et al.[9] reported that copolymer films of a diacrylic resin and 2-(dimethylamino)ethyl methacrylate (DMAEMA), quaternized with 16 carbon atoms, exhibited enhanced bactericidal activity compared to those quaternized with an alkyl halide with two carbon atoms. This finding was attributed to the fact, that longer alkyl chains can interact more strongly with the lipid cell wall and, therefore, destabilize more effectively the bacterial membrane. Since then, numerous studies have employed ammonium salt derivatives with longer ACL to obtain surfaces with superior biocidal performance.[10] Roy et al.[11] stated that an ACL of eight carbon atoms is ideal to maintain a hydrophilic/hydrophobic balance and a superior biocidal efficacy of cationic polymer brushes.

In another approach, the antibacterial potency of surfaces has been achieved by repelling the bacteria in the vicinity of the surface (antifouling). The antifouling property of polymer brushes was realized via negatively charged polymer chains for the electrostatic repulsion of the negatively charged bacteria, highly hydrophilic PEG-based surfaces for the steric repulsion of bacteria or polymers with intrinsic low surface energies for the hydrophobic repulsion of bacteria.

Overall, bactericidal activity can be realized either by bactericide-releasing or contact-killing antimicrobial surfaces or both.[12]

The first part of this Chapter investigates the influence of the ACL of the quaternization agent on the antimicrobial activity of well-defined, quaternized poly(DMAEMA) (PQDMAEMA) brushes. First, PDMAEMA chains were grown by surface-initiated atom transfer radical polymerization (SI-ATRP) on glass and silicon substrates, followed by post polymerization quaternization of the PDMAEMA brushes using alkyl halides of different ACL. The quaternization of the tertiary amine groups of PDMAEMA yields a strong polyelectrolyte brush with permanent cationic charges along the polymer chains and induces a potential antimicrobial action to the polymer.[8a-c, 10b, 13] Although quaternized PDMAEMA brushes have been examined as antimicrobial surfaces in the literature, to the best of our knowledge, a systematic study of the effect of the ACL (ranging from one to eighteen carbon atoms) of the quaternary ammonium salt moieties on the contact-active antibacterial activity of PQDMAEMA brushes has not been reported so far. In the second part, the influence of the fluorinated alkyl chain length (FCL) of semi-fluorinated methacrylate brushes on their bacterial-releasing properties is examined. PTFEMA, POFPMA and PTDFOMA brushes bearing

1, 4 or 6 fluorocarbon atoms on the side group, were synthesized via SI-ATRP on glass and silicon substrates. To the best of our knowledge, the effect of the FCL of the side group on the bacterial-releasing activity of the semi-fluorinated brushes has not been reported so far.

In the final part of this study, mixed PQDMAEMA and PTFEMA, POFPMA or PTDFOMA brushes were examined in terms of the antimicrobial behavior. The binary mixed brushes not only maintained the bactericidal character of the PQDMAEMA surfaces, but also endowed the surfaces with a bacterial release property as a result of the low surface energy of the PTFEMA, POFPMA or PTDFOMA chains.[14]

## 6.2 Results & discussion

### 6.2.1 Homopolymer brushes

#### 6.2.1.1 Surface accessible quaternary ammonium salt moieties

Previous studies have shown that the number of quaternary ammonium salt moieties present on a surface is a critical factor determining its antibacterial properties, and charge densities (CDs) above a critical threshold of $1\times10^{14}$ $N^+$ $cm^{-2}$ and surface charge densities (SCDs) above $1\times10^{13}$ $N^+$ $cm^{-2}$ are required for an antibacterial active surface.[5a, 15] The CDs and SCDs of the $PQDMAEMA_1$ brushes prepared in this work were calculated from the degrees of quaternization of the polymer brushes, by UV-Vis spectroscopy, using a colorimetric method based on fluorescent complexation, described in Chapter 3 (Table 6.1). The CDs ranged from $3\times10^{15}$ to $1\times10^{16}$ $N^+$ $cm^{-2}$ and the respective SCDs from $7\times10^{13}$ to $3\times10^{14}$ $N^+$ $cm^{-2}$ therefore, all the $PQDMAEMA_1$ brushes prepared in this work are expected to exhibit effective antibacterial action.[5a, 8a, 13a]

**Table 6.1.** Homopolymer brushes evaluated as antimicrobial surfaces

| Brush | Thickness (nm) | DQ (mol %) by UV-Vis | Charge density ($N^+$ $cm^{-2}$) | SCD ($N^+$ $cm^{-2}$) |
|---|---|---|---|---|
| $PDMAEMA_1$ | 24 | - | - | - |
| $PQDMAEMA_1$-C1 | 46 | 94 | $1\times10^{16}$ | $3\times10^{14}$ |
| $PQDMAEMA_1$-C2 | 43 | 78 | $9\times10^{15}$ | $2\times10^{14}$ |
| $PQDMAEMA_1$-C3 | 43 | 65 | $8\times10^{15}$ | $2\times10^{14}$ |
| $PQDMAEMA_1$-C6 | 40 | 48 | $6\times10^{15}$ | $1.5\times10^{14}$ |
| $PQDMAEMA_1$-C12 | 37 | 30 | $4\times10^{15}$ | $1\times10^{14}$ |
| $PQDMAEMA_1$-C16 | 36 | 29 | $4\times10^{15}$ | $1\times10^{14}$ |
| $PQDMAEMA_1$-C18 | 34 | 24 | $3\times10^{15}$ | $7\times10^{13}$ |
| PTFEMA | 14 | - | - | - |
| POFPMA | 15 | - | - | - |
| PTDFOMA | 12 | - | - | - |

#### 6.2.1.2 Bacterial contact-killing of the PQDMAEMA brushes

The antibacterial activity of the PQDMAEMA brushes was studied against both gram-negative (*E. coli*) and gram-positive (*B. cereus*) bacteria strains. So far, a reliable and effective protocol to evaluate the antimicrobial efficiency of bactericidal surfaces is lacking. Recently, van de Lagemaat and coworkers compared several different methods to assess the bactericidal activity of surfaces.[16] They concluded that, the most frequently used methods in the literature, determine the antibacterial efficacy against bacteria strains in the supernatant solution, while neglecting the surface itself, whereas, the combination of these antibacterial methods with the, often employed, LIVE-DEAD assay is not reliable because in many cases bacteria indicated as dead by the staining method, can form colonies and proliferate.[16-17] Therefore, FESEM or LIVE-DEAD staining gives only an indication of the membrane damage and safe conclusions on the bacterial cell death can only be drawn by culture-based assays.

Herein, the bactericidal activity of the polymer surfaces was quantified, in terms of log reduction of the number of viable bacteria colonies after contact with the polymer brush, by a plate counting method (PCM).[8b, 13a] It is noted, that the alive bacteria adhered very strongly onto the $PQDMAEMA_1$ brushes quaternized with short ACLs (C1-C3), via electrostatic interactions, and could not be desorbed even after extensive washing of the polymer surface (which may have resulted in the contradictory bactericidal results published in the literature), therefore, the substrates were completely wrecked to recover all bacteria and evaluate the actual bactericidal efficiency of the polymer brushes.

Figure 6.1 shows the logarithmic reduction in the number of bacteria for the two representative strains, as a function of the ACL of the quaternization agent, for the $PQDMAEMA_1$ brushes. The horizontal line denotes an effective bactericidal surface with a 99% or 2log reduction in the number of colony-forming units (CFU) at the bacterial challenge, with respect to control silicon surfaces. The non-quaternized $PDMAEMA_1$ brush showed minimal bactericidal activity, attributed to the protonation of a few tertiary amine groups of PDMAEMA ($pK_\alpha \sim 7.0$) at neutral pH, which induces some positively charged groups on the polymer surface. On the other hand, quaternization induced discrete antimicrobial activities to the $PQDMAEMA_1$ brushes (Figure 6.1). An enhanced, ~2-3log (99-99.9%) reduction, was found for the hydrophilic cationic polymer brushes (C1, C2, C3), while a very moderate decrease of <1log (<90%), similar to that observed for the PDMAEMA brush, was measured for the hydrophobic cationic brushes (C≥6) (Table 6.2). From these results, it becomes apparent that the ACL of the quaternary ammonium salt moieties of the PQDMAEMA brushes dominates the interactions of the cationic brushes with the bacteria cells. For long ACLs (C≥6), the efficient killing of the bacteria by the cationic polymer surface is significantly hindered because of the formation of a cumbersome hydrophobic barrier by the long alkyl substituents, which compromises the interactions between the positively charged moieties of the brush and the bacteria deposited on the surface. On the other hand, the quaternized polymer chains with short ACLs are freely mobile in the aqueous bacteria culture medium and their positively charged units can interact effectively with the negatively charged wall of the bacteria, resulting in the perforation and lysis of their membrane. Since the SCDs of all brushes were found above the required threshold value, the antibacterial performance of the brushes is dictated by the

accessibility of the cationic charges to the bacteria cell wall, which is affected by the surface wettability and the mobility of the cationic brushes in the aqueous medium.[18] The observed differences in the bacteria reduction for the two representative strains are attributed to the much-complicated cell membrane structure of the gram-negative microorganism, comprising an extra peptidoglycan layer, which seals a higher protection to the integrity of the bacteria structure.[19] From these results, we can conclude that the optimal ACL for the antimicrobial action of the $PQDMAEMA_1$ brushes is in the C1-C3 range, exhibiting a 99% and 99.9% reduction of the adhered viable *E. coli* and *B. cereus* bacteria, respectively, and we adopt the definition of "bactericidal cationic brushes" referring to hydrophilic PQDMAEMA brushes with short ACL (C1-C3), and "non-bactericidal cationic brushes" referring to the hydrophobic PQDMAEMA brushes with long ACLs (C≥6).

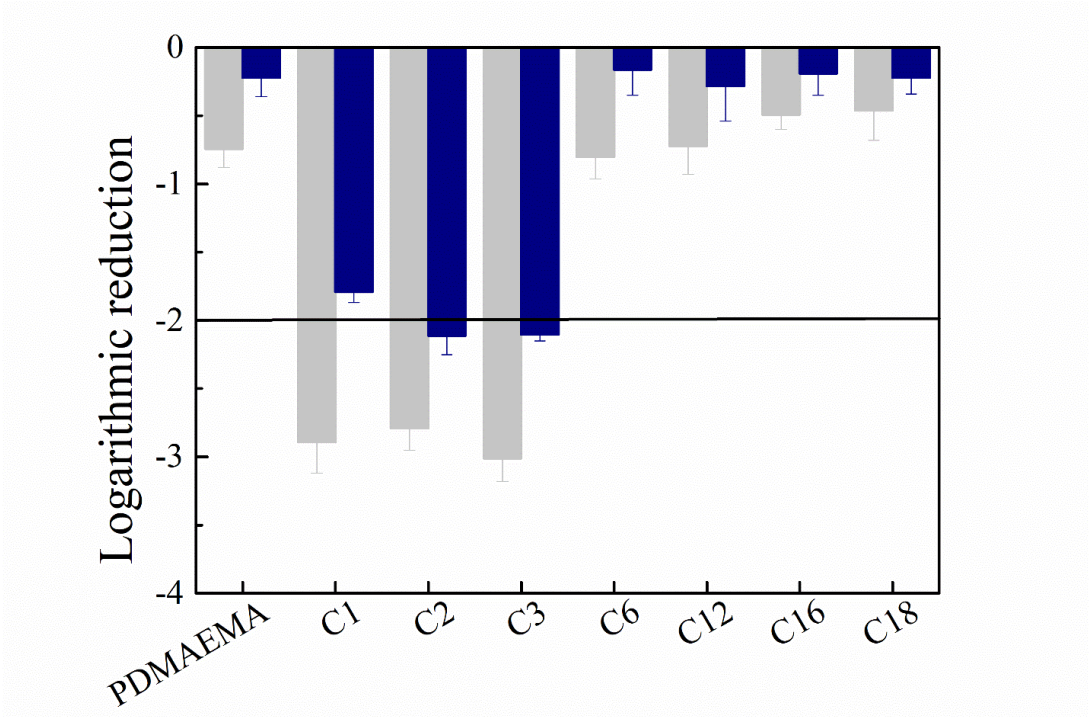


**Figure 6.1.** Bactericidal activity of the $PQDMAEMA_1$ brushes after 5 h contact with *B. cereus* (grey bars) and *E. coli* (blue bars) at 37 °C. Each bar represents the log reduction from 3 different experiments carried out in duplicates (mean ± SD). The black line denotes the minimum value for effective bactericidal action (2log reduction).

**Table 6.2.** Homopolymer brushes evaluated as antimicrobial surfaces

| Brush | %Bacterial-releasing | | %Contact-killing | |
|---|---|---|---|---|
| | *B. cereus* | *E. coli* | *B. cereus* | *E. coli* |
| $PDMAEMA_1$ | - | - | 81.8 | 40.4 |
| $PQDMAEMA_1$-C1 | - | - | 99.8 | 98.4 |
| $PQDMAEMA_1$-C2 | - | - | 99.7 | 99.2 |
| $PQDMAEMA_1$-C3 | - | - | 99.9 | 99.0 |
| $PQDMAEMA_1$-C6 | - | - | 77.1 | 31.7 |
| $PQDMAEMA_1$-C12 | - | - | 81.1 | 47.6 |
| $PQDMAEMA_1$-C16 | - | - | 67.7 | 36.5 |
| $PQDMAEMA_1$-C18 | - | - | 65.4 | 40.7 |
| $PTFEMA_3$ | 50.9 | 85.0 | - | - |
| $POFPMA_3$ | 99.5 | 91.8 | - | - |
| $PTDFOMA_3$ | 99.6 | 92.4 | - | - |

To elucidate further the antibacterial activity of the PQDMAEMA brushes, the adhesion and morphology of the bacteria incubated on the polymer surfaces (washed with PBS, but not wrecked) were examined by FESEM analysis.[20] Figure 6.2 shows characteristic FESEM images of the bacteria cells on the polymer surfaces. All quaternized and non-quaternized PDMAEMA brushes suffered from extensive bacterial adhesion, nevertheless with distinct antimicrobial action. A vast number of adherent bacteria were observed on the non-quaternized $PDMAEMA_1$ brush attributed to the high surface energy of the film which rendered the surface adhesive. On the other hand, the hydrophobic $PQDMAEMA_1$-C18 surface exhibited a lower number of adherent bacteria compared to the moderate hydrophilic $PDMAEMA_1$ brush, attributed to the lower surface energy of the film (see Figure 6.2c), which induces the removal of a large number of alive bacteria, upon washing with PBS.

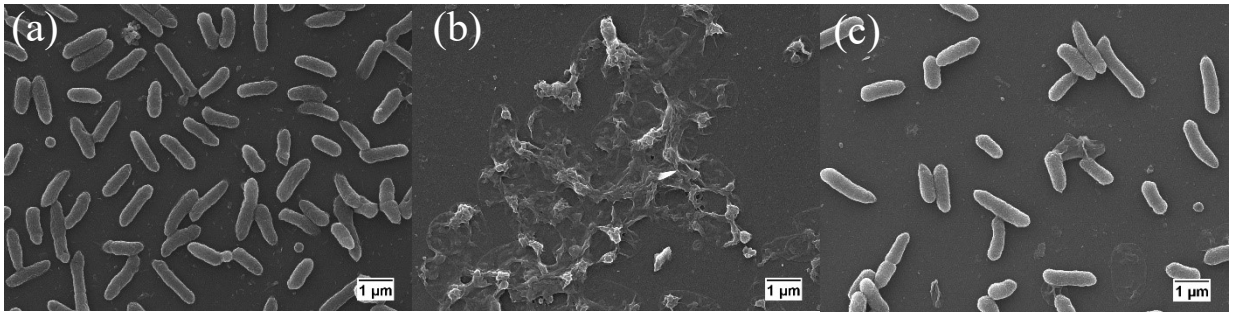


**Figure 6.2.** Representative FESEM images of adherent *E. coli* bacteria on the (a) $PDMAEMA_1$, (b) $PQDMAEMA_1$-C3 and (c) $PQDMAEMA_1$-C18 brushes.

The cells maintained their smooth shape on the non-quaternized $PDMAEMA_1$ brush, due to the inability of the surface to efficiently kill the bacteria. Similarly, the $PQDMAEMA_1$-C18 brush exhibited intact adhered bacteria with only very few killed ones, despite the high SCD of the brush, suggesting an insufficient bactericidal activity of the polymer film. Finally, the $PQDMAEMA_1$-C3 brush exhibited a high bactericidal efficacy and a large amount of debris of killed bacteria with collapsed cell morphology and damaged bacterial cell membranes, implying that the charged hydrophilic brush interacted strongly with the microbe cell membranes and killed he bacteria by the lysis of their cytoplasm, in agreement with the PCM results discussed above.

#### 6.2.1.3 Zone of Inhibition test

A contact killing mechanism is proposed for the cationic polymer brushes prepared herein, since the antimicrobial polymer chains are covalently attached to the surfaces. In order to eliminate possible leaching of bactericidal species from the brush, which would interfere with the contact-active bactericidal action of the surfaces, all samples were studied by the disc diffusion method (Figure 6.3). No inhibition zones were observed around the $PDMAEMA_1$, $PQDMAEMA_1$-C3 and $PQDMAEMA_1$-C18 brushes against *B. cereus* and *E. coli*, verifying that the antimicrobial polymer chains would not leach from the polymer film during the antimicrobial tests.

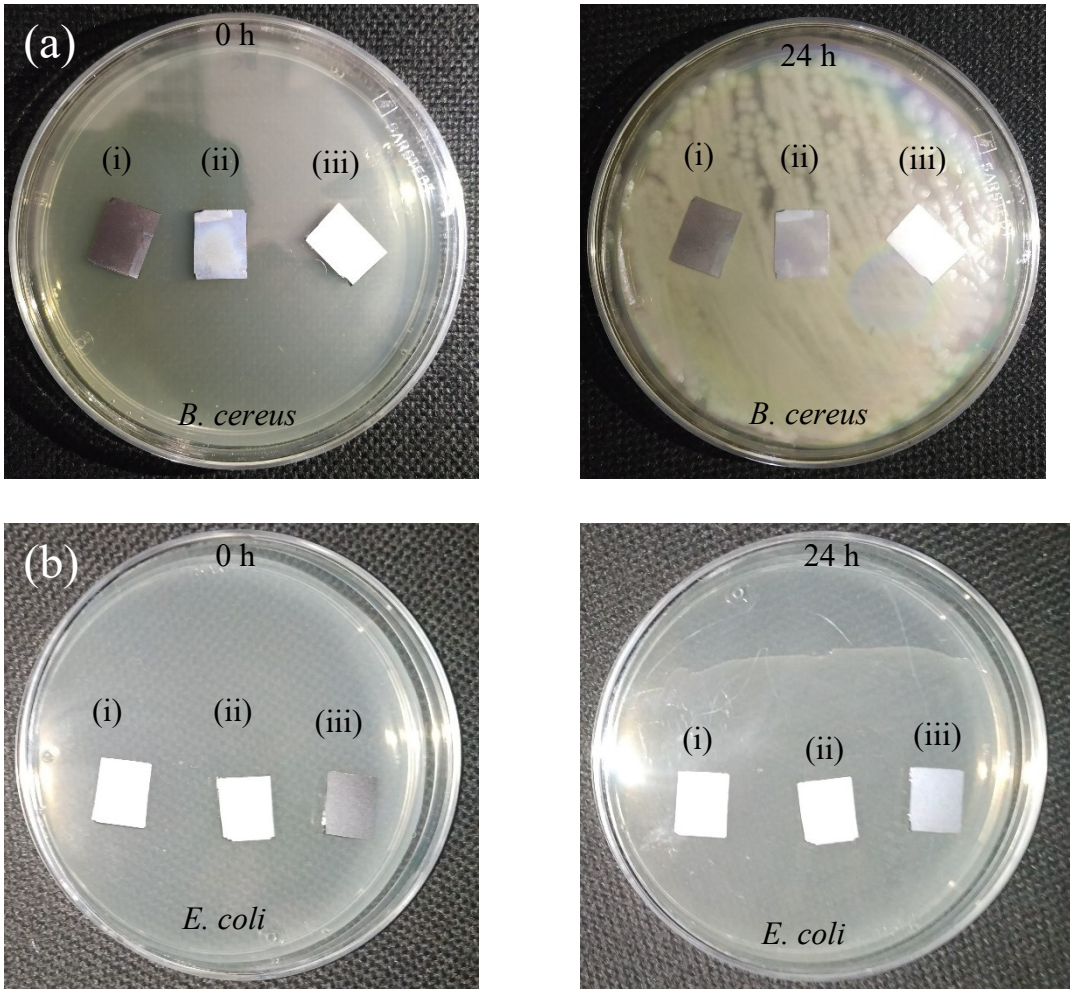


**Figure 6.3.** Zone of inhibition test for the (i) $PDMAEMA_1$, (ii) $PQDMAEMA_1$-C3 and (iii) $PQDMAEMA_1$-C18 brushes in (a) *B. cereus* and (b) *E. coli* culture lawns after 24 h incubation.

A favorable mechanism of antibacterial action suggests that locally enhanced attractive forces between the anionic lipids of the bacteria envelope and the positively charged quaternary ammonium species ("phospholipid sponge effect") of the polymer, which can be also accompanied by the release of phospholipids from the cell wall, lead to bacteria death.[5c] An integral key factor affecting the bactericidal efficiency of a polymer film in this mechanism has been proved to be the charge density of the surface, which enhances the adhesion forces between the bacteria and the immobile cations. Herein, it is demonstrated that the ACL of the substituent of the immobilized quaternary ammonium salt groups is vital for the accessibility of the positively charged moieties and the phospholipid attack in the cell culture medium. PQDMAEMA brushes with C1-C3 ACLs are effective bactericidal surfaces against both gram-positive and gram-negative bacteria, whereas, PDMAEMA brushes quaternized with C6, C12, C16 and

C18 alkyl chains exhibited a moderate antifouling action, but were found ineffective to kill the bacteria. In all cases, we evidence that bacteria first adsorb onto the polymer surfaces via electrostatic attraction. For the hydrophilic quaternized polymer brushes, the chains are mobile in the aqueous bacteria medium allowing the positively charged polymer units to effectively interact with the negatively charged walls of the bacteria, leading to the perforation and lysis of the cell membrane. On the contrary, bacteria adhere on the hydrophobic cationic polymer brushes, quaternized with long ACLs, however the hydrophobic polymer chains are immobile in the aqueous medium and thus the positively charged groups are inaccessible to the bacteria resulting in the suppression of the bactericidal action of the brush.[13a]

#### 6.2.1.4 Bacterial-releasing properties of the fluorinated brushes

To prevent the irreversible bacterial contamination and biofilm formation on surfaces, it is important to inhibit or release initial adhered bacteria. The hydrophilicity/hydrophobicity and the surface energy of polymer films constitute important properties that can affect their biological action and the adhesion of cells, bacteria and proteins. Highly hydrophilic surfaces with high surface energies are well known to resist the adsorption of proteins/cells/bacteria, due to an exclusive volume effect.[21] On the other hand, hydrophobic surfaces are more susceptible to protein or bacterial adhesion. However, hydrophobic polymer surfaces of very low surface energies and high interfacial energies with water, have been shown to exhibit very weak protein or bacterial adhesion and the facile detachment of the contaminants by water molecules under low applied frictional forces (i.e. water flow).[22]

Herein, the antifouling activity, based on their low-surface energy values, of the fluorinated homopolymer brushes was studied against the adhesion of both gram-negative (*E. coli*) and gram-positive (*B. cereus*) bacteria strains. All homopolymer brushes were incubated in a 1 ml bacterial suspension, with concentration $10^8$ CFU/ml, for 2 h and were washed with PBS under gentle agitation at 150 rpm for 1 h, to examine the bacterial-releasing efficacy of the surfaces.

The bacterial releasing properties of the homopolymer brushes were quantified using a plate counting method (Figure 6.4) (Table 6.2). A large number of *B. cereus* ($1.1\times10^6$

CFU/cm$^2$) and *E. coli* ($5\times10^6$ CFU/cm$^2$) bacteria adhered on the control silicon surfaces after 2 h, and their adherence was irreversible since the bacteria could not be detached through the rinsing and agitation process. Moreover, a vast number of adherent bacteria were found on the PDMAEMA brushes ($2.5\times10^6$ CFU/cm$^2$ for *B. cereus* and $8.2\times10^6$ CFU/cm$^2$ for *E. coli*), attributed to the partial protonation of the polymer at neutral pH (p$K_\alpha$ ~ 7.0) and the high surface energy of the film. Higher bacterial adhesion is expected for the PQDMAEMA brushes, which however, possess positively charged quaternary ammonium salt groups that act as contact-killing moieties, as discussed above in Section 6.2.1.2, and therefore, exhibited lower adhesion of the negatively charged *B. cereus* ($4.0\times10^4$ CFU/cm$^2$) and *E. coli* ($1.3\times10^6$ CFU/cm$^2$) bacteria. On the other hand, the non-contact killing fluorinated PTFEMA, POFPMA and PTDFOMA brushes, exhibited a much lower number of adhered bacteria colonies, attributed to the lower surface energy (10 to 23 mN/m) and the hydrophobicity of their surface (WCA 97$^o$ to 115$^o$) compared to the bare silicon and the PDMAEMA brushes. For the PTFEMA brush, the decrease in the number of adhered, *B. cereus* and *E. coli,* was 51% and 85%, respectively. The increase of the FCL in the POFPMA brush layer, decreased further the adhered bacteria by ~2.5log (99.5%) and ~1log (91.8%) for *B. cereus* and *E. coli*, respectively, whereas similar results were obtained for the PTDFOMA brush, with ~2.5log (99.6%) and ~1.2log (92.4%) reduction for *B. cereus* and *E. coli*, respectively. From the above it is evident that the length of the FCL plays a key role in the bacterial-releasing behavior of the brushes for both bacterial strains, whereas, the differences in the release of the two representative bacteria are attributed to their different cell membrane structure, which mediates the bacterial adhesion.[23]

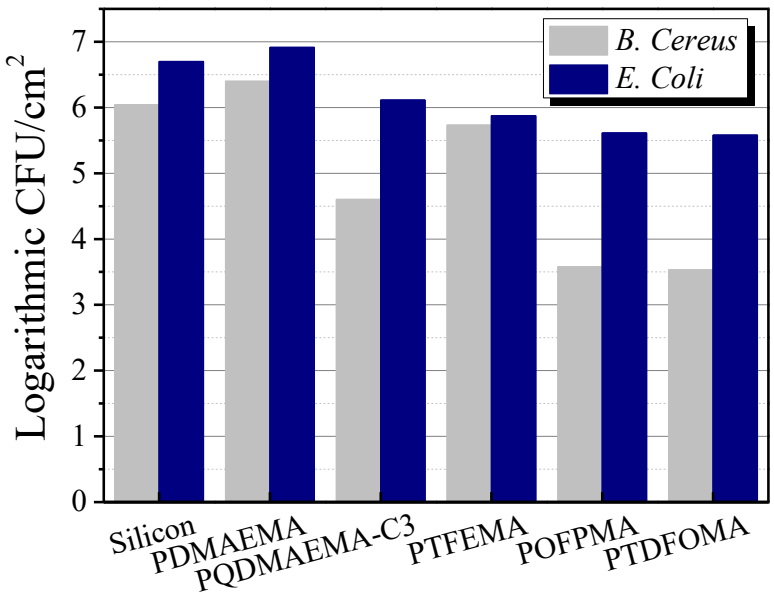


**Figure 6.4.** Quantitative analysis of adherent B. cereus and E. coli bacteria on the control silicon, the PDMAEMA, PQDMAEMA and the fluorinated PTFEMA, POFPMA and PTDFOMA brushes, after exposure in a suspension of $10^8$ CFU/ml for both strains, at 37 ºC for 2 h.

FESEM analysis verify qualitatively the bacterial adhesion, *E. coli* (Figure 6.5) and *B. cereus* (Figure 6.6), on the polymer films. The PDMAEMA brushes, show a large number of adhered bacteria after incubation for 2 h, which is irreversible since the bacteria could not be detached through the rinsing and agitation processes. The massive attachment of bacteria on the PQDMAEMA brushes, stems from the electrostatic attractions between the negatively charged bacteria and the positively charged quaternary ammonium salt groups of PQDMAEMA. In striking contrast to the almost complete coverage of the PQDMAEMA brushes by *E. coli* or *B. cereus* the semi-fluorinated PTFEMA, POFPMA and PTDFOMA brushes reduced the bacterial attachment. This is attributed to the low-surface energy of the fluorinated homopolymer brushes which facilitates the detachment of the bacteria following agitation in water.

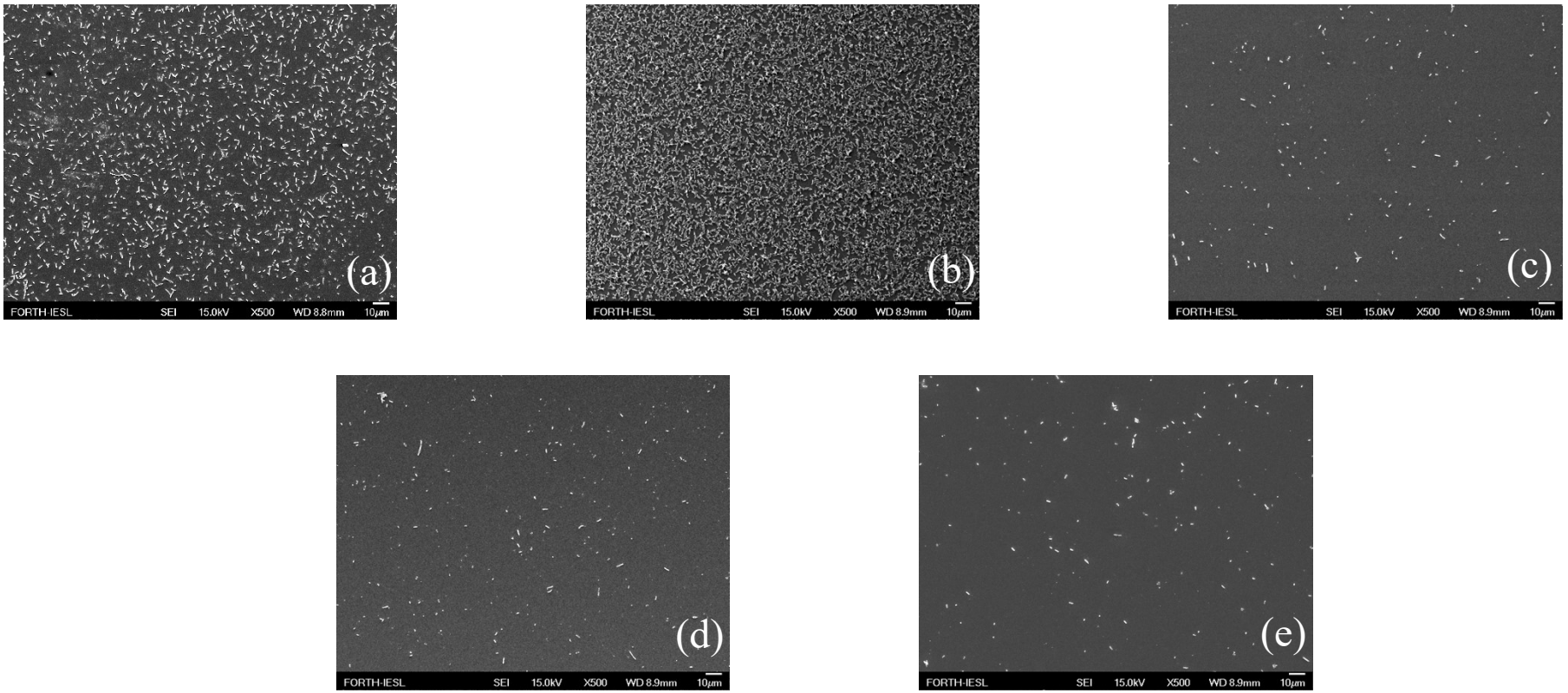


**Figure 6.5.** FESEM images of the (a) PDMAEMA, (b) PQDMAEMA-C3, (c) PTFEMA, (d) POFPMA and (e) PTDFOMA homopolymer brushes following incubation with *E. coli* at 37 ºC for 2 h and rinsing with PBS for 1 h. Scale bar: 10 μm.

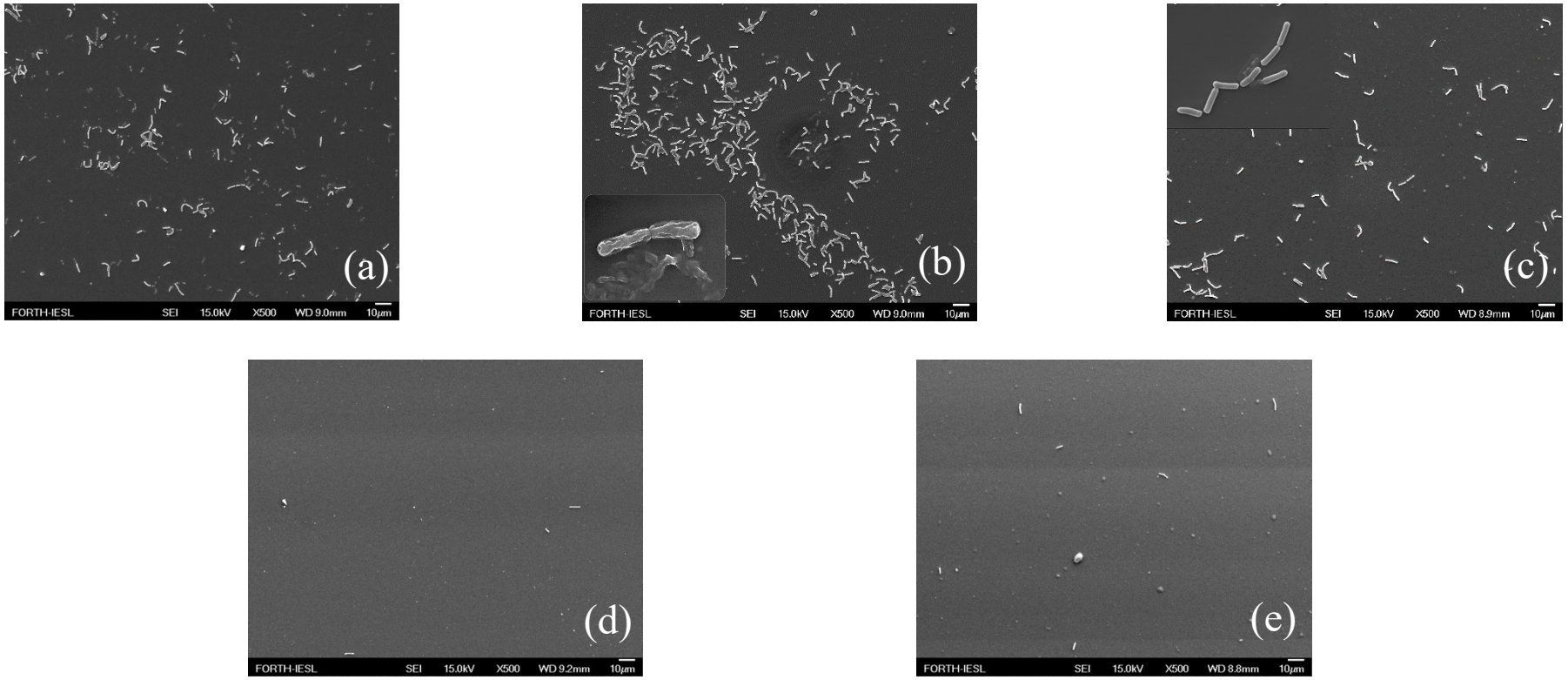


**Figure 6.6.** FESEM images of the (a) PDMAEMA, (b) PQDMAEMA-C3, (c) PTFEMA, (d) POFPMA and (e) PTDFOMA homopolymer brushes following incubation with *B. cereus* at 37 ºC for 2 h and rinsing with PBS for 1 h. Scale bar: 10 μm. Insets: Higher magnification images.

### 6.2.2 Binary mixed polymer brushes

The binary mixed polymer brushes, combine the antifouling properties of the fluorinated PTFEMA, POFPMA and PTDFOMA chains (hydrophobic and low surface energy moieties with $C_F1$, $C_F4$ and $C_F6$ FCLs) with the bactericidal activity of the cationic PQDMAEMA chains (hydrophilic QAS moieties with C3 ACL). The phase segregated domains of the brushes are in the range of nanometers (see Chapter 5) whereas, the bacteria are of micrometer size, and therefore the attached bacteria will come in contact with both the cationic and the fluorinated polymer chains.[24] Upon contamination, we envisage that these surfaces could be easily cleaned under the flow of water, whereas simultaneously their bactericidal action will inactivate any bacteria that are eventually irreversibly attached.

#### 6.2.2.1 Bacterial-releasing properties of the binary mixed brushes

In the present study, two representative bacteria strains, *B. cereus* and *E. coli,* were used to study the antifouling activities of the PTFEMA/PQDMAEMA, POFPMA/PQDMAEMA and PTDFOMA/PQDMAEMA mixed brushes. The characteristics of the mixed polymer brushes are summarized in Table 5.3 (see chapter 5).

To quantify the bacterial releasing ability of our polymer brushes, the number of bacteria attached on the surface after extensive rinsing with PBS was calculated by a plate counting method. As seen in Figure 6.7, the number of adhered bacteria on the binary mixed surfaces was lower compared to those found on the PQDMAEMA surfaces. The low surface energy of the mixed brushes, induced by the fluorinated polymer chains, resulted in the increased bacterial release following bacterial adhesion for short incubation times (2 h). For the PTFEMA/PQDMAEMA brush, a decrease in the number of adhered *B. cereus* and *E. coli* bacteria by 97.9% and 75.8%, respectively was found, compared to the bare silicon surface, whereas increasing the FCL from $C_F1$ to $C_F4$ resulted in a further decrease to 99.9% (~3log) and 99.8% (~2.7log) for *B. cereus* and *E. coli*, respectively, for the POFPMA/PQDMAEMA brush layer (see Table 6.3). Similar bacterial releasing properties were found for the PTDFOMA/PQDMAEMA brush with $C_F6$ (99.9% (~3log) for *B. cereus*, and 93.6% (~1.1log) for *E. coli*). The

observed differences in the bacteria releasing behavior for the two representative strains are attributed to the differences in their cell membrane structure, which mediates the adhesion of the bacteria on the surfaces. In fact, bacterial adhesion on a surface is a complex process that has several parameters as determinants (the properties of the bacterial cell surface, the liquid environment, and the properties of the material surface, *etc.*). According to the Baier curve of self-cleaning surfaces against biofilm formation, surfaces with intermediate WCA and high surface energy values are more prone to microbial fouling, whereas low surface energy and hydrophobic surfaces are less susceptible to fouling.[25] In this work, the fluorine component on the treated fabric surface in this work seems to play an important role in bacterial anti-adhesion because of their low surface energy. The bacterial-releasing efficacy of the PTFEMA/PQDMAEMA brushes was lower than that of the PTFEMA brush analogues, which suggests that the presence of PQDMAEMA results to the increase of the surface energy (~46 mN/m) and the attraction of negatively charged bacteria, by the positively charged quaternary ammonium salt groups of PQDMAEMA. In striking contrast, the bacterial-releasing efficacy of the binary mixed brushes is higher compared to that of the fluorinated homopolymer brush analogues, thus it is anticipated that a second mechanism takes place (contact-killing by the PQDMAEMA chains) enhancing the sterilization process of the mixed polymer surfaces from the *E. coli* and *B. cereus* bacteria strains. The surface energy values of these systems were shown to remain low (see Table 6.3), preventing the colonization of bacteria and fewer bacteria to contact and adhere on the surface so as to enhance the bacterial anti-adhesion.

**Table 6.3.** Binary mixed brushes evaluated as antimicrobial surfaces

| Brush | SFE (mN/m) | %Bacterial-releasing | | %Contact-killing | |
|---|---|---|---|---|---|
| | | *B. cereus* | *E. coli* | *B. cereus* | *E. coli* |
| PTFEMA/PQDMAEMA | 46 | 97.9 | 75.8 | 99.4 | 77.7 |
| POFPMA/PQDMAEMA | 25 | 99.9 | 99.8 | 98.7 | 90.2 |
| PTDFOMA/PQDMAEMA | 19 | 99.9 | 93.6 | 21.6 | 0.0 |

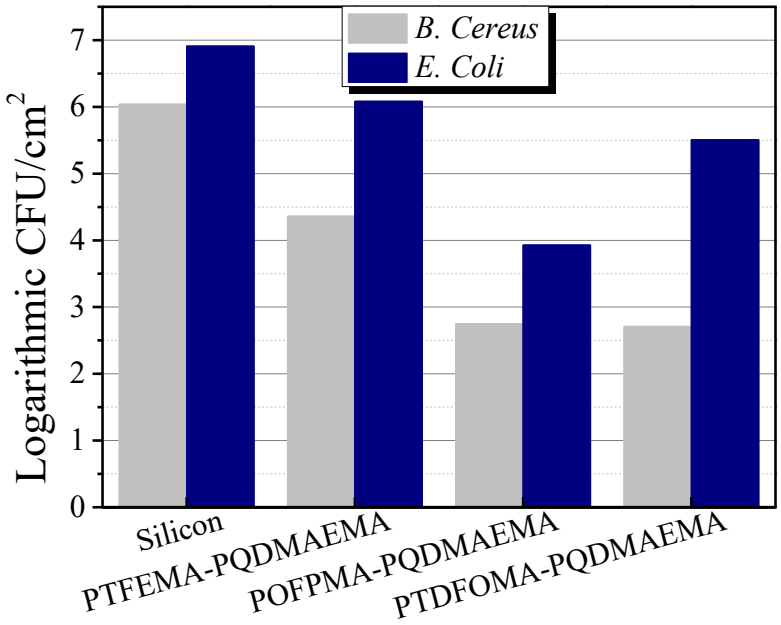


**Figure 6.7.** Logarithmic reduction of adherent B. cereus and E. coli bacteria on a control silicon substrate and the mixed polymer brushes following exposure in a 1 ml suspension of $10^8$ CFU/ml, at 37 ºC for 2 h.

FESEM was employed to verify the extent of bacterial adhesion on the polymer surfaces following immersion in the bacterial inoculums of *B. cereus* and *E. coli* (Figure 6.8). The PQDMAEMA brushes, which exhibit a large number of adhered bacteria due to electrostatic interactions between the positively charged polymer moieties and the negatively charged bacteria membranes, were compared to the mixed polymer brushes.

It is clearly seen that bacteria adhesion is reduced on the PTFEMA/PQDMAEMA mixed brushes, nevertheless, adhesion is higher compared to that on the PTFEMA homopolymer brushes, which is attributed to the presence of the positively charged quaternary ammonium salt groups in the mixed brushes, that attract the negatively charged bacteria. On the other hand, while the PTFEMA/PQDMAEMA brushes presented a relatively large number of adhered bacteria after 2 h of contact, the $C_F4$ and $C_F6$ FCLs, reduced significantly bacterial attachment on the POFPMA/PQDMAEMA and PTDFOMA/PQDMAEMA brushes, due to the lower surface energy. In particular, a much higher reduction in bacteria adhesion is observed for *E. coli* on the POFPMA/PQDMAEMA brushes compared to the PTDFOMA/PQDMAEMA brushes. This result is in good agreement with the PCM results discussed above and suggests

that a second mechanism takes place (contact-killing by the PQDMAEMA chains), and it is possible to enhance the preventing of the *E. coli* colonization in P POFPMA/PQDMAEMA brushes, whereas in PTDFOMA/PQDMAEMA brushes, the bacterial-releasing efficacy of PTDFOMA chains dominates on the outer surface of the brush, and the second mechanism is not favorable towards the more complex structure of *E. coli* compared to *B. cereus*.

Finally, the observed morphological changes of the bacteria on the mixed polymer brushes (see inset in Figure 6.8) suggest that the besides the bacteria-releasing behavior of the polymer brushes upon contact, attributed to the low-surface energy properties of the fluorinated homopolymer chains, which leads to the detachment of the bacteria after agitation in water, a contact-killing action of the remaining bacteria, from the cationic PQDMAEMA chains (see section 6.2.2.2 below) also takes place. Therefore, the mixed binary brushes display an effective dual-action (antifouling and bactericidal) against the initial bacterial adhesion, offering better protection to the surface and retarding biofilm formation.

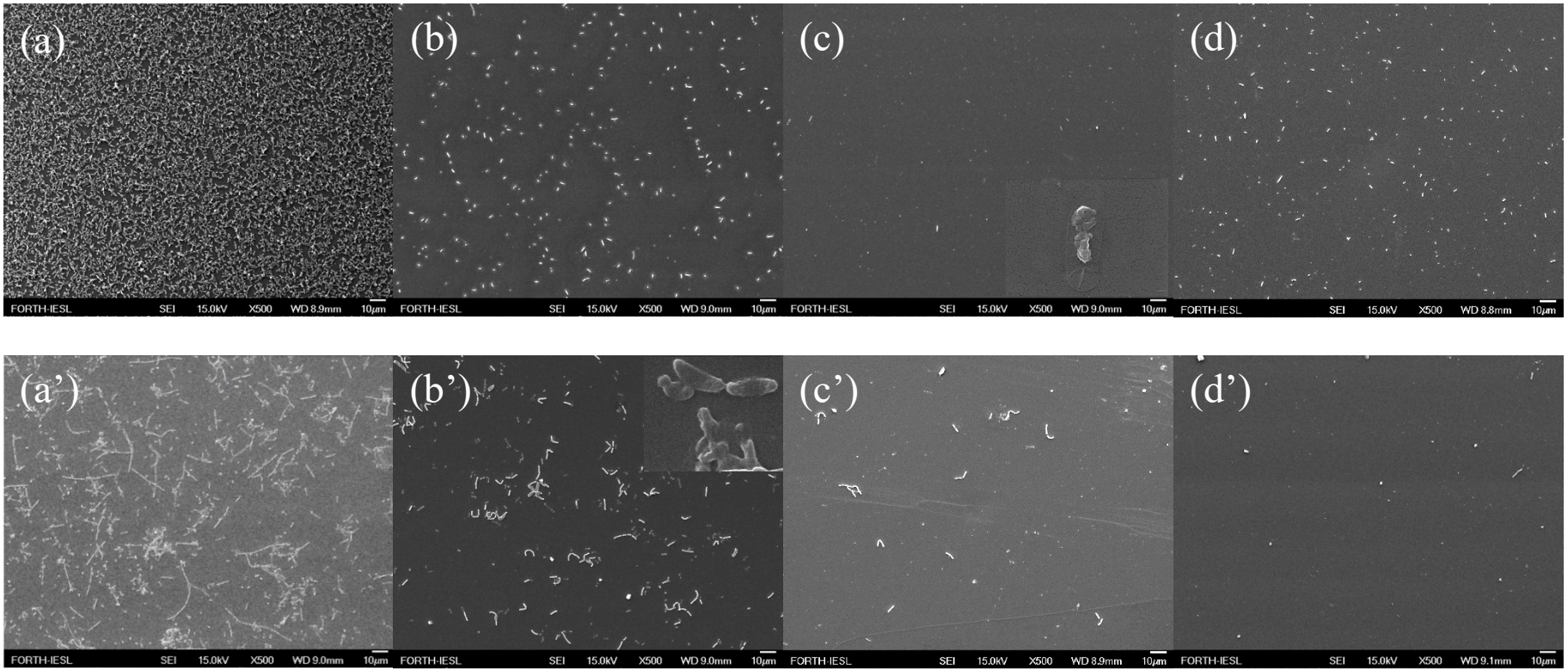


**Figure 6.8.** FESEM images of the (a,a') PQDMAEMA, (b,b') PTFEMA/PQDMAEMA, (c,c') POFPMA/PQDMAEMA and (d,d') PTDFOMA/PQDMAEMA brushes following incubation with (a,b,c and d) *E. coli* and (a',b',c' and d') *B. cereus* at 37 ºC for 2 h. Scale bar: 10 μm. Insets: Higher magnification images.

#### 6.2.2.2 Bacterial contact-killing activity of the binary mixed brushes

The remaining attached bacteria on a surface, following the release of the initially loosely adhered microorganisms, constitutes a significant issue. Killing these residual bacteria by a contact-killing mechanism is crucial to prevent the subsequent surface contamination and biofilm formation. The bactericidal activity of the PTFEMA/PQDMAEMA, POFPMA/PQDMAEMA and PTDFOMA/PQDMAEMA mixed polymer brushes was evaluated using the bactericidal assay described above for the homopolymer brushes (see Table 6.3). The surfaces were brought in contact with a bacterial suspension of *B. cereus or E. coli* for 5 h after which the supernatant was cultured on LB agar culture plates. Figure 6.9 shows the logarithmic reduction of the bacterial cells after being brought in contact with the quaternized binary mixed brushes. The PQDMAEMA-C3 homopolymer brush was used as a negative control. A very moderate decrease of 0.6log was measured for the PTFEMA/PQDMAEMA mixed brush against E. coli and a 2.2log reduction against *B. cereus*. On the other hand, the PTDFOMA/PQDMAEMA mixed brush showed no bactericidal activity against both bacterial strains, attributed to the high hydrophobicity of the brush (CA ~91º - 97º), which suggests that the contact-killing activity is impeded by the PTDFOMA chains. Finally, the POFPMA/PQDMAEMA brush exhibited a 1log (90%) and 1.9log (98.7%) reduction of the adhered viable *E. coli* and *B. cereus* bacteria, respectively, despite the moderate hydrophobicity (CA ~83º - 88º) of the brush. The observed differences in the bacteria killing for the two representative strains are attributed to the much-complicated cell membrane structure of the gram-negative microorganism, comprising an extra peptidoglycan layer.[19] It is also noted that for both *B. cereus and E. coli* the bactericidal reduction was larger for the $PQDMAEMA_1$-C3 homopolymer brush, with ~3log and ~2log reduction, respectively, which might be related to the lower number of positively charged moieties in the outer surface of the mixed brushes (~75%) compared to the PQDMAEMA brush. From the above results, it becomes apparent that the POFPMA/PQDMAEMA mixed brushes exhibit optimal antimicrobial properties, since these systems combine the bacterial-releasing properties of POFPMA and the contact-killing efficacy of PQDMAEMA-C3.

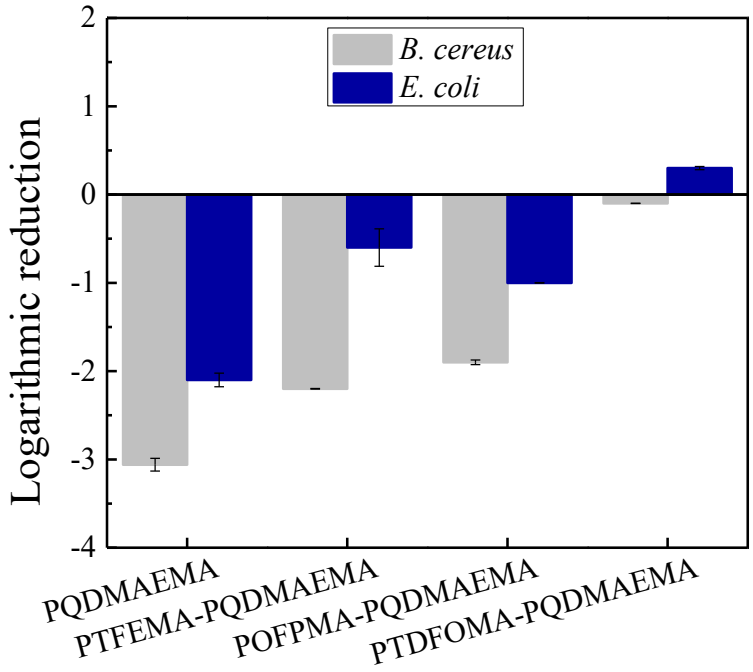


**Figure 6.9.** Bactericidal activity of the PQDMAEMA$_1$-C3, PTFEMA/PQDMAEMA, POFPMA/PQDMAEMA and PTDFOMA/PQDMAEMA brushes after 5 h contact with *B. cereus* (grey bars) and *E. coli* (blue bars) at 37 °C. Each bar represents the bacteria log reduction from 2 different experiments carried out in duplicates (mean ± SD).

## 6.3 Conclusions

In the present work, the effect of the ACLs of the quaternary ammonium salt moieties of quaternized PDMAEMA brushes was investigated and was shown to play a significant role on the bactericidal activity of the polymer brushes. Bactericidal, hydrophilic, cationic brushes, with high antimicrobial activity against both gram-positive and gram-negative bacteria strains are obtained for short ACLs as opposed to non-bactericidal, hydrophobic, cationic surfaces for ACLs with more than six carbon atoms. This dependence of the antibacterial activity of the PQDMAEMA brushes on the ACL of the quaternization agent provides new insights in the design of effective cationic bactericidal polymer surfaces to combat biofilm formation.

In addition, the antifouling efficacy of semi-fluorinated brushes bearing different FCLs on the polymer side groups was examined. Higher bacteria-release, under the flow of sterile water, was found for POFPMA ($C_F4$) and PTDFOMA ($C_F6$) against *B. cereus*

and *E. coli*. This improved antifouling performance is clearly related to the low surface energy of these polymers which prevents strong bacteria adhesion.

Finally, mixed amphiphilic polymer brushes comprising bactericidal PQDMAEMA and bacteria-release PTFEMA, POFPMA and PTDFOMA chains, were grown on silicon surfaces via SI-ATRP. Amongst these polymer brushes the POFPMA/PQDMAEMA system has provided effective dual-action antimicrobial properties. The initial adhesion of *B. cereus* and *E. coli* on this brush is reduced by more than 99.9% (~3log) and 99.8% (~2.7log), respectively, while simultaneously over 90% (1log) and 98.8% (1.9log) of the adhered *B. cereus* and *E. coli* bacteria, respectively, are killed by the cationic moieties, leading to a possible overall 99.99% (~4log) antimicrobial action.

## 6.4 References

1. Alvarez-Paino, M.; Munoz-Bonilla, A.; Fernandez-Garcia, M., Antimicrobial Polymers in the Nano-World. *Nanomaterials (Basel)* **2017,** *7* (2).
2. Jiao, Y.; Niu, L.-n.; Ma, S.; Li, J.; Tay, F. R.; Chen, J.-h., Quaternary ammonium-based biomedical materials: State-of-the-art, toxicological aspects and antimicrobial resistance. *Prog Polym Sci* **2017,** *71*, 53-90.
3. (a) Xue, Y.; Xiao, H.; Zhang, Y., Antimicrobial Polymeric Materials with Quaternary Ammonium and Phosphonium Salts. *International Journal of Molecular Sciences* **2015,** *16* (2); (b) Jain, A.; Duvvuri, L. S.; Farah, S.; Beyth, N.; Domb, A. J.; Khan, W., Antimicrobial Polymers. *Adv Healthc Mater* **2014,** *3* (12), 1969-1985.
4. (a) Siedenbiedel, F.; Tiller, J. C., Antimicrobial Polymers in Solution and on Surfaces: Overview and Functional Principles. *Polymers-Basel* **2012,** *4* (1), 46-71; (b) Asri, L. A. T. W.; Crismaru, M.; Roest, S.; Chen, Y.; Ivashenko, O.; Rudolf, P.; Tiller, J. C.; van der Mei, H. C.; Loontjens, T. J. A.; Busscher, H. J., A Shape- Adaptive, Antibacterial- Coating of Immobilized Quaternary- Ammonium Compounds Tethered on Hyperbranched Polyurea and its Mechanism of Action. *Adv Funct Mater* **2014,** *24* (3), 346-355; (c) Madkour, A. E.; Dabkowski, J. M.; Nüsslein, K.; Tew, G. N., Fast Disinfecting Antimicrobial Surfaces. *Langmuir* **2009,** *25* (2), 1060-1067; (d) Bieser, A. M.; Tiller, J. C., Mechanistic Considerations on Contact-Active Antimicrobial Surfaces with Controlled Functional Group Densities. *Macromol Biosci* **2011,** *11* (4), 526-534.
5. (a) Kugler, R.; Bouloussa, O.; Rondelez, F., Evidence of a charge-density threshold for optimum efficiency of biocidal cationic surfaces. *Microbiol-Sgm* **2005,** *151*, 1341-1348; (b) Timofeeva, L.; Kleshcheva, N., Antimicrobial polymers: mechanism of action, factors of activity, and applications. *Appl Microbiol Biotechnol* **2011,** *89* (3), 475-92; (c) Gao, J.; White, E. M.; Liu, Q. H.; Locklin, J., Evidence for the Phospholipid Sponge Effect as the Biocidal Mechanism in Surface-Bound Polyquaternary Ammonium Coatings with Variable Cross-Linking Density. *Acs Appl Mater Inter* **2017,** *9* (8), 7745-7751.

6. (a) Li, M.; Liu, X. H.; Liu, N.; Guo, Z. H.; Singh, P. K.; Fu, S. Y., Effect of surface wettability on the antibacterial activity of nanocellulose-based material with quaternary ammonium groups. *Colloid Surface A* **2018,** *554*, 122-128; (b) Buffet-Bataillon, S.; Tattevin, P.; Bonnaure-Mallet, M.; Jolivet-Gougeon, A., Emergence of resistance to antibacterial agents: the role of quaternary ammonium compounds—a critical review. *International Journal of Antimicrobial Agents* **2012,** *39* (5), 381-389; (c) Li, F.; Weir, M. D.; Xu, H. H. K., Effects of Quaternary Ammonium Chain Length on Antibacterial Bonding Agents. *J Dent Res* **2013,** *92* (10), 932-938.
7. Tiller, J. C.; Liao, C. J.; Lewis, K.; Klibanov, A. M., Designing surfaces that kill bacteria on contact. *P Natl Acad Sci USA* **2001,** *98* (11), 5981-5985.
8. (a) Murata, H.; Koepsel, R. R.; Matyjaszewski, K.; Russell, A. J., Permanent, non-leaching antibacterial surfaces—2: How high density cationic surfaces kill bacterial cells. *Biomaterials* **2007,** *28* (32), 4870-4879; (b) Karamdoust, S.; Yu, B. Y.; Bonduelle, C. V.; Liu, Y.; Davidson, G.; Stojcevic, G.; Yang, J.; Lau, W. M.; Gillies, E. R., Preparation of antibacterial surfaces by hyperthermal hydrogen induced cross-linking of polymer thin films. *J Mater Chem* **2012,** *22* (11), 4881-4889; (c) Ozcam, A. E.; Roskov, K. E.; Spontak, R. J.; Genzer, J., Generation of functional PET microfibers through surface-initiated polymerization. *J Mater Chem* **2012,** *22* (12), 5855-5864; (d) Yan, S. J.; Luan, S. F.; Shi, H. C.; Xu, X. D.; Zhang, J. D.; Yuan, S. S.; Yang, Y. M.; Yin, J. H., Hierarchical Polymer Brushes with Dominant Antibacterial Mechanisms Switching from Bactericidal to Bacteria Repellent. *Biomacromolecules* **2016,** *17* (5), 1696-1704; (e) Huang, C. J.; Chen, Y. S.; Chang, Y., Counterion-activated nanoactuator: reversibly switchable killing/releasing bacteria on polycation brushes. *ACS Appl Mater Interfaces* **2015,** *7* (4), 2415-23; (f) Li, H. R.; Bao, H. Q.; Bok, K. X.; Lee, C. Y.; Li, B.; Zin, M. T.; Kang, L. F., High durability and low toxicity antimicrobial coatings fabricated by quaternary ammonium silane copolymers. *Biomater Sci-Uk* **2016,** *4* (2), 299-309.
9. Gozzelino, G.; Lisanti, C.; Beneventi, S., Quaternary ammonium monomers for UV crosslinked antibacterial surfaces. *Colloid Surface A* **2013,** *430*, 21-28.
10. (a) Zhao, J.; Millians, W.; Tang, S. D.; Wu, T. H.; Zhu, L.; Ming, W. H., Self-Stratified Antimicrobial Acrylic Coatings via One-Step UV Curing. *Acs Appl Mater Inter* **2015,** *7* (33), 18467-18472; (b) Zhao, J.; Ma, L.; Millians, W.; Wu, T. E. H.; Ming, W. H., Dual-Functional Antifogging/Antimicrobial Polymer Coating. *Acs Appl Mater Inter* **2016,** *8* (13), 8737-8742; (c) Koromilas, N. D.; Lainioti, G. C.; Vasilopoulos, G.; Vantarakis, A.; Kallitsis, J. K., Synthesis of antimicrobial block copolymers bearing immobilized bacteriostatic groups. *Polym Chem-Uk* **2016,** *7* (21), 3562-3575; (d) Druvari, D.; Koromilas, N. D.; Lainioti, G. C.; Bokias, G.; Vasilopoulos, G.; Vantarakis, A.; Baras, H.; Dourala, N.; Kallitsis, J. K., Polymeric Quaternary Ammonium-Containing Coatings with Potential Dual Contact-Based and Release-Based Antimicrobial Activity. *Acs Appl Mater Inter* **2016,** *8* (51), 35593-35605; (e) Kurt, P.; Wood, L.; Ohman, D. E.; Wynne, K. J., Highly effective contact antimicrobial surfaces via polymer surface modifiers. *Langmuir* **2007,** *23* (9), 4719-4723; (f) He, J. W.; Soderling, E.; Vallittu, P. K.; Lassila, L. V. J., Investigation of double bond conversion, mechanical properties, and antibacterial activity of dental resins with different alkyl chain length quaternary ammonium methacrylate monomers (QAM). *J Biomat Sci-Polym E* **2013,** *24* (5), 565-573.
11. Roy, D.; Knapp, J. S.; Guthrie, J. T.; Perrier, S., Antibacterial cellulose fiber via RAFT surface graft polymerization. *Biomacromolecules* **2008,** *9* (1), 91-99.
12. Lin, J.; Chen, X.; Chen, C.; Hu, J.; Zhou, C.; Cai, X.; Wang, W.; Zheng, C.; Zhang, P.; Cheng, J.; Guo, Z.; Liu, H., Durably Antibacterial and Bacterially

Antiadhesive Cotton Fabrics Coated by Cationic Fluorinated Polymers. *Acs Appl Mater Inter* **2018,** *10* (7), 6124-6136.
13. (a) Yang, Y. F.; Hu, H. Q.; Li, Y.; Wan, L. S.; Xu, Z. K., Membrane surface with antibacterial property by grafting polycation. *J Membrane Sci* **2011,** *376* (1-2), 132-141; (b) Guo, S. T.; Zhang, Q.; Wang, D. H.; Wang, L.; Lin, F.; Wilson, P.; Haddleton, D. M., Bioinspired coating of TiO2 nanoparticles with antimicrobial polymers by Cu(0)-LRP: grafting to vs. grafting from. *Polym Chem-Uk* **2017,** *8* (42), 6570-6580.
14. Xu, B.; Liu, Y.; Sun, X.; Hu, J.; Shi, P.; Huang, X., Semifluorinated Synergistic Nonfouling/Fouling-Release Surface. *Acs Appl Mater Inter* **2017,** *9* (19), 16517-16523.
15. Kaur, R.; Liu, S., Antibacterial surface design - Contact kill. *Prog Surf Sci* **2016,** *91* (3), 136-153.
16. van de Lagemaat, M.; Grotenhuis, A.; van de Belt-Gritter, B.; Roest, S.; Loontjens, T. J. A.; Busscher, H. J.; van der Mei, H. C.; Ren, Y., Comparison of methods to evaluate bacterial contact-killing materials. *Acta Biomater* **2017**.
17. Hammes, F.; Berney, M.; Egli, T., Cultivation-independent Assessment of Bacterial Viability. **2010,** *124*, 123-150.
18. Choi, G.; Jeong, G. M.; Oh, M. S.; Joo, M.; Im, S. G.; Jeong, K. J.; Lee, E., Robust Thin Film Surface with a Selective Antibacterial Property Enabled via a Cross-Linked Ionic Polymer Coating for Infection-Resistant Medical Applications. *ACS Biomaterials Science & Engineering* **2018,** *4* (7), 2614-2622.
19. (a) Xue, Y.; Guan, Y.; Zheng, A.; Wang, H.; Xiao, H., Synthesis and Characterization of Ciprofloxacin Pendant Antibacterial Cationic Polymers. *Journal of Biomaterials Science, Polymer Edition* **2012,** *23* (8), 1115-1128; (b) Pant, J.; Gao, J.; Goudie, M. J.; Hopkins, S. P.; Locklin, J.; Handa, H., A multi-defense strategy: Enhancing bactericidal activity of a medical grade polymer with a nitric oxide donor and surface-immobilized quaternary ammonium compound. *Acta Biomater* **2017,** *58*, 421-431.
20. Li, P.; Poon, Y. F.; Li, W.; Zhu, H. Y.; Yeap, S. H.; Cao, Y.; Qi, X.; Zhou, C.; Lamrani, M.; Beuerman, R. W.; Kang, E. T.; Mu, Y.; Li, C. M.; Chang, M. W.; Leong, S. S.; Chan-Park, M. B., A polycationic antimicrobial and biocompatible hydrogel with microbe membrane suctioning ability. *Nat Mater* **2011,** *10* (2), 149-56.
21. Chen, S.; Li, L.; Zhao, C.; Zheng, J., Surface hydration: Principles and applications toward low-fouling/nonfouling biomaterials. *Polymer* **2010,** *51* (23), 5283-5293.
22. Krishnan, S.; Weinman, C. J.; Ober, C. K., Advances in polymers for anti-biofouling surfaces. *J Mater Chem* **2008,** *18* (29), 3405-3413.
23. Hori, K.; Matsumoto, S., Bacterial adhesion: From mechanism to control. *Biochemical Engineering Journal* **2010,** *48* (3), 424-434.
24. Zdyrko, B.; Klep, V.; Li, X. W.; Kang, Q.; Minko, S.; Wen, X. J.; Luzinov, I., Polymer brushes as active nanolayers for tunable bacteria adhesion. *Mat Sci Eng C-Bio S* **2009,** *29* (3), 680-684.
25. Magin, C. M.; Cooper, S. P.; Brennan, A. B., Non-toxic antifouling strategies. *Materials Today* **2010,** *13* (4), 36-44.

# Chapter 7

Conclusions & Future Perspectives

## 7.1 Conclusions

In this thesis, we have synthesized functional non-fluorinated and semi-fluorinated polymer brushes on silicon/glass substrates via SI-ATRP. The main directions pursued were to investigate the impact of the polymer functionality and architecture on the surface properties and the antimicrobial performance of these systems, grafted from solid substrates. The three brush architectures explored were homopolymer, diblock copolymer and binary mixed polymer brushes. The solvato-responsive behavior of these brushes was investigated using a variety of experimental techniques such as ellipsometry, contact angle measurements, AFM, LFM, ATR-FTIR spectroscopy and their interactions with representative Gram-positive and Gram-negative bacteria was assessed.

### 7.1.1. Surface properties of the homopolymer brushes

In the first part of the work, we report the synthesis of homopolymer brushes with different functionalities. Amine-based polymer brushes (PDMAEMA), leading to hydrophilic surfaces, and hydrophobic semi-fluorinated polymer brushes (based on PTFEMA, POFPMA and PTDFOMA), bearing different fluorinated side groups, were grown from silicon surfaces.

PDMAEMA brushes were successfully grown from silicon surfaces, fully-coated with a BIDS ATRP initiator monolayer. Next, PQDMAEMA brushes bearing different ACLs were prepared, by a facile post polymerization quaternization reaction of the tertiary amine groups of PDMAEMA using suitable alkyl halides. Quaternization with short ACLs (C1-C3), resulted in hydrophilic surfaces, due to the permanent positive charges on the polymer side groups. On the other hand, post modification with long ACLs (C≥6) yielded hydrophobic surfaces verifying that the alkyl chains dominate the surface wettability of the films. Based on the degrees of the quaternization and the swelling of the polymer films, it is suggested that the diffusion of alkyl halides with long ACLs (C ≥ 6) in the brush is hindered, forming an upper layer of quaternized moieties. On the contrary, small alkyl halides can diffuse easily within the dense polymer film and react almost quantitatively with the PDMAEMA amine groups. Overall, partially quaternized brushes with long ACLs can retain their pH-responsive

character, after quaternization which is lost for the PQDMAEMA brushes with short ACLs.

The fluorinated polymers resulted in moderate hydrophobic surfaces, with the hydrophobicity increasing with the FCL of the side group. Moreover, the surface free energies diminished with the increase of the FCL. Adhesion and friction studies between the semi-fluorinated brushes and inorganic silicon nitride surfaces (AFM tip) revealed that the fluorinated moieties introduce dry lubricant properties to the polymer layers and reduce their interaction with the tip.

Finally, the synthesized PDMAEMA and PQDMAEMA brushes suffered a profound loss of the grafted polymer chains after a few days. This process is detrimental, because the morphology and the composition of the polymer films change and therefore, their application underwater for prolonged periods of time is impossible. The degrafting process was not observed for the semi-fluorinated polymer brushes grafted on the same substrate, suggesting the action of the chains as a "polymer carpet" underwater to repel the water molecules from the polymer-substrate interface, which prevents the hydrolysis process and stabilizes the grafted polymer layer.

### 7.1.2. Responsive amphiphilic diblock copolymer brushes

Solvent-responsive polymeric surfaces, based on amphiphilic diblock copolymer brushes (PDMAEMA-*b*-PTFEMA, PDMAEMA-*b*-POFPMA, PDMAEMA-*b*-PTDFOMA) that can reversibly switch from the hydrophobic to the hydrophilic state, were synthesized. Two families of brushes were prepared, the first comprising a lower content of the fluorocarbon blocks compared to the hydrophilic segments and the second comprising almost symmetric amphiphilic diblock copolymer chains. The symmetric diblock copolymers could not undergo re-arrangement of their chains following exposure to water, whereas the re-arrangement took place for the copolymers with a higher content of the inner PDMAEMA block. The latter smart surfaces are able to alter their surface properties, from hydrophilic (~60º) to hydrophobic (94º -110º), following immersion in water (selective solvent for PDMAEMA) and hexafluoroisopropanol (HFiP) (selective solvent for the semi-fluorinated segments), respectively, for at least 5 solvent cycles.

In addition, it was shown that quaternization of the amine groups of the responsive diblock copolymer brushes, deteriorated their responsiveness. This was attributed to the larger χ value between the two blocks after quaternization, due to the presence of two very dissimilar polymers, charged PQDMAEMA and fluorinated PTFEMA, POFPMA or PTDFOMA chains which leads to phase separation with both polymers being present at the polymer-air interface.

Finally, undesired degrafting was observed, attributed to the hydrolysis of the ester or siloxane bonds of the surface-bound initiator, following exposure of the diblock copolymer brushes in aqueous media for prolonged time periods, which compromises their use in underwater applications. It was also found, that the stability of the amphiphilic diblock copolymer brushes depends on the charge density along the polymer chains, with the PQDMAEMA brushes undergoing significant degrafting in the first week in water, whereas the non-quaternized analogues were stable for the first two weeks, after which they exhibited significant degrafting in the aqueous medium.

### 7.1.3. Binary mixed polymer brushes with tunable surface and friction properties

Well defined amphiphilic binary mixed brushes were synthesized by two sequential SI-ATRP steps from mixed-silane ATRP initiator modified surfaces using TFEMA, OFPMA and TDFOMA as the fluorinated monomers and DMAEMA as a functional hydrophilic monomer. The surface properties (wettability and surface energy) were tuned following immersion of the mixed brushes in water (selective solvent for PDMAEMA) and hexafluoroisopropanol (HFiP) (selective solvent for the semi-fluorinated segments), respectively. An excellent switching behavior with a reversible transition from the hydrophilic to the hydrophobic state was found for all polymer brushes, for at least 6 solvent cycles. In addition, a reversible transition from low to high adhesion/friction, was observed, upon immersion of the films in HFiP and water, respectively, rendering these mixed polymer brushes attractive for use as switchable dry lubricant surfaces. Their responsive wettability was lost after quaternization of the DMAEMA moieties with propyl iodide, attributed to the increase of the Flory-Higgins χ parameter between the cationic and fluorinated polymer chains. Nevertheless, their

surface energy values indicated a compositional heterogeneity of their surface which may favor their use in dual action, non-fouling and bactericidal, applications.

Finally, the stability of the polymer films upon prolonged immersion in water, was studied. The increased stability of the polyelectrolyte chains during long-term exposure in aqueous media was attributed to the localization of the fluorinated chains at the polymer-substrate interface, which hinders the access of water to the surface and diminishes the hydrolysis of the ester or siloxane bonds of the surface-bound initiator, enabling the use of the polymer brushes in underwater applications.

### 7.1.4. Antimicrobial surfaces

The antimicrobial efficiency of the homopolymer and binary mixed polymer brushes against Gram-positive and Gram-negative bacteria strains was investigated.

The facile quaternization reaction of PDMAEMA produced cationic homopolymer brushes with high antibiotic performance. The effect of the ACLs of the quaternary ammonium salt moieties of the quaternized PDMAEMA brushes was investigated and was shown to influence the bactericidal performance of the polymer brushes. Bactericidal, hydrophilic, cationic brushes, with high antimicrobial activity against both bacteria strains were obtained for short ACLs as opposed to the non-bactericidal, hydrophobic, cationic surfaces for ACLs with more than six carbon atoms. These results create new understanding on the dependence of the antibacterial activity of the PQDMAEMA brushes on the ACL of the quaternized moieties and allows the design of effective surfaces to combat biofilm formation in various applications.

The antifouling activity of the semi-fluorinated homopolymer brushes, bearing different FCLs on the polymer side groups, was examined. An increased bacteria-release, under the flow of sterile water, was found for the POFPMA ($C_F4$) and PTDFOMA ($C_F6$) brushes against *B. cereus* and *E. coli*, signifying the requirement for a minimum number of fluorine atoms, which correlates with a low surface free energy of the brush, for effective antifouling performance.

Finally, dual-action, amphiphilic, mixed polymer brushes comprising bactericidal PQDMAEMA and antifouling PTFEMA, POFPMA or PTDFOMA chains, were grown

on silicon surfaces via SI-ATRP. The mixed POFPMA/PQDMAEMA brush exhibited the stronger antimicrobial activity, combining effective dual-action bactericidal and bacterial-releasing properties. The fluorinated POFPMA chains exhibited a high antifouling action against the initial adhesion of both *B. cereus* and *E. coli* on the mixed brush 99.9% (~3log) and 99.8% (~2.7log), while, simultaneously the positively charged PQDMAEMA chains demonstrated a strong contact killing action 90% (1log) and 98.8% (1.9log), of the adhered *B. cereus* and *E. coli* bacteria, respectively, leading to a profound antimicrobial efficacy of ~4log reduction.

## 7.2 Future Perspectives

This thesis presents the synthesis and characterization of novel smart polymer brushes to realize the influence of polymer functionality and architecture on the surface properties and the antimicrobial performance of thin polymer films. Three brush architectures were explored, namely homopolymer, diblock copolymer and binary mixed polymer brushes.

Future work in this field would require the detailed investigation of the dependence of the degree of quaternization of the PQDMAEMA brushes bearing long ACLs (C≥6) on the polymer grafting density. PDMAEMA brushes with lower grafting densities can be prepared to possibly access higher degrees of quaternization and thus a different dependence of the surface properties of the PQDMAEMA brushes on the ACL of the quaternization agent. Additional work is also required to characterize the formation of an outermost quaternized layer in the polymer brush when using alkyl halides with long ACLs. XPS measurements could help in the characterization of this upper layer in the brushes (~10 nm penetration depth). Another interesting study could focus on the synthesis of a first thin, grafted semi-fluorinated layer at the polymer-substrate interface, followed by chain extension with DMAEMA to prepare the strong polyelectrolyte brushes, that would act as a barrier for the penetration of water molecules into the interphase and thus postpone or even completely eliminate the detrimental degrafting of the hydrophilic polymer chains.

The responsive behavior of the amphiphilic PDMAEMA-*b*-PTFEMA, PDMAEMA-*b*-POFPMA and PDMAEMA-*b*-PTDFOMA diblock copolymer brushes as a function of

solution pH and/or temperature should be addressed. Moreover, the synthesis of PTFEMA-*b*-PDMAEMA, POFPMA-*b*-PDMAEMA and PTDFOMA-*b*-PDMAEMA diblock copolymer brushes is proposed which could possibly retain their solvato-responsive behavior, while, simultaneously preventing the degrafting process. In addition, the characterization of the rearrangement of the amphiphilic block copolymer chains upon immersion in different selective solvents holds great promise, since we evidenced a complex behavior with no obvious phase separation, implying the lateral organization of the end-grafted chains. Finally, the determination of the $\chi$ parameter and the solubility parameters of the PDMAEMA, PQDMAEMA and the semi-fluorinated polymer chains could help to understand the phase behavior of the diblock and mixed polymer brushes and its influence on the organization of the polymer chains and the responsive properties on the surfaces.

The PQDMAEMA brushes exhibited effective bactericidal activity, against both gram-positive and gram-negative bacteria strains for short ACLs as opposed to the cationic surfaces with ACLs of more than six carbon atoms. Quaternization of PDMAEMA with appropriate alkylating agents to introduce more than one quaternary ammonium group per monomer repeat unit, will introduce a larger number of charges which might help to increase the bactericidal activity of the brushes. In this case the optimum chain length might also be different, due to the subtle balance between the number of changes and the hydrophilicity/hydrophobicity of the surface. In addition, a wider range of bacterial strains should be tested to broaden the scope of potential applications of these polymer surfaces. On the other hand, the semi-fluorinated chains, namely PTFEMA, POFPMA and PTDFOMA brushes, exhibited high bacterial-releasing properties for both E. coli and B. cereus. The antifouling performance of the brushes was shown to increase with the fluorinated chain length ($C_F1$ to $C_F4$ to $C_F6$), which is clearly related to the low surface energy of these polymers providing antifouling surfaces under a flow of water. A closer resemblance to real life conditions could use a flow chamber that can apply the velocity of a marine boat to investigate the bacteria-release behavior of these surfaces against biofilm formation.